Technical Report Documentation Page

1. Report No. FHWA/TX-09/9-5498-2	2. Government Accession No.	3. Recipient's Catalog No.
4. Title and Subtitle The Tensile Capacity of Welded Shear Studs		5. Report Date October 2008 6. Performing Organization Code
7. Author(s) Joshua M. Mouras, James P. Sutton, Karl H. Frank, Eric B. Williamson		8. Performing Organization Report No. 9-5498-2
9. Performing Organization Name and Address Center for Transportation Research The University of Texas at Austin 3208 Red River, Suite 200 Austin, TX 78705-2650		10. Work Unit No. (TRAIS) 11. Contract or Grant No. 0-5498
12. Sponsoring Agency Name and Address Texas Department of Transportation Research and Technology Implementation Office P.O. Box 5080 Austin, TX 78763-5080		13. Type of Report and Period Covered Technical Report 14. Sponsoring Agency Code
15. Supplementary Notes Project performed in cooperation with the Texas Department of Transportation and the Federal Highway Administration.		
16. Abstract The ability of shear studs to transfer vertical tension forces from a fractured girder to intact bridge components was investigated. The effect of haunches in the deck, stud length, number of studs, and arrangement of the studs was evaluated in static and dynamic tests. Revised stud strength provisions were developed, which included the effect of a haunch upon stud capacity.		
17. Key Words Bridges, shear studs, fracture critical.	18. Distribution Statement No restrictions. This document is available to the public through the National Technical Information Service, Springfield, Virginia 22161; www.ntis.gov.	

19. Security Classif. (of report) Unclassified	20. Security Classif. (of this page) Unclassified	21. No. of pages 166	22. Price

Form DOT F 1700.7 (8-72) Reproduction of completed page authorized

The Tensile Capacity of Welded Shear Studs

Joshua M. Mouras
James P. Sutton
Karl H. Frank
Eric B. Williamson

CTR Technical Report:	9-5498-2
Report Date:	October 14, 2008
Project:	0-5498
Project Title:	Methods of Evaluating the Redundancy of Steel Bridges
Sponsoring Agency:	Texas Department of Transportation
Performing Agency:	Center for Transportation Research at The University of Texas at Austin

Project performed in cooperation with the Texas Department of Transportation and the Federal Highway Administration.

Center for Transportation Research
The University of Texas at Austin
3208 Red River
Austin, TX 78705

www.utexas.edu/research/ctr

Disclaimers

Author's Disclaimer: The contents of this report reflect the views of the authors, who are responsible for the facts and the accuracy of the data presented herein. The contents do not necessarily reflect the official view or policies of the Federal Highway Administration or the Texas Department of Transportation (TxDOT). This report does not constitute a standard, specification, or regulation.

Patent Disclaimer: There was no invention or discovery conceived or first actually reduced to practice in the course of or under this contract, including any art, method, process, machine manufacture, design or composition of matter, or any new useful improvement thereof, or any variety of plant, which is or may be patentable under the patent laws of the United States of America or any foreign country.

Engineering Disclaimer

NOT INTENDED FOR CONSTRUCTION, BIDDING, OR PERMIT PURPOSES.

Project Engineer: Karl H. Frank
Professional Engineer License State and Number: Texas No. 48953

Acknowledgments

The authors wish to express their thanks for the guidance from the TxDOT Project Directors Ronnie Medlock, Keith Ramsey and Alan Kowalik, the Project Monitoring Committee, and Peter Forsling of the FHWA for his role as a Project Advisor. Bryce Neuman's help in the fabrication and testing of the specimens is gratefully acknowledged.

Table of Contents

Chapter 1: Introduction....1
1.1 Background....1
1.2 Test Bridge....1
1.3 Goals of Current Research and Outline of Work....4
Chapter 2: Strength of Embedded Shear Studs under Tensile Loading....5
2.1 Introduction....5
2.2 Tensile Strength of Concrete Anchors - ACI 318 Appendix D....5
2.2.1 Overview....5
2.2.2 Steel Failure....7
2.2.3 Concrete Breakout Strength....8
2.2.4 Pullout Strength....11
2.3 Summary....12
Chapter 3: Testing Program....13
3.1 Introduction....13
3.2 Test Specimens....13
3.2.1 Specimen Details....13
3.2.2 Stud Welding....20
3.2.3 Formwork....21
3.2.4 Concrete Mix....22
3.3 Test Setup....22
3.3.1 Loading Arrangement and Test Setup....22
3.3.2 Dynamic Test Setup....24
3.4 Instrumentation....25
3.4.1 Shear Studs....25
3.4.2 Reinforcing Steel....26
3.4.3 Load and Displacement....27
3.5 Testing Procedure....28
3.5.1 Static Testing Procedure....28
3.5.2 Dynamic Testing Procedure....29
Chapter 4: Test Results....31
4.1 General Components....31
4.2 Series I Summary - Five-Inch Studs Spaced Transversely....31
4.3 Series II Results - Five-Inch Studs Spaced Longitudinally....33
4.3.1 Strength....33
4.3.2 Behavior at Failure....35
4.3.3 Shear Stud Gage Data....42
4.3.4 Reinforcing Steel Gage Data....46
4.3.5 Slab Deflection....52
4.3.6 Concrete Cylinder Tests....54
4.4 Series III Results - Taller Studs and Eccentric Loading... 54
4.4.1 Strength....54
4.4.2 Behavior at Failure....56
4.4.3 Shear Stud Gage Data....61
4.4.4 Reinforcing Steel Gage Data....69
4.4.5 Slab Deflection....73
4.4.6 Concrete Cylinder Tests....75
4.5 Series IV Results - Dynamic Loading....76
4.5.1 Strength....76

4.5.2 Behavior at Failure....78
4.5.3 Shear Stud Gage Data....82
4.5.4 Reinforcing Steel Gage Data....87
4.5.5 Slab Strength....90
Chapter 5: Analysis and Discussion of Test Results....93
5.1 Introduction....93
5.2 Evaluation of Tested Shear Stud Details....93
5.2.1 Strength....93
5.2.2 Ductility....107
5.2.3 Efficiency....111
5.2.4 Summary....111
5.3 Proposed Shear Stud Configurations and Modifications to Code Strength Calculations....114
5.3.1 General Comments....114
5.3.2 Code Modifications - Haunch Effect....114
5.3.3 Code Modifications - Transversely Spaced Studs....116
5.3.4 Code Modifications - Longitudinally Spaced Studs....120
5.3.5 Code Modifications - Summary....124
5.3.6 Recommended Additional Testing....126
5.3.7 Summary....127
Chapter 6....129
6.1 Conclusions and Recommendations....129
6.1.1 Summary and Objectives....129
6.1.2 Conclusions....129
6.1.3 Recommendations for Design and Future Work....130
Appendix A: Selected Tensile Strength Calculations using ACI Appendix D Existing Provisions and Proposed Modifications....131
Appendix B: Complete Test Specimen Details....145
References....151

List of Figures

Figure 1.1: Picture of FSEL Test Bridge 2
Figure 1.2: Schematic of FSEL Test Bridge (Rebar Omitted from Drawing) 2
Figure 1.3: Test Bridge Shear Stud Detail with 3-Haunch, Spaced 22 in On Center 3
Figure 2.1: Geometry of 7/8-in Diameter by 5-in Tall Test Studs 6
Figure 2.2: Tensile Failure Modes of Shear Studs (ACI 318-08) 7
Figure 2.3: Physical Breakout Failure Cone of (a) a Single Stud (b) Multiple Studs Grouped Together 8
Figure 2.4: CCD Method Assumed Failure Cone and Projected Area. 9
Figure 2.5: Illustration of Edge Effect on Projected Failure Cone Area 11
Figure 2.6: Illustration Showing (a) Assumed Full Depth Edge (b) Actual Partial Depth Edge of Haunch 11
Figure 3.1: Moment Distribution in Test Bridge and Test Specimen 14
Figure 3.2: Longitudinal and Transverse Labeling, Rebar Configuration 15
Figure 3.3: Specimen Nomenclature 16
Figure 3.4: Series I Stud Details, 5-in Studs Spaced Transversely (a), (c), (e) with a Haunch and (b), (d), (f) without a Haunch 18
Figure 3.5: Series II Stud Details, 5-in Studs Spaced Longitudinally (a), (d), (f) with a Haunch and (b), (c), (e), (g) without a Haunch 19
Figure 3.6: Series III Stud Details, 7-in and 9-in Studs Spaced (a), (c), (e) Transversely and (b), (d), (f) Longitudinally 20
Figure 3.7: (a) Stud Welding (b) Bend Over Test 21
Figure 3.8: Formwork for Specimens with a (a) Haunch (b) 3-in Haunch 22
Figure 3.9: Basic Test Configuration, Static and Dynamic 23
Figure 3.10: Connector Plates for (a) Standard Loading (b) Eccentric Loading 23
Figure 3.11: Dynamic Test Setup Showing Hydraulics 25
Figure 3.12: Shear Stud Gages (a) Installation (b) Shear Stud after Gage Installation (c) Drawing of Typical Stud Gage Placement 26
Figure 3.13: Strain Gages on Reinforcing Bars 27
Figure 3.14: Labeling Scheme of Gages (a) in Studs and (b) on Reinforcing Steel 27
Figure 3.15: Linear Pot Installation 28
Figure 3.16: Load Cell Attachment to Ram and Specimen 28
Figure 3.17: Overall Test Setup 29
Figure 4.1: Failure Cone (a) Around Stud (b) Cone Void in Slab 32
Figure 4.2: Normalized Peak Strength vs. Number of Studs for 5-in Studs Spaced Transversely 32
Figure 4.3: Series I Failures (a) Splitting of Haunch (b) Separation of Haunch 33
Figure 4.4: Normalized Peak Strength vs. Number of Studs for 5-in Studs Spaced Longitudinally 34
Figure 4.5: Group Effect in Concrete Failure Cone 35
Figure 4.6: Applied Load vs. Average Stud Pullout for 3-in Haunch Specimens 36
Figure 4.7: Haunch Specimen (a) Flexural Cracks (b) Cracking at Peak Load (c) Separated Haunch 37
Figure 4.8: Load-Deflection Plot for Specimen 5:3-3La 38
Figure 4.9: Specimen 5:3-3La (a) Pullout Engaging Bottom Rebar (b) Schematic Showing Rebar-Stud Interlock 38
Figure 4.10: Load-Deflection Plot for Specimens without a Haunch 39
Figure 4.11: Specimens with No Haunch (a) First Flexural Crack (b) Single Stud Failure Cone 40
Figure 4.12: Longitudinally Spaced Stud Specimen Cracking (a) Horizontal Crack Formation (b) Horizontal Crack Growth(c) Side Cracking and Separation from the Interior Failure Cone 41
Figure 4.13: Displacement Gradient of WT with Concentric Loading 42
Figure 4.14: Forces and Friction Transfer on a Shear Stud 43

Figure 4.15: Applied Force vs. Stud Force, Two Studs No Haunch 44
Figure 4.16: Applied Force vs. Stud Force, Three Studs No Haunch Specimens 44
Figure 4.17: Applied Force vs. Stud Force, Four Studs No Haunch Specimens 45
Figure 4.18: Applied Force vs. Stud Force, Three Studs 3-in Haunch Specimens 46
Figure 4.19: Slab (a) Strain and (b) Stress at First Yield 47
Figure 4.20: Slab (a) Strain and (b) Stress at Ultimate Moment 48
Figure 4.21: Applied Load vs. Rebar Strain for 3-in Haunch Specimens 50
Figure 4.22: Applied Load vs. Rebar Strain for No-Haunch Specimens with One Stud 51
Figure 4.23: Applied Load vs. Rebar Strain for No-Haunch Specimens with Two or More Studs 51
Figure 4.24: Applied Load vs. Slab Deflection for Series II Specimens 52
Figure 4.25: Applied Load vs. Slab Deflection for Specimen 5:0-4Lb 53
Figure 4.26: Specimen Showing Significant Arching 53
Figure 4.27: Normalized Peak Strength vs. Number of Studs for Series III Specimens 55
Figure 4.28: Load-Deflection Plots for Specimens with Tall Studs Spaced Transversely 57
Figure 4.29: Failure Sequence for 7-in Studs Spaced Transversely (a) Horizontal Crack Formation (b) Haunch Splitting (c) Split Haunch with Failure Cone 57
Figure 4.30: Failure Sequence for 9-in Studs Spaced Transversely (a) Horizontal Crack forming Concrete Ridge (b) Rebar Supporting WT 58
Figure 4.31: Load-Deflection Plots for Specimens Tall Studs Spaced Longitudinally 59
Figure 4.32: Load-Deflection Plots for Specimens Loaded Eccentrically 60
Figure 4.33: Failure Sequence for No-Haunch Specimen Loaded Eccentrically (a) Horizontal Crack Formation (b) WT and Failure Cone Rotation (c) Back Side Hinge Crack 61
Figure 4.34: Applied Force vs. Stud Force, Specimen 9:3-1 62
Figure 4.35: Applied Force vs. Stud Force, Two Studs Spaced Transversely 63
Figure 4.36: Applied Force vs. Stud Force, Three Studs Spaced Transversely 64
Figure 4.37: Applied Force vs. Stud Force, Two Studs Spaced Longitudinally 65
Figure 4.38: Applied Force vs. Stud Force, Three Studs Spaced Longitudinally 66
Figure 4.39: Schematic of Prying Forces in an Eccentrically Loaded Stud 67
Figure 4.40(a): Applied Force vs. Stud Force, Specimen 5:3-3LE 67
Figure 4.40(b): Applied Force vs. Stud Force, Specimen 5:0-3LE 68
Figure 4.41: Error in Applied Moment compared to Stud Moment for Eccentrically Loaded Specimens 69
Figure 4.42: Applied Load vs. Rebar Strain for Specimens with Tall Studs Spaced Transversely 70
Figure 4.43: Applied Load vs. Rebar Strain for Specimens with Tall Studs Spaced Longitudinally (a) With Two Studs (b) with Three Studs 71
Figure 4.44: Applied Load vs. Rebar Strain for Eccentrically Loaded Specimens (a) without a Haunch (b) with a 3-in Haunch 73
Figure 4.45(a): Applied Load vs. Slab Deflection for Specimens with Brittle Haunch Failure 75
Figure 4.45(b): Applied Load vs. Slab Deflection for Specimens with Ductile Stud Pullout 75
Figure 4.46: Dynamic Strength Factor vs. Number of Studs for Series IV Specimens 77
Figure 4.47: Load-Deflection Plots for 3-in Haunch Specimens Loaded Dynamically 79
Figure 4.48: Dynamic Specimens with a Haunch (a) Fractured Haunch with Multiple Pieces (b) Connected Haunch Segment Showing 45-Degree Failure Angle 80
Figure 4.49: Failure of Specimen 5:3-3LDa 80
Figure 4.50: Load-Deflection Plots for No-Haunch Specimens Loaded Dynamically 81
Figure 4.51: Failure of Dynamic Specimens 5:0-3LD (a) Cracking Patterns (b) Fractured Failure Cone 81
Figure 4.52: Applied Force vs. Stud Force, Specimens 5:3-1D 83
Figure 4.53: Applied Force vs. Stud Force, Specimens 5:3-3LD 84
Figure 4.54: Applied Force vs. Stud Force, Specimens 5:3-3TD 84
Figure 4.55: Applied Force vs. Stud Force, Specimens 5:0-1D 85

Figure 4.56: Applied Force vs. Stud Force, Specimens 5:0-3LD 86
Figure 4.57: Applied Force vs. Stud Force, Specimens 5:0-3TD 86
Figure 4.58: Applied Load vs. Rebar Strain Dynamically Loaded Haunch Specimens (a) with Studs Spaced Transversely (b) with Studs Spaced Longitudinally 88
Figure 4.59: Applied Load vs. Rebar Strain Dynamically Loaded No-Haunch Specimens with (a) Studs Spaced Transversely (b) Studs Spaced Longitudinally 90
Figure 5.1: Dimensioned Projected Failure Cone Areas for (a) 1 Stud (b) 3 Studs Spaced Transversely (c) 3 Studs Spaced Longitudinally, all without a Haunch 96
Figure 5.2: Dimensioned Projected Failure Cone Areas for (a) 3 Studs Spaced Transversely and (b) 3 Studs Spaced Longitudinally, both in a Haunch 97
Figure 5.3: Measured and Predicted Strengths of 5-in Tall Studs Loaded Statically 99
Figure 5.4: Code (Dashed) and Observed (Solid) Failure Cones with Pictures for (a) Single Studs without A Haunch (b) Multiple Studs without a Haunch 100
Figure 5.5: Code (Dashed) and Observed (Solid) Failure Cones with Picture for Studs Spaced Transversely in a Haunch 101
Figure 5.6: Methods of Dealing with Haunch Effect on Failure Cone Area (a) Full Height Action (b) Confined Haunch Action (c) Real Failure Cone 101
Figure 5.7: Code (Dashed) and Observed (Solid) Failure Cones with Picture for Studs Spaced Longitudinally without a Haunch 102
Figure 5.8: Code (Dashed) and Observed (Solid) Failure Cones with Picture for Studs Spaced Longitudinally with a Haunch 102
Figure 5.9: Measured and Predicted Strengths of Dynamically Loaded 5-in Studs Spaced 103
Figure 5.10: Measured and Predicted Strengths of 7-in and 9-in Tall Studs Spaced 104
Figure 5.11: Code (Dashed) and Observed (Solid) Failure Cones for Studs Spaced Longitudinally (a) 7 in Tall (b) 9 in Tall (c) Picture of Failure Cone 105
Figure 5.12: Code (Dashed) and Observed (Solid) Failure Cones with Pictures for Studs Spaced Transversely (a) 7 in Tall (b) 9 in Tall 106
Figure 5.13: Failure Cone of a Stud Spaced Transversely, Showing Rebar near the edge of the Failure Surface 108
Figure 5.14: Failure Cone of 7-in Studs Spaced Longitudinally Enclosing Bottom Mat Reinforcement 109
Figure 5.15: Measured and WT-Rotation-Predicted Load-Displacement Plots for Specimen 5:0-3LE 110
Figure 5.16: Failure Measured and WT-Rotation-Predicted Load-Displacement Plots for Specimen 5:3-3LE 110
Figure 5.17: Flowchart Showing Possible Configuration Options and their Strength and Ductility Behavior 113
Figure 5.18: Pictorial Definition of Terms for Effective Stud Height Term 115
Figure 5.19: Code (Dashed) and Proposed Modified (Solid) Failure Cones for 9 in. Studs (Configurations Not Pictured had no Change in Cone Projected Area) 116
Figure 5.20: Comparison of Modified Code Strengths to Measured Strengths for Statically Loaded Studs Spaced Transversely 118
Figure 5.21: Comparison of Modified Code Strengths to Measured Strengths for Dynamically Loaded Studs Spaced Transversely 119
Figure 5.22: Comparison of Modified Code Strengths to Measured Strengths for Taller Studs Spaced Transversely 119
Figure 5.23: Comparison of Modified Code Strengths to Measured Strengths for Statically Loaded Studs Spaced Longitudinally 122
Figure 5.24: Comparison of Modified Code Strengths to Measured Strengths for Dynamically Loaded Studs Spaced Longitudinally 123
Figure 5.25: Comparison of Modified Code Strengths to Measured Strengths for Taller Studs Spaced Longitudinally 123

Figure A.1: Code (Green) and Proposed (Purple) Projected Failure Cone Areas for 5:0-1 131
Figure A.2: Code (Green) and Proposed (Purple) Projected Failure Cone Areas for 5:3-1 132
Figure A.3: Code (Green) and Proposed (Purple) Projected Failure Cone Areas for 5:3-3T 133
Figure A.4: Code (Green) and Proposed (Purple) Projected Failure Cone Areas for 5:0-3L 135
Figure A.5: Code (Green) and Proposed (Purple) Projected Failure Cone Areas for 5:3-3L 137
Figure A.6: Code (Green) and Proposed (Purple) Projected Failure Cone Areas for 9:3-3T 138
Figure A.7: Code (Green) and Proposed (Purple) Projected Failure Cone Areas for 9:3-3L 140
Figure A.8: Code (Green) and Proposed (Purple) Projected Failure Cone Areas for 5:3-3LE 142
Figure B.1: Standard Specimen Slab Details 145
Figure B.2: Shear Studs Details, 5-in Studs Spaced Transversely 146
Figure B.3: Shear Studs Details, 5-in Studs Spaced Longitudinally 147
Figure B.4: Shear Studs Details, 7-in Studs 148
Figure B.5: Shear Studs Details, 9-in Studs 149

List of Tables

Table 4.1 Peak Strengths of Specimens with 5-in Studs Spaced Transversely....31
Table 4.2: Peak Strengths of Specimens with 5-in Studs Spaced Longitudinally....34
Table 4.3: Series II Specimens, No Haunch, Comparison of Stud and Applied Forces....43
Table 4.4: Series II Specimens, 3-in Haunch, Comparison of Stud and Applied Forces....45
Table 4.5: Series II Slab Critical Loads....49
Table 4.6: Series II Concrete Test Data....54
Table 4.7: Peak Strengths of Series III Specimens....54
Table 4.8: Peak Strengths of Specimens with Three 5-in Studs Spaced Longitudinally....56
Table 4.9: Series III Specimen with Studs Spaced Transversely, Comparison of Stud and Applied Forces....62
Table 4.10: Series III Specimens with Studs Spaced Longitudinally, Comparison of Stud and Applied Forces....65
Table 4.11: Series III Slab Critical Loads....69
Table 4.12: Series III Concrete Test Data....76
Table 4.13: Peak Strengths and Dynamic Strength Factors for Series IV Specimens....76
Table 4.14: Strain Rates and Dynamic Strength Factors for Series IV Specimens....78
Table 4.15: Series IV Specimens, 3-in Haunch, Comparison of Stud and Applied Forces....83
Table 4.16: Series IV Specimens, No Haunch, Comparison of Stud and Applied Forces....85
Table 4.17: Series IV Slab Critical Loads....87
Table 4.18: Series IV Concrete Test Data....91
Table 5.1: Values used to Calculate ACI 318, Appendix D Specimen Strength....95
Table 5.2: Comparison of Code Predicted and Measured Strengths....98
Table 5.3: Values used to calculate Eccentrically Loaded Specimen Strength....107
Table 5.4: Comparison of Code-Predicted and Measured Strengths for Eccentrically Loaded Specimens....107
Table 5.5: Comparative Ranking of Major Stud Configurations....114
Table 5.6: Measured Strength to Haunch-Height-Modified Strength Ratios for Studs Spaced Transversely....117
Table 5.7: Values of the Group Effect Modification Factor for Studs Spaced Transversely....117
Table 5.8: Comparison of Modified Code Strengths to Original Code and Measured Strengths for Studs Spaced Transversely....118
Table 5.9: Measured Strength to Haunch-Height-Modified Strength Ratios for Studs Spaced Longitudinally....121
Table 5.10: Values of the Group Effect Modification Factor for Studs Spaced Longitudinally....121
Table 5.11: Comparison of Modified Code Strengths to Original Code and Measured Strengths for Studs Spaced Longitudinally....122
Table 5.12: Comparison of Modified Code Strengths to Measured Strengths for Eccentrically Loaded Specimens....124
Table 5.13: Predicted-to-Measured Strength Ratios for Code and Modified Strengths of all Test Specimens....124

Chapter 1: Introduction

1.1 Background

The ability of a twin girder bridge to maintain its structural integrity after the facture of one of the girders depends upon the ability of the bridge system to redistribute the load carried by the fractured girder to the other intact girder. The element connecting the girders is the concrete bridge deck. The deck must have sufficient moment and shear capacity to transmit the load from the damaged girder to the intact girder. The calculation of the moment and shear capacity of the deck slab is relatively straightforward and can be done using conventional reinforced concrete design principles. An initial evaluation of the post fracture behavior of a twin trapezoidal box girder bridge, later tested as part of this research project, revealed the shear and flexural strength of the deck was adequate to transfer the load between the girders. Though the bridge deck strength was sufficient for transferring loads, the tensile capacity of the shear studs connecting the girder to the deck was found to control the response (Sutton, 2007). The shear studs used to connect the deck and girder are designed to transmit the horizontal shear force between the two elements to provide flexural conformance. They tensile strength of the connection is not considered in the design of the shear studs. The research presented in this report was undertaken to examine the tensile strength of the connection and to develop predictive equations of the connection strength.

1.2 Test Bridge

In an effort to examine the redundancy of facture critical bridge systems in a controlled setting, the Texas Department of Transportation (TxDOT) sponsored an investigation with the Phil M. Ferguson Structural Engineering Laboratory (FSEL) at the University of Texas at Austin. Because TxDOT has many twin box girder bridges across Texas, they opted to examine this design for the research. Twin box girder bridges, with only two girders in each span, are classified as fracture critical bridges because a fracture in a lower tension flange of one box girder has the ability to propagate through the entire section, severing the girder and leaving the remaining girder to support the entire bridge. In the case of twin box girder bridges, the fracture inspection requires the inspectors to examine the inside of the girder, a very difficult task. TxDOT was retiring a twin box girder bridge on Interstate 10 in Houston. A 120-ft span of the bridge was removed and shipped to FSEL for use in a full-scale fracture test. Figure 1.1 shows the test bridge in place at the laboratory. Figure 1.2 is a drawing of the cross-section of the bridge, including its deck slab and barrier rails. The bridge was erected as a statically determinate simple span so that the loss in moment capacity of a fractured girder would form a collapse mechanism. The bridge was instrumented so that the load transfer from the fractured to the intact girder could be observed during a fracture event.

Figure 1.1: Picture of FSEL Test Bridge

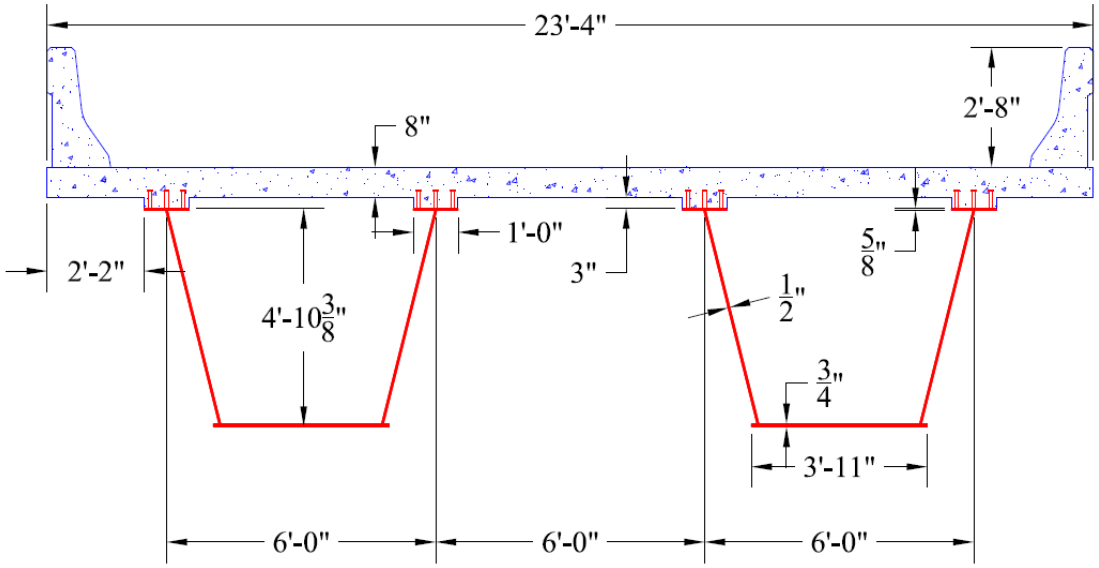

Figure 1.2: Schematic of FSEL Test Bridge
(Rebar Omitted from Drawing)

The load transfer path was of critical interest for the test; if the strength of the individual elements in the load path could be evaluated, it would be possible to determine by simple analysis if the bridge had sufficient redundant strength to support itself under facture and post-fracture loads. Sutton (2007) examined this load transfer path in detail for the bridge with a full-depth fracture in one girder. It was assumed that the fractured girder would be supported by the unfractured girder with the load transferred through the bridge deck. This load path has three elements: the unfractured girder, the bridge deck slab between girders, and the shear studs connecting the fractured girder to the bridge deck slab. Each element's strength had to be evaluated to determine the overall load path strength. The first element, the unfractured bridge girder, had to be checked to ensure it had sufficient plastic moment capacity to support

the entire bridge load. The second element, the bridge deck slab, had to be checked to ensure that it had enough moment and shear capacity to support the load and self weight of the fractured girder. The third element, the shear studs, had to be able to develop sufficient tensile strength to transfer the load from the fractured girder to the intact girder. After fracture, the fractured girder would hang from the slab, loading the shear studs in tension. Determining the forces carried by these three elements during a fracture event and comparing these values against calculated strengths was a key goal of the fracture test.

Calculation of the strengths for the shear and moment capacity of the deck was straightforward using traditional reinforced concrete design procedures. However, calculation of the shear stud tensile strength was complicated by the presence of the haunch around the studs. The haunch is a thickened portion of slab over the top flange of the girders. A haunch is used to maintain the distance between the top of the web and bottom of the bridge deck when the flange thickness is reduced. The haunch and shear stud detail for the test bridge are shown in Figure 1.3. The haunch depth of 3 inches is the largest allowed in Texas. The American Concrete Institute specification, ACI 318, has in its Appendix D a method for calculating the tensile strength of headed shear studs embedded in concrete, but it does not have provisions to address the presence of a haunch. Further, based on the initial stud strength predicted by the ACI code equations, 87% of the shear studs on the fractured girder were needed to support the load, which required that the shear stud connection detail have sufficient ductility to allow for nearly all of the studs to mobilize their full strength (Sutton, 2007). If the connections behaved in a brittle manner, then it was possible the first group of studs near the fracture would fail before the rest of the studs could be mobilized, transferring their load back to the next group of studs, which would also be overloaded. This action would result in an 'unbuttoning' of the fractured girder from the deck for part or all of its length. Given the importance and uncertainty surrounding the shear stud connection detail, a series of full-size laboratory tests were performed to determine the stud connection's strength and ductility.

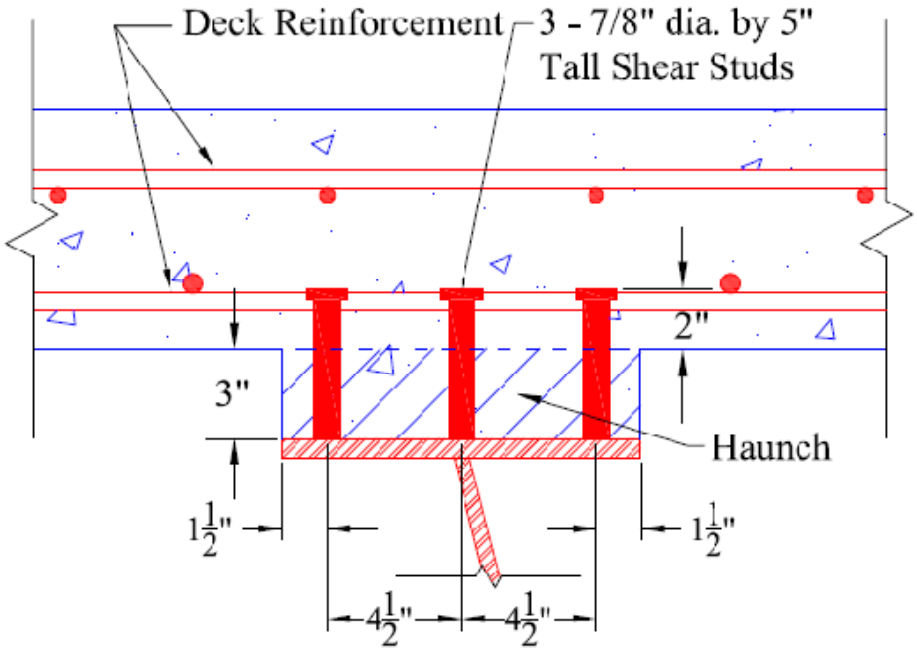

Figure 1.3: Test Bridge Shear Stud Detail with 3-in Haunch, Spaced 22 in On Center

1.3 Goals of Current Research and Outline of Work

The initial phase of the study was to determine the tensile strength of the stud detail used in the test bridge and the effect of the haunch upon the strength and ductility of the connection (Sutton, 2007). After these initial tests, the research was expanded to other shear stud configurations that might have both greater strength and ductility than current configurations. The results of the early work by Sutton are summarized, and the details of the follow-up tests are presented in this report. Also, a method of prediction for the strengths of both current and new stud details is provided. Additional aims are to examine shear stud behavior under other loading conditions, including the effects of eccentric loading and dynamic loading on the strength and the ductility of the connection. New shear stud details are compared to one another as well as the existing details, and an overview of new recommended shear stud connection details is presented.

A common means for evaluating the tensile strength of shear studs is given in ACI 318, Appendix D, which will be the basis of prediction for stud strengths used in this report. The relevant portions of Appendix D that help explain stud tensile behavior are summarized in Chapter 2. The test series and specimens, their configuration and instrumentation, as well as the testing procedure, are covered in Chapter 3. The data from the tests, as well as comments on individual specimen behavior, are presented in Chapter 4. Chapter 5 includes a comparison of the strengths and ductilities of the different stud configurations and has details that are most desirable for achieving good strength and ductility. Chapter 5 also includes proposed modifications to ACI 318, Appendix D to predict the tensile strength of shear stud details for bridge decks in a more accurate manner than current guidelines provide. Chapter 6 gives a concise summary of the results of the research, as well as recommended additional investigations.

Chapter 2: Strength of Embedded Shear Studs under Tensile Loading

2.1 Introduction

The tensile strength of shear studs embedded in a concrete deck slab were evaluated using the provisions of ACI 318, Appendix D. The provisions of Appendix D are broad in scope, covering cast-in-place and post-installed anchorages to concrete, both individually and in groups, under a combination of tension and shear. Headed shear studs fall under the classification of cast-in-place anchors and will be the focus of the information presented in this chapter. In addition to providing predictive strength equations, ACI 38, Appendix D explains the behavior of shear studs under tensile loads, illustrating each of the possible failure mechanisms and the factors that influence each mechanism.

In both the analysis and the testing considered in this research, only tensile loading is considered. While shear can interact with and potentially reduce the tensile strength of studs, this research only focuses on the characterization of the tensile behavior. Typically, shear at the location of highest positive bending in a girder (where fracture is likely to occur) is small, and the shear demand on the studs is negligible. Strengths based on ACI 318, Appendix D are used in comparison to measured connection strengths throughout this work, and improved prediction methods recommended in Chapter 5 are modifications of this section of the ACI code.

2.2 Tensile Strength of Concrete Anchors — ACI 318 Appendix D

2.2.1 Overview

ACI 318, Appendix D is intended to cover the tensile and shear strengths of anchors embedded in concrete, including headed shear stud behavior, which is most typically found in anchoring weld plates in precast construction. The geometry of headed shear studs is standardized and controlled by the AASHTO/AWS D1.5 Bridge Welding Code, Section 7.3, which includes required minimum yield and tensile strengths. Figure 2.1 illustrates the as-installed dimensions for the 7/8-in diameter studs used in this research, of heights varying from the standard 5-in stud employed in the test bridge (shown) to taller 7-in and 9-in studs. 7-in and 9-in studs have all the same dimensions as the 5-in tall studs with the exception of a 2-in and 4-in increase in shaft length, respectively. Included in the dimensions is the value of the effective stud height to the underside of the head, h_{ef}, which is of significant importance in the strength calculations presented later in this report. Studs are required to have a minimum yield strength of 50 ksi and a minimum tensile strength of 60 ksi.

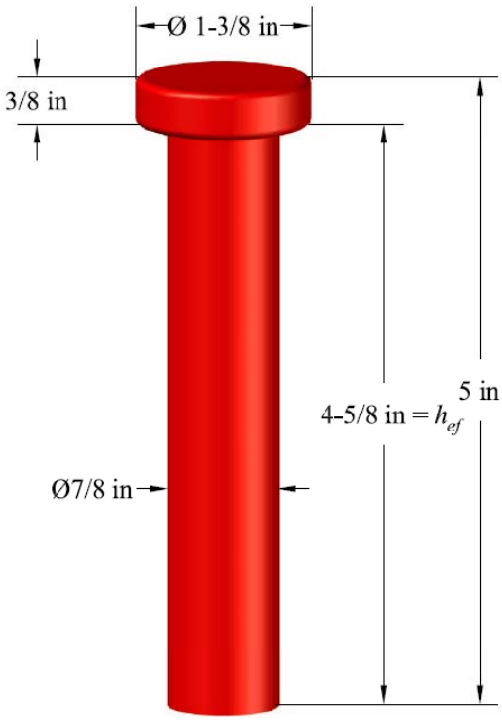

Figure 2.1: Geometry of 7/8-in Diameter by 5-in Tall Test Studs

ACI 318, Appendix D recognizes four failure modes for shear studs loaded in tension, with the minimum capacity mode controlling: (1) steel failure of the studs, (2) concrete breakout of both the studs and the surrounding concrete, (3) pullout of the studs from the concrete, and (4) side face blowout of studs spaced near an edge. Figure 2.2 illustrates these basic failure mechanisms. Of these four modes, only the first three are applicable to the discussion of shear studs embedded in a concrete deck. Because of the presence of the slab in all directions confining the stud head, side face blowout will never govern for this application of tensile loading. Each of the three remaining failure modes is described in detail below.

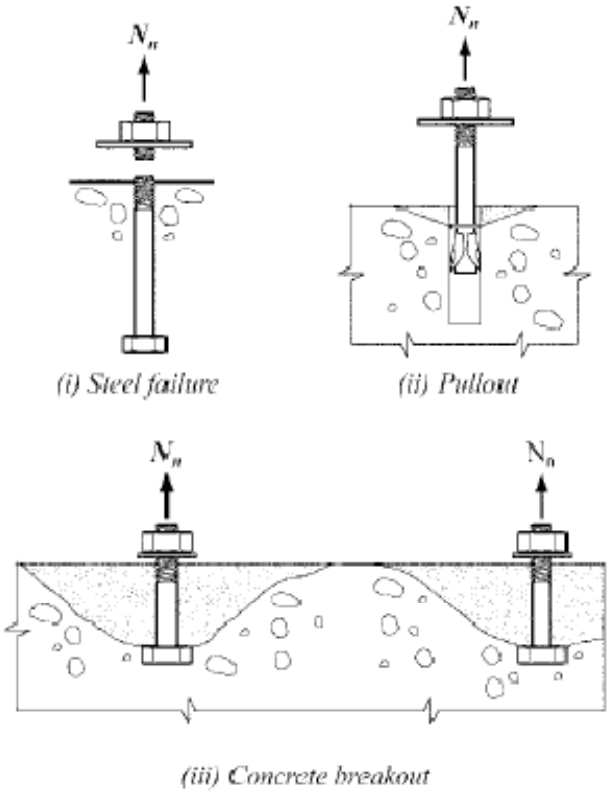

Figure 2.2: Tensile Failure Modes of Shear Studs (ACI 318-08)

While the goal of this research is to characterize the actual tensile strength of shear studs, it is important to note how Appendix D accounts for ductility through the determination of the strength reduction factor, ϕ, as applied to the nominal strength, N_n. The code varies the strength reduction factor based on the type of anchorage used, the loads applied, and the governing mode of failure. It classifies the steel anchor element as brittle or ductile, with ductility being defined by a minimum failure strain and area reduction. For the relatively mild steel used in shear studs, the requirements are satisfied, and the stud can be treated as a ductile steel element with $\phi = 0.75$ if stud failure controls. The strength reduction factor for cast in-place studs subject to tensile loads is $\phi = 0.70$ if pullout controls or if breakout controls and no reinforcement crosses the failure surfaces. The strength reduction factor ϕ is increased to 0.75 if breakout controls and reinforcement is present. This distinction between the presence of reinforcement crossing the failure surfaces in breakout, or if steel strength governs, are the only distinctions the code gives for ductility in the overall connection behavior (with steel failure or breakout with reinforcement being ductile failure modes). No method is provided for explicitly quantifying a connection's ductility.

2.2.2 Steel Failure

The first, and simplest, failure mode to check is that of steel failure. Steel failure is determined by Equation 2.1:

$$N_{sa} = nA_{se}f_{uta} \qquad \text{Equation 2.1 (ACI 318-08)}$$

where: N_{sa} = nominal strength of shear stud connection governed by steel failure (lb)
n= number of studs in a group
A_{se}= effective cross-sectional area of a stud (in^2)

f_{uta}= specified tensile strength of a stud (psi)

For shear studs, the effective cross-sectional area is the area of the circular stud shaft, calculated using the stud diameter. The tensile strength of a stud is used to find the ultimate plastic strength of a connection. The steel strength represents the upper limit on the connection strength because once the steel strength has been reached, no additional changes in the manner of embedment or reinforcing can increase the stud strength. Adding more studs to a connection is the only way to increase the steel failure strength. The stud strength will not control for typical bridge applications.

2.2.3 Concrete Breakout Strength

The second failure mode for shear studs in tension is concrete breakout strength, and it is typically the dominate failure mode for the bridge shear stud connection detail. Breakout occurs when the concrete mobilized by the shear stud head cracks and separates from the main concrete mass of the slab. In plain concrete the cracks are observed to propagate at 45 degrees, and the resulting shape of the breakout cone for a single stud is a 45 degree cone, shown in Figure 2.3(a). When multiple studs are in close proximity to one another, their failure cones overlap and produce a single large failure cone, as shown in Figure 2.3(b).

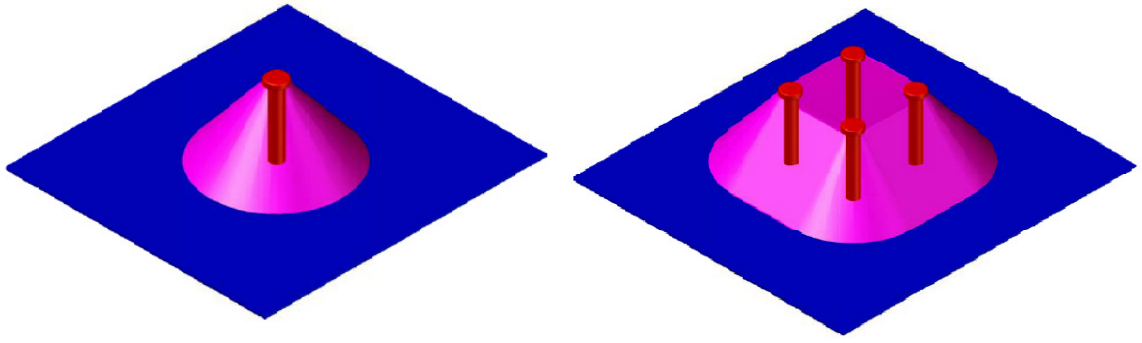

(a) ***(b)***

Figure 2.3: Physical Breakout Failure Cone of (a) a Single Stud (b) Multiple Studs Grouped Together

While the physical failure surface is a cone with a length-to-height ratio of 1:1, the method used by Appendix D is the Concrete Capacity Design (CCD) Method, which models the failure cone as pyramidal and spreading at a ratio of 1.5:1, as pictured in Figure 2.4. This method is used by the ACI Code because it is simple to apply and produces predictions that accurately match test data average strengths (Fuchs, Eligehausen, and Breen, 1995). The CCD method replaced the older method from ACI 349, which assumes a projected conical 45 degree failure cone (Shirvani, Klingner, and Graves, 2004). Sutton investigated the ACI 349 method and found it did not agree with test results of studs in a haunch (Sutton, 2007). This method was not used in this research. The equations of the CCD method, which ACI 318-08 uses to predict breakout strength, are listed below:

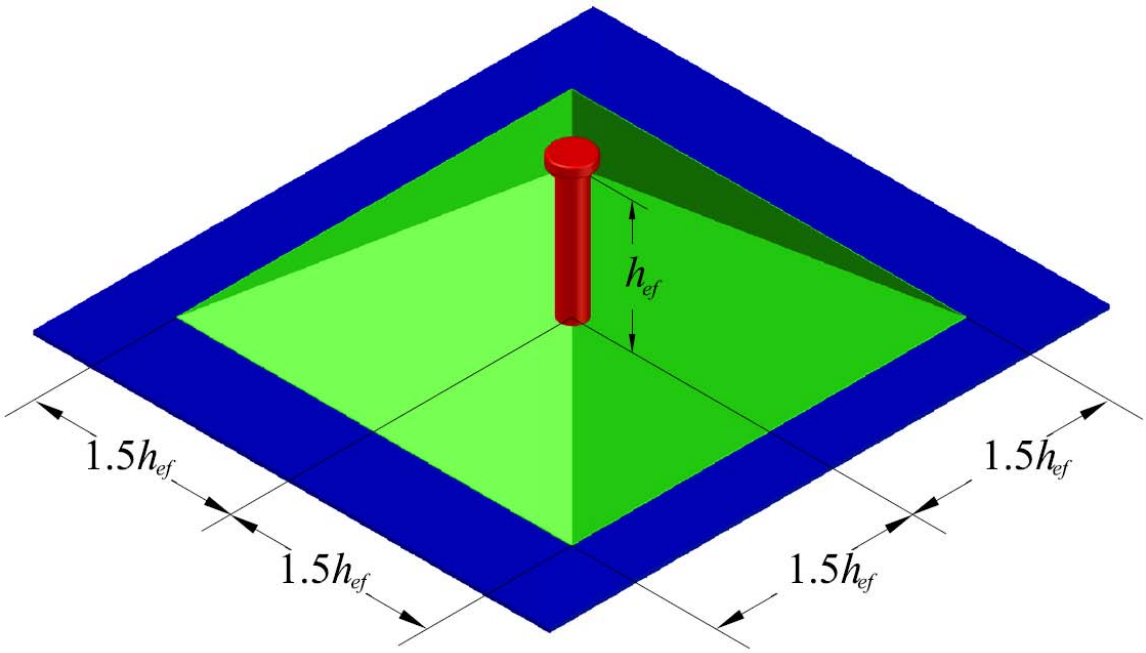

Figure 2.4: CCD Method Assumed Failure Cone and Projected Area

Basic Single Stud Strength:

$$N_b = k_c \sqrt{f_c'} h_{ef}^{1.5}$$ Equation 2.2 (ACI 318-08)

where: N_b = concrete cone breakout strength of a single isolated stud in a continuous piece of cracked concrete (lb)
k_c = 24 for cast-in-place anchors
f_c' = specified compressive strength of concrete (psi)
h_{ef} = effective height of shear stud in concrete (in)

General Breakout Strength:

$$N_{cbg} = \frac{A_{Nc}}{A_{Nco}} \psi_{ec,N} \psi_{ed,N} \psi_{c,N} \psi_{cp,N} N_b$$ Equation 2.3 (ACI 318-08)

where: N_{cbg} = design concrete breakout strength of a stud or group of studs (lb)
A_{Nc} = projected concrete cone failure area of a stud group (in^2)
A_{Nco} = projected concrete cone failure area of a single stud in continuous concrete (= $9h_{ef}^2$) (in^2)
$\psi_{ec,N}$ = eccentric load modification factor
$\psi_{ed,N}$ = edge distance modification factor (when distance is less than $1.5h_{ef}$)
$\psi_{c,N}$ = cracked concrete modification factor
$\psi_{cp,N}$ = post-installed anchor modification factor (=1.0)

N_b = concrete cone breakout strength of a single isolated stud in a continuous piece of cracked concrete (lb)

Because the concrete breakout cone extends from the underside of the stud head, it is the distance from the underside of the head to the base of the stud, the effective stud height, h_{ef}, that governs the size of the failure cone and the breakout strength. For a single stud, because of the pyramidal shape, the projected failure cone area is a square $3h_{ef}$ on a side, for a total area of $9h_{ef}^2$. The group projected failure area is the composite of the individual failure cone areas and takes into account any overlap of intersecting failure cones. The group failure cone area is bounded by any concrete edges present, so close proximity to an edge reduces the area engaged. The ratio of A_{Nc}/A_{Nco} is used in lieu of the number of studs, n, because as the studs become more closely spaced, the failure cones overlap and each cone cannot mobilize its full projected single stud area to contribute to strength.

The modification factors in Equation 2.3 account for several conditions that cover eccentric loading, edge distance, concrete cracking, and post-installed anchor splitting. The eccentric load modification factor, $\psi_{ec,N}$, considers the combination of tension and moment on shear stud connections:

$$\psi_{ec,N} = \frac{1}{\left(1 + \frac{2e'_N}{3h_{ef}}\right)} \leq 1.0 \qquad \text{Equation 2.4 (ACI 318-08)}$$

where: $\psi_{ec,N}$ = eccentric load modification factor
e'_N = eccentricity of resultant stud tensile load
h_{ef} = effective height of shear stud in concrete (in)

The eccentricity of the load is measured from the geometric center of all the studs in a group subjected to tension. For single-stud cases, the eccentric load modification factor is always 1.0.

The edge distance modification factor, in addition to the group projected failure cone area, takes into account the proximity of studs to a concrete edge and the effect this proximity has on stress distributions within the concrete (Fuchs, Eligehausen, and Breen, 1995). Equation 2.5 shows how the factor is calculated:

$$\psi_{ed,N} = 0.7 + 0.3\frac{c_{a,\min}}{1.5h_{ef}} \leq 1.0 \qquad \text{Equation 2.5 (ACI 318-08)}$$

where: $\psi_{ed,N}$ = edge distance modification factor (when distance is less than $1.5h_{ef}$)
$c_{a,min}$ = smallest edge distance measured from center of a stud
shaft to the edge of concrete (in)
h_{ef} = effective height of shear stud in concrete (in)

If the minimum edge distance, $c_{a,min}$, is greater than $1.5h_{ef}$, the failure cone is not limited by the concrete edge, and the modification factor equals 1.0. Figure 2.5 illustrates $c_{a,min}$ and how an edge reduces the projected group failure cone area, A_{Nc}. Of note is that, while the breakout equation has provisions for edges, it assumes these edges extend the full height of the stud. This assumption does not apply for the partial depth edges of a haunch, shown in Figure 2.6, so it is unclear how such an edge should be treated.

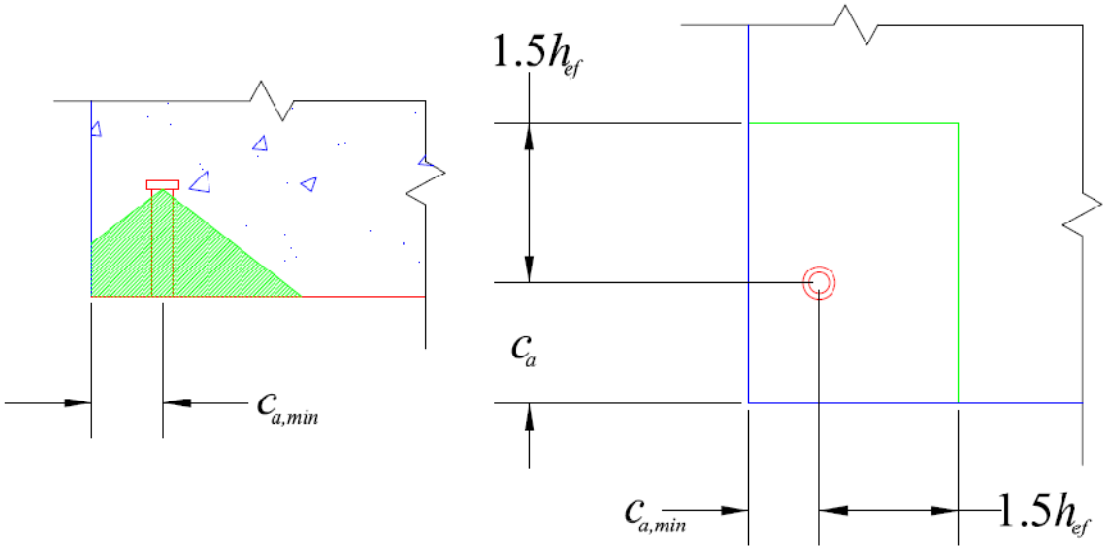

Figure 2.5: Illustration of Edge Effect on Projected Failure Cone Area

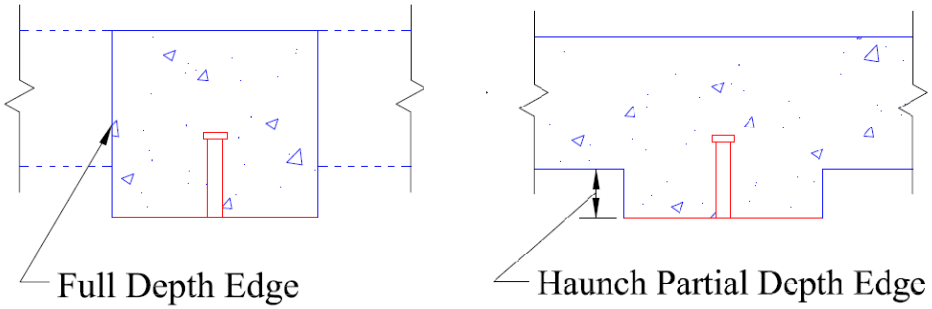

(a) ***(b)***

Figure 2.6: Illustration Showing (a) Assumed Full Depth Edge (b) Actual Partial Depth Edge of Haunch

The cracked concrete modification factor, $\psi_{c,N}$, recognizes the benefit to stud strength when the concrete cone is uncracked prior to breakout. When no cracking is present around the studs before breakout, the factor equals 1.25, otherwise it is equal to 1.0.

The post-installed anchor modification factor takes into account the increased possibility of concrete splitting around post-installed anchors. Because the bridge deck shear studs are cast-in-place, the factor is equal to 1.0.

In summary, concrete breakout strength is based on a number of factors, principally the height of the shear studs, the strength of the concrete, and the spacing of the studs, both to each other and to any free edges. Given that breakout typically controls the strength of the connections of interest in this research, the combinations of these three key factors govern a connection's strength. Chapter 3 includes a discussion of how these factors were varied in each series of tests to examine their effect on concrete tensile strength.

2.2.4 Pullout Strength

Pullout strength differs from breakout strength because, instead of mobilizing a large cone of concrete, it is governed by crushing of the concrete directly under the shear stud head. Once crushing

begins, stiffness of the connection is greatly reduced and rapidly leads to full pullout of the studs from the concrete. Equation 2.6 shows the calculation of shear stud pullout strength for headed shear studs:

$$N_{pn} = 8A_{brg}f_c'\psi_{c,P} \qquad \text{Equation 2.6 (ACI 318-08)}$$

where: N_{pn} = pullout strength of a single stud in tension (lb)
A_{brg} = shear stud head bearing area (in^2)
$\psi_{c,P}$ = pullout cracking modification factor

The concrete crush strength is a function of the concrete compressive strength and the bearing area of the stud head. For all 7/8-in diameter studs, the head bearing area is equal to 0.75 in^2. The cracking modification factor for pullout functions the same way as for breakout, but the value for uncracked concrete is 1.4, while the cracked concrete value is 1.0. Because pullout strength for a given stud diameter is only a function of concrete strength, as a stud gets taller its breakout strength increases, but its pullout strength is constant. This condition makes pullout strength the governing capacity only for tall studs deeply embedded in concrete.

2.3 Summary

ACI 318, Appendix D provides a simple and straightforward means of calculating the tensile strength of a shear stud connection. For tensile loadings, there are three possible failure modes that govern, with concrete breakout being more common than steel or pullout failures. The individual failure modes are governed by concrete strength, diameter and height of the shear studs, the spacing configuration of studs with respect to one another, and the studs' location within a concrete slab. While these equations provide a prediction for strength, they do not provide a means of accounting for the effects of a haunch on the shear stud strength, nor do they provide an explicit means of accounting for ductility. To determine the haunch effect on connection strength as well as to examine how differing stud configurations change connection strength and ductility, a testing regime was developed and is described in Chapter 3. By comparing the test data to the ACI predicted strengths, the effectiveness of the code for predicting shear stud tensile strengths in fracture critical bridges can be determined.

Chapter 3: Testing Program

3.1 Introduction

As reported by Sutton (2007), the presence of a haunch greatly affects the tensile behavior of shear studs embedded in concrete. A haunch and its associated edge effect reduce the strength of grouped shear studs compared to both a single stud in a haunch and to the same number of studs without a haunch. The haunch also reduces the ductility of test specimens. Both high connection strength and ductility are desirable to allow for load redistribution in fracture critical bridges. Accordingly, alternative shear stud connection designs were investigated in search of improved ductility and strength.

Using Sutton's tests as a first series (Series I), three additional series of tests of twelve specimens each were conducted to evaluate the effects of possible alternative stud configurations, including rearranging the shear studs parallel to the girder web (Series II), and increasing the height of the shear studs (Series III). Also, as part of Series III, two tests were performed with the load applied at an eccentricity to create non-uniform displacement of the shear studs. Series IV was conducted by testing the studs under dynamic tensile loading to evaluate changes in connection response due to a sudden load event.

Orienting the studs parallel to the girder web increases the size of the predicted breakout cone and increases the distance from the studs to the concrete edges, both of which should increase the strength of the connection over an equivalent section with the original, perpendicular spacing. Increasing stud height increases the size of the projected failure cone area, increasing strength over shorter studs. Also, increased stud height allows studs in a haunch to engage the reinforcement in the slab, which may provide greater connection ductility. Non-uniform displacement of the specimens is expected to produce lower strengths compared to an equivalent uniformly displaced specimen. Because a fracture event in a girder occurs very rapidly, dynamic tests of previously investigated stud configurations are also examined to see if dynamic loading rates change the ductility or strength behavior of the tested connections.

Experiments were performed similarly to Sutton, with the intent that experiments match both the geometry and loading conditions of the test bridge. When the girder in the test bridge is fractured, it should attempt to drop away from the bridge deck, creating tension in the shear studs and flexure in the slab. However, not all existing stress conditions were captured in the four testing series, as prior to girder fracture shear studs are in shear from composite girder behavior, and no shear was applied during specimen testing.

3.2 Test Specimens

3.2.1 Specimen Details

Four series of twelve specimens each were tested to examine shear stud strength and ductility behavior. Series I examined the behavior of current standard connection details and was conducted and reported by Sutton (2007). The subsequent three series used the same test specimen geometry as Sutton, but they examined variations in stud spacing, height, and loading rate.

As detailed by Sutton, all test specimen geometry was based off of the full-scale bridge test. Spacing between girder webs on the test bridge is 6 ft, and assuming the fractured girder deflects vertically when cut (with little twisting or lateral motion), the slab deck between girders is forced into double curvature, creating maximum moments at the shear studs, as shown in Figure 3.1. Given this geometry and expected behavior, specimens were designed as simply supported with a midspan point load, having a clear span of 6 ft, and 6 in of bearing length on each end, for a total specimen length of 7-ft 0-in. Specimens are 2-ft wide, intending to approximately match the stud group center-to-center spacing of the test bridge, which is 22 in. These dimensions created a group of studs centered in the concrete

specimen, with the span-wise sides of the concrete representing a plane of symmetry with the hypothetical next group of studs and their associated failure cones. Specimens are 8-in thick to match the test bridge slab thickness.

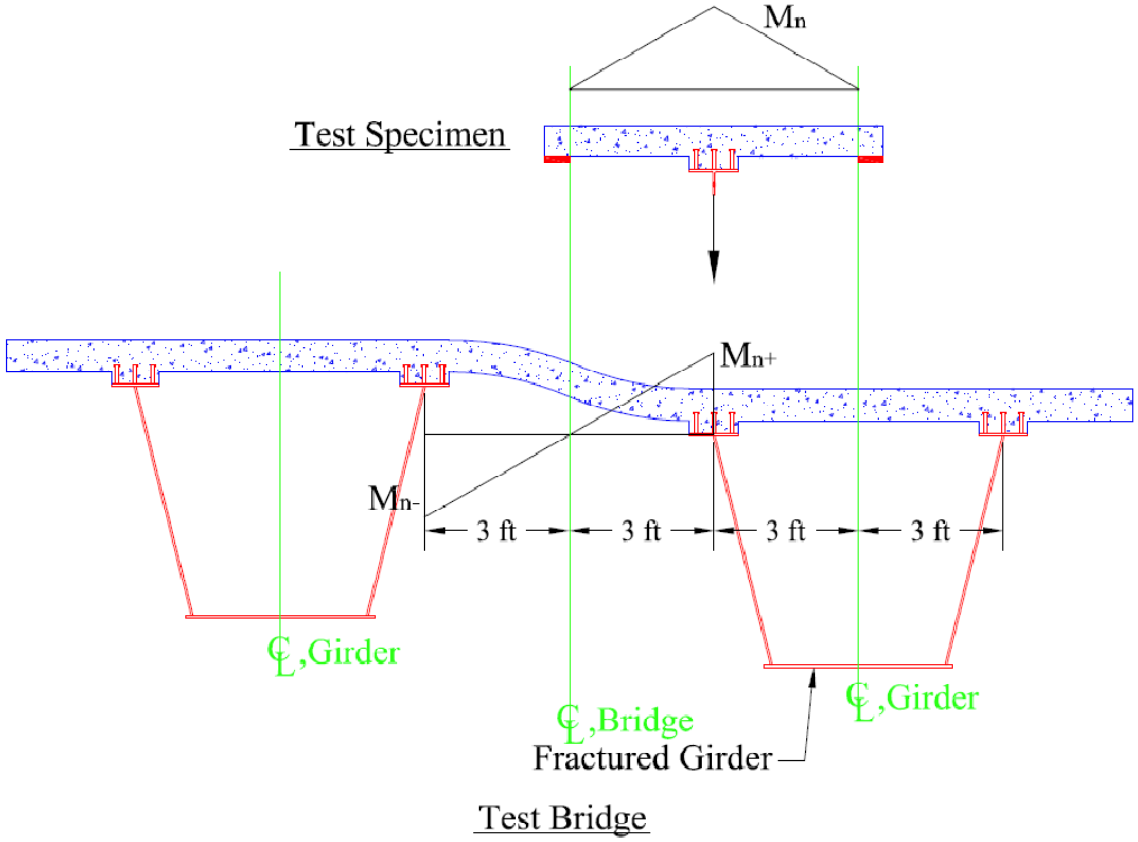

Figure 3.1: Moment Distribution in Test Bridge and Test Specimen

For those specimens with a haunch, a 3-in haunch was used to match the test bridge haunch size. A 3-in haunch is also the deepest haunch permitted by TxDOT and AASHTO standards for a 5-in stud, the most commonly used stud size (AASHTO requires that studs extend a minimum of 2 in above the top of a haunch). Rebar size and spacing in the specimens also matched the configuration found in the test bridge and TxDOT details. In order to remain consistent with the test bridge, the same configuration terminology is used: the span direction of the specimen is perpendicular to the girder web and long axis of the test bridge and is thus called the *transverse direction*. The short dimension of the specimen is parallel to the bridge long axis and is referred to as the *longitudinal direction* (see Figure 3.2 for illustration of terms and rebar layout). In the specimens, all transverse reinforcing bars, as well as the bottom mat longitudinal bars, were #5 rebar, while the top mat longitudinal bars were #4 rebar. Clear cover under the bottom mat was 1-1/4 in, while the clear cover over the top mat was 2 in. Clear cover on all sides to the nearest bar was 1-1/2 in. According to TxDOT standard details, the transverse rebar was spaced 6 in on center, with both mats of reinforcing having the same bar locations. The longitudinal bars were spaced 9 in on center, with top and bottom mats staggered 4-1/2 in.

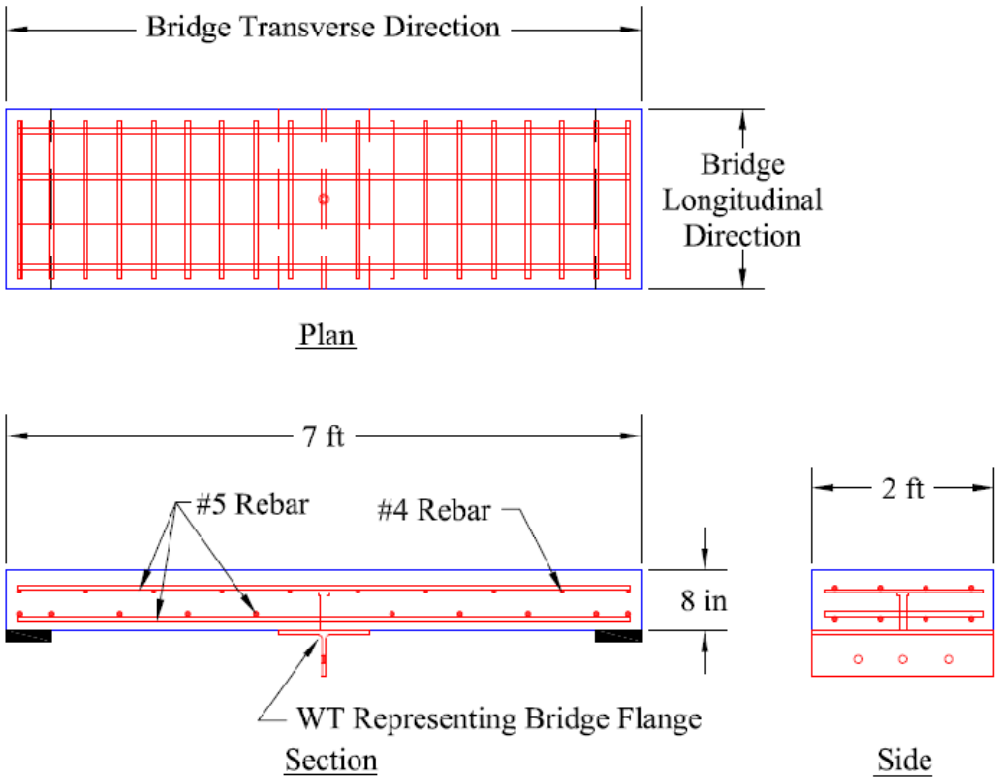

Figure 3.2: Longitudinal and Transverse Labeling, Rebar Configuration

A WT 6×39.5 was used in the specimens to represent the top flange and web of the girder from the test bridge. This WT shape has similar web thickness (1/2 in), top flange thickness (3/4 in), and width (12 in), as the test bridge girder.

Shear studs used in the specimens were standard 7/8-in diameter headed shear studs with head dimensions of 1-3/8-in diameter by 3/8-in thickness. All studs, with the exception of those in Series III, had an installed height of 5 in. Studs in Series III had installed heights of 5-1/4 in, 7-1/4 in, and 9-1/4 in depending on the specimen (the extra 1/4 in is explained in Section 3.2.2). Studs were welded to the flange of the WT in the given test configurations, as summarized in Table 3.1. The nomenclature of the specimens is explained in Figure 3.3.

Table 3.1: Test Series Configurations

Series, Test Speed	Specimen Number	Stud height, in	Haunch Size, in	Number of Studs	Stud Orientation
Series I	5:0-1a,b	5.0	0.0	1	
Static	5:0-2Ta,b	5.0	0.0	2	Transverse
	5:0-3Ta,b	5.0	0.0	3	Transverse
	5:3-1a,b	5.0	3.0	1	Transverse
	5:3-2Ta,b	5.0	3.0	2	Transverse
	5:3-3Ta,b	5.0	3.0	3	Transverse
Series II	5:0-1a,b	5.0	0.0	1	
Static	5:0-2La,b	5.0	0.0	2	Longitudinal
	5:0-3La,b	5.0	0.0	3	Longitudinal
	5:0-4La,b	5.0	0.0	4	Longitudinal
	5:3-2La,b	5.0	3.0	2	Longitudinal
	5:3-3La,b	5.0	3.0	3	Longitudinal
Series III	7:3-1	7.25	3.0	1	
Static	7:3-2L	7.25	3.0	2	Longitudinal
	7:3-3L	7.25	3.0	3	Longitudinal
	7:3-2T	7.25	3.0	2	Transverse
	7:3-3T	7.25	3.0	3	Transverse
	9:3-1	9.25	3.0	1	
	9:3-2L	9.25	3.0	2	Longitudinal
	9:3-3L	9.25	3.0	3	Longitudinal
	9:3-2T	9.25	3.0	2	Transverse
	9:3-3T	9.25	3.0	3	Transverse
	5:0-3LE	5.25	0.0	3	Longitudinal
	5:3-3LE	5.25	3.0	3	Longitudinal
Series IV	5:0-1Da,b	5.0	0.0	1	
Dynamic	5:0-3LDa,b	5.0	0.0	3	Longitudinal
	5:0-3TDa,b	5.0	0.0	3	Transverse
	5:3-1Da,b	5.0	3.0	1	
	5:3-3LDa,b	5.0	3.0	3	Longitudinal
	5:3-3TDa,b	5.0	3.0	3	Transverse

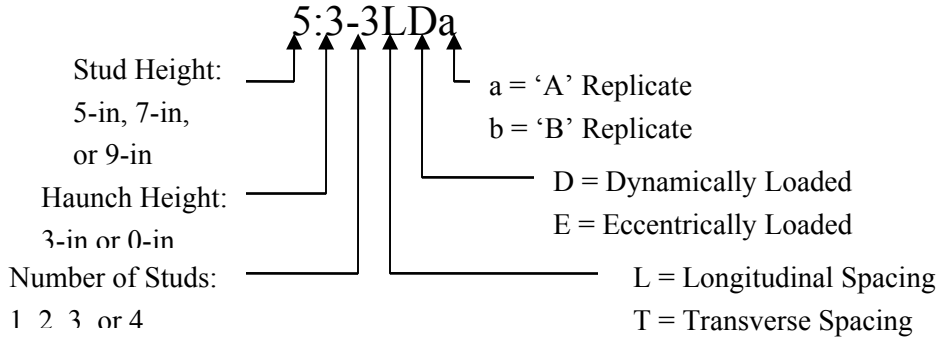

Figure 3.3: Specimen Nomenclature

For Series I, transverse spacings were tested as shown in Figure 3.4. A single stud was welded over the WT web, centered in the specimen. Two studs were welded equally spaced, with 4 in from edge-of-flange to center of each stud and 4 in center-to-center between studs. Both studs were centered

longitudinally in the specimen. For three studs, TxDOT details required a minimum of 2 in from edge-of-flange to center of first stud, making the center-to-center stud distance 4 in. Again, all studs were centered longitudinally.

Series II tests utilized longitudinal spacings, with all studs centered transversely (Figure 3.5). Studs were equally spaced down the WT, with one stud centered at 24 in (12 in from each edge of the specimen), two at 12 in, three at 8 in, and four at 6 in center-to-center. Closer spacings are prohibited by AASHTO provisions on minimum spacing (6 times the stud diameter or 5-1/4 in for 7/8-in diameter studs). Series III used the same transverse and longitudinal configurations as Series I and II but with longer studs that are 7 in and 9 in tall (Figure 3.6). Series IV utilizes 5-in studs with the same geometries as in Series I and II.

Figures 3.4-3.6 illustrate the stud configurations for each test series. For transverse spacings (Figure 3.4), the detail shows the midspan of the specimen with haunch details, if present. For longitudinal spacings (Figure 3.5), the detail shows the end view of the specimen with studs spaced over the web. For taller studs (Figure 3.6), the same views for longitudinal and transverse spacings are used as before, and both stud heights are illustrated in the details. In Figure 3.6, 7-in studs are shown in red and 9-in studs are shown in green (9-in studs have filled-in heads).

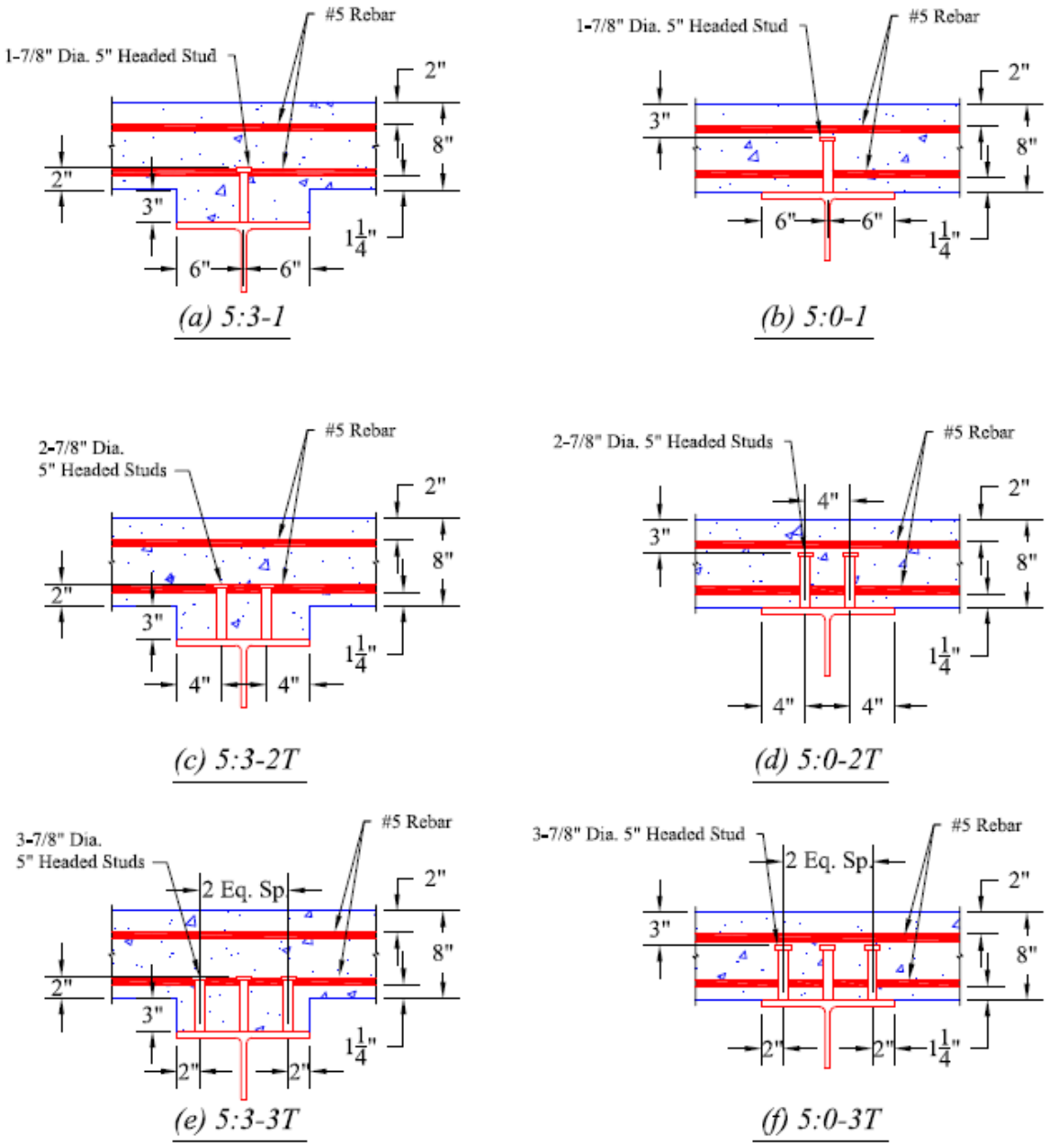

Figure 3.4: Series I Stud Details, 5-in Studs Spaced Transversely (a),(c),(e) with a Haunch and (b),(d),(f) without a Haunch

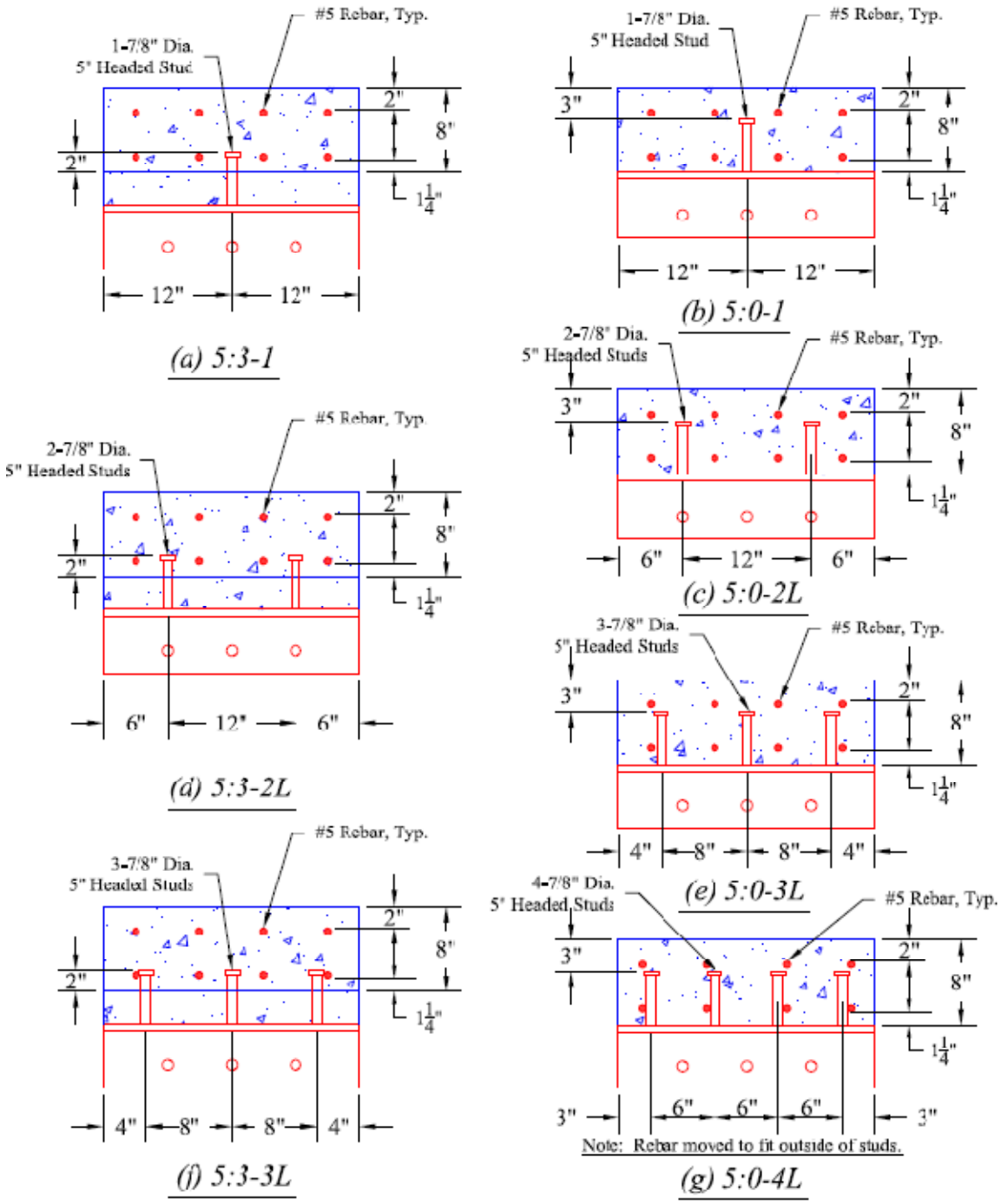

Figure 3.5: Series II Stud Details, 5-in Studs Spaced Longitudinally (a),(d),(f) with a Haunch and (b),(c),(e),(g) without a Haunch

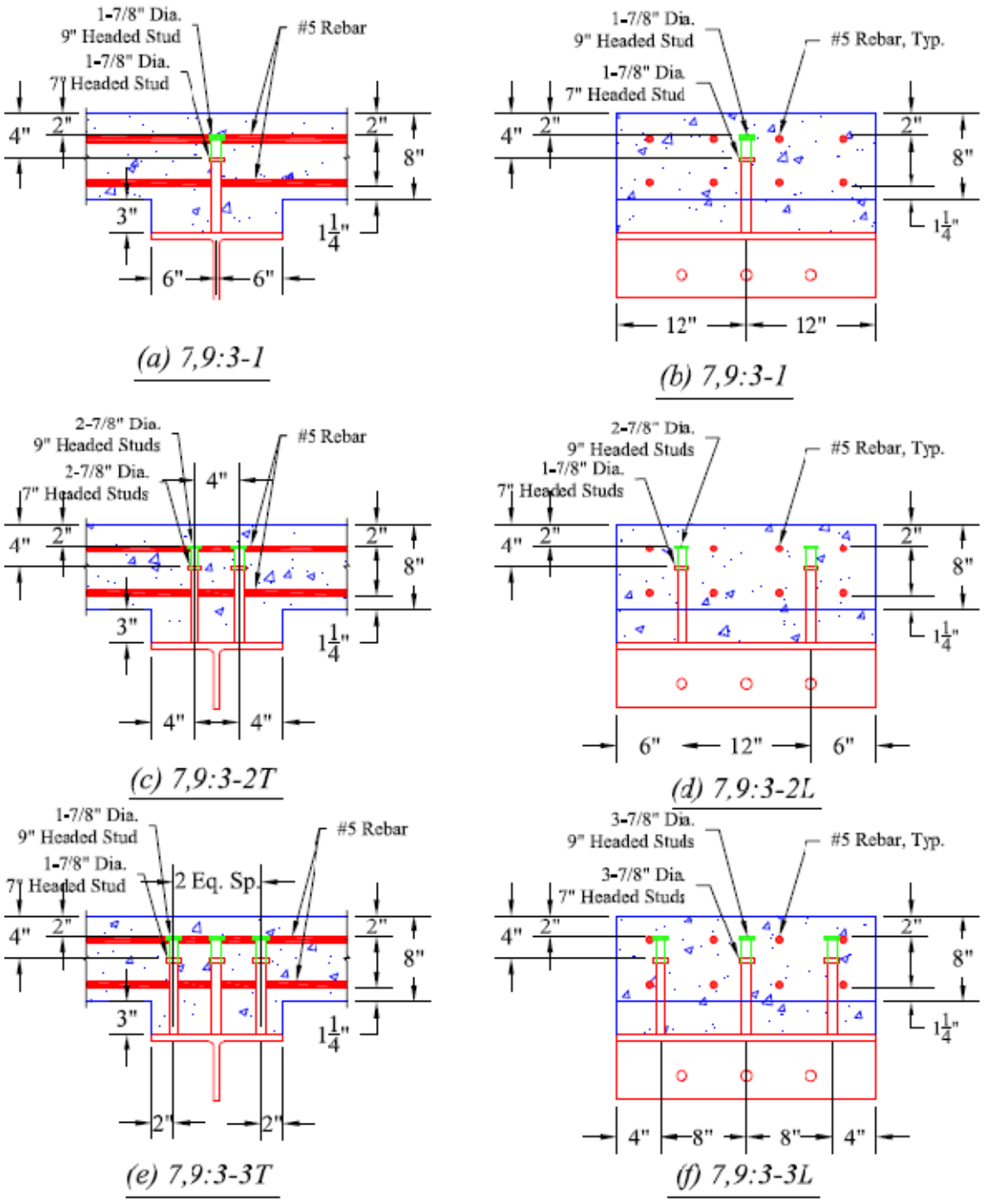

Figure 3.6: Series III Stud Details, 7-in and 9-in Studs Spaced (a),(c),(e) Transversely and (b),(d),(f) Longitudinally

3.2.2 Stud Welding

The headed shear studs were attached to the WT sections by two methods. For Series I and II, the studs were welded using conventional stud welding equipment (Figure 3.7) from a stud supplier to match typical field conditions. For Series III, the supplier was unavailable; therefore the studs were fillet welded to the WTs. Fillet welding was found to produce satisfactory strength in the studs, as shown by a bend

over test (Figure 3.7(b)). A bend over test was performed by bending a welded stud horizontally to validate that the weld had sufficient strength to support the maximum force the stud can develop. Shear studs are manufactured 1/4 in longer than the final installed height because conventional stud welding uses the stud as the electrode, resulting in the bottom 1/4 in of the stud melting during the welding process. Because the fillet welding did not use the stud as an electrode, all studs in Series III were 1/4 in taller than the nominal height. Based on the results from Series III, Series IV studs were also fillet welded. For Series IV studs, the bottom 1/4 in of the stud was cut off to bring the installed stud height to exactly 5 inches.

(a) ***(b)***

Figure 3.7: (a) Stud Welding (b) Bend Over Test

3.2.3 Formwork

All four series of tests were cast in the same two sets of forms, each built to accommodate six specimens (all twelve specimens in a series were always cast simultaneously). Forms are shown in Figure 3.8, both with and without a haunch. Forms were adjustable so that each bay of a form could be individually set to form either no haunch or a 3-in haunch as needed in each series. All forms were stripped, cleaned, and reassembled after each cast.

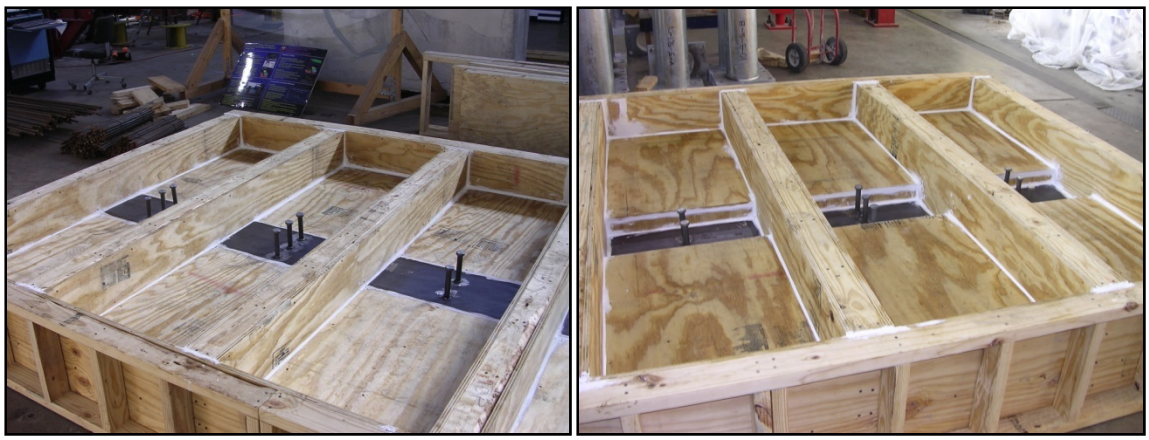

(a) ***(b)***

Figure 3.8: Formwork for Specimens with (a) No Haunch (b) 3-in. Haunch

3.2.4 Concrete Mix

All concrete used in the test specimens conformed to the details of TxDOT class "S" concrete mix. Class "S" concrete has a minimum compressive strength of 4000 psi, a maximum water/cement ratio of 0.45, and course aggregate ranging between 3/4 in and 1-1/2 in.

For each series, twelve 6-in by 12-in concrete cylinders were cast with the specimens. Specimens and cylinders were tested on or after a 28- day curing period, with three compression cylinders tested on the same day as the first specimen in the series. Six cylinders were tested after half the specimens in a series had been tested (typically 7 to 10 days after the first test). Three of these specimens were tested to determine the unconfined compressive strength, and the other three were subject to split cylinder tests to establish the concrete tensile strength. The last three compression cylinders were tested on the same day as the last test in the series (2 to 3 weeks after the first test). Taken together, the cylinder tests bracketed each series and captured changes in compressive strength over the duration of series testing. They also provided valuable information on the concrete tensile strength, which was essential to the evaluation of pullout cone behavior.

3.3 Test Setup

3.3.1 Loading Arrangement and Test Setup

Each of the specimens was tested as a simply supported beam with a point load applied at midspan (Figure 3.9). Load was applied with a hydraulic ram, driven by a pneumatic pump and connected to the stem of the WT embedded in the slab. The ram was attached via a chevron of pinned connecting plates attached to the web at the quarter points, 6 in from each end of the specimen, to evenly distribute the load among the studs (Figure 3.10(a)). For the eccentrically loaded specimens, the ram was attached by a pair of pinned connector plates directly underneath the quarter point on the WT web (Figure 3.10(b)). All specimens were supported at each end by 6-in long elastomeric bearing pads. The bearing pads were spaced two inches away from the edge of the support blocks to allow for rotation of the specimen ends. Given this rotation, the span length was taken as the distance between the centers of the bearing pads, 6-ft 6-in.

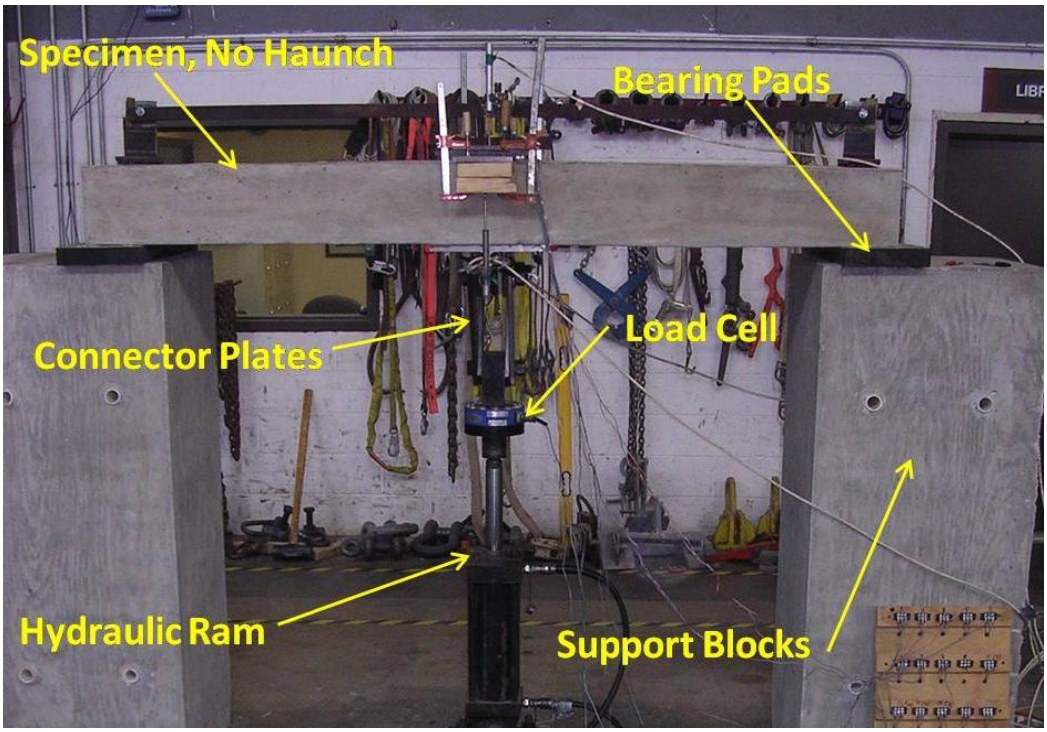

Figure 3.9: Basic Test Configuration, Static and Dynamic

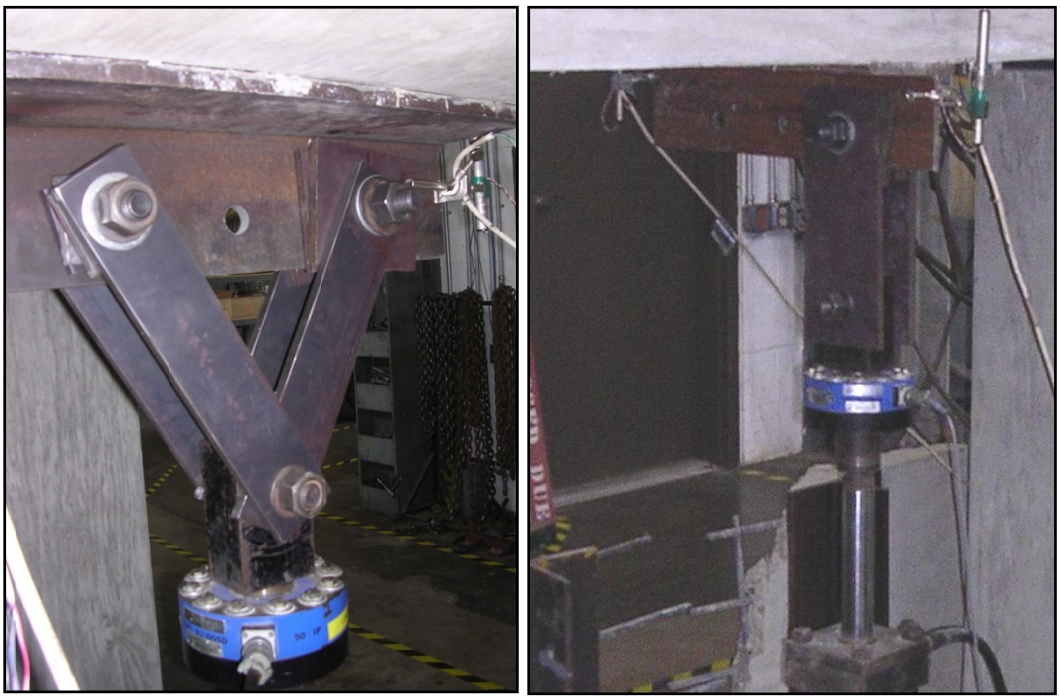

(a) ***(b)***

Figure 3.10: Connector Plates for (a) Standard Loading (b) Eccentric Loading

3.3.2 Dynamic Test Setup

The dynamic testing series had the same test configuration as the static test series, but the hydraulic system used to load the specimen was substantially different. The same hydraulic ram was used in both testing configurations, but for the dynamic tests, the pneumatic pump was included in a separate loop to the ram, which could be isolated from the rest of the hydraulic system. This pump was used to position the ram so it could be connected and disconnected from the specimen.

The main system, shown in Figure 3.11, included a constant pressure electric pump, a pressure accumulator, a line conditioner (pressure accumulator and line conditioner are mounted on a support frame to prevent movement during testing), and a sump. The electric pump supplied oil pressurized to 3,000 psi to the 10 gallon accumulator where it was stored for use in the test. The line conditioner connected the line between the accumulator and the ram and contained a solenoid valve that could be opened to full pressure nearly instantaneously, allowing a fast release of the high pressure oil. The dynamic test configuration produced an average loading rate of between 900 and 1100 kips per second, compared to the average static loading rate of 0.05 to 0.07 kips per second. Oil exiting the ram drained into the sump through a large diameter line to prevent a pressure buildup that could slow the ram's descent during a test. Every two to three tests, the sump had to be emptied back into the electric pump to return oil to the pressure accumulator. Safety valves between the line conditioner and ram, and ram and sump, prevented an accidental firing of the system once the accumulator was pressurized. A wooden catch stand was placed around the ram to stop the WT from falling onto and damaging the ram after it had separated from the specimen.

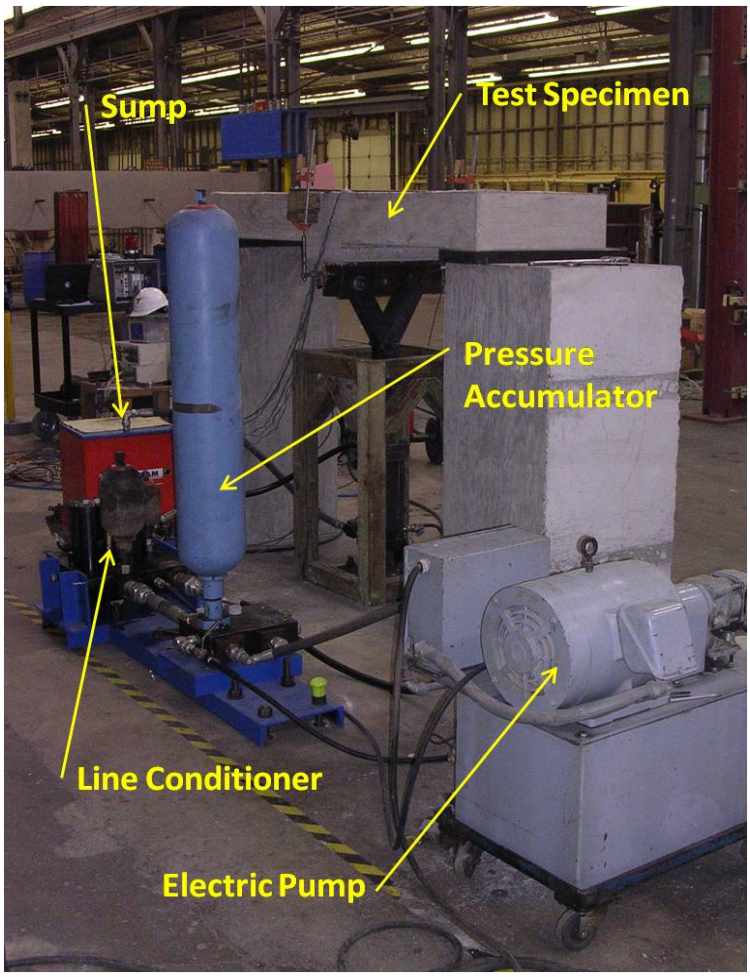

Figure 3.11: Dynamic Test Setup showing Hydraulics

3.4 Instrumentation

3.4.1 Shear Studs

Each shear stud was instrumented with a strain gage. These gages were originally designed for use inside the shank of high tension bolts. Before the studs were installed on the WTs, 2-mm holes were drilled into the head of the shear studs. After installation, strain gages were inserted into the holes to a depth of 1-3/8 in, as shown in Figure 3.12(c), to reach a range of relatively uniform stress below the stud head. Once the gage was inserted, the hole was filled with an epoxy. The gage instructions then called for the gages and epoxy to be heated to 280 degrees Fahrenheit for 3 hours and allowed to cure at room temperature for 12 hours to bond the strain gage to the shear stud. It was impractical to heat the entire WT with studs as specified, so each stud was warmed with a heat gun for a few minutes and allowed to cure for one day. Figure 3.12 illustrates the gage installation process.

(a)

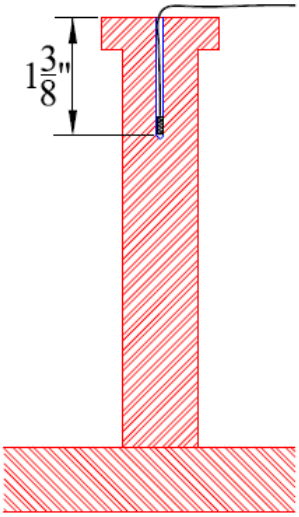

(b) **(c)**

Figure 3.12: Shear Stud Gages (a) Installation (b) Shear Stud after Gage Installation (c) Drawing of Typical Stud Gage Placement

3.4.2 Reinforcing Steel

For all specimens, each of the eight transverse bars of reinforcement was instrumented with a strain gage at midspan to measure slab behavior. The only exception to this pattern was in Series IV, where each 'b' replicate had only the center four bars instrumented because previous tests showed that all four bars in each mat of reinforcement had nearly the same strain. Each gage was applied to a section of rebar surface that had been ground smooth and flat and cleaned with acetone to remove imperfections and grit. Each gage was also covered with wax, heat-shrink waterproofing tape, and a waterproofing sealant to make sure the surrounding concrete did not damage the gage (Figure 3.13). Gages were labeled 1-8, with "T" indicating top-mat reinforcement gages and "B" indicating bottom-mat gages, as shown in Figure 3.14.

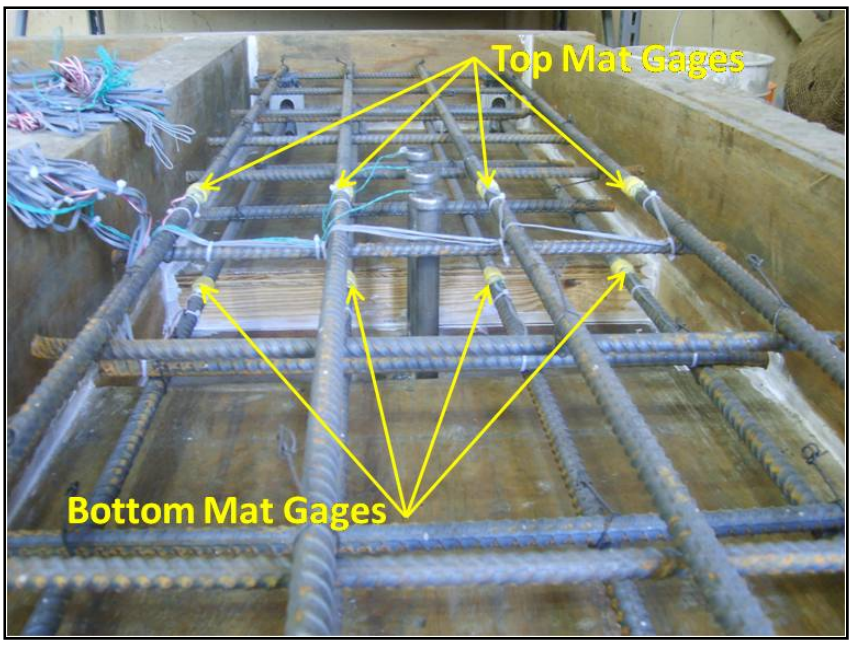

Figure 3.13: Strain Gages on Reinforcing Bars

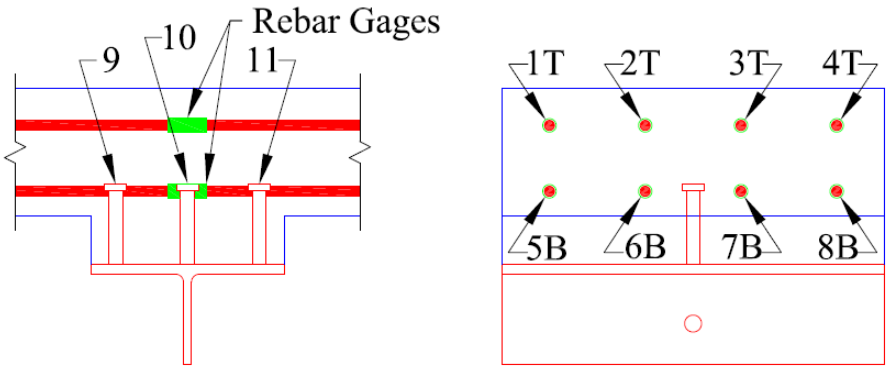

Figure 3.14: Labeling Scheme of Gages (a) in Studs and (b) on Reinforcing Steel

3.4.3 Load and Displacement

Deflection of the slab and pullout of the shear studs were measured with three linear potentiometers. Slab deflection under load was measured with a single potentiometer at midspan, clamped to a rigid frame resting on the slab directly above the bearing pads. This configuration eliminated the deformation of the bearing pad from the measurement and directly gave the slab deflection (this measurement was omitted in the dynamic tests for safety reasons). Pullout of the shear studs (and the WT) from the concrete slab was measured with two linear potentiometers, one attached to the WT on each side of the specimen (Figure 3.15). The potentiometers measured the distance between the WT and a plate with shims placed on top of the slab. Because stud pullout was often to some degree unsymmetrical, the average of the two gages was used to give the separation between the studs and the concrete slab. Load was measured with a load cell mounted to the end of the hydraulic ram immediately before the clevis attaching the ram to the connector plates, as shown in Figure 3.16.

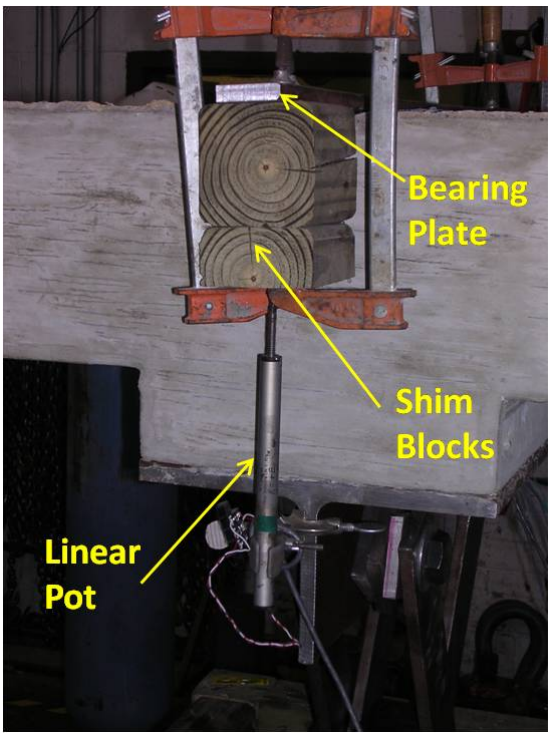

Figure 3.15: Linear Pot Installation

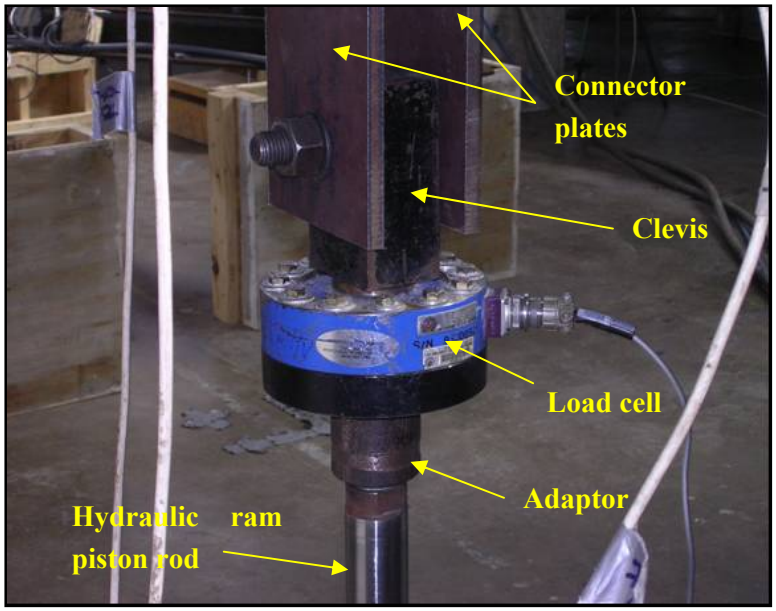

Figure 3.16: Load Cell Attachment to Ram and Specimen

3.5 Testing Procedure

3.5.1 Static Testing Procedure

For static tests (Series I, II, and III), after installation of all linear potentiometers, the hydraulic ram was raised and bolted onto the spreader plates. The assembled test setup is shown in Figure 3.17. At this point, all gage readings would be zeroed, and data collection begun. Load was steadily applied by the

ram, creating tension in the studs and moment in the slab. Periodically, loading would be paused to allow for the mapping and photographing of cracks in the concrete slab. Loading was continued until either the load in the specimen dropped to two kips or the linear pots had reached full extension and no more displacement data could be collected. Loading was stopped prior to zero force because large pieces of the haunch, and sometimes the entire WT, would break away from the specimen and damage the ram when complete pullout occurred.

3.5.2 Dynamic Testing Procedure

Dynamic testing (Series IV) began with raising the ram and connecting it to the spreader plates using the pneumatic pump, after the linear pots were installed (similarly to Figure 3.17). At this point, the data acquisition system was calibrated and zeroed, and the pneumatic pump was isolated from the ram system. The electric pump was used to charge the accumulator to 3000 psi, and the relief valve to the ram sump was opened. Once the accumulator was charged, the safety valve between the accumulator and the ram was opened, and data collection was initiated. Immediately after data collection was triggered, the solenoid valve in the line conditioner was fired, opening the line and releasing the pressurized oil to the ram, which loaded the specimen nearly instantaneously. After firing, the ram would displace its full stroke, with loading and displacement rates varying by the slabs' individual strength and stiffness. Especially for brittle specimens, full ram displacement resulted in the WT, studs, and pieces of concrete completely separating from the slab and resting on the catch stand. Each test was filmed with a video camera to record specimen behavior.

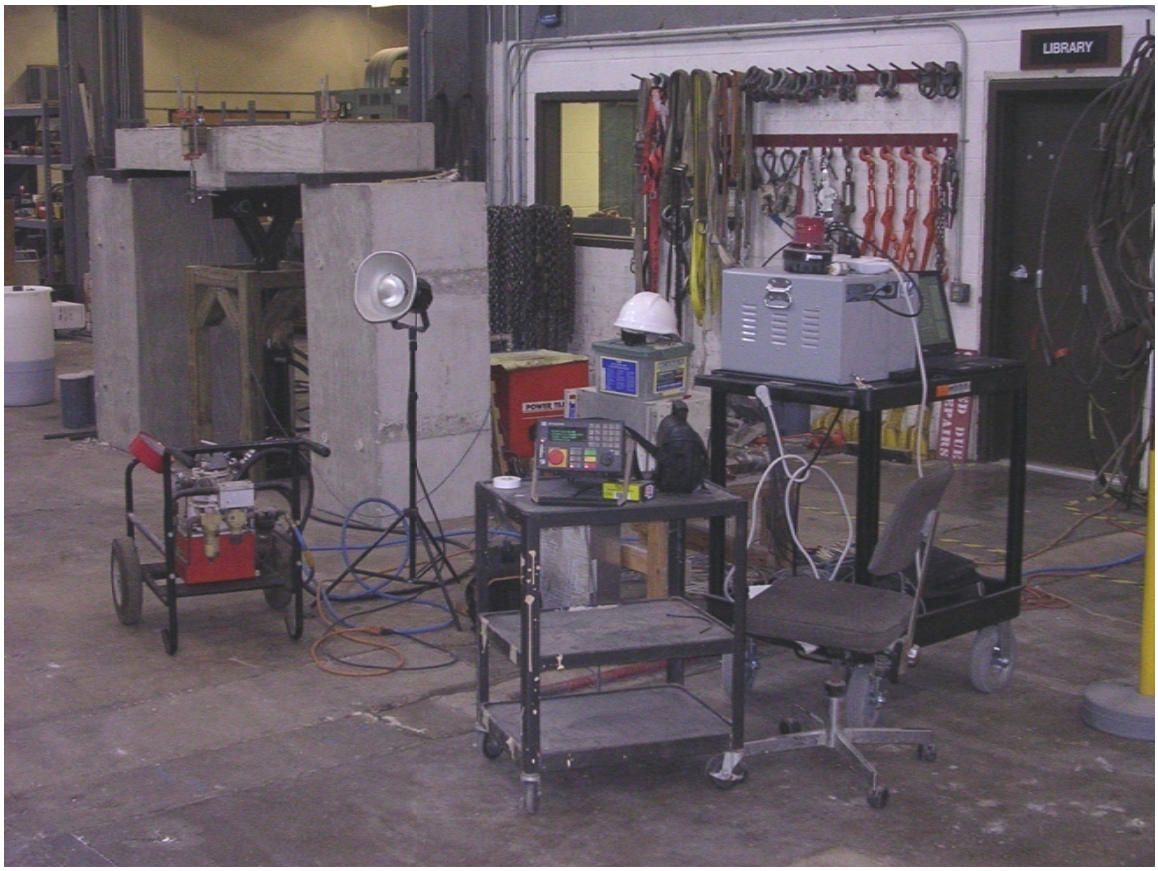

Figure 3.17: Overall Test Setup

The above testing and construction procedures were used for all four test series. The tests themselves produced considerable data from the various measuring devices, with relatively few instances of strain gages on the rebar or in the shear studs malfunctioning, though falling concrete from a test damaged the load cell's electrical cable and invalidated one test in Series IV. The data collected from the various gages, as well as observations during the tests, are discussed in Chapter 4.

Chapter 4: Test Results

4.1 General Components

The three series of tests conducted for this research produced considerable data on the tensile behavior of shear studs. All specimens failed by some variation of tensile cone pullout. Each series was tested over a two-to-three week period, and the four series were tested over the course of one year. This chapter includes the results of each series in detail, beginning with a summary of the related tests performed by Sutton. The details of Sutton's tests are given in his thesis (Sutton, 2007).

4.2 Series I Summary — Five-Inch Studs Spaced Transversely

Series I test results, covering studs spaced transversely with and without a haunch, are presented by Sutton (2007); they are summarized here for reference. Strengths for each test in Series I are shown in Table 4.1.

Table 4.1 Peak Strengths of Specimens with 5-in Studs Spaced Transversely

Number of Studs, No Haunch	Peak Strength (kips)	Average Strength (kips)	Number of Studs, 3-in Haunch	Peak Strength (kips)	Average Strength (kips)
1	21.3	20.9	1	23.4	22.3
	20.4			21.2	
2	25.3	24.6	2	18.5	19.2
	23.8			19.9	
3	26.2	25.9	3	16.4	17.3
	25.6			18.2	

All specimens without a haunch fail by cone formation around the studs, as shown in Figure 4.1. Specimens demonstrate very little post-peak load strength, indicating no engagement between failure cones and rebar. Increasing the number of studs increases the total strength for specimens without a haunch. For three studs, the increase is an average of 20% more than for a single stud, as shown in Figure 4.2. For Figure 4.2 and all Peak Load versus Number of Studs plots, the peak load is normalized by the concrete tensile strength because tensile strength is the critical factor governing concrete failure. All references to relative strengths of tests are expressed in terms of this normalized value. Concrete tensile strength was determined using split cylinder tests as described in Chapter 3, with results reported in the Concrete Cylinder Test section of each series.

(a) ***(b)***

Figure 4.1: Failure Cone (a) Around Stud (b) Cone Void in Slab

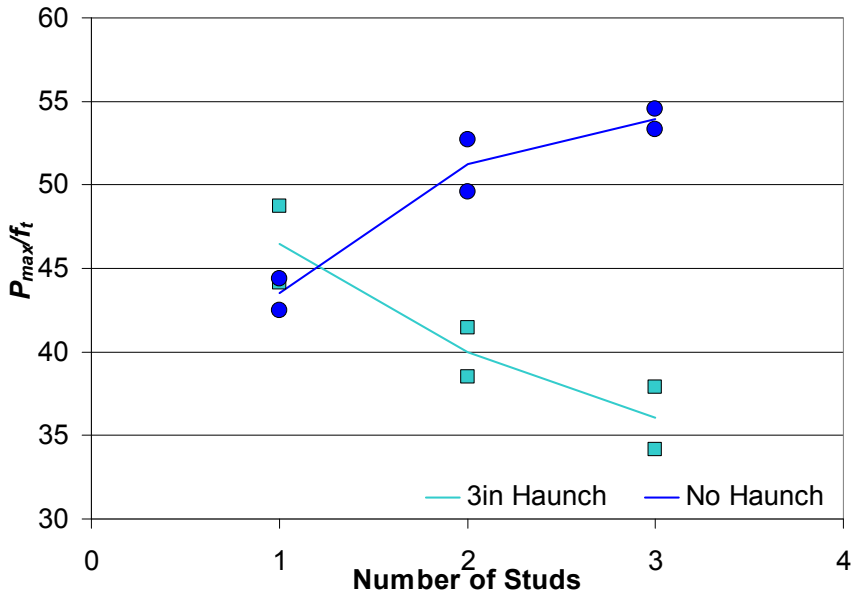

Figure 4.2: Normalized Peak Strength vs. Number of Studs for 5-in Studs Spaced Transversely

Failure of specimens with a haunch occurs by splitting and tensile failure of the unreinforced concrete haunch (Figure 4.3), sometimes leading to complete separation of the haunch from the slab. The specimens show essentially no post-peak-load strength. The strength of a single stud with a haunch is greater than for a single stud without a haunch because the haunch limits cracking around the studs. For more than one stud, specimens without a haunch have much higher strengths than specimens with a haunch. For specimens with a haunch, the total strength decreases as the number of studs increases and studs become more closely spaced to the edge of the haunch (Figure 4.2).

(a) (b)

Figure 4.3: Series I Failures (a) Splitting of Haunch (b) Separation of Haunch

4.3 Series II Results - Five-inch Studs Spaced Longitudinally

4.3.1 Strength

Longitudinally spaced studs are intended to increase overall strength by reducing the edge effect of studs in a haunch and increasing the size of the projected failure cone area for all specimens. As shown in Figure 4.4, two 5-in studs spaced longitudinally have an increase in strength over a single stud, both for specimens with and without a haunch. For three and four studs spaced longitudinally, strength is relatively similar to the respective two-stud case for specimens with and without a haunch. Table 4.2 lists the measured strengths for each replicate in the series.

For specimens without a haunch, single-stud tests have nearly the same strength, within 4%, of Series I. This similarity is expected because both specimens have the same configuration. The strength of two studs spaced longitudinally increases 40% over a single stud (14% over equivalent transverse spacing). For three studs spaced longitudinally, the strength increases 46% over one stud (13% over equivalent transverse spacing). The strength of the four-stud configuration tested in Series II is also 40% greater than a single stud without a haunch, but 6% lower than a three-stud grouping. This reduction is believed to be due to the two end studs' proximity to the transverse edges of the slab.

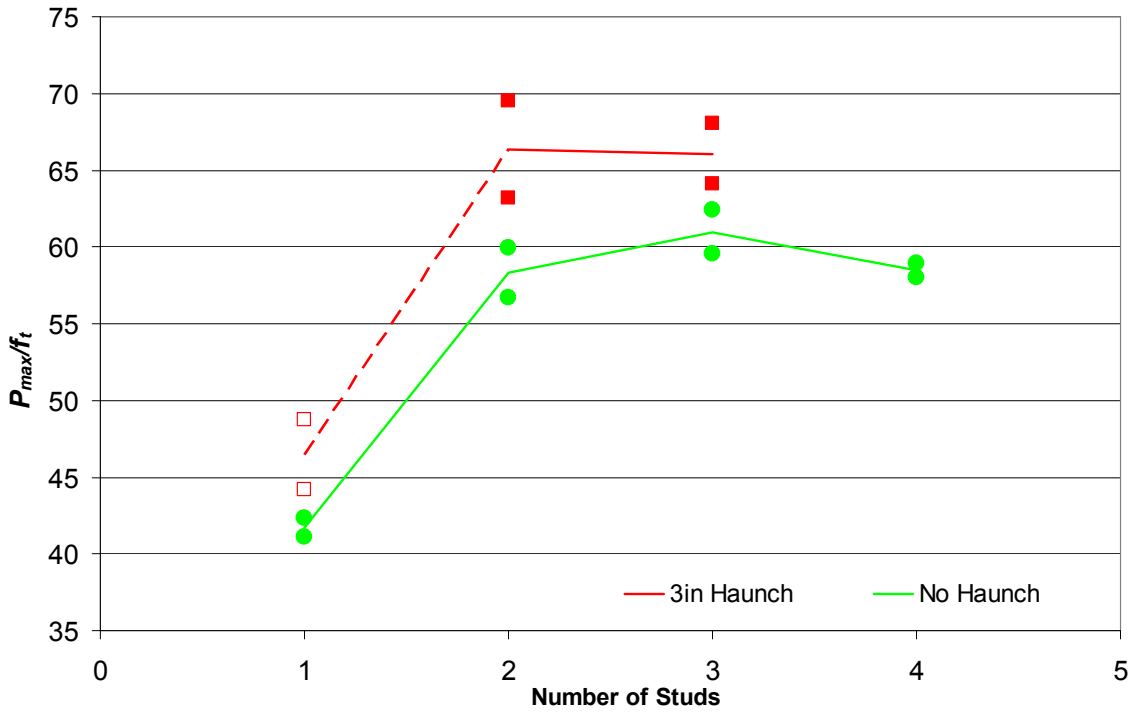

Figure 4.4: Normalized Peak Strength vs. Number of Studs for 5-in Studs Spaced Longitudinally

Table 4.2: Peak Strengths of Specimens with 5-in Studs Spaced Longitudinally

Number of Studs, No Haunch	Peak Strength (kips)	Average Strength (kips)	Number of Studs, 3-in Haunch	Peak Strength (kips)	Average Strength (kips)
1	20.9	20.6	1 (from Series I)	23.4	22.3
	20.3			21.2	
2	28.0	28.8	2	31.2	32.7
	29.6			34.3	
3	30.8	30.1	3	31.6	32.6
	29.4			33.6	
4	28.6	28.9			
	29.1				

For specimens with a haunch, no replicate one-stud specimens were tested because it was expected that, like the no-haunch tests, a single stud has a strength similar to the same configuration in Series I. For graphing purposes, the Series I single-stud with haunch test results are used when plotting the Series II results (Series I results are the dashed line and data points in Figure 4.4). For two studs spaced longitudinally in a haunch, the strength increases (rather than decreases as with a transverse spacing) 43% over a single stud (66% greater than the equivalent transverse spacing). For three studs spaced longitudinally, the strength is 42% greater than a single stud (82% greater than the equivalent transverse spacing).

The plateau in peak strengths for specimens with studs spaced longitudinally, both with and without a haunch, is explained by the overlap of the studs' failure cones. Once studs are spaced apart longitudinally less than a distance, *s*, which is defined as three times the effective stud height (13.875 in for a 5-in stud, as specified by ACI 318-08 Appendix D), the individual failure cones overlap as shown in Figure 4.5. The failure cone overlap creates a continuous failure surface across the entire specimen (a concrete 'ridge') that does not change size as the number of studs within the failure surface increases. In the Series II specimens, two studs centered longitudinally are spaced 12 in apart, less than the maximum

threshold to create group failure. Three and four studs centered longitudinally are even more closely spaced, at 8 in and 6 in apart, respectively. Because all of these specimens are under the threshold for group failure, they all have the same failure surface and approximately the same strength.

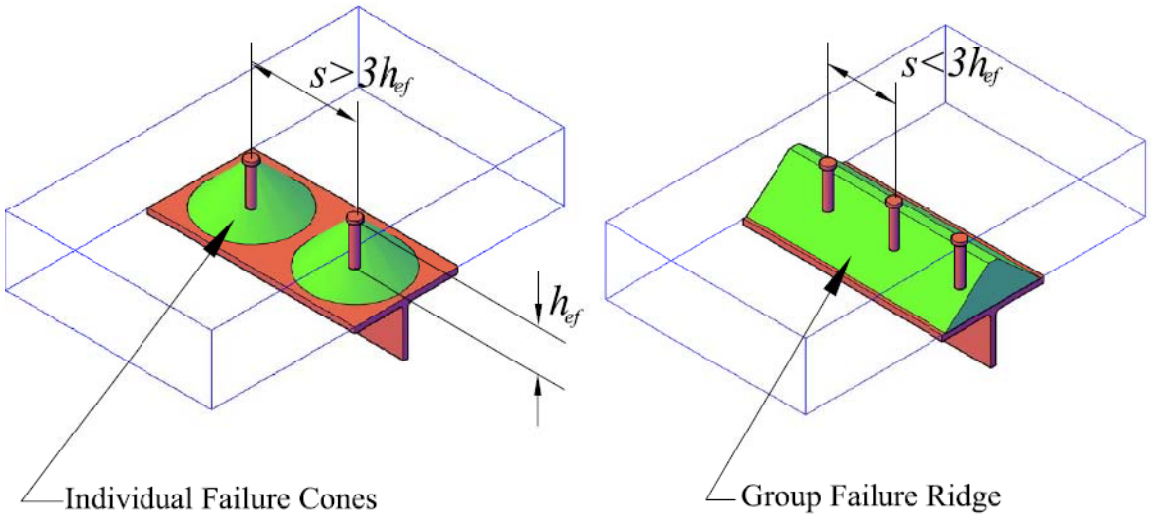

Figure 4.5: Group Effect in Concrete Failure Cone

In Series I, specimens with a haunch have lower strengths than specimens without a haunch. In Series II, the converse is true: specimens without a haunch have lower strengths than specimens with a haunch. Two competing factors influence the effect of the haunch, causing the change from Series I to Series II: the edge effect and the uncracked concrete effect. The edge effect reduces stud strength in a haunch (relative to studs without a haunch) because the stress in the concrete at the corner of the haunch and the slab increases as studs are spaced closer to a haunch edge. The uncracked concrete effect increases stud strength in a haunch (relative to studs without a haunch) because the increased depth of the haunch reduces concrete stresses from slab flexure and eliminates flexural cracking in the haunch. Without flexural cracks crossing the failure cone, shear stud tensile strength is increased. Studs spaced transversely in a haunch have very small edge distances, resulting in high stresses at the haunch corner that outweigh the benefit from the uncracked concrete, resulting in low strengths. For studs spaced longitudinally, edge distances are larger and associated corner stresses are smaller, allowing the uncracked concrete effect to dominate and increase overall strength above similar studs without a haunch. ACI 318, Appendix D accounts for both of these effects with modification factors to the stud breakout strength. The edge effect is accounted for with the edge effect modification factor, which reduces strength as edge distance decreases. The uncracked concrete effect is accounted for with the cracked concrete modification factor, which increases the strength when the concrete is uncracked.

4.3.2 Behavior at Failure

For Series II specimens, a greater degree of cone development and ductility is observed than in Series I because of the studs' longitudinal spacing. This greater cone development increases the strength of all sections relative to transverse spacings and, in some cases, also increases the post-peak load carrying strength significantly.

Specimens with a Haunch

While studs spaced longitudinally in a haunch have a higher strength than those spaced transversely, the lack of reinforcement in the haunch still leads to a sudden, brittle failure at or

immediately after peak load in all but one specimen. Figure 4.6 shows applied load versus the average displacement of the WT (relative to the slab) and is typical for longitudinal studs in a haunch. Of note in Figure 4.6 is the horizontal axis, which has been magnified for better resolution. Because the WT is very stiff, average stud displacement is assumed to be the same as average WT displacement. For all displacement plots, the average displacement is calculated as the mean of the displacements measured at each end of the WT.

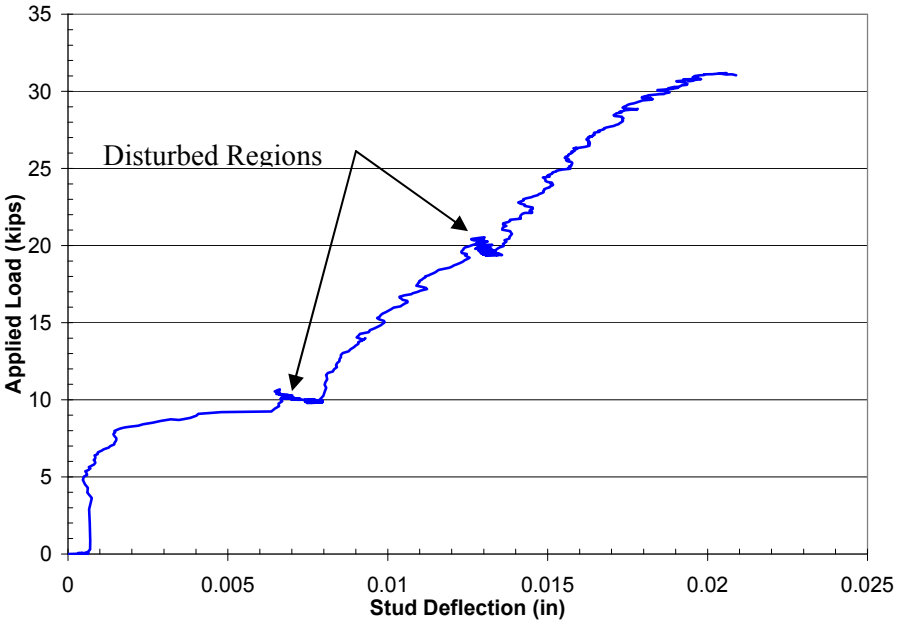

Figure 4.6: Applied Load vs. Average Stud Pullout for 3-in Haunch Specimens

All specimens with a haunch reach peak load between 0.02-in and 0.04-in of displacement. Of note on the load-displacement plots are the "disturbed" regions on each graph, shown on Figure 4.6. These regions are caused by pauses in loading to photograph the specimen and mark cracks. When paused, the hydraulic pressure in the ram drops slightly, resulting in the load and deflection variations seen in the plot. As load is applied, flexural cracks first occur at the edges of the haunch as shown in Figure 4.7(a), similarly to those seen by Sutton (2007). Flexural cracks grow as the load increases and, in the case of three studs spaced longitudinally, grow up to the top mat of reinforcement. At peak load, the two centermost flexural cracks join over the haunch, as shown in Figure 4.7(b). Immediately after peak load, a horizontal failure plane occurs across the top of the haunch. As the failure plane forms, all strength is lost, and the haunch concrete, still attached to the studs and WT, breaks away from the specimen as shown in Figure 4.7(c). The lack of reinforcement within the haunch results in the brittle concrete tensile failure observed, with virtually no ductility.

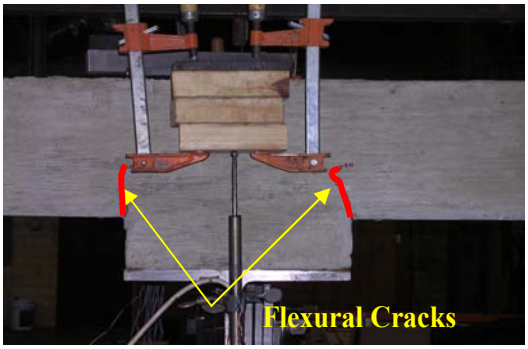

(a)

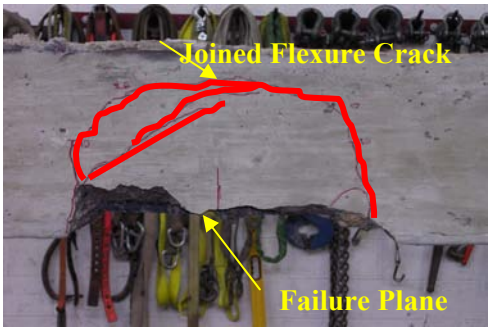

(b) *(c)*

Figure 4.7: Haunch Specimen (a) Flexural Cracks (b) Cracking at Peak Load (c) Separated Haunch

The single exception to the brittle haunch behavior is specimen 5:3-3La, whose load-deflection behavior is shown in Figure 4.8. Specimen 5:3-3La develops a complete cone pullout, engaging the bottom rebar mat as shown in Figure 4.9(a). This failure is very similar to the failure patterns of specimens with no haunch. The specimen demonstrates considerable ductility by sustaining an average load of 10 kips until a deflection of 1.75 in. At 1.75 in the load drops to around 7 kips and is maintained to a deflection of 2.6 in. This ductile behavior is caused by the special geometry of specimen 5:3-3La. The shear stud spacing for this specimen places the outer studs in direct contact with the rebar, and the height of the stud in the 3-in haunch causes the heads of the studs to bear directly against the rebar, as shown in Figure 4.9(b). The stud head overlapping the rebar creates a mechanical interlock that forces the studs and rebar to deform together, resulting in the ductile failure.

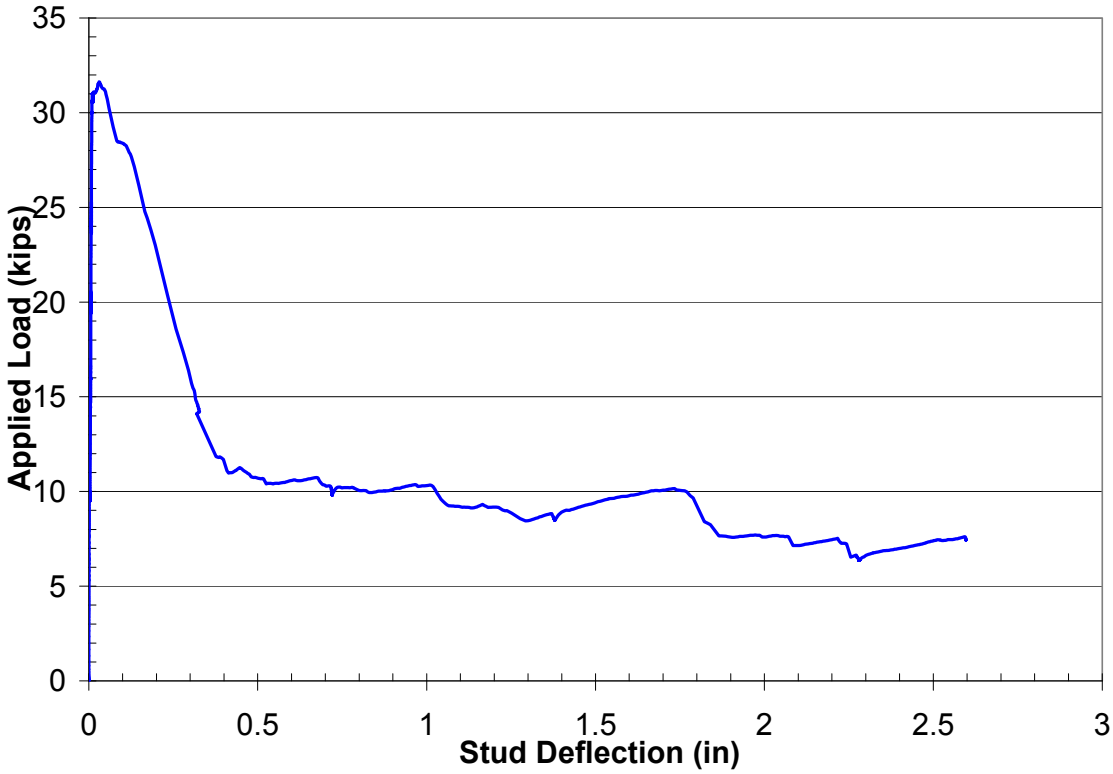

Figure 4.8: Load-Deflection Plot for Specimen 5:3-3La

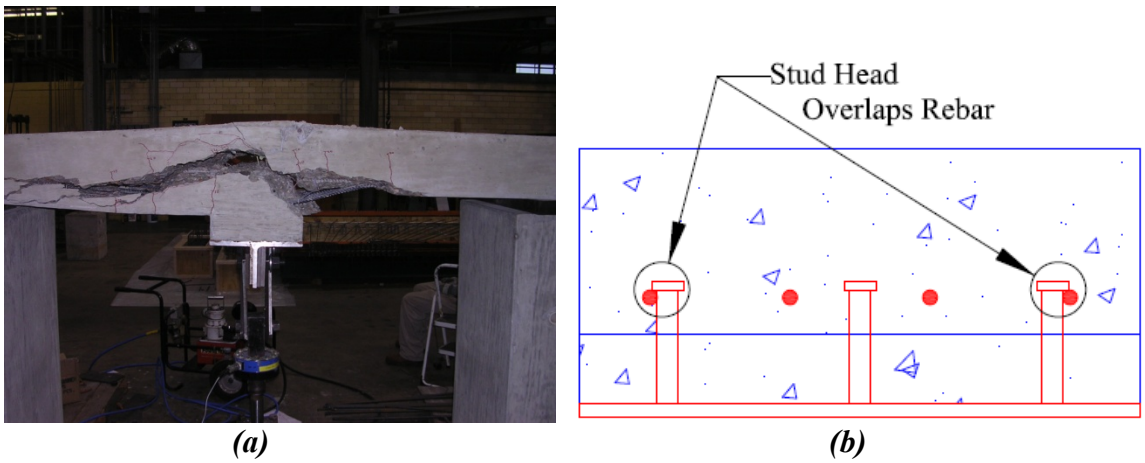

(a) ***(b)***

Figure 4.9: Specimen 5:3-3La (a) Pullout Engaging Bottom Rebar (b) Schematic Showing Rebar-Stud Interlock

Specimens with No Haunch

All specimens with longitudinally spaced studs and no haunch have significantly more ductility than studs spaced longitudinally or transversely in a haunch and studs spaced transversely without a haunch. All specimens without a haunch have rebar engaging the concrete failure cone of the shear studs, and all show a controlled unloading curve. This unloading curve indicates ductility and is influenced by the number of studs and the specific failure behavior of each specimen. Eccentricity in the stud displacement reduces, but does not eliminate, the ductility of some specimens relative to their replicates. Load-displacement plots for specimens with no haunch are shown in Figure 4.10. As the number of studs

increases the ultimate displacement achieved on the unloading curve also increases, indicating that ductility increases with the number of studs even though the strength remains approximately the same with two or more studs.

All no-haunch specimens, with the exception of single-stud specimens, reach a peak load at deflections between 0.02 and 0.04 inches, similarly to specimens with a haunch. Single-stud specimens have peak load at slightly larger deflections, between 0.05 and 0.07 inches.

As load is applied, the first flexural crack always occurs at the center of the specimen, right down the line of the studs (Figure 4.11a). For specimens with a single stud, a ring of failure cracks forms on the underside of the specimen around the stud just after peak load (Figure 411.b). After failure crack formation, the failure cone and WT pull out together, rapidly losing load as deflection increases.

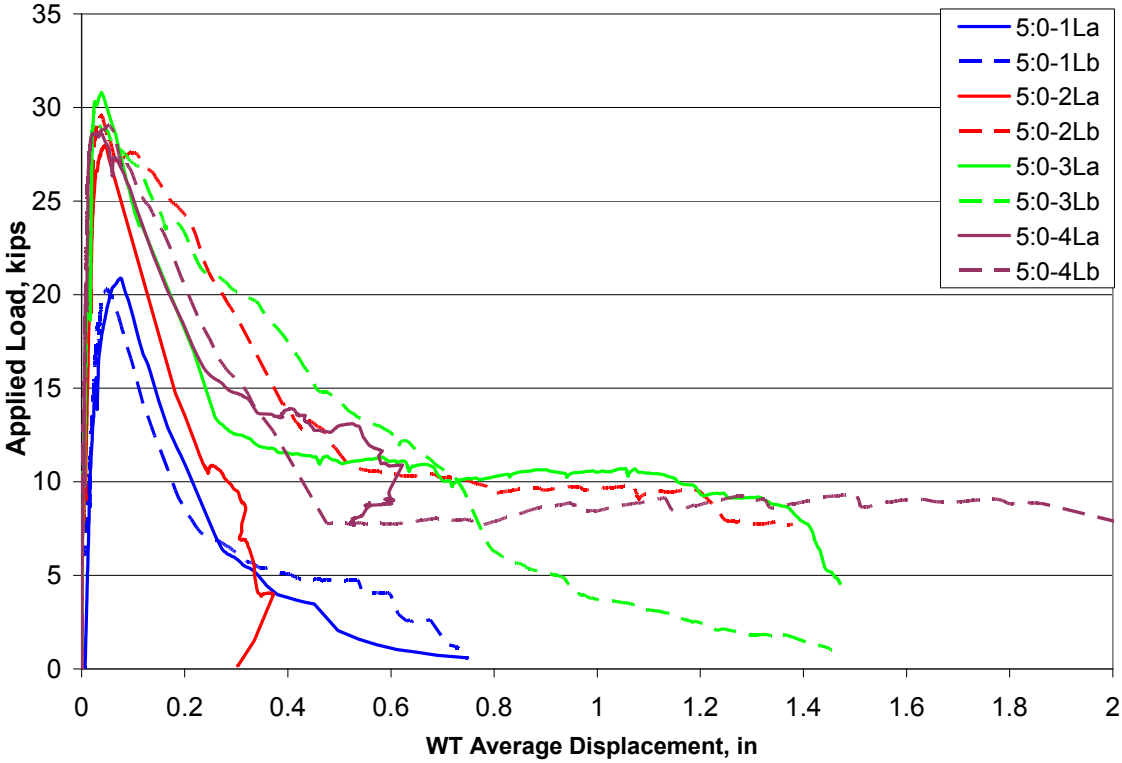

Figure 4.10: Load-Deflection Plot for Specimens without a Haunch

(a) **(b)**

Figure 4.11: Specimens with No Haunch (a) First Flexural Crack (b) Single Stud Failure Cone

For specimens with more than one stud, just after peak load, a horizontal crack forms at midspan in the 1-in tall region between the top of the studs and the top mat of reinforcing. This horizontal crack propagates quickly in both directions. Often the horizontal crack merges with a flexural crack on one or both sides of the studs, turning down towards the bottom of the specimen (Figure 4.12(a)). As displacement increases, the horizontal crack opens, and portions of the bottom cover concrete spall (Figure 4.12(b)). As deflections continue to increase, the sides of the slab crack and separate from the central failure cone, leaving only the interior cone of concrete to continue displacing (Figure 4.12(c)). This side cracking is especially pronounced in tests with four studs, where the end studs in the group are 3 inches from the edge of the slab, creating an edge effect promoting side cracking.

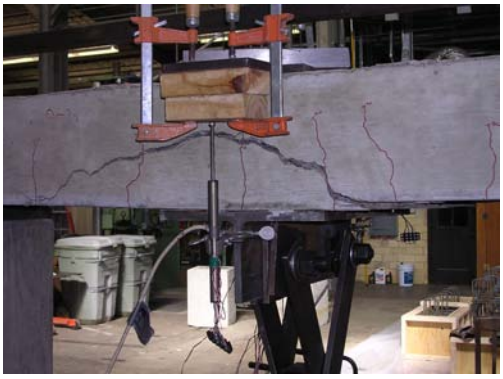

(a)

(b)

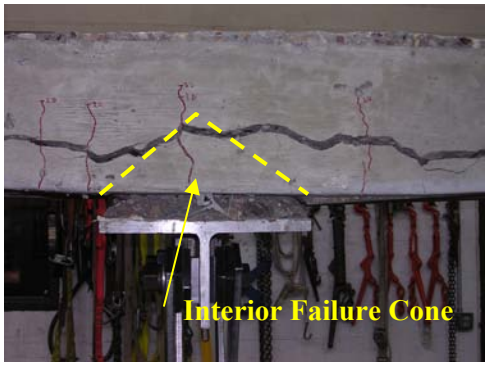

(c)

Figure 4.12: Longitudinally Spaced Stud Specimen Cracking (a) Horizontal Crack Formation (b) Horizontal Crack Growth(c) Side Cracking and Separation from the Interior Failure Cone

Several of the no-haunch specimens (as indicated above in Figure 4.10) exhibit a post-peak load plateau at large displacements while their replicates show a steady decrease in load after peak strength. This steadily decreasing load is due to eccentric pullout of the WT, as shown in Figure 4.13. During loading, one edge of the WT begins to pull out faster than the other edge, creating a displacement gradient down the length of the WT. This displacement gradient causes additional cracking around the shear studs, reducing the load-carrying capacity of the studs at large displacements. Specimens showing a load plateau and specimens with a haunch pull out evenly, with both edges of the WT displacing at roughly the same rate. Eccentric loading of the studs may occur during a bridge fracture; therefore, tests of eccentrically loaded specimens in Series III were performed to better understand how this behavior impacts specimen strength and ductility.

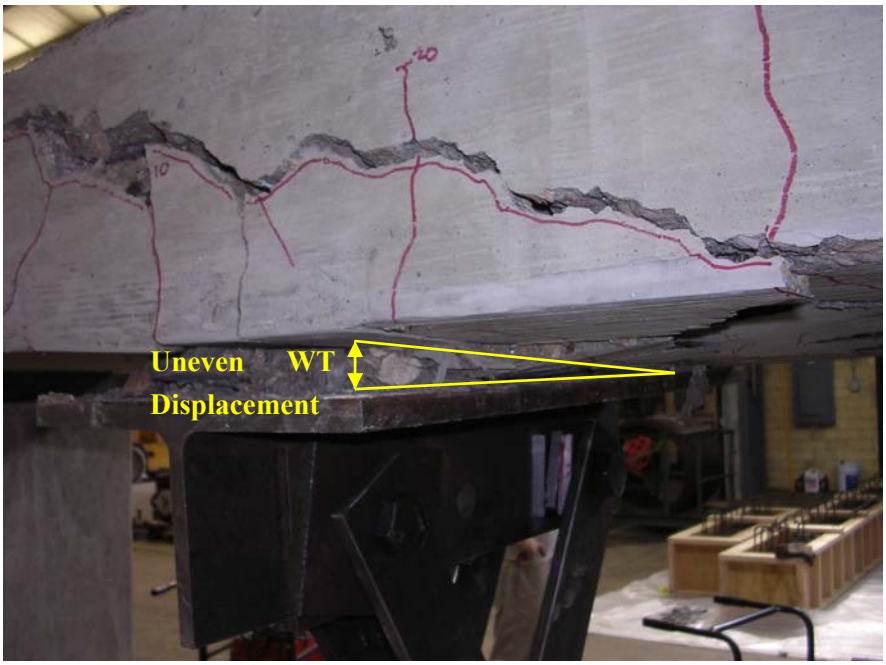

Figure 4.13: Displacement Gradient of WT with Concentric Loading

4.3.3 Shear Stud Gage Data

Analysis of Data

Data collected from the strain gages placed inside of the shear studs were used to determine the distribution of forces among studs in a specimen. The sum of the calculated stud forces is compared to the measured applied load to verify the load path between ram, shear studs, and concrete slab. Because the strain gages were placed in the center of the stud, any bending strains will be negligible. Measured strains are assumed uniform across the stud cross section. Thus, multiplying the strain by the modulus of elasticity of steel (taken as 29,000 ksi here and throughout this work) and multiplying by the nominal area of the 7/8-in diameter shaft gives the force in each stud. For studs spaced longitudinally, peak stresses are relatively low, below 45% of yield in all cases.

For all plots and tables of stud forces, gage data are terminated when strain gages fail. Cracking of the concrete near peak load frequently breaks the gage lead wires, failing the gages. When gages fail after peak load, strain and load data in the stud force tables are reported for the peak load time step. When gages fail before peak load, forces in all studs are calculated at the last time step where all strain gages have data. The applied force used for comparison to the stud force is taken from the same time step as the stud gage strains. For reference, the line for applied force equaling stud force (in black) is shown on all graphs. All shear stud gages are numbered consecutively from one side of the specimen to the other, either down the WT web for longitudinal spacings or across the WT web for transverse spacings. On all stud force plots, studs begin to acquire significant force only after a certain applied load is reached. This load is the specimen's first cracking load. Prior to cracking, stud friction and steel-concrete bond with the WT allow the load to be applied directly to the concrete through the WT and not in bearing by the shear stud head. The strain gage is embedded near the top of the stud and only measures strains from forces transferred in bearing above it. The majority of the load transfer from friction occurs below the strain gage, as shown in Figure 4.14, and is not measured. Once the first crack forms in the specimen, steel-concrete bond is lost and the load is transferred by bearing under the heads of the studs, creating a characteristic bend in stud force plots. After cracking, a portion of the load is still transferred by steel-concrete friction, resulting in forces calculated from the shear stud strain gages being less than the applied

load. All stud force plots show the same disturbances found in load-displacement plots because of load pauses. In stud force plots, these disturbances resemble V-shaped indentations or overlapping sections of the curve.

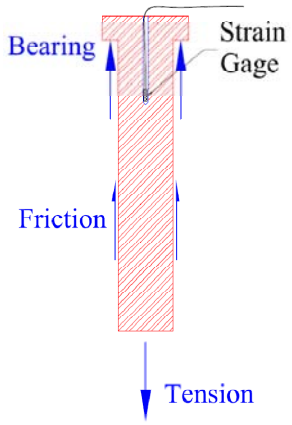

Figure 4.14: Forces and Friction Transfer on a Shear Stud

Specimens with No Haunch

Single-stud specimens without a haunch do not have strain gages installed in them because single stud tests by Sutton (2007) showed that the majority of the applied force is carried in tension by the single shear stud. For all specimens, the sum of the forces measured in the studs is less than the applied force, as shown in Table 4.3. The portion of the applied load not measured by the stud gages in Table 4.3 is transferred in shear by steel-concrete friction around the shaft of the stud. The footnote for table 4.3 notes that the sum of stud forces in specimen 5:0-4Lb just before peak load is different from the sum at peak load. This change occurs when failure cracks begin to form around the studs, eliminating the studs' friction action with the concrete.

Table 4.3: Series II Specimens, No Haunch, Comparison of Stud and Applied Forces

Specimen	Stud Location	Strain (in/in)	Stress (ksi)	Force (kips)	% Total Stud Force	Total Stud Force (kips)	Applied Force (kips)	% Difference
5:0-2La	**Both Gages Failed**							
5:0-2Lb	Left	0.000828	24.01	14.44	51.8%	27.90	28.06	-0.57%
	Right	0.000772	22.39	13.46	48.3%			
5:0-3La	Left	0.000403	11.69	7.03	32.3%	21.76	22.83	-4.67%
	Center	0.000385	11.17	6.71	30.8%			
	Right	0.000460	13.34	8.02	36.9%			
5:0-3Lb	**Gage Failed**							
5:0-4La	Outer Left	0.000348	10.09	6.07	22.2%	27.40	28.59	-4.18%
	Inner Left	0.000437	12.67	7.62	27.8%			
	Inner Right	0.000441	12.79	7.69	28.1%			
	Outer Right	0.000345	10.01	6.02	22.0%			
5:0-4Lb†	Outer Left	0.000398	11.54	6.94	24.1%	28.76	28.97	-0.74%
	Inner Left	0.000479	13.89	8.35	29.0%			
	Inner Right	0.000446	12.93	7.78	27.0%			
	Outer Right	0.000326	9.45	5.68	19.8%			

†immediately prior to final cracking at peak load, % difference between stud and applied forces is -8.3%

For specimens with two studs spaced longitudinally without a haunch, stud forces are distributed nearly equally between the two studs, as shown by Figure 4.15. Stud data for the two-stud specimens comes solely from specimen 5:0-2Lb because both stud gages in specimen 5:0-2La malfunctioned.

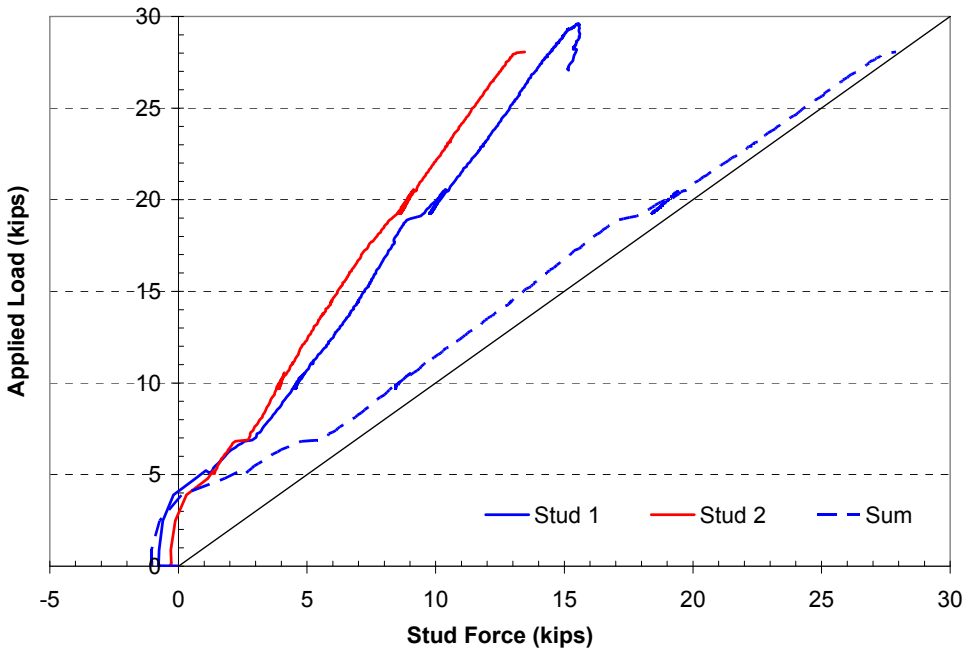

Figure 4.15: Applied Force vs. Stud Force, Two Studs No Haunch

For specimens with three studs, forces are again distributed nearly equally among all three studs (particularly during the early stages of response), as shown in Figure 4.16. Both specimens show a very good correlation between measured peak stud forces and applied forces, with less than 5% of the applied load transferred by friction and not measured by the stud gages.

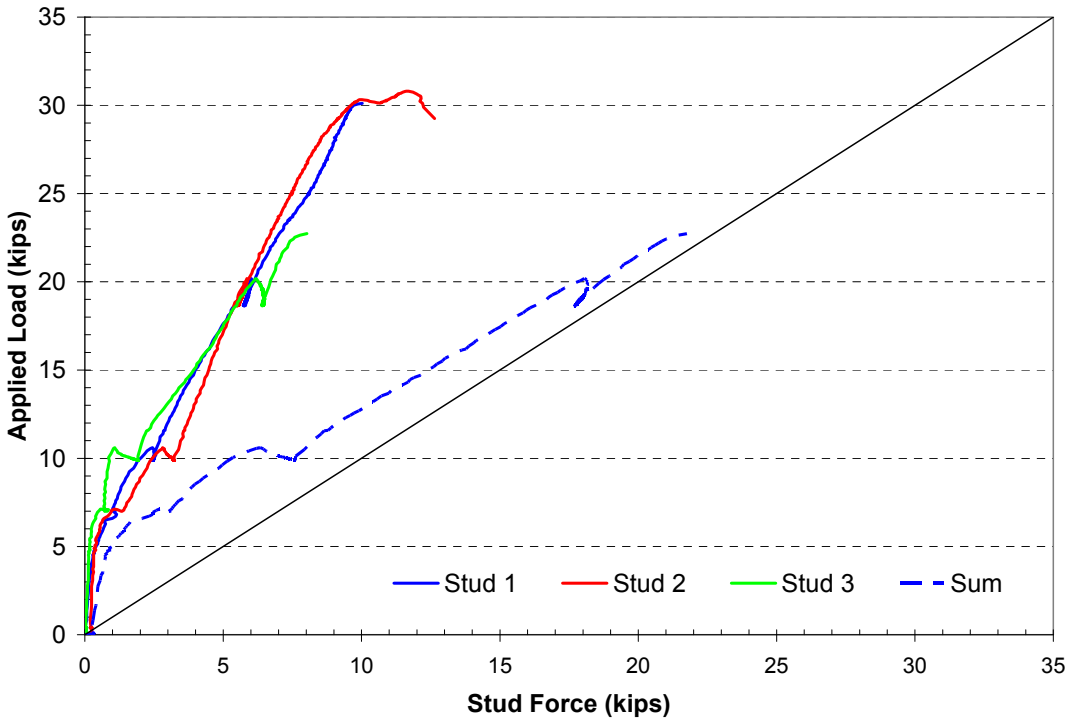

Figure 4.16: Applied Force vs. Stud Force, Three Studs No Haunch Specimens

For specimens with four studs spaced longitudinally, the outer two studs (Studs 1 and 4) typically carry more force than the inner two studs (Studs 2 and 3), up to 60% more as shown in Figure 4.17. Each set of inner and outer studs carry roughly the same force. The force distribution evens out among all four studs as the applied load approaches its maximum. The reduction of force in the outer studs is most likely due to cracking near the edge of the concrete. As noted in the footnote of Table 4.3, specimen 5:0-4Lb has a difference between measured stud and applied load of 8.3% just before peak load. The difference of 8.3% at peak load is typical of the other specimens. Specimen 5:0-4L, the replicate specimen, had a difference of 4.8%.

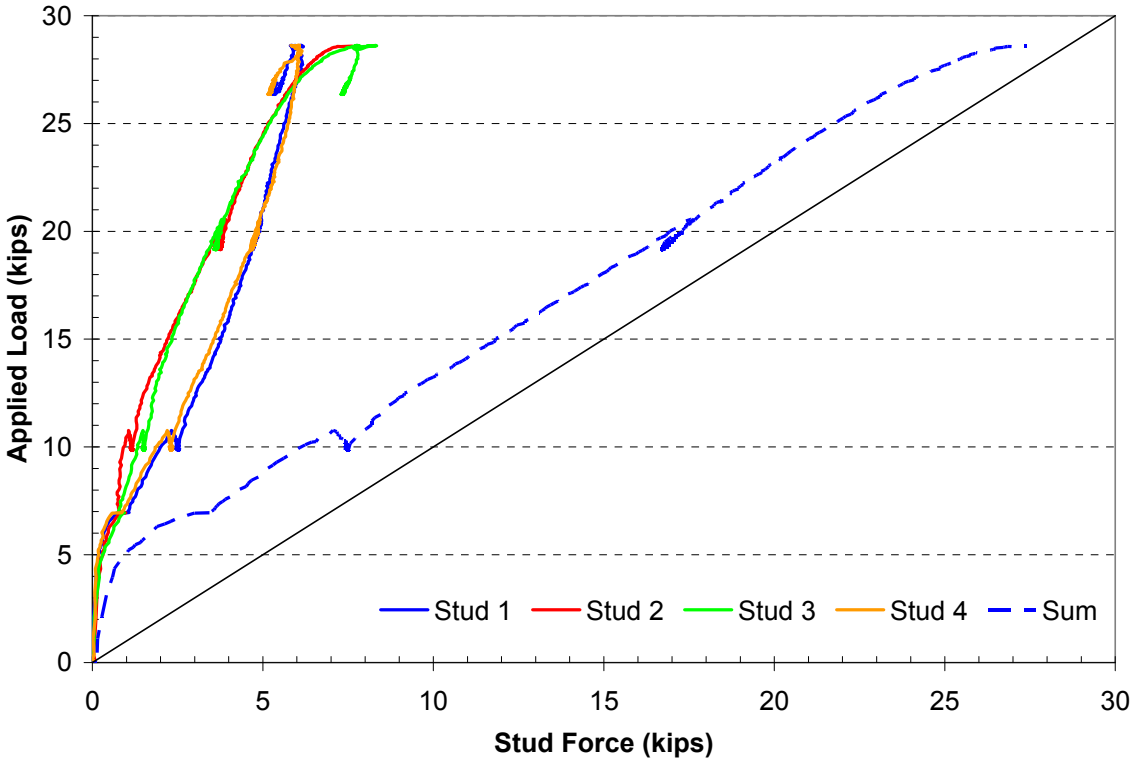

Figure 4.17: Applied Force vs. Stud Force, Four Studs No Haunch Specimens

Specimens with a Haunch

Several stud strain gages in two-stud specimens with a haunch malfunctioned, limiting the available data. The data for all functioning gages are summarized in Table 4.4.

Table 4.4: Series II Specimens, 3-in Haunch, Comparison of Stud and Applied Forces

Specimen	Stud Location	Strain (in/in)	Stress (ksi)	Force (kips)	% Total Stud Force	Total Stud Force (kips)	Applied Force (kips)	% Difference
5:3-2La	**Gage Failed**							
5:3-2Lb	**Both Gages Failed**							
5:3-3La	Left	0.000399	11.57	6.96	27.0%	25.77	31.63	-18.51%
	Center	0.000529	15.34	9.22	35.8%			
	Right	0.000550	15.95	9.59	37.2%			
5:3-3Lb	Left	0.000636	18.44	11.09	35.5%	31.25	31.12	0.42%
	Center	0.000621	18.01	10.83	34.7%			
	Right	0.000535	15.52	9.33	29.9%			

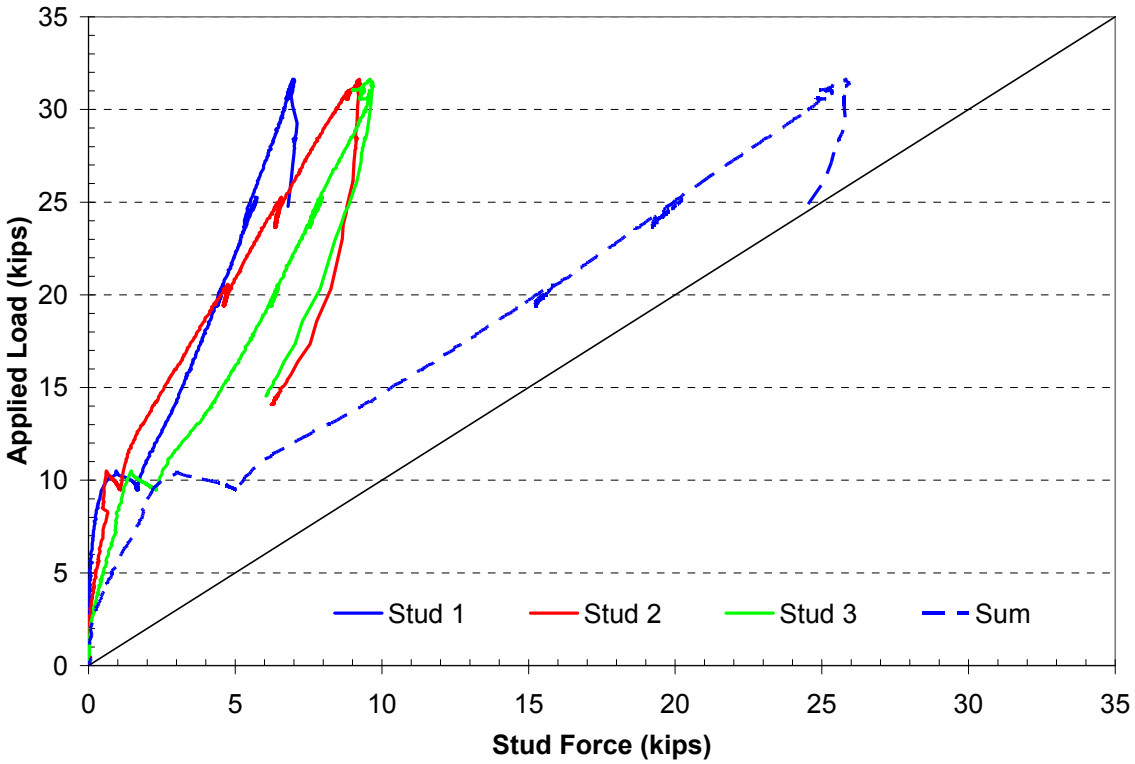

Figure 4.18: Applied Force vs. Stud Force, Three Studs 3-in Haunch Specimens

For three-stud specimens with a haunch, load distribution among the studs is not equal, as shown in Figure 4.18. The reason for the variation in force among the three studs is unclear. The sum of the stud forces for specimen 5:3-3La, as shown in Table 4.4, is considerably less than the applied peak load. This large difference is typical of most specimens with a haunch where the concrete around the studs remains uncracked throughout the test. Uncracked concrete does not lose the concrete-steel bond that reduces measured stud forces. Specimen 5:3-3Lb is an exception to this pattern and shows a stud force equal to the applied peak load because of eccentric pullout. Eccentric pullout creates prying action in the specimen (prying action is discussed in Section 4.3.3.4, below), resulting in increased stud forces.

4.3.4 Reinforcing Steel Gage Data

Concrete Slab Predicted Behavior

The strain gages placed on the rebar provide data on how the slab portion of the specimen behaved during a test. Three critical points in the slab analysis are first cracking in the specimen, yield of the tensile reinforcement, and ultimate strength of the slab. These points, calculated using beam theory, allow the slab to be checked for conformance to simple beam bending behavior.

The specimen is treated as a simply supported beam with a point load at midspan. By idealizing the bearing pads as pins at the center of the pad, a span of 6 ft-6 in is obtained. Self-weight of the specimen is small compared to the applied load and is neglected. The peak moment in the specimen at the location of the point load is $PL/4$, as determined by equilibrium, where P is the applied load and L is the span. For specimens with a haunch, the increased slab thickness reduces stresses in the haunch. The stress reduction moves the critical section to the edge of the haunch, 6-in from slab midspan. For the assumed slab span, the moment at the critical section is $11PL/52$. Given these relationships, moments at the three critical stages of slab behavior can be converted into loads for data comparison.

The design dimensions for the specimens are used in the analyses presented below. Slab thickness is 8 in, with the effect of the haunch neglected for purposes of calculating slab stiffness. The haunch is neglected because it only extends over a short section of the total span. The width is 24 in, and the depths from the top of the slab to the top and bottom mats of reinforcement are 2-5/16 in and 6-7/16 in, respectively. All flexural #5 rebar is assumed to have a cross-sectional area of 0.31 in^2. Rebar yield strength is taken as 60 ksi, the minimum value of yield for the rebar. For Series II, concrete compressive strength is taken as 7.5 ksi, the mean value of all the compression cylinder tests (see Section 4.2.6).

The cracking tensile stress of the concrete in flexure is taken as 7.5 times the square root of the compressive strength, as per ACI 318-08. Given this value of stress, the cracking moment in the slab is found by Equation 4.1 below:

$$M_{cr} = \frac{\sigma_{cr} I}{c} = \frac{7.5\sqrt{f_c'}\, I}{c} \qquad \text{Equation 4.1}$$

where:
- M_{cr} = cracking moment (lb-in.)
- σ_{cr} = cracking tensile stress of concrete (= 650 psi)
- I = gross moment of inertia of the slab (= 1024 in^4)
- c = distance from neutral axis to extreme stress (= 4 in)
- f'_c = concrete compressive strength (= 7,500 psi)

Using Equation 4.1 and the values listed, the cracking moment is calculated as 166 kip-in. Using the statics relationships already described, the cracking load for specimens without a haunch is 8.5 kips. For specimens with a haunch, the load to cause cracking at the haunch edge is 10.1 kips.

The next critical point in the slab is first yield of the tensile reinforcement. At first yield, the concrete stress block is assumed to obey Hook's Law for stresses below 70% of the concrete compressive strength. The modulus of elasticity is taken as 57 times the square root of the compressive strength, as recommended by ACI 318-08. An illustration of the stress and strain diagrams on the section at first yield is shown in Figure 4.19. The value c is the distance from the top of the slab to the neutral axis. The top mat of reinforcement is initially assumed to be in tension. By setting the forces in the steel equal to the forces in the concrete, Equation 4.2 is derived:

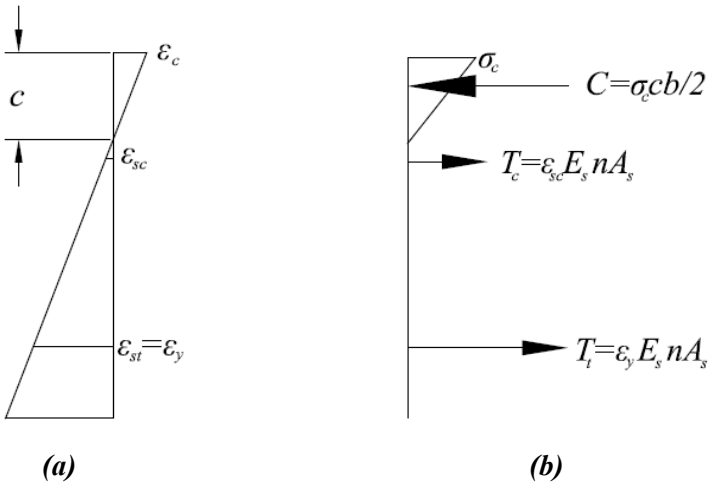

Figure 4.19: Slab (a) Strain and (b) Stress at First Yield

$$nA_s E_s \frac{\varepsilon_y (d_c - c)}{(d_t - c)} + nA_s E_s \varepsilon_y = 57\sqrt{f'_c}\,\frac{c}{(d_t - c)}\frac{cb}{2} \qquad \text{Equation 4.2}$$

where:

n	=	number of rebars in one mat of reinforcement (= 4)
A_s	=	area of a single rebar (= 0.31 in^2)
E_s	=	modulus of elasticity of steel (= 29,000,000 psi)
ε_y	=	yield strain of rebar (= 0.00207 in/in)
d_t	=	depth from top of slab to bottom rebar (= 6.44 in)
d_c	=	depth from top of slab to top rebar (= 2.31 in)
c	=	depth of neutral axis (in)
f'_c	=	compressive strength of concrete (=7500 psi)
b	=	width of slab (= 24 in)

Solving this equation for c provides the location of the neutral axis, allowing the forces in the concrete and both mats of reinforcement to be calculated. Once these forces are determined, the yield moment in the slab is calculated by summing moments about the neutral axis. For Series II specimens, this moment is 439 kip-in, giving a yield force of 22.5 kips for specimens without a haunch. For specimens with a haunch, the force needed to reach the yield moment at the haunch edge is 26.6 kips.

Ultimate moment in the slab is calculated using the Whitney stress block method recommended by ACI 318-08 and shown schematically in Figure 4.20. The concrete compression stress is taken as 0.85 times the compressive strength. The depth of the stress block is a, equal to $\beta_1 c$, where c is the distance to the neutral axis and β_1 is a coefficient based on the compressive strength of the concrete, defined in ACI 318-08. The tensile mat of reinforcement is assumed to be yielded with strains in the yield plateau. This assumption makes rebar stress equal to yield, taken as the minimum 60 ksi for analysis. The maximum concrete strain is taken conservatively as 0.003 in/in by ACI 318-08, though in certain circumstances it can be higher. The force in the top mat of steel is based on its strain from the strain gradient. By setting the compression force in the concrete equal to the tension forces in the steel, Equation 4.3 is derived:

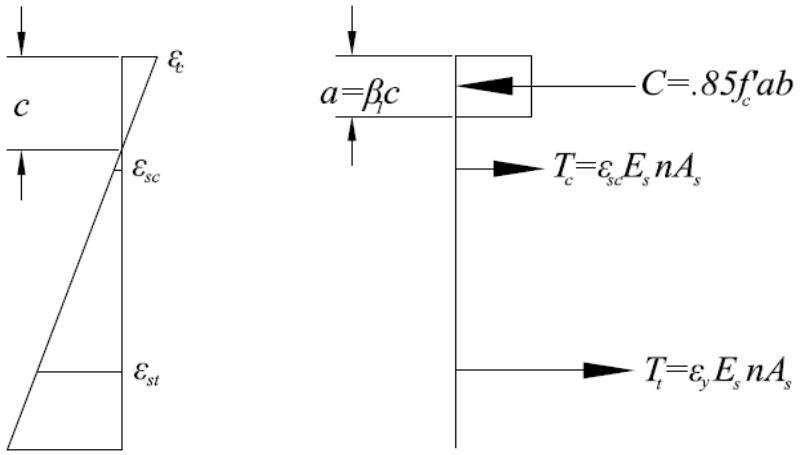

Figure 4.20: Slab (a) Strain and (b) Stress at Ultimate Moment

$$\varepsilon_c \frac{(d_c - c)}{c} E_s n A_s + E_s \varepsilon_y n A_s = 0.85 f'_c b \beta_1 c \qquad \text{Equation 4.3}$$

where:
- ε_c = maximum concrete strain (= 0.003 in/in)
- d_c = depth from top of slab to top rebar (= 2.31 in)
- c = depth of neutral axis (in)
- E_s = modulus of elasticity of steel (= 29,000,000 psi)
- n = number of rebars in one mat of reinforcement (= 4)
- A_s = area of a rebar (= 0.31 in^2)
- ε_y = yield strain of rebar (= 0.00207 in/in)
- f'_c = compressive strength of concrete (=7500 psi)
- b = width of slab (= 24 in)
- β_1 = width of slab (= 0.68 for f'_c=7.5 ksi)

By solving this equation for *c,* the location of the neutral axis and the forces in the concrete and each mat of steel can be computed. Once these forces are found, summing moments about the neutral axis gives the ultimate moment, which for Series II specimens is 573 kip-in. By statics, this moment gives an ultimate load of 29.4 kips for specimens without a haunch. For specimens with a haunch, the load to create the ultimate moment at the haunch edge is 34.7 kips. Shear failure must also be considered at ultimate load, but for the given test specimen geometry and range of compressive strengths, it does not govern. A summary of the critical slab points for Series II is given in Table 4.5.

Table 4.5: Series II Slab Critical Loads

Slab State	Moment (kip-in)	Load (kips), No Haunch	Load (kips), 3-in Haunch
Cracking	166	8.5	10.1
First Yield	438	22.5	26.6
Ultimate Strength	573	29.4	34.7

Specimens with a Haunch

All four specimens with a haunch show limited rebar yielding and very little inelastic behavior. Only one of the four tests, specimen 5:3-3Lb, shows significant yielding of the bottom mat of rebar, even though all four tests have peak loads well above the predicted yield load. Specimen 5:3-3La appears on the verge of yielding rebar when its horizontal crack develops, reducing overall specimen strength and strains in the rebar. All four tests show stresses among individual bars of a given mat are similar during the loading process.

Figure 4.21 shows the load-strain plot typical for both two-stud and three-stud haunch specimens. Gages labeled “T” refer to top mat reinforcing, and gages labeled “B” refer to the bottom mat of reinforcing. This nomenclature is typical for all rebar-strain graphs. The plotting of the strain gage data is terminated when a gage output either ceases or becomes erratic due to damage in the lead wires. Because failure cracks frequently damage the lead wires, very little of the descending load branch for many tests is captured. Yield of the rebar is marked by a bold vertical line on the plot at 0.00207 in/in, the steel strain corresponding to 60 ksi yield. A gage omitted from a graph means it did not function. Cracking load is indicated by a sharp change in the slope of the load-strain curves when the cracked concrete begins to actively utilize the rebar. All four haunch specimens have a cracking load between 8.0 and 9.0 kips, lower than anticipated for haunch specimens. Of note in Figure 4.21 is that, prior to cracking, all four top mat bars are in compression. After the cracking load, the top bars rapidly go into tension as the neutral axis of the slab moves above the top mat of reinforcing.

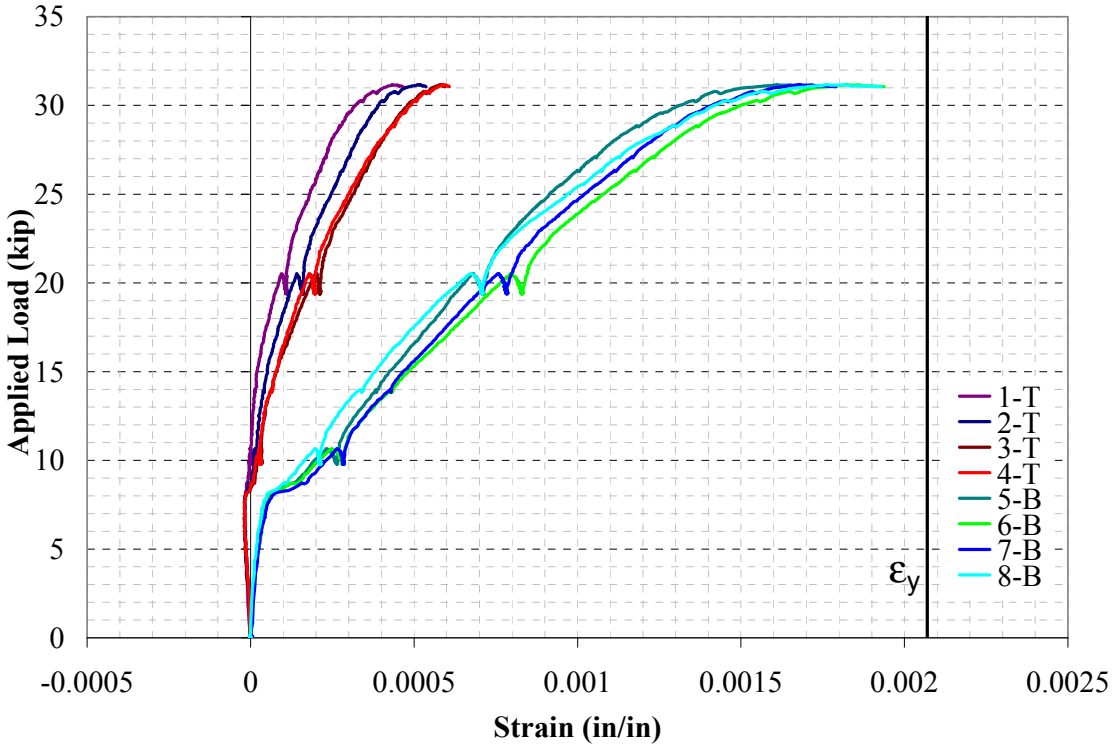

Figure 4.21: Applied Load vs. Rebar Strain for 3-in Haunch Specimens

Specimens with no Haunch

Specimens without a haunch show a distinct difference in rebar strain behavior depending on the number of studs in the specimen. Single-stud specimens show no yielding of the rebar, while specimens with more than one stud show substantial yielding and slab deformation.

The load-rebar strain plot for a single stud without a haunch is shown in Figure 4.22 and looks very similar to that of a specimen with a haunch. Cracking occurs at 8.0 kips, close to the predicted value. Rebar strains are just below yield at peak load. This behavior corresponds well to predicted behavior, with the specimen's peak strength, 20.5 kips, just below the predicted yield load of 22.5 kips. After peak load, all the rebar begins to lose strain rapidly. All strains in top bar mats are nearly identical during loading, while bottom mat bars show slight variations in strain for a given load, most likely due to uneven engagement of the rebar by the stud failure cone.

All specimens with more than one stud spaced longitudinally without a haunch have similar load-rebar strain plots, represented by Figure 4.23. Cracking load varies between 7.0 and 9.0 kips, depending on the specimen. During loading, all of the bars in each mat of reinforcement have similar strains. The bottom mat of reinforcement begins to yield just prior to peak load. Shortly after yielding, the bottom bars experience large increases in strain with little increase in load as failure occurs. After peak load, all reinforcement begins to lose strain with decreasing load.

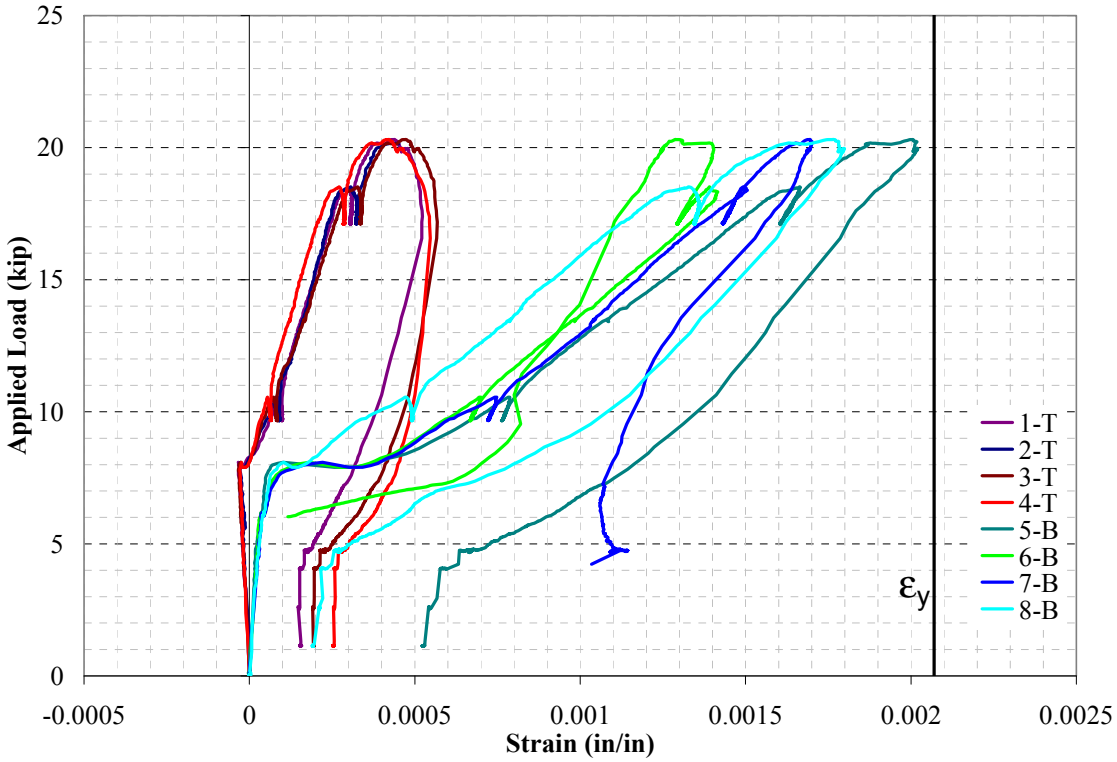

Figure 4.22: Applied Load vs. Rebar Strain for No-Haunch Specimens with One Stud

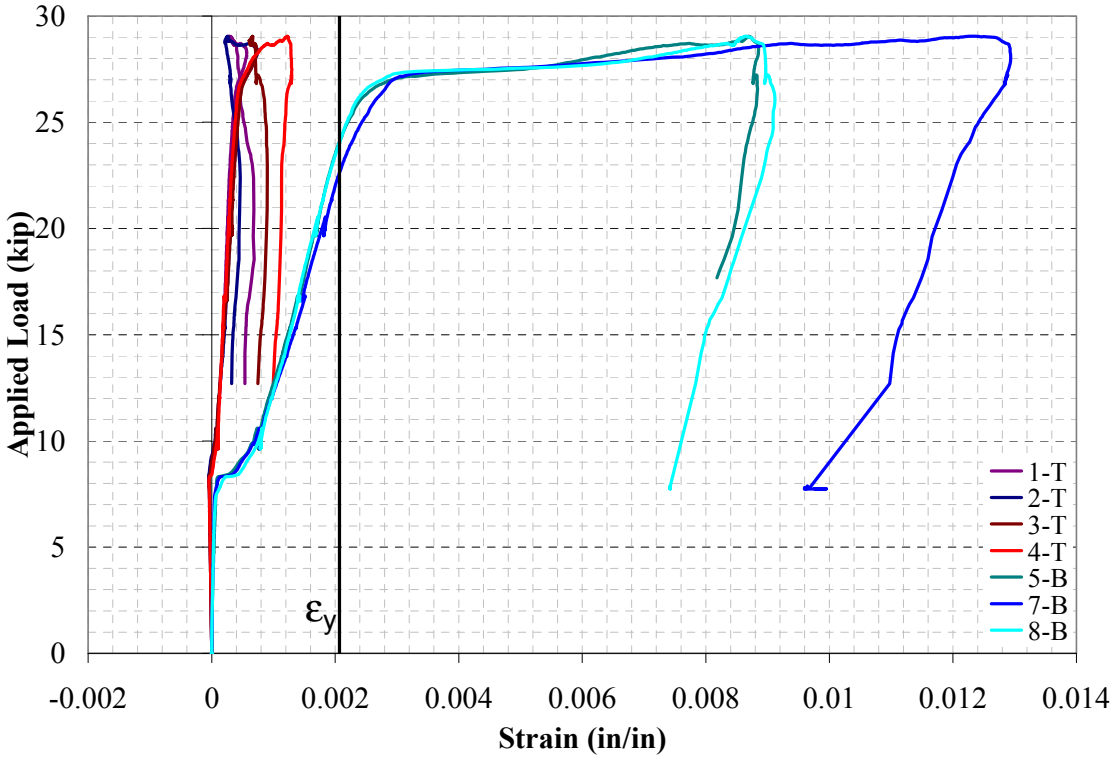

Figure 4.23: Applied Load vs. Rebar Strain for No-Haunch Specimens with Two or More Studs

4.3.5 Slab Deflection

Slab midspan deflection, like rebar strain gages, provides a measure of concrete slab response during specimen tests. Slab behavior for all specimens is very similar prior to peak loading. After peak loading, slab behavior is determined by the presence or lack of a haunch; Figure 4.24 illustrates the load-deflection plots for both cases. All specimens show a similar steep initial stiffness, indicating uncracked concrete flexure in the slab. The sharp change in slope comes at first flexural cracking. For all specimens, the cracking load indicated by slab deflection corresponds very closely with the cracking load indicated by rebar strains. After cracking, the specimens all have a similar low stiffness and maintain this stiffness until the load approaches its peak value.

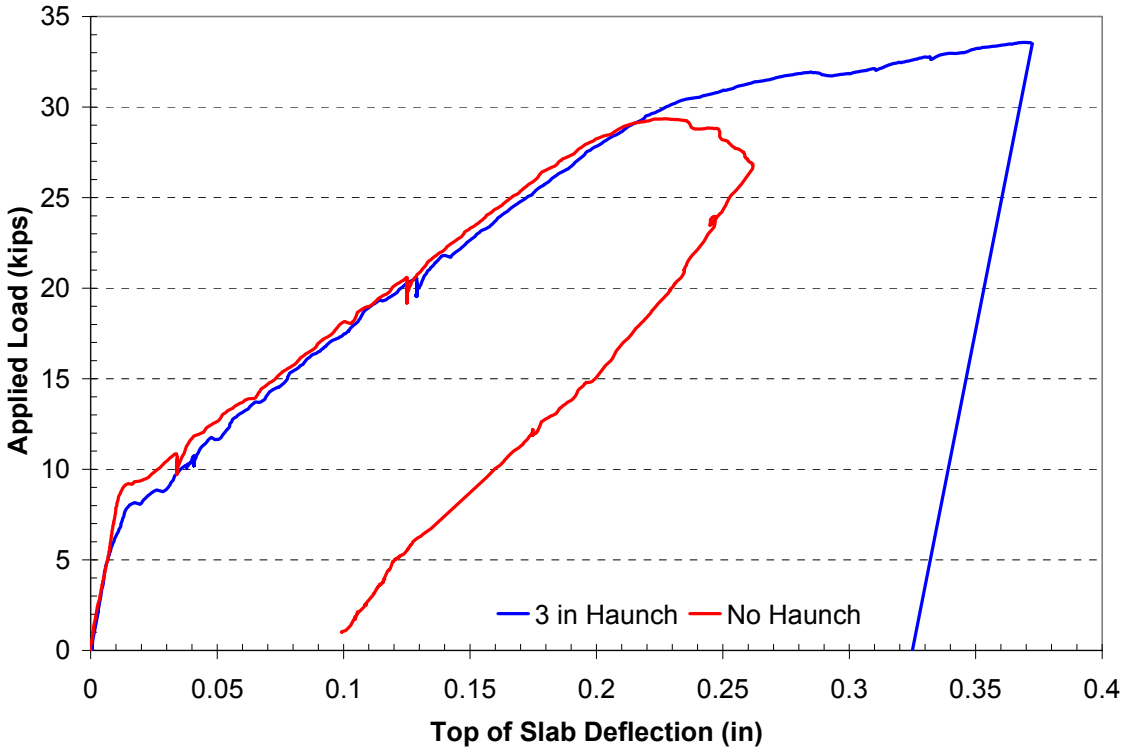

Figure 4.24: Applied Load vs. Slab Deflection for Series II Specimens

For specimens without a haunch, slab stiffness is at or near zero at peak load. After peak load, the slab deflection decreases rapidly as the WT and studs pull away from the slab. Deflections at peak load are typically between 0.25 and 0.40 in, with the exception of the single-stud specimens with peak deflections around 0.20 in. Typically, most specimens have a permanent deflection in the slab after the test due to the missing concrete pulled out by the studs. Specimen 5:0-4b, whose load-deflection plot is shown in Figure 4.25, has a variation of the typical permanent deck deflection. Arching of the top rebar causes negative deflections in the slab of this specimen as shown in Figure 4.26. Arching occurs when the bottom mat of reinforcing draws down with the studs after development of the failure cone, pulling the ends of the specimen toward each other and causing the top rebar mat to deflect upwards.

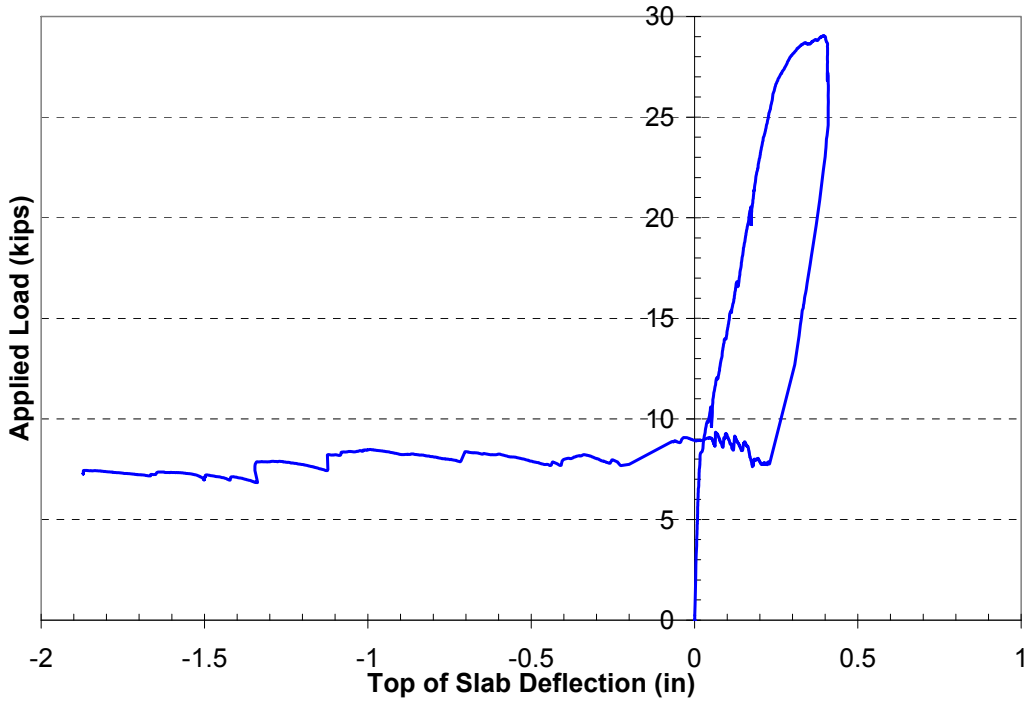

Figure 4.25: Applied Load vs. Slab Deflection for Specimen 5:0-4Lb

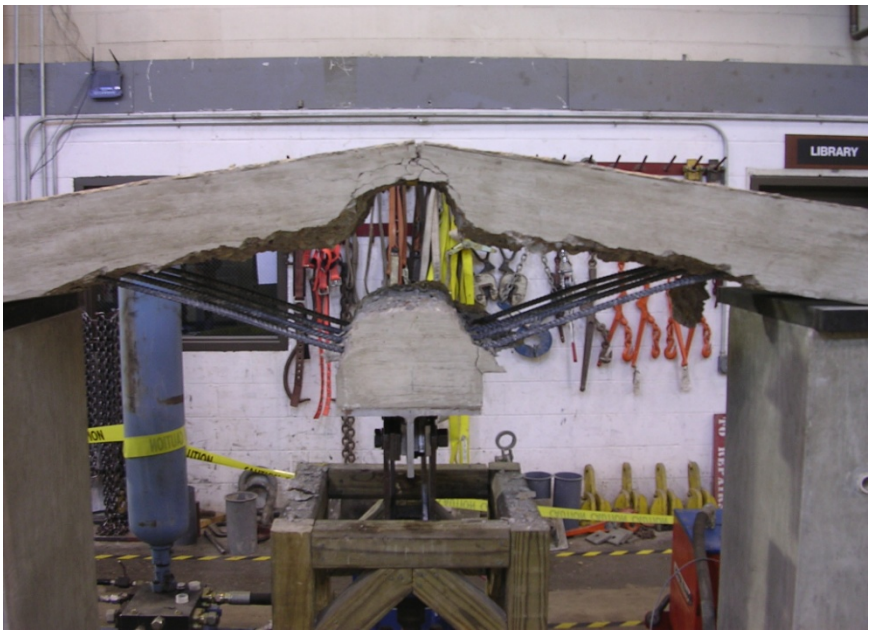

Figure 4.26: Specimen Showing Significant Arching

Specimens with a haunch behave similarly to specimens without a haunch until peak load. At peak load, a specimen's haunch separates and the slab rebounds, with all specimens having a permanent slab deflection. The single exception to this observed behavior is specimen 5:3-3La, which behaves similarly to specimens without a haunch because of rebar-stud interlock. Peak load deflections for all haunch specimens, similarly to specimens without a haunch, are between 0.25 and 0.40 in.

4.3.6 Concrete Cylinder Tests

As described in Chapter 3, compressive and split cylinder tensile tests were performed on 6-in by 12-in concrete cylinders cast as part of each series pour. The cylinders were tested at the beginning, middle (after six specimens were tested), and end of each series. The results from these tests are summarized in Table 4.6. The concrete compressive strength for Series II is much higher than the required minimum compressive strength of 4.0 ksi. The tensile strength of the concrete corresponds well to ACI standard values of concrete tensile strength between 4 and 6 times the square root of the compression strength.

Table 4.6: Series II Concrete Test Data

Compression Tests		**Split Cylinder Tensile Tests**		
Days after Casting	Mean Compressive Strengh, f'_c (psi)	Days after Casting	Cracking Tensile Strength, f_t (psi)	$f_t/\sqrt{f'_c}$
28	7,347	35	433	5.0
35	7,550			
41	7,520			

Series Mean Strength: 7.5 ksi

4.4 Series III Results — Taller Studs and Eccentric Loading

4.4.1 Strength

Data collected from Series I and Series II show that, depending on spacing, studs in a haunch can develop greater strength than without a haunch, and studs without a haunch but engaging the bottom mat of reinforcement have considerable ductility. Using taller studs than the 5-in standard combines these two trends to create studs in a haunch that engage the reinforcement, providing both strength and ductility. Seven-inch and nine-inch studs were tested in a 3-in haunch, spaced both transversely and longitudinally. A 7-in stud in a 3-in haunch has the same height penetrating the slab as 4-in studs in a slab without a haunch. A 9-in stud in a 3-in haunch has the same height in the slab as 6-in stud in a slab without a haunch. The heads of both 7-in and 9-in studs were above the bottom mat of reinforcement. Two 5-in stud specimens with three studs spaced longitudinally were also eccentrically tested, with the load applied 6 in off center to examine the ability of longitudinal stud groups to redistribute load. Strengths for all Series III tests are shown in Table 4.7.

Table 4.7: Peak Strengths of Series III Specimens

Number of 7-in Studs	Configuration	Peak Strength (kips)	Number of 9-in Studs	Configuration	Peak Strength (kips)	Eccentric Loading, Three Longitudinal Studs	Peak Strength (kips)
1		26.2	1		28.4	No Huanch	22.1
2	Longitudinal	27.2	2	Longitudinal	29.5	3-in Haunch	19.6
3	Longitudinal	28.3	3	Longitudinal	30.0		
2	Transverse	25.1	2	Transverse	27.7		
3	Transverse	20.3	3	Transverse	31.4		

The strengths of taller studs spaced longitudinally follow the same trend as 5-in studs in Series II without a haunch as shown in Figure 4.27. The single taller stud has higher strength than a single 5-in stud without a haunch (24% in the case of 7-in studs and 34% in the case of 9-in studs) because of the uncracked concrete effect from the haunch. With two studs or more, the strengths of the 5-in and 9-in studs are very similar (two 9-in studs are 0.3% less strong than 5-in studs, and three 9-in studs are 3.0% less strong). This similarity is attributable to the similar failure cones both cases develop. Seven-inch

studs are effectively shorter than the 5-in studs due to the 3-in haunch and do not develop as large a failure cone, resulting in slightly reduced strengths (two 7-in studs are 8.0% less strong than using 5-in studs, and three 7-in studs are 8.5% less strong than three 5-in studs). Nine-inch studs have almost exactly the same strength increase over 7-in studs for all numbers of studs, 8.4%, except in the case of three studs, where the increase is 6.1%.

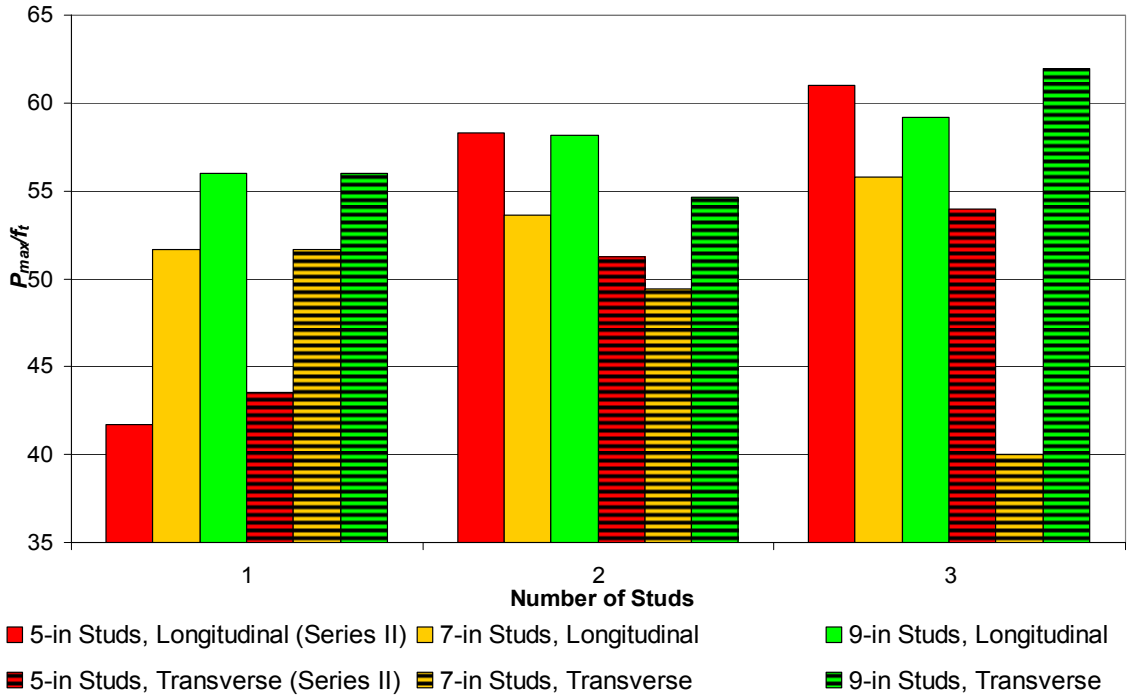

Figure 4.27: Normalized Peak Strength vs. Number of Studs for Series III Specimens

The strength trend for taller studs spaced transversely changes as stud height increases, as seen in Figure 4.27. The strengths of 7-in studs spaced transversely are lower than for 7-in studs spaced longitudinally. The strengths of the 9-in studs spaced transversely are similar to longitudinally spaced 9-in studs. The 7-in tall studs reflect the previously established behavior of studs spaced transversely in a haunch. The initial strength for a single 7-in stud is high (20% over a 5-in stud without a haunch), while strength is rapidly lost as studs are added because of the edge effect in the haunch (a 4% decrease for two 7-in studs and 23% decrease for three 7-in studs).

The behavior for the 9-in studs spaced transversely is similar to transverse 5-in studs without a haunch. The strength of two 9-in studs increases 6% over 5-in studs, and increases 17% in the case of three studs. Based on the limited test data, the two 9-in stud specimen strength is believed to be low for this series. The two 9-in stud case has a strength less than a single 9-in stud (2.4% lower), when a value higher than the single-stud case is expected based on the 5-in stud trend. It is unclear why the two-stud specimen has such a low strength.

For the eccentric tests, there is a significant difference in strength between the specimens with and without a haunch, as shown in Table 4.8. Eccentric loading reduces the strength of both specimens compared to the concentrically loaded tests, with the haunch specimen showing a very significant reduction. Five-inch studs without a haunch show a 29% decrease in strength over the same concentrically loaded specimen. The 5-in studs with haunch show a 42% decrease in strength over the same specimen concentrically loaded.

Table 4.8: Peak Strengths of Specimens with Three 5-in Studs Spaced Longitudinally

Loading	Strength, No Haunch (kips)	Strength, 3-in Haunch (kips)
Concentric	30.1	32.6
Eccentric	22.1	19.6

4.4.2 Behavior at Failure

For all concentrically loaded specimens in Series III, normal flexural cracking occurs first during loading, with the first flexural cracks forming at the edges of the haunch. Breakout cracking patterns and failure mode are determined by whether the shear stud failure cone engages the bottom mat rebar (ductile, group failure) or is only plain concrete (brittle separation failure).

Specimens with Studs Spaced Transversely

For taller studs spaced transversely in a haunch, stud height has a significant effect on the load-displacement behavior, as shown in Figure 4.28. Tall, 9-in studs are able to engage the rebar, supporting higher loads at larger displacements and resulting in more ductility than 7-in or 5-in studs. The 7-in studs are not tall enough to develop a failure cone intersecting the bottom rebar mat.

Because the pullout cone did not engage the rebar, all the 7-in stud specimens have a rapid decrease in strength after peak load, showing only limited ductility. For 7-in stud specimens, just after peak load, a horizontal crack appears on the side face of the concrete specimen near the level of the bottom mat of reinforcement, growing rapidly to cross the haunch (Figure 4.29(a)). At the same time, a vertical crack in the haunch occurs at the center of the slab, splitting the haunch into two pieces (Figure 4.29(b)). As displacements increase, these two split pieces of haunch rotate down with the WT, and the shear stud pullout cone develops on the underside of the slab (Figure 4.29(c)). Specimens reach peak load at displacements between 0.02 and 0.04 inches, with an increasing number of studs decreasing the displacement at peak load.

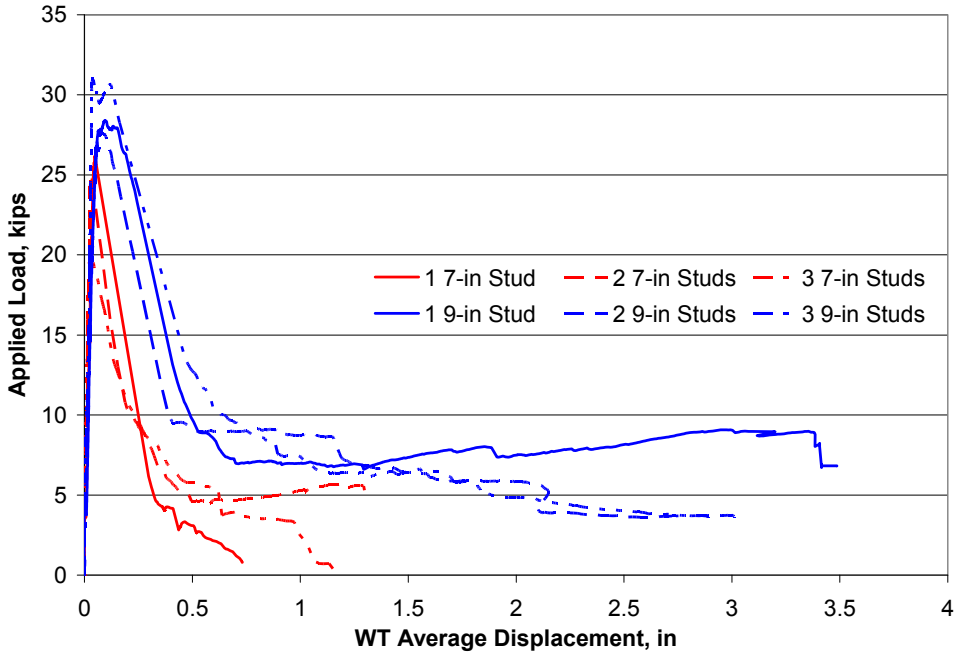

Figure 4.28: Load-Deflection Plots for Specimens with Tall Studs Spaced Transversely

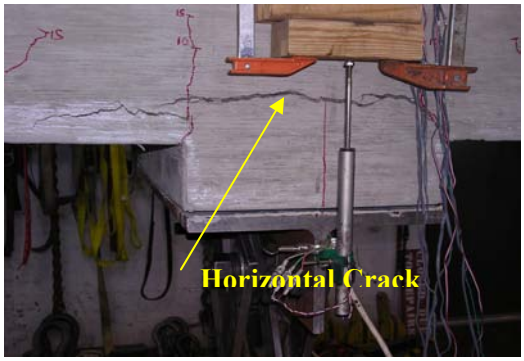

(a)

(b)

(c)

Figure 4.29: Failure Sequence for 7-in Studs Spaced Transversely (a) Horizontal Crack Formation (b) Haunch Splitting (c) Split Haunch with Failure Cone

Nine-inch studs in a 3-in haunch are tall enough to engage the bottom rebar with their pullout cones, creating considerably more post-peak strength and ductility than with 7-in studs. Just after peak load, a horizontal crack forms on the side of the specimen near the level of the top mat of reinforcing. This crack quickly grows and turns downwards until it reaches the bottom mat of reinforcing, creating a ridge of concrete around the studs (Figure 4.30(a)). As the studs continue to displace, the horizontal crack grows, often until it reaches the ends of the specimen. Under larger deflections, the WT, studs, and ridge of concrete hang from the exposed bottom rebar, which shows considerable bending, as shown in Figure 4.30(b). The development of this ridge of uncracked concrete around the studs provides an intact load path between the rebar supporting the WT and the shear studs. This load path allows for substantial loads, on the order of 7 kips, to be carried by the specimens, even at very large displacements (exceeding 2.5 in).

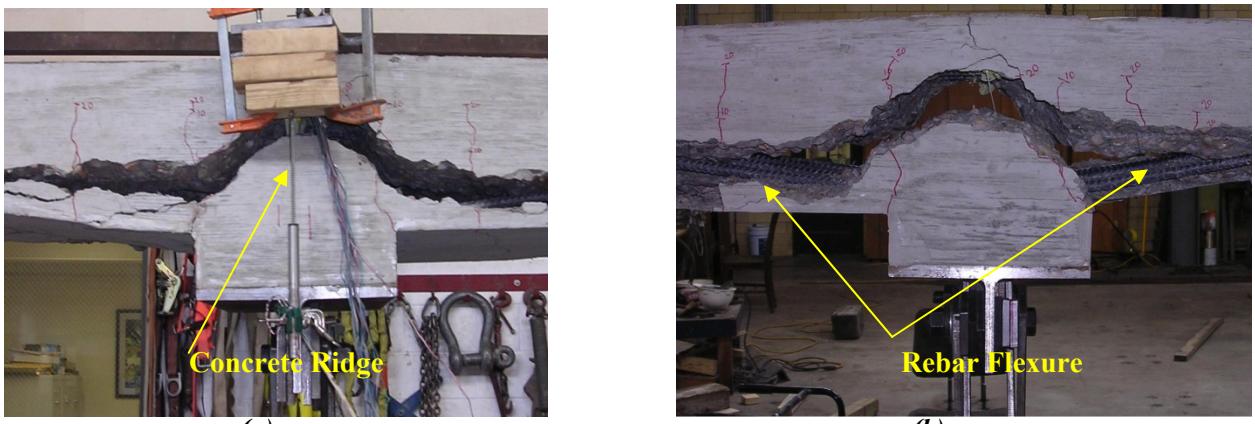

(a) ***(b)***

Figure 4.30: Failure Sequence for 9-in Studs Spaced Transversely (a) Horizontal Crack forming Concrete Ridge (b) Rebar Supporting WT

Specimens with Studs Spaced Longitudinally

Tall studs spaced longitudinally in a 3-in haunch very consistently show significant post-peak strength at large deflections, as shown by Figure 4.31. This ductility significantly exceeds the ductility of all specimens with 5-in studs. Nearly all longitudinally spaced studs, 7-in or 9-in, have similar cracking and failure behavior. The haunch remains intact and uncracked for all of the longitudinal specimens except 7:3-1, which behaves like 7-in studs spaced transversely. The single 7-in stud specimen has a splitting failure at the center of the haunch and has a rapid loss in strength after peak load. Just after peak load, a horizontal crack forms on the edges of the specimen near the height of the stud head. The crack rapidly grows horizontally and downwards to the bottom mat of reinforcing to form the same ridge of concrete as seen in 9-in stud transversely spaced specimens. As displacements increase, the horizontal crack grows, often to the ends of the specimen. Concrete on the bottom face of the slab spalls as the rebar begins to flex. The rebar continues to bend and support a substantial load, between 6 and 8 kips, until the end of the test. Peak load occurs at displacements of 0.02 to 0.06 in, with an increasing number of studs decreasing the displacement at peak load.

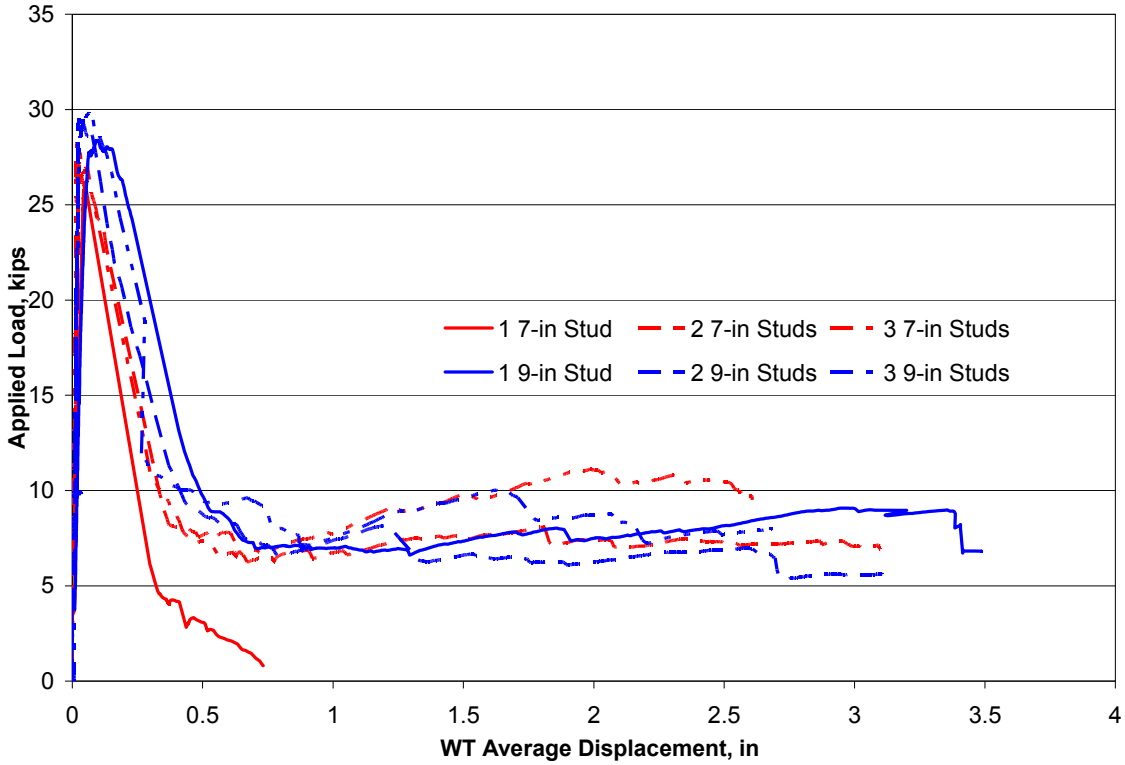

Figure 4.31: Load-Deflection Plots for Specimens Tall Studs Spaced Longitudinally

Specimens Loaded Eccentrically

The two eccentrically loaded specimens show very different load-displacement plots from one another depending on if a haunch is present or not, as shown in Figure 4.32 (displacement is still the average of the displacements at each edge of the WT). The no-haunch specimen exhibits ductility, but at lower values than for the same stud configuration loaded concentrically. The 3-in haunch specimen shows virtually no ductility.

For three 5-in studs spaced longitudinally without a haunch, considerable post-peak strength is achieved as the specimen displaces. As load is applied, flexural cracks form first, with the first crack forming at midspan at the location of the studs. Just after peak load, a horizontal crack forms on the side of the specimen nearest the applied load. The horizontal crack starts at the level of the top mat of reinforcing and grows rapidly down and over to the bottom mat of reinforcing (Figure 4.33(a)). As displacements increase, the side and bottom cover concrete near the applied load spall. Under increasing displacements the WT rotates as a rigid body about the back edge of the slab (Figure 4.33(b)). A horizontal crack forms on the back side of the specimen opposite from the load as displacements increase further. This back side horizontal crack represents the hinge between the slab and the concrete rotating with the WT. (Figure 4.33(c)). The specimen continues to carry load at large displacements (5 kips up to 1.2 in), until the center stud pulls free of the surrounding rebar. After the center stud pulls free, the load drops to 1.4 kips for the remainder of the test. Peak load occurs at a displacement of 0.02 in, less than the 0.04 in from the concentrically loaded test.

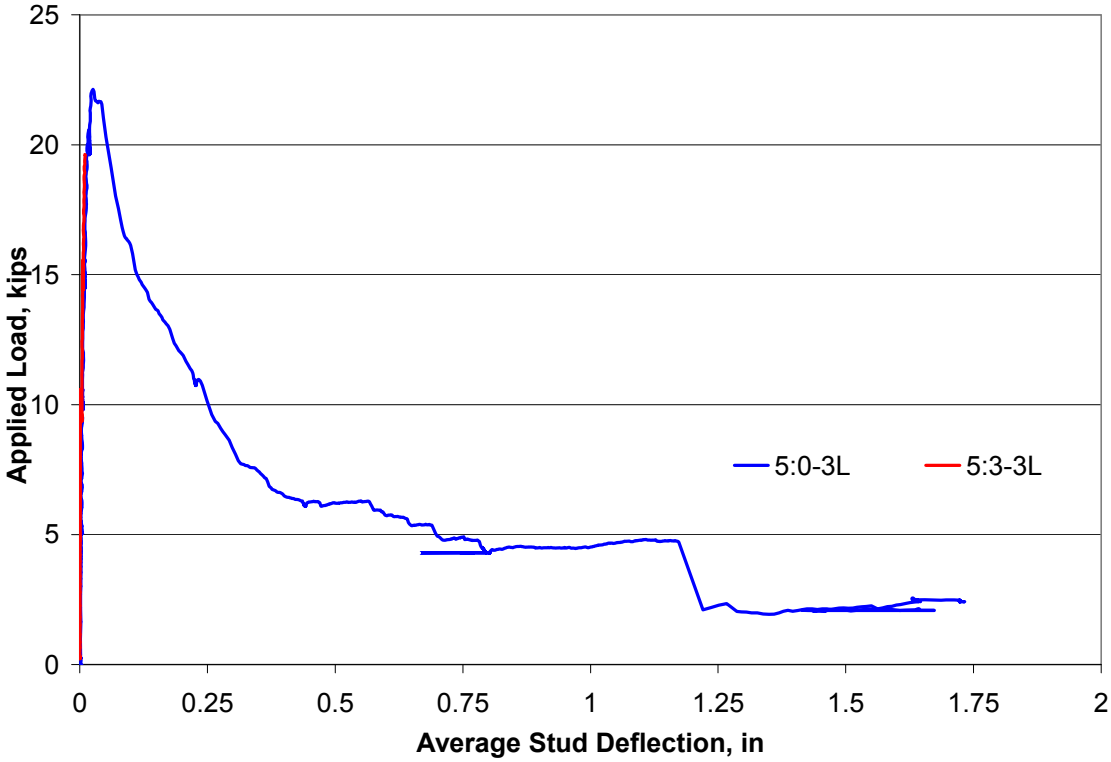

Figure 4.32: Load-Deflection Plots for Specimens Loaded Eccentrically

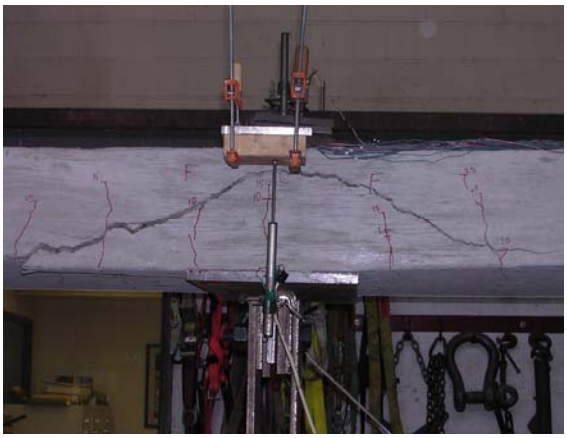

(a)

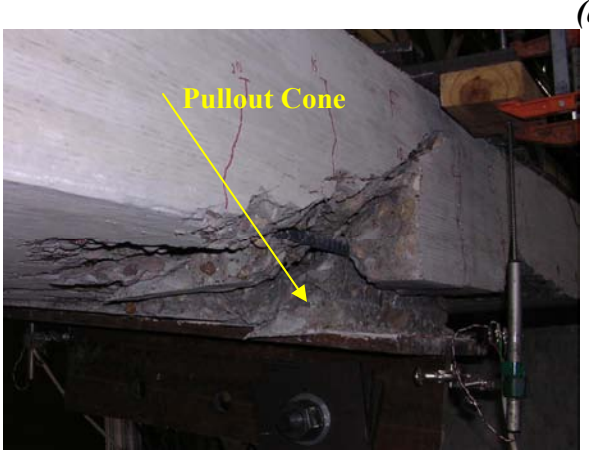

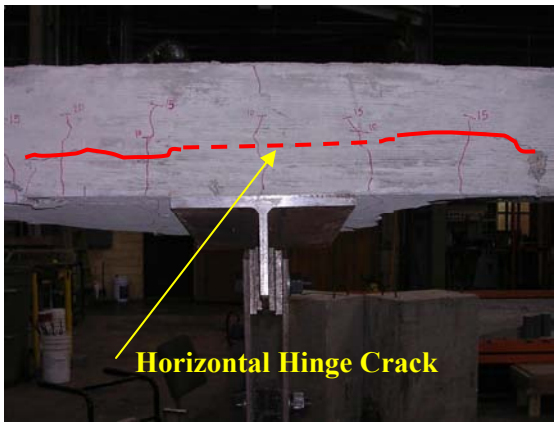

(b) *(c)*

Figure 4.33: Failure Sequence for No-Haunch Specimen Loaded Eccentrically (a) Horizontal Crack Formation (b) WT and Failure Cone Rotation (c) Back Side Hinge Crack

For three 5-in studs spaced longitudinally in a 3-in haunch, the cracking and load behavior is very different than the specimen without a haunch. The first flexural cracks form at the sides of the haunch as seen in all haunch specimens. At peak load, a horizontal crack forms at the top of the haunch, separating the haunch across nearly its entire area. The haunch remains connected only at the back edge of the slab, which acts as the haunch pivot point. At the formation of the horizontal crack, all load carrying capacity of the specimen is lost. Peak load occurs at a displacement of 0.01 in, less than the 0.02-in displacement in the concentric tests.

4.4.3 Shear Stud Gage Data

Stud behavior, in terms of force distribution and total load, correlates very well between tall studs and their respective 5-in stud geometries. All data analyzed here uses the same formats as established in Section 4.2.3. With the exception of the single stud cases, which reach stresses of 80% of yield, most studs are stressed to less than 40% of yield.

Specimens with Studs Spaced Transversely

All specimens with studs spaced transversely, whether 7-in or 9-in studs, have the same basic applied load-stud force plots as their respective 5-in stud specimens. The taller transversely spaced studs

also have more eccentric WT pullout than 5-in studs, producing strain-gage-based stud forces higher than the applied load. The single 7-in stud specimen had a malfunctioning stud gage, and no data are available for this case. The single 9-in stud specimen shows forces at or above the applied force during the majority of the test, as shown in Figure 4.34. The increase in stud load over applied load is reflected in Table 4.9, which compares stud forces for all transversely spaced specimens. This behavior is due to eccentric pullout of the studs, which results in prying action.

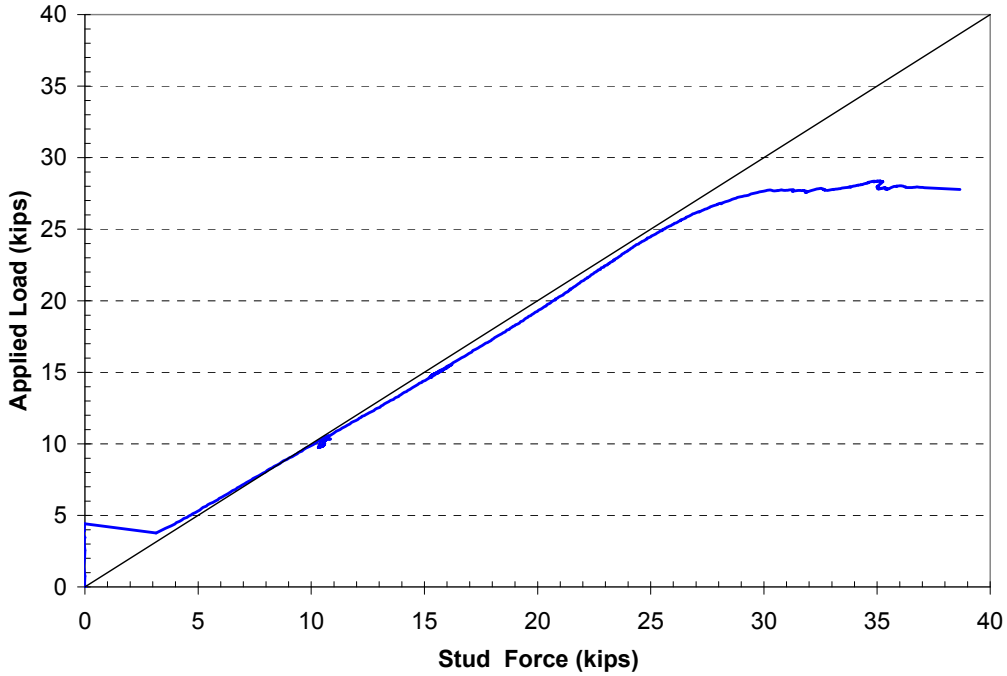

Figure 4.34: Applied Force vs. Stud Force, Specimen 9:3-1

Table 4.9: Series III Specimen with Studs Spaced Transversely, Comparison of Stud and Applied Forces

Specimen	Stud Location	Strain (in/in)	Stress (ksi)	Force (kips)	% Total Stud Force	Total Stud Force (kips)	Applied Force (kips)	% Difference
7:3-1	**Gage Failed**							
7:3-2T	Left	0.000713	20.68	12.43	51.2%	24.27	25.03	-3.02%
	Right	0.000679	19.69	11.84	48.8%			
7:3-3T†	Left	0.000336	9.74	5.86	27.1%	21.59	20.31	6.30%
	Center	0.000580	16.82	10.11	46.8%			
	Right	0.000322	9.34	5.62	26.0%			
9:3-1	Center	0.001665	48.29	29.03	100.0%	29.03	27.29	6.39%
9:3-2T‡	Left	0.000827	23.98	14.42	50.6%	28.53	27.69	3.03%
	Right	0.000809	23.46	14.11	49.4%			
9:3-3T	Left	0.000328	9.51	5.72	20.9%	27.40	31.37	-12.67%
	Center	0.000741	21.49	12.92	47.2%			
	Right	0.000502	14.56	8.75	32.0%			

†immediately prior to final cracking at peak load, % difference between stud and applied forces is -12.7%

‡immediately prior to final cracking at peak load, % difference between stud and applied forces is -3.7%

Two-stud specimens, shown in Figure 4.35, have very little difference between the forces in the two studs, indicating a uniform force distribution during the test. Both 7-in and 9-in stud specimens show a similar degree of measured force transfer to concrete friction transfer, between 3.0% and 3.7%, just before final cracking at peak load, as indicated in the footnote of Table 4.9.

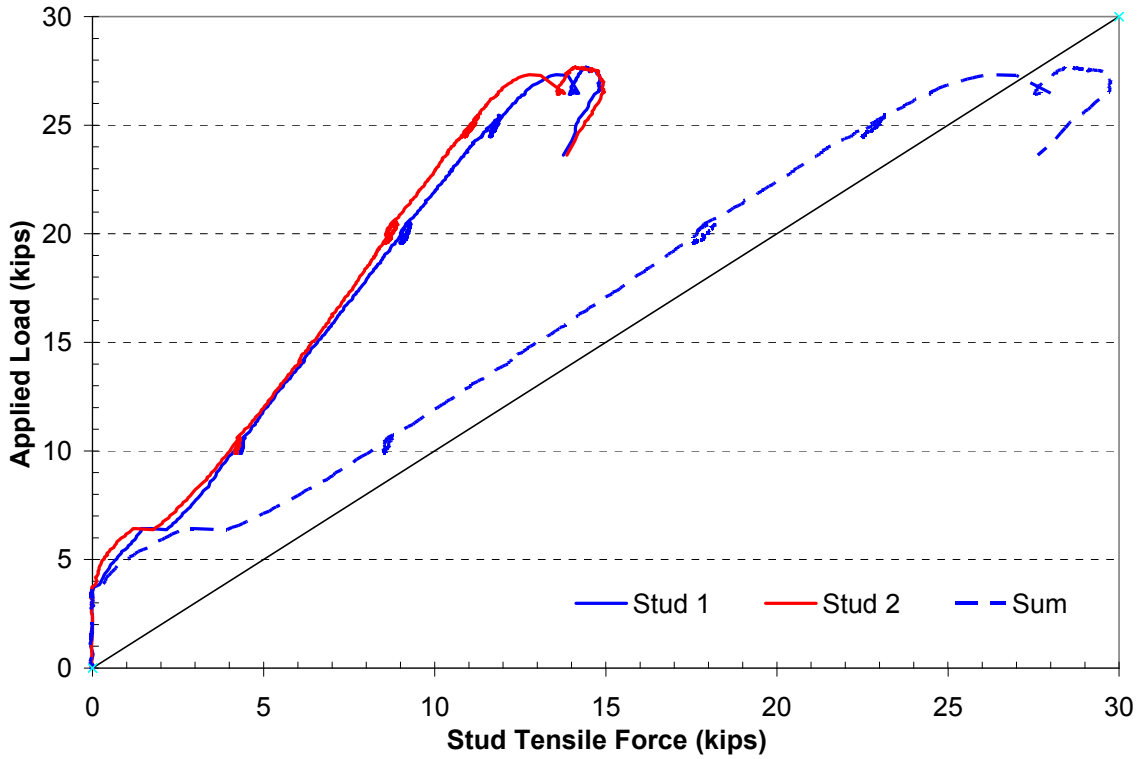

Figure 4.35: Applied Force vs. Stud Force, Two Studs Spaced Transversely

For specimens with three studs spaced transversely, the center stud carries significantly more load than either of the outer studs, with differences between 50% and 75%. Figure 4.36 (representative of both stud heights) shows how this percentage remains fairly constant as load increases. Both specimens show a roughly 13% lower measured force caused by transfer of the force by concrete friction before cracking at peak load, as noted in the footnote to Table 4.9. This high percentage of friction load transfer is attributed to the large section of uncracked concrete in the haunch around the three studs. The haunch configuration provides substantial surface area for skin friction, undisturbed by cracking.

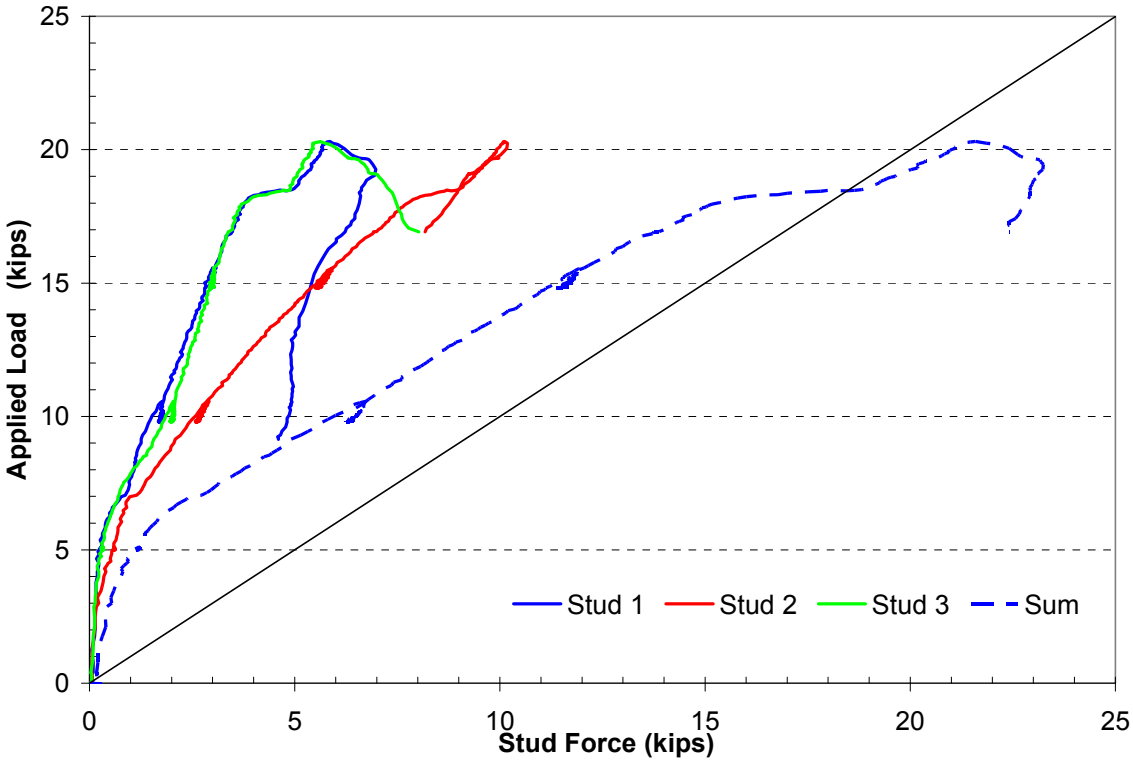

Figure 4.36: Applied Force vs. Stud Force, Three Studs Spaced Transversely

Specimens with Studs Spaced Longitudinally

As with transversely spaced stud specimens, specimens with studs spaced longitudinally have stud forces similar to their respective 5-in stud tests. Both studs in specimens with two studs spaced longitudinally have nearly the same force throughout the test, indicating a roughly uniform force distribution, as shown in Figure 4.37 (representative of both tests). Both studs also have a small amount of concrete friction load transfer, 3.0% to 5.0%, as shown in Table 4.10.

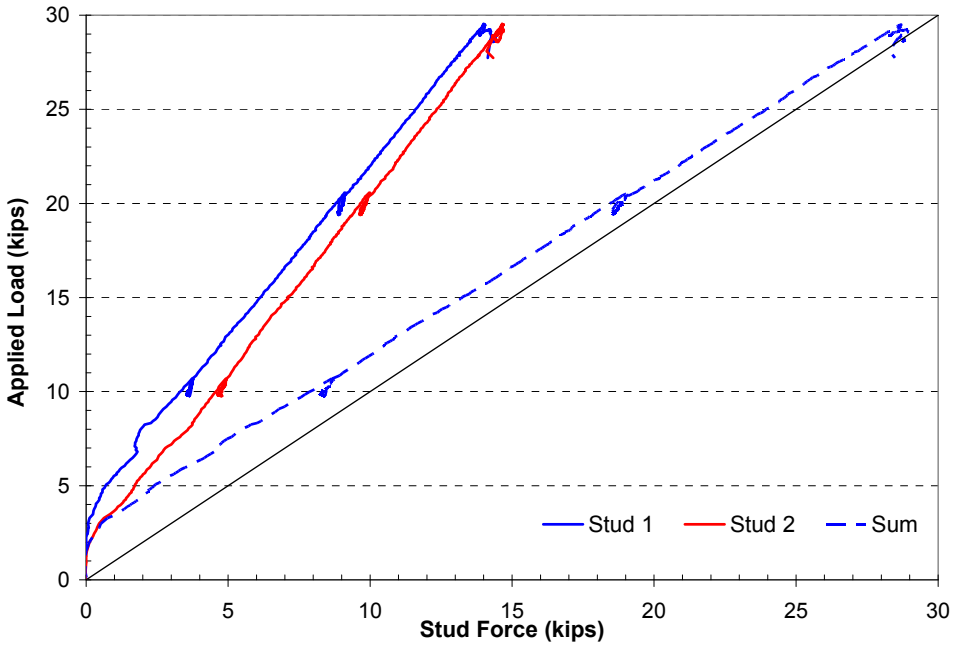

Figure 4.37: Applied Force vs. Stud Force, Two Studs Spaced Longitudinally

Table 4.10: Series III Specimens with Studs Spaced Longitudinally, Comparison of Stud and Applied Forces

Specimen	Stud Location	Strain (in/in)	Stress (ksi)	Force (kips)	% Total Stud Force	Total Stud Force (kips)	Applied Force (kips)	% Difference
7:3-2L	Left	0.000695	20.16	12.12	46.9%	25.84	27.21	-5.02%
	Right	0.000787	22.82	13.72	53.1%			
7:3-3L	Left	0.000555	16.10	9.68	37.7%	25.69	28.28	-9.17%
	Center	0.000408	11.83	7.11	27.7%			
	Right	0.000510	14.79	8.89	34.6%			
9:3-2L	Left	0.000803	23.29	14.00	48.9%	28.65	29.54	-3.01%
	Right	0.000840	24.36	14.65	51.1%			
9:3-3L	Left	0.000570	16.53	9.94	36.5%	27.24	29.96	-9.08%
	Center	0.000519	15.05	9.05	33.2%			
	Right	0.000473	13.72	8.25	30.3%			

In the specimen with three 7-in studs spaced longitudinally, the inner stud carries approximately 40% less load than the outer studs. Both outer studs have nearly identical forces throughout the test, as shown in Figure 4.38, representative of both tests. Both specimens have force transfers by concrete friction near 9.0% at peak load. As observed for studs spaced transversely, these friction values appear to be larger than the friction values for two studs because of the increased contact area of the third stud.

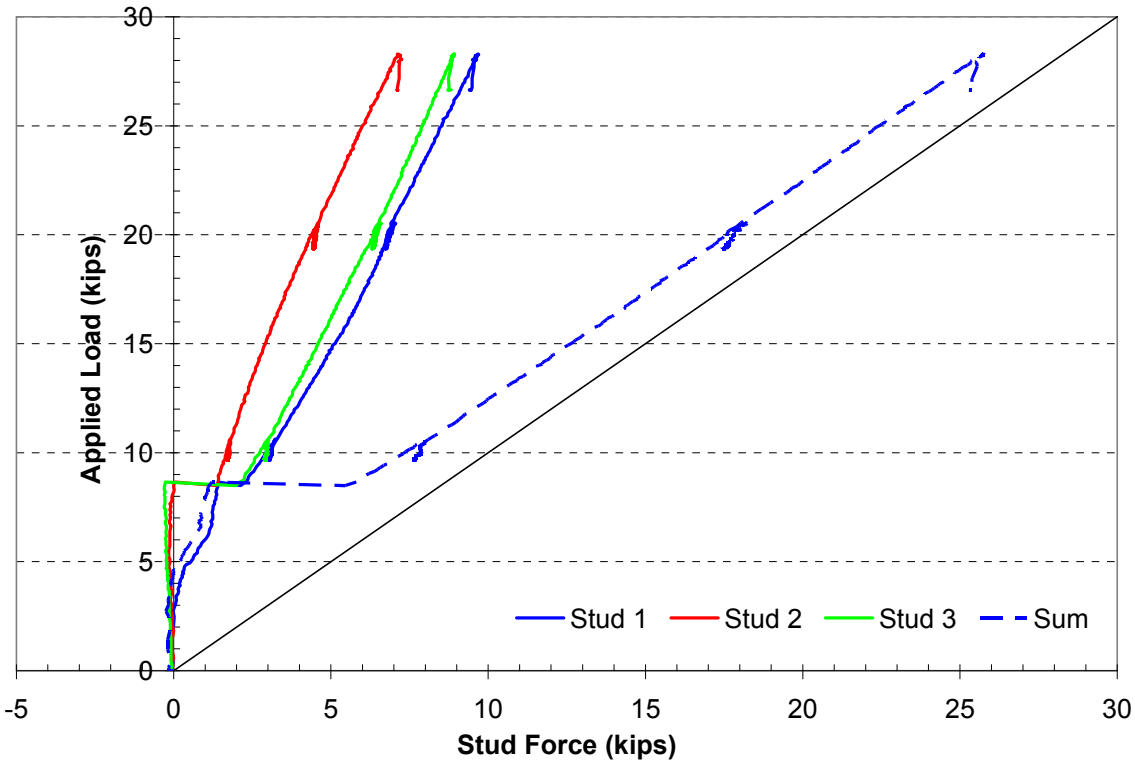

Figure 4.38: Applied Force vs. Stud Force, Three Studs Spaced Longitudinally

Specimens Loaded Eccentrically

The two specimens loaded eccentrically have significantly different behavior than concentrically loaded specimens. Because of the significant displacement gradient, the WT, studs, and haunch concrete (if present) act as a rigid body pivoting about the back edge of the specimen, as shown in Figure 4.39. At the pivot point, compression forces are developed that must also be resisted by the shear studs. This extra force reduces the stud strength available to resist the applied load and results in the lower measured strengths. The distribution of these forces for both the no-haunch and 3-in haunch specimens is shown in Figure 4.40 (in both cases load is applied under Stud 3). Especially for the 3-in haunch specimen, stud force is directly related to the stud's distance from the hinge as depicted in Figure 4.39. The ratio of the individual stud forces does not change significantly during the test. In both specimens, Stud 1 is in compression, acting as part of a hinge zone prior to flexural cracking. After first cracking, it goes into tension as the hinge location moves to the back edge of the slab.

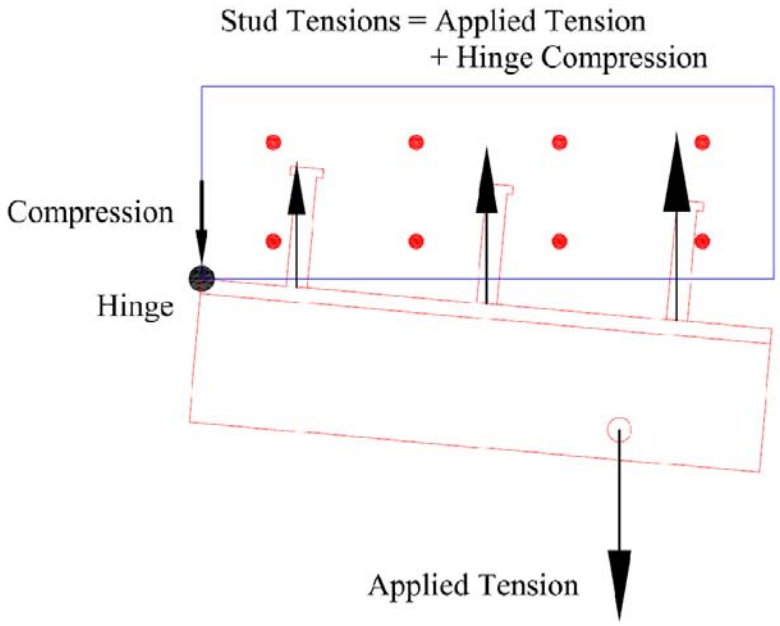

Figure 4.39: Schematic of Prying Forces in an Eccentrically Loaded Stud

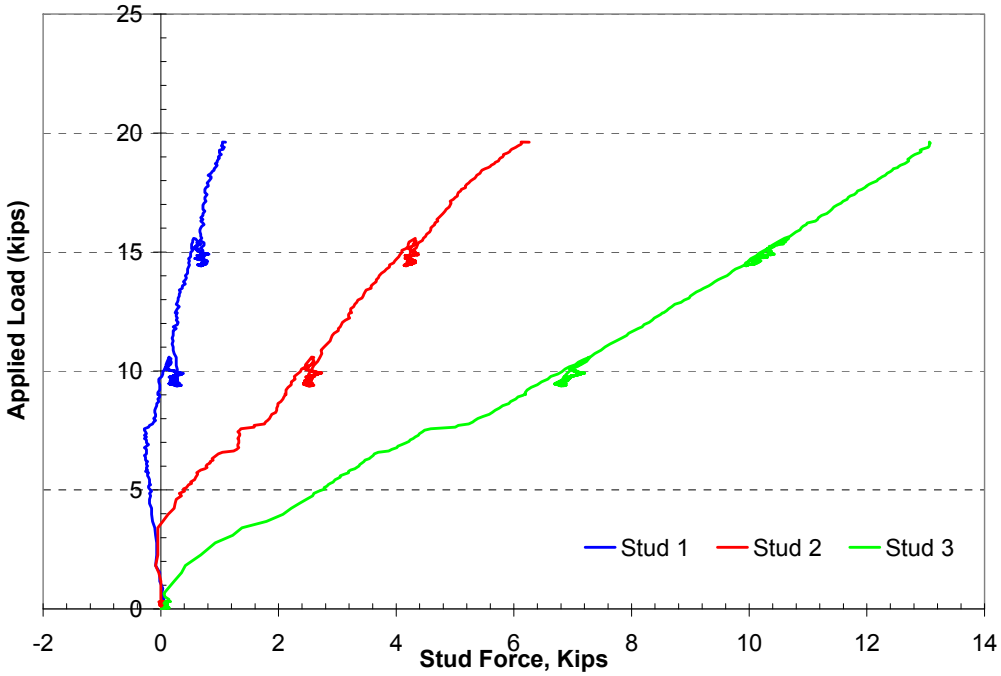

Figure 4.40(a): Applied Force vs. Stud Force, Specimen 5:3-3LE

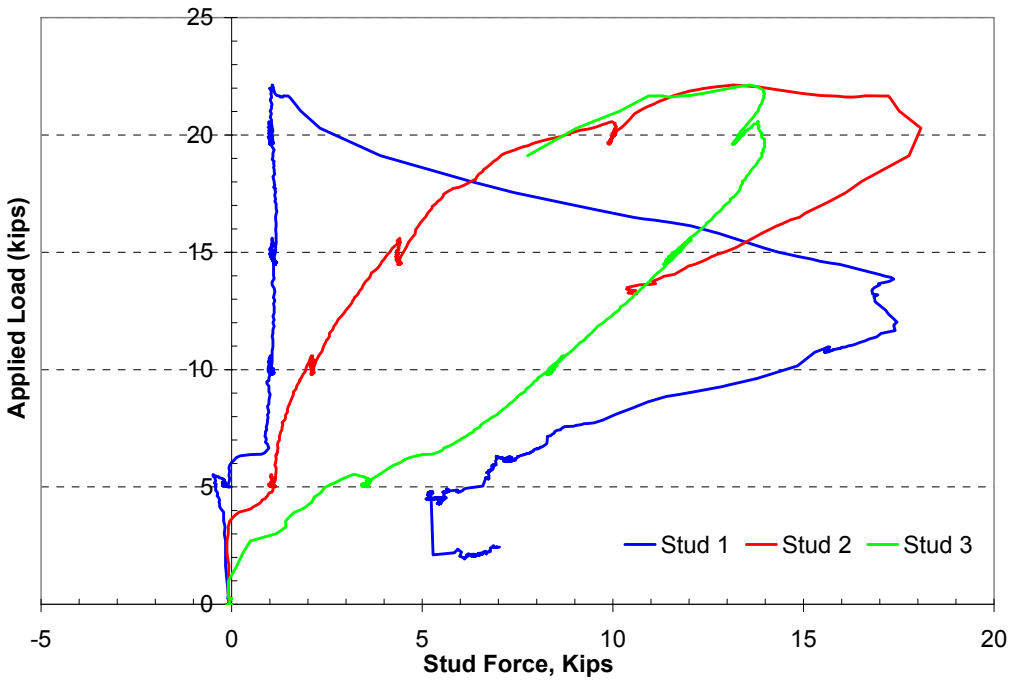

Figure 4.40(b): Applied Force vs. Stud Force, Specimen 5:0-3LE

For the specimen with no haunch, the gradient in stud forces relative to distance from the hinge point is non-uniform. After flexural cracking, Stud 1 has very little load increase, while Stud 3 supports substantial load. Near peak load, Stud 3 begins to lose force as its pullout cone begins to separate, shedding load to Stud 2. After peak load, Stud 2 begins to separate from the slab, and Stud 1 begins to carry more load. The specimen resistance to applied load decreases rapidly once Stud 2 separates.

To account for prying action and evaluate the agreement between measured and calculated stud gage results, moments are summed about the edge of the slab for the three studs and the applied load. The percentage error between the applied moment and moment calculated from the stud force for both specimens is shown in Figure 4.41. The sections of each curve that form horizontal plateaus indicate the disturbed regions of the plot where loading is paused. For the specimen with a haunch, percentage error begins around -10% at low force levels, then decreases to -3.7% at peak load. As with most concentrically loaded cases, measured force is less than applied force because of concrete-stud friction. The effects of concrete-stud friction decrease as load increases and the studs begin to slip past the concrete. For the no haunch specimen, the error begins around +6.0% and reaches +9.0% at peak load. It is unclear why these values are greater than the applied load.

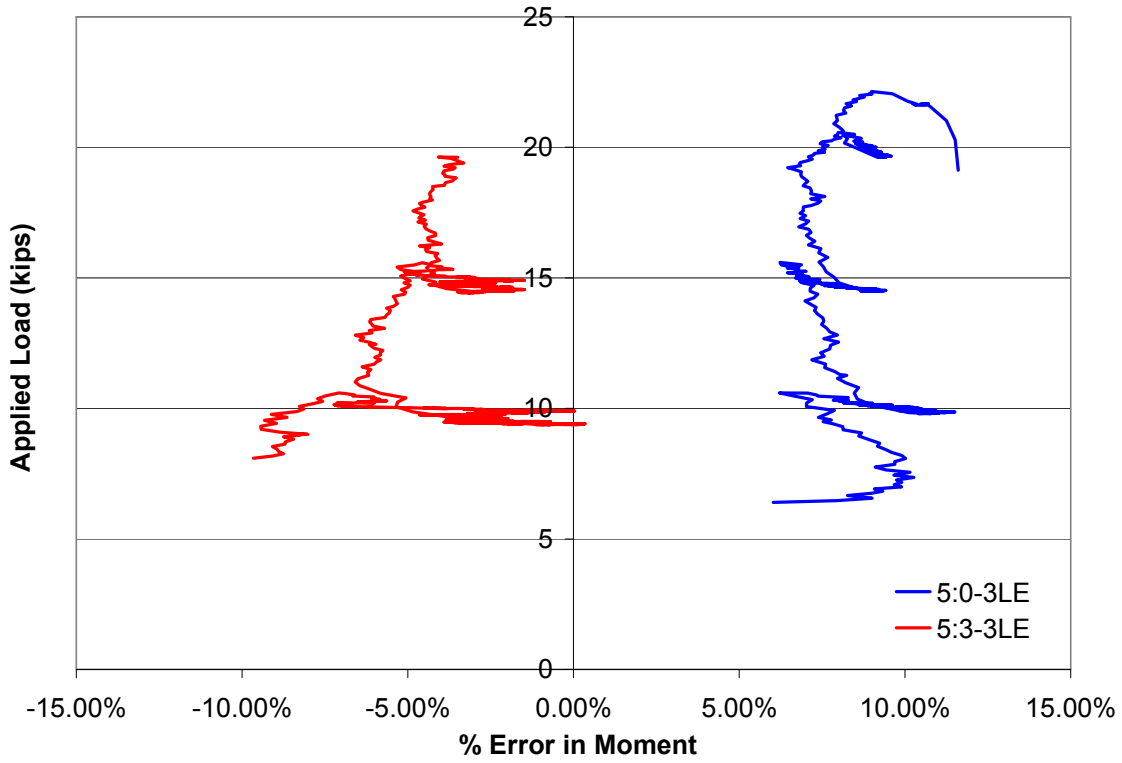

Figure 4.41: Error in Applied Moment compared to Stud Moment for Eccentrically Loaded Specimens

4.4.4 Reinforcing Steel Gage Data

Concrete Slab Predicted Behavior

Cracking, yield, and ultimate loads for Series III are predicted using the same methods as presented in Section 4.2.4. For Series III, the compressive concrete strength has a mean value of 5.1 ksi, with a corresponding β_1 value of 0.795. Table 4.11 summarizes the critical points of slab behavior for Series III.

Table 4.11: Series III Slab Critical Loads

Slab State	Moment (kip-in)	Load (kips), No Haunch	Load (kips), 3-in Haunch
Cracking	137	7.0	8.3
First Yield	442	22.7	26.8
Ultimate Strength	524	26.9	31.8

Specimens with Studs Spaced Transversely

All specimens with studs spaced transversely have the same basic load-rebar strain plot with very little rebar yielding, as shown in Figure 4.42. Strain gage data from specimen 7:3-1 are very noisy, and its data are omitted from analysis. Most of the specimens have a peak load greater than the predicted yield load (and greater than the estimated ultimate load in some cases), but no specimen shows any

substantial yielding in the rebar. Again, these low strains are attributed to the haunch reducing stresses in the rebar.

Cracking load is between 8.0 and 9.0 kips for all specimens, very close to the predicted cracking load. After cracking, all rebar goes into tension, and the top mat rebar shows very similar strains for each bar. The bottom mat rebar shows more variation in strain, typically with two bars on one side of the specimen carrying more strain than the other two. This pattern of strain is a result of the WT pulling out eccentrically in many of the transversely spaced stud tests. In no case is the difference between maximum and minimum strains greater than 50% in the bottom mat rebar. At peak load, the strain gages begin to show increasing strains with no load increase. After the studs begin to pull out, strains in the rebar drop rapidly.

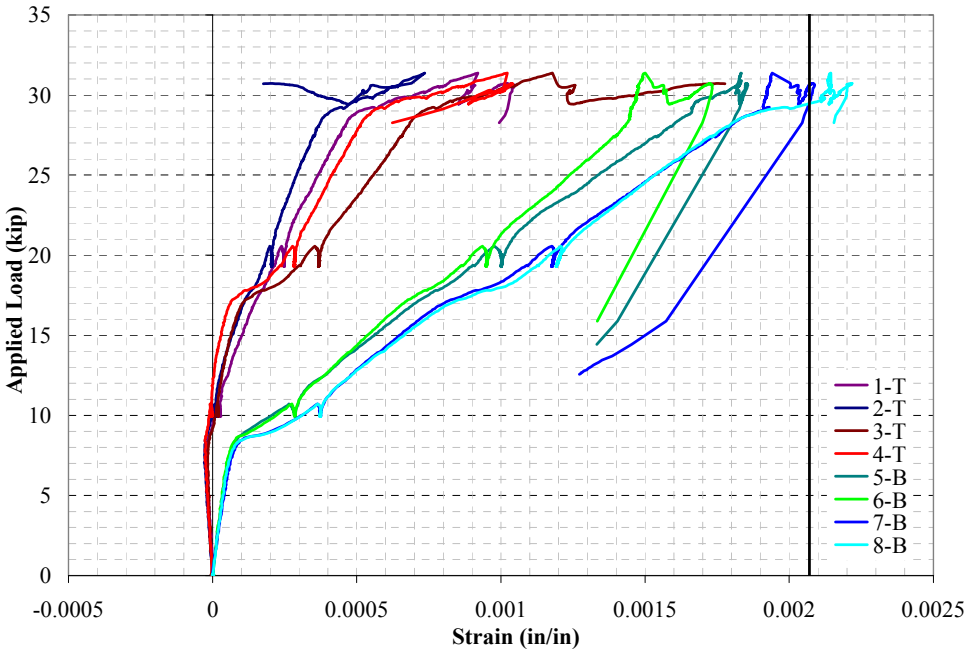

Figure 4.42: Applied Load vs. Rebar Strain for Specimens with Tall Studs Spaced Transversely

Specimens with Studs Spaced Longitudinally

Tall studs spaced longitudinally have two different load-rebar strain plots, shown in Figure 4.43. Two-stud specimens show very little yielding, while three-stud specimens have significant yielding and inelastic deformation. All specimens have a peak load greater than the estimated yield load, but the two-stud specimens show no significant yielding. The three-stud specimens show bottom mat yielding at loads near the estimated yield load.

For specimens with two studs and with three studs, the loading portion of the curves is nearly the same. Cracking occurs between 7.0 and 8.0 kips, which is lower than predicted. For loads above cracking, all of the rebar goes into tension, with the top mat rebar showing very little variation in strain. The bottom mat of reinforcing again shows variation in strain among the individual bars, with rebar on one side of the specimen showing greater strains than the other.

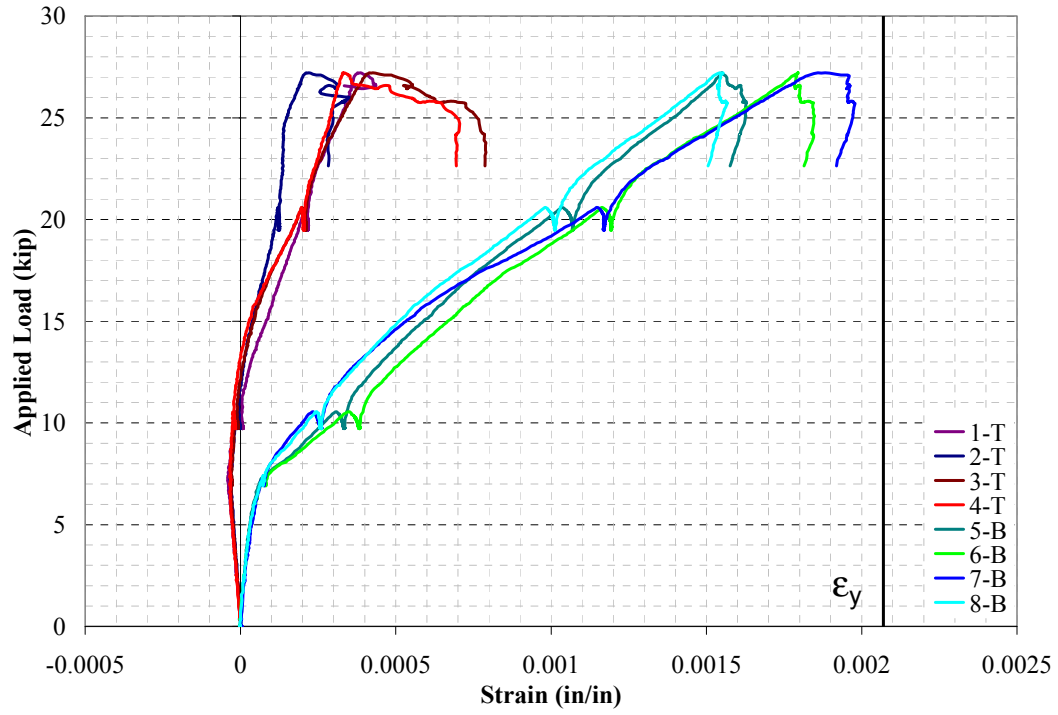

(a)

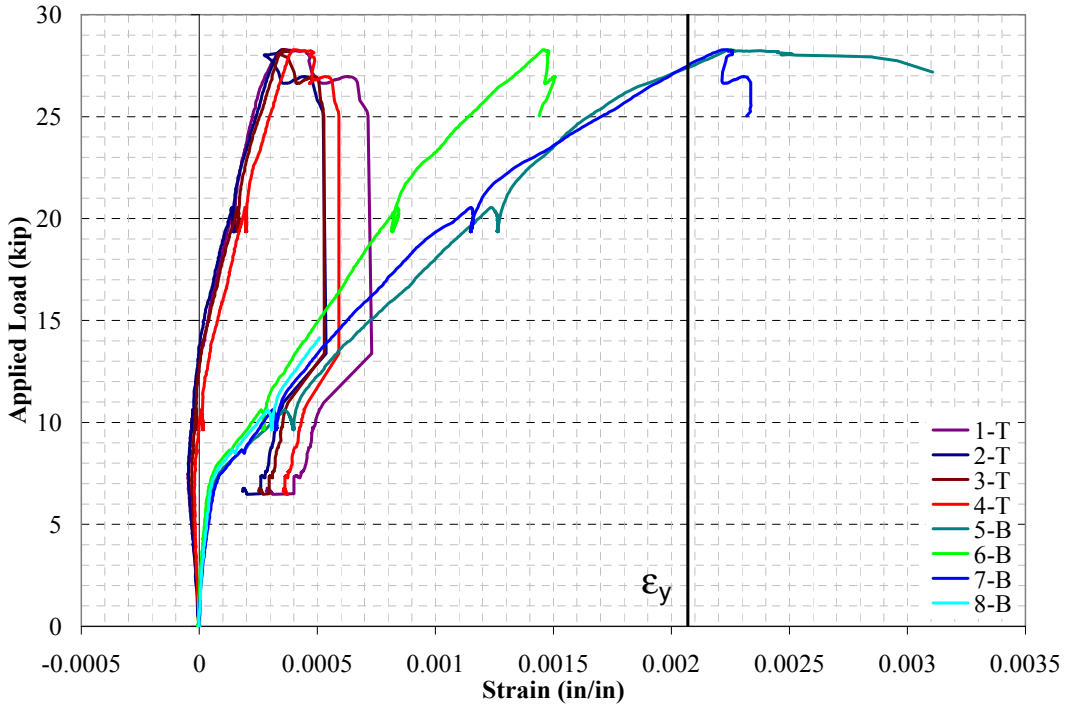

(b)

Figure 4.43: Applied Load vs. Rebar Strain for Specimens with Tall Studs Spaced Longitudinally (a) with Two Studs (b) with Three Studs

For two-stud specimens, strains in all of the rebar begin to decrease after peak load. For three-stud specimens at peak load, the gages show increasing strain with no load increase. Strains in the bottom

mat rebar are well past yield. This strain behavior, as before, is indicative of the large deformations the slab experiences as the WT and studs pull out. Specimen 9:3-3L is an exception to the above behavior; at peak load, the top mat of reinforcing begins to go into compression. This compression is caused by arching in the slab. After peak load, strains in all of the gages decrease.

Specimens Loaded Eccentrically

The two specimens loaded eccentrically have very different behaviors depending on the presence of the haunch. In both cases, the eccentricity of the load is reflected in non-uniform strains of the reinforcement. The specimen with a haunch shows strains above the yield strain near peak load, while the specimen with a haunch has no yielding in the slab. For the specimen without a haunch (Figure 4.44(a)), cracking occurs at 6.3 kips, slightly lower than the expected 7.0 kips. After cracking, all of the rebar goes into tension, with a clear gradient of strains in both mats of rebar. The top and bottom rebar both show highest tensile strains on the outermost bar (on the same side as the applied load). Peak load of the specimen corresponds to the estimated yield load, and at least two of the bottom bars yield. After peak load, strains in all bars drop rapidly.

The specimen with a haunch (Figure 4.44(b)) has a cracking load of 9.0 kips, close to the predicted haunch cracking load. After cracking, all rebar goes into tension, with the top rebar showing virtually no variation in strain among individual bars. The bottom mat reinforcing does show a strain gradient; strains increases with proximity to the applied load. While peak load in the specimen, 19.6 kips, is less than the predicted yield load of 26.8 kips, all rebar strains are well below yield. This lack of yielding is again attributed to the effects of the haunch reducing strains in the rebar.

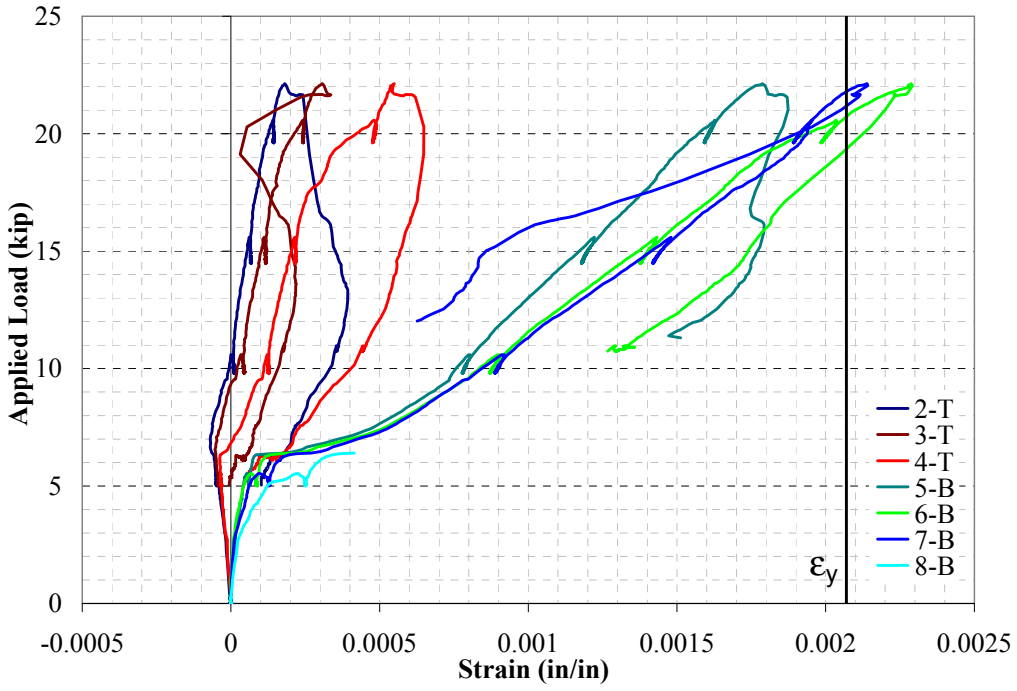

(a)

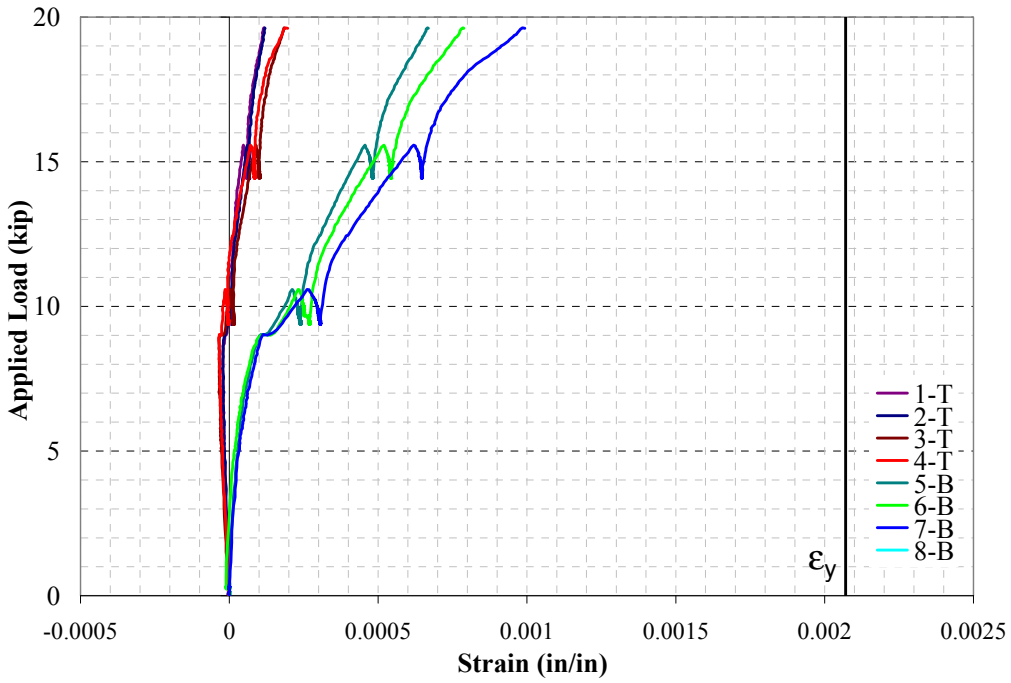

(b)

Figure 4.44: Applied Load vs. Rebar Strain for Eccentrically Loaded Specimens (a) without a Haunch (b) with a 3-in Haunch

4.4.5 Slab Deflection

Slab deflections of specimens with tall studs fall into two categories depending on their mode of failure. The two modes are shown in Figure 4.45. Specimens failing by splitting and separation of the haunch (7-in studs spaced transversely) have a brittle failure as shown by Figure 4.45(a). Note the horizontal axis in Figure 4.45(a) is at a smaller scale than Figure 4.45(b) for improved resolution. Specimens that engage the bottom mat of reinforcing (7-in studs spaced transversely and all 9-in studs) have a more ductile failure than those that do not as shown in Figure 4.45(b). The negative deflection shown in Figure 4.45(b) is due to arching action of the slab. All specimens have cracked and uncracked stiffnesses nearly identical to one another and to the tests in Series II. All specimens have slab-deflection-based cracking loads that agree well with rebar-gage-based cracking loads.

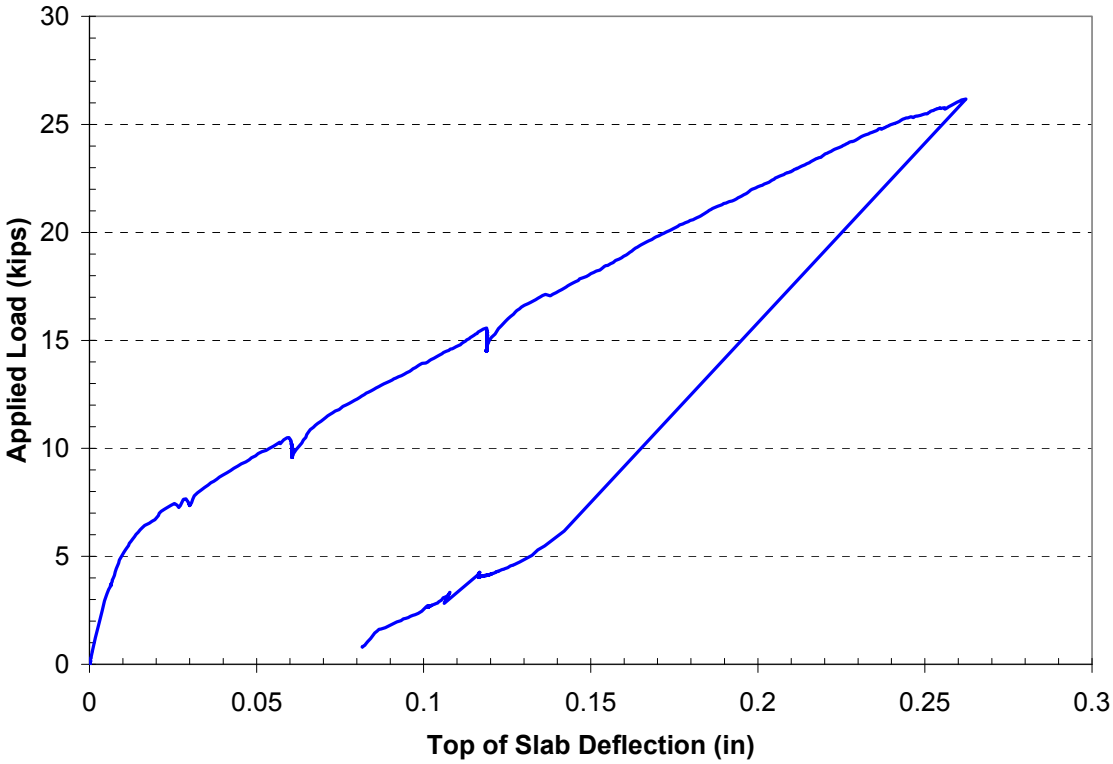

Figure 4.45(a): Applied Load vs. Slab Deflection for Specimens with Brittle Haunch Failure

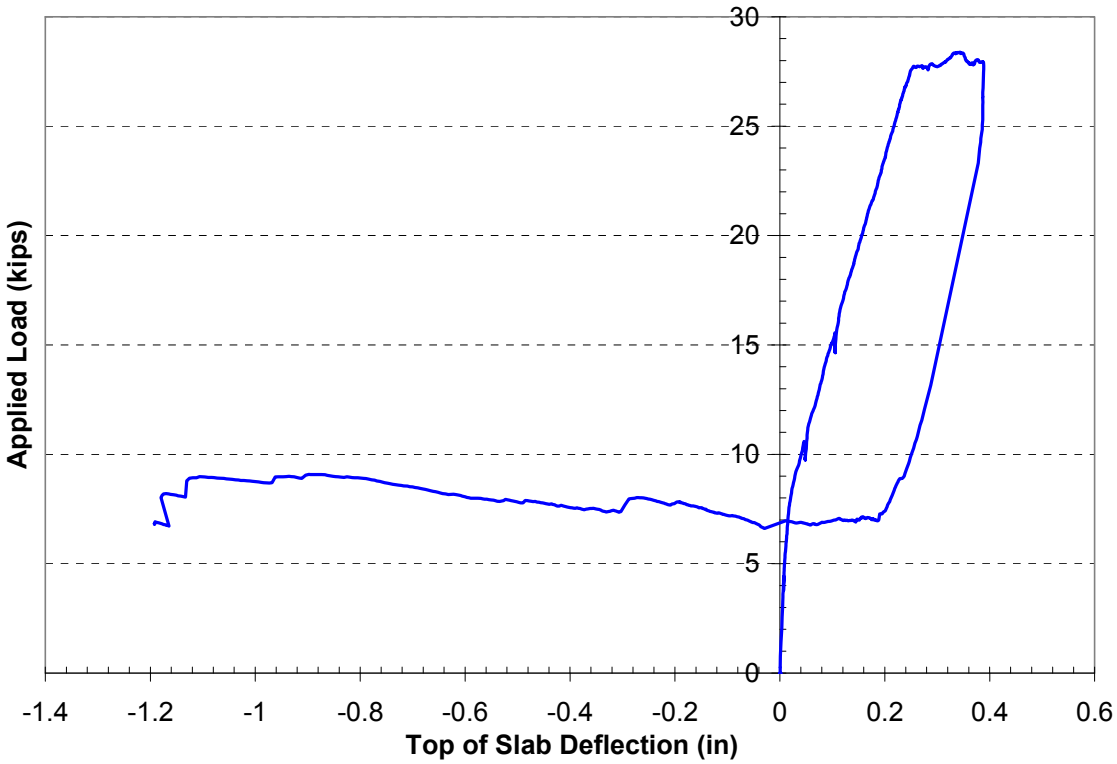

Figure 4.45(b): Applied Load vs. Slab Deflection for Specimens with Ductile Stud Pullout

All specimens with a brittle failure have very little loss in stiffness near peak load. Deflections decrease rapidly as the haunch separates, with all slabs having a permanent slab deformation. Peak load deflections are in the range of 0.20 to 0.25 in, which are similar to the haunch specimens in Series II. Specimens with a ductile failure show a region of low or zero stiffness at peak load at the same time as formation of the horizontal failure crack. Deflections then decrease rapidly as the stud failure cone pulls away from the slab. Nearly all ductile specimens experience upward deflections because of arching in the top mat of reinforcement, up to 1.2 in for some specimens.

Eccentrically loaded specimens show slab deflection behavior very similar to their respective concentrically loaded cases in Series II, including cracked and uncracked stiffnesses, peak load deflections, and post-peak load behavior.

4.4.6 Concrete Cylinder Tests

Cylinder testing for Series III was performed using the same procedure as in Series II. Table 4.12 summarizes the results. While the concrete compressive strength is still higher than the required minimum strength by TxDOT standards, it is much lower than in Series II. The concrete tensile strength is higher than in Series II, increasing 17% to 507 psi. This tensile strength is very high for the average compressive strength.

Table 4.12: Series III Concrete Test Data

Compression Tests		Split Cylinder Tensile Tests		
Days after Casting	Mean Compressive Strengh, f'_c (psi)	Days after Casting	Cracking Tensile Strength, f_t (psi)	$f_t/\sqrt{f'_c}$
41	5,192	49	507	7.1
49	5,039			
64	4,922			

Series Mean Strength: 5.1 ksi

4.5 Series IV Results — Dynamic Loading

4.5.1 Strength

Series IV investigated the dynamic behavior for many of the previously tested stud configurations, examining changes in strength and ductility associated with high loading rates. Dynamic loading causes a general increase in the strength of every configuration without changing the failure mode significantly. The increase in strength was quantified as the dynamic strength factor, DSF, which is the ratio of the dynamic and the quasi-static test strength results. To calculate the dynamic strength factor, the average dynamic peak strength of a stud configuration is normalized by the corresponding measured concrete tensile strength. The same normalization is performed for the average static peak strength of the same configuration. The normalized dynamic strength is divided by the normalized static strength to yield the dynamic strength factor. Table 4.13 lists average peak specimen strengths and their dynamic strength factors. Of note in Table 4.13 is that all studs spaced transversely (including single studs) have a similar dynamic strength factor, 1.29 to 1.43, while studs spaced longitudinally have a lower factor, 1.15 to 1.18.

Table 4.13: Peak Strengths and Dynamic Strength Factors for Series IV Specimens

Number of Studs, No Haunch	Configuration	Peak Strength (kips)	Average Strength (kips)	Dynamic Strength Factor	Number of Studs, 3-in Haunch	Configuration	Peak Strength (kips)	Average Strength (kips)	Dynamic Strength Factor
1		26.1	27.0	1.29	1		32.6	31.9	1.43
		27.9					31.1		
2	Longitudinal	33.6	34.5	1.18	2	Longitudinal	36.4	36.6	1.15
	Longitudinal	35.4				Longitudinal	36.7		
3	Transverse	33.9	33.9	1.31	3	Transverse	23.4	24.4	1.41
	Transverse	†				Transverse	25.3		

†Load Cell Failed

Figure 4.46 shows the dynamic strength factors of all configurations. The strength trends of each configuration of studs are the same as for static loading. For the case of a single stud with a haunch, the dynamic strength factor is 1.43, and for three studs spaced transversely with a haunch, the dynamic strength factor is 1.41. Three studs spaced transversely with a haunch still exhibits reduced strength relative to the respective single stud case. For three studs spaced longitudinally with a haunch, the dynamic strength factor is 1.15, indicating that studs spaced longitudinally have lower dynamic strength factors than studs spaced transversely. For a single stud without a haunch, the dynamic strength factor is 1.29. For three studs spaced transversely without a haunch, the dynamic strength factor is 1.41, while for three studs spaced longitudinally without a haunch the dynamic strength factor is 1.18.

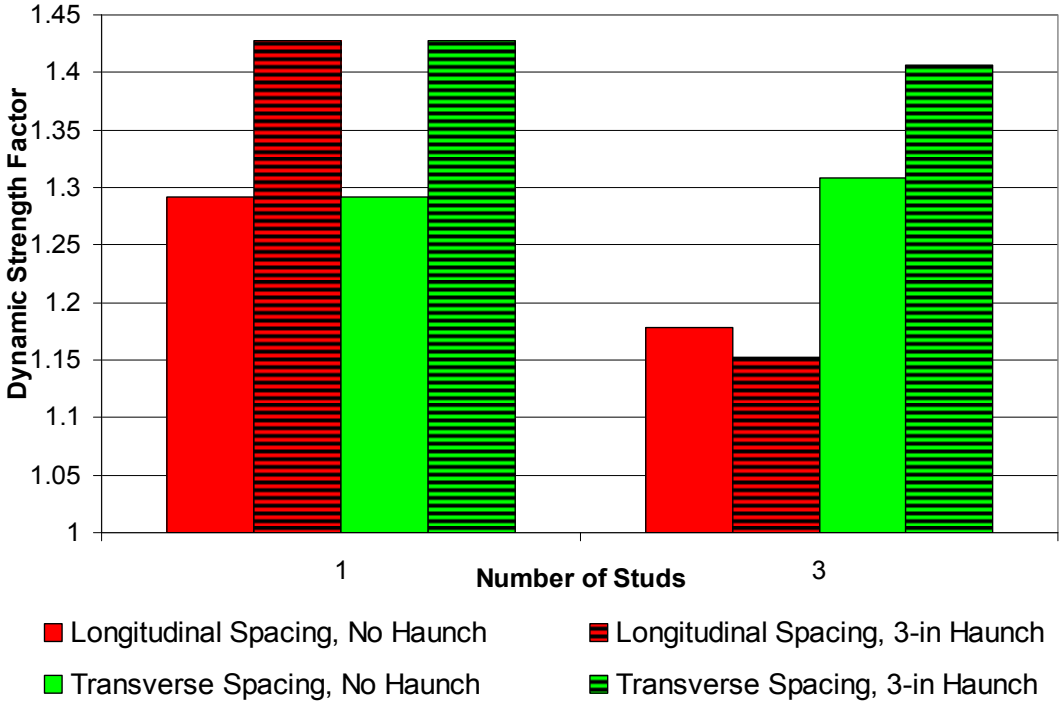

Figure 4.46: Dynamic Strength Factor vs. Number of Studs for Series IV Specimens

The dynamic strength factors for the dynamically loaded specimens were evaluated using the measured strain rates in the rebar and the shear studs. The *mean strain rates* of both the rebar and the shear studs during loading were computed for the purposes of calculating the dynamic strength factor (DSF). These mean rates are not representative of measured strain rates at any given time because strain rates varied significantly during loading. The mean strain rates of the shear studs and the rebar were used to calculate dynamic material strength increase factors from the plots of dynamic increase in steel yield strength versus strain rate (Army Technical Manual TM 5-1300, 1990). Concrete strain rates were not measured directly but were back-calculated from measured applied load data. Using a concrete modulus of elasticity of $57{,}000\sqrt{f_c'}$ and a flexural cracking stress of $7.5\sqrt{f_c'}$ as recommended by ACI 318-08, the concrete strain at cracking was calculated. The average concrete strain rate in the slab was calculated by dividing this strain by the measured time interval from zero load to first cracking. These strain rates were then converted into dynamic strength factors using plots of dynamic increase in concrete strength versus strain rate (Army Technical Manual TM 5-1300, 1990). The calculations of rebar, shear stud, and concrete strain rates and calculated dynamic strength factors are shown in Table 4.14.

Table 4.14: Strain Rates and Dynamic Strength Factors for Series IV Specimens

Number of Studs	Haunch Depth (in)	Spacing	Measured Dynamic Strength Factor (DSF)	Average Rebar Strain Rate (in/in/sec)	Rebar DSF	% Error	Average Stud Strain Rate (in/in/sec)	Stud DSF	% Error
1	0		1.29	4.6E-02	1.13	-12.4%	4.4E-02	1.13	-12.4%
1	0		1.29	6.1E-02	1.15	-10.9%	5.7E-02	1.14	-11.6%
3	0	Longitudinal	1.18	7.0E-02	1.15	-10.9%	2.1E-02	1.11	-14.0%
3	0	Longitudinal	1.18	3.4E-02	1.13	-12.4%	1.9E-02	1.09	-15.5%
3	0	Transverse	1.31	3.5E-02	1.13	-12.4%	1.6E-02	1.08	-16.3%
3	0	Transverse	1.31	6.5E-02	1.15	-10.9%	2.3E-02	1.11	-14.0%
1	3		1.43	3.0E-02	1.12	-13.2%	7.0E-02	1.15	-10.9%
1	3		1.43	2.8E-02	1.12	-13.2%	5.6E-02	1.14	-11.6%
3	3	Longitudinal	1.15	2.6E-02	1.12	-13.2%	1.3E-02	1.07	-17.1%
3	3	Longitudinal	1.15	8.7E-03	1.06	-17.8%	8.9E-03	1.05	-18.6%
3	3	Transverse	1.41	2.6E-02	1.11	-14.0%	1.2E-02	1.07	-17.1%
3	3	Transverse	1.41	3.2E-02	1.12	-13.2%	1.9E-02	1.09	-15.5%

Cracking Stress = $7.5\sqrt{f'_c}$ Concrete Modulus of Elasticity = $57,000\sqrt{f'_c}$ Cracking Strain = $\frac{7.5\sqrt{f'_c}}{57,000\sqrt{f'_c}}$ Concrete Strain Rate = $\frac{7.5}{57,000}\frac{1}{t_c}$

Number of Studs	Haunch Depth (in)	Spacing	Measured Dynamic Strength Factor (DSF)	Time to Cracking, t_c (sec)	Average Concrete Strain Rate (in/in/sec)	Concrete DSF	% Error
1	0		1.29	0.01	1.3E-02	1.60	24.0%
1	0		1.29	0.008	1.6E-02	1.60	24.0%
3	0	Longitudinal	1.18	0.012	1.1E-02	1.70	31.8%
3	0	Longitudinal	1.18	0.0097	1.4E-02	1.60	24.0%
3	0	Transverse	1.31	0.0113	1.2E-02	1.65	27.9%
3	0	Transverse	1.31	**Load Cell Failed**			
1	3		1.43	**Noisy Data**			
1	3		1.43	0.011	1.2E-02	1.65	27.9%
3	3	Longitudinal	1.15	0.0117	1.1E-02	1.70	31.8%
3	3	Longitudinal	1.15	0.0153	8.6E-03	1.75	35.7%
3	3	Transverse	1.41	0.012	1.1E-02	1.70	31.8%
3	3	Transverse	1.41	0.012	1.1E-02	1.70	31.8%

As Table 4.14 shows, the rebar strain rates, 0.035 to 0.07 in/in/sec for no-haunch specimens and 0.0087 to 0.032 in/in/sec for 3-in haunch specimens, predict dynamic strength factors between 11% and 18% less than measured values. The strain rates in the shear studs of 0.044 to 0.07 in/in/sec for single-stud specimens and 0.0089 to 0.023 in/in/sec for three-stud specimens also predicted DSFs less than the measured values by between 11% and 19%. Neither the yielding of the rebar or the shear stud was the controlling limit state for the specimens. The calculated average concrete strain rates of 0.011 to 0.016 in/in/sec for specimens without a haunch and 0.0086 to 0.012 in/in/sec for specimens with a haunch over-predict the measured dynamic strength factor significantly, between 24% and 32%. Because the failure of the specimens was a concrete failure, it was expected that the concrete DSF would be better correlated with the measured DSF. The lack of correlation and unconservative prediction indicates further work is required to define the strain rate in the specimens and its correlation to the strength of the concrete.

4.5.2 Behavior at Failure

In general, the behavior of the dynamic tests, in terms of cracking patterns, pullout cone geometry, and load-deflection curves, is very similar to the respective static tests. The most significant change in behavior for studs loaded dynamically is the dynamic increase of strengths mentioned previously. This strength increase applies both to the peak strength of specimens and the magnitude of the load plateau at large displacements. While the magnitude of the load plateau is increased in dynamic specimens, the maximum displacements over which the studs carry load decreases from static tests (the exception is three studs spaced longitudinally in a haunch, discussed below). This trend indicates a general loss in ductility for dynamically loaded specimens relative to their static counterparts.

Specimens with a Haunch

Because the dynamic tests occur over a very short time interval, only the final crack patterns could be observed and not their propagation. Based on the observed final crack patterns, specimen response was found to be very similar to the respective static cases. For a single stud and three studs spaced transversely, very little ductility was achieved. For three studs spaced longitudinally, rebar-stud interlock created a ductile response. Load-displacement plots for dynamically loaded specimens with a haunch are shown in Figure 4.47.

For a single stud and three studs spaced transversely, the haunch separates with very little cracking beyond the flexural cracking at the edges of the haunch. At peak load, horizontal cracking just above the haunch occurs, similarly to the static specimens. Unlike the static specimens where the haunch split into only two pieces, for dynamic specimens the haunch splits into three or more pieces, as shown in Figure 4.48(a). The first crack is at the location of the stud, and additional cracking planes occur at roughly a 45-degree angle, behaving as a continuation of the shear stud failure cone. It appears these cracks are a secondary failure plane that occurs after haunch separation. In some cases, the portion of the haunch not in contact with the studs remains loosely attached to the edge of the slab, even though the failure plane has severed nearly the entire piece from the slab, as shown in Figure 4.48(b). For single-stud specimens and three studs spaced transversely with a haunch, peak load occurs at displacements that are similar to static displacements, between 0.05 and 0.06 in.

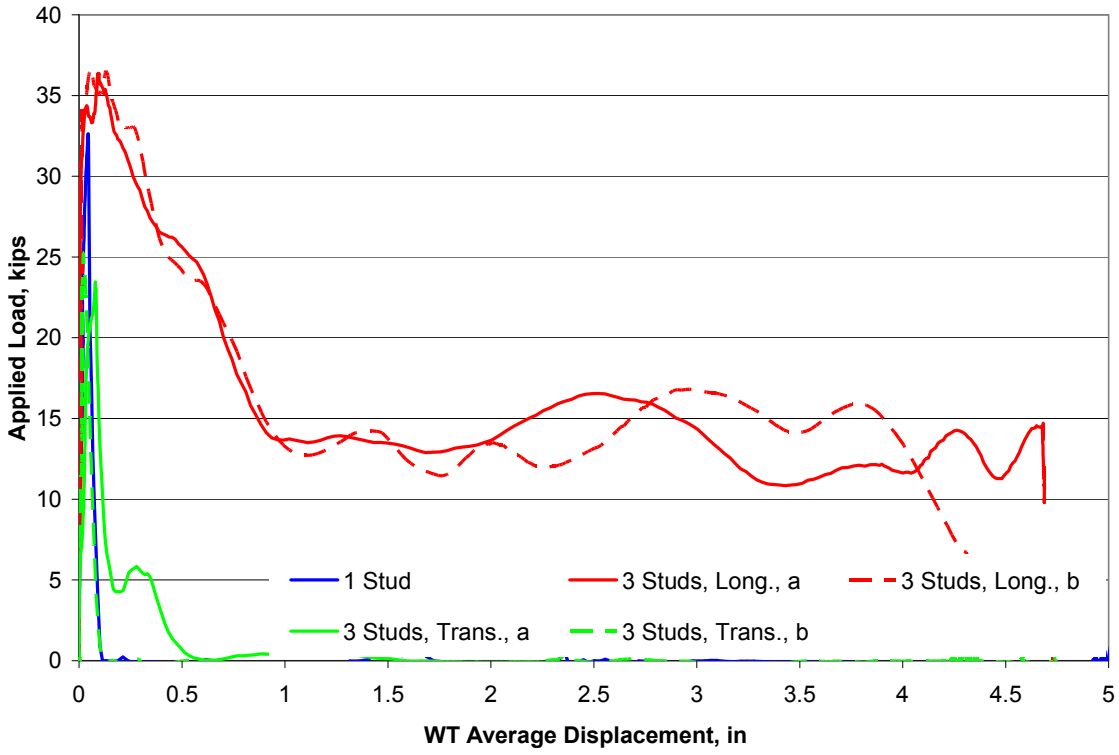

Figure 4.47: Load-Deflection Plots for 3-in Haunch Specimens Loaded Dynamically

Figure 4.48: Dynamic Specimens with a Haunch (a) Fractured Haunch with Multiple Pieces (b) Connected Haunch Segment Showing 45-Degree Failure Angle

For three studs spaced longitudinally, the cracking and load-deflection behavior is very different from other haunch cases under dynamic load. Both specimen replicates had a similar behavior to static specimen 5:3-3La in Series II, where the exterior studs mechanically engaged with the rebar. The result of this rebar-stud interlock is failure by a major horizontal crack growing out to the edges of the specimen and substantial bottom mat rebar flexure, as shown in Figure 4.49. Both specimens show substantial post-peak load strength, on the order of 12 to 18 kips, for the full range of measured displacements.

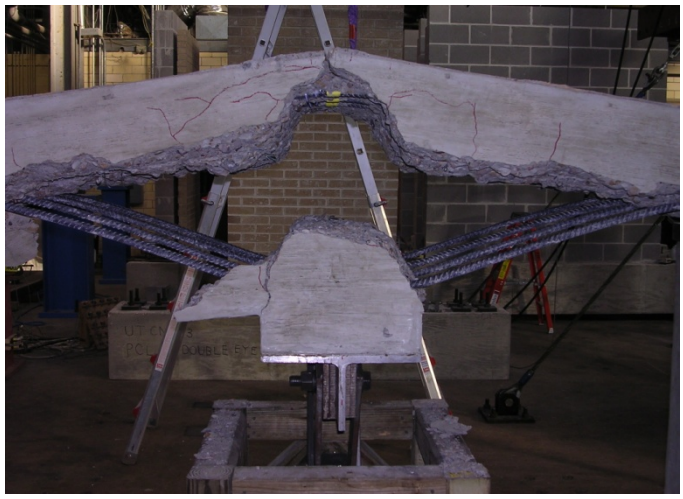

Figure 4.49: Failure of Specimen 5:3-3LDa

Specimens with no Haunch

As with the 3-in haunch specimens, the dynamically loaded no-haunch specimens behave very similarly to their respective static cases. Strengths of all specimens are higher, while the ductilities are lower than the respective static tests. Load-displacement plots for dynamically loaded no-haunch specimens are shown in Figure 4.50. Specimen 5:0-3Tb had a damaged load cell and produced no data. Specimens with a single stud and specimens with three studs spaced transversely have very similar behavior. Both configurations had a complete separation of the haunch from the slab after the formation of the horizontal failure cracks and a sudden drop in load as shown in Figure 4.50. For single-stud specimens, the applied load reaches zero around 1 in of displacement, indicating very little ductility. For

three studs spaced transversely, the specimen is able to maintain load for larger displacements, reaching a minimal level of load (2 kips) at 2 in of displacement.

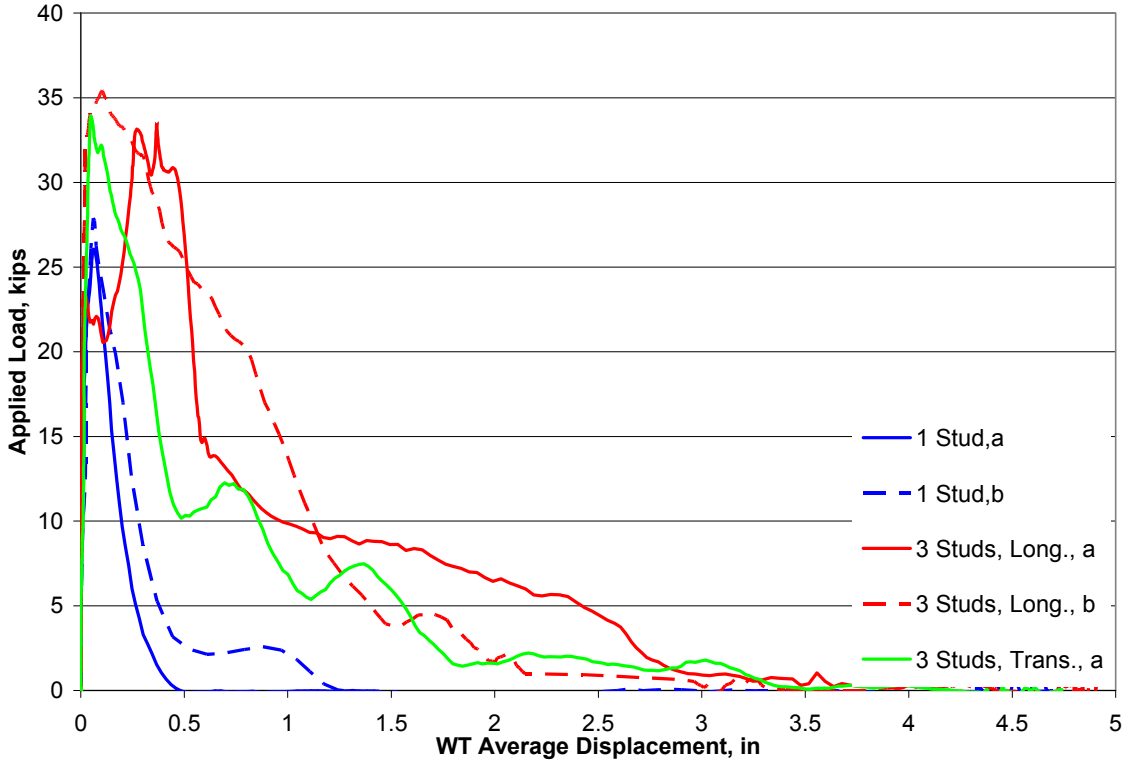

Figure 4.50: Load-Deflection Plots for No-Haunch Specimens Loaded Dynamically

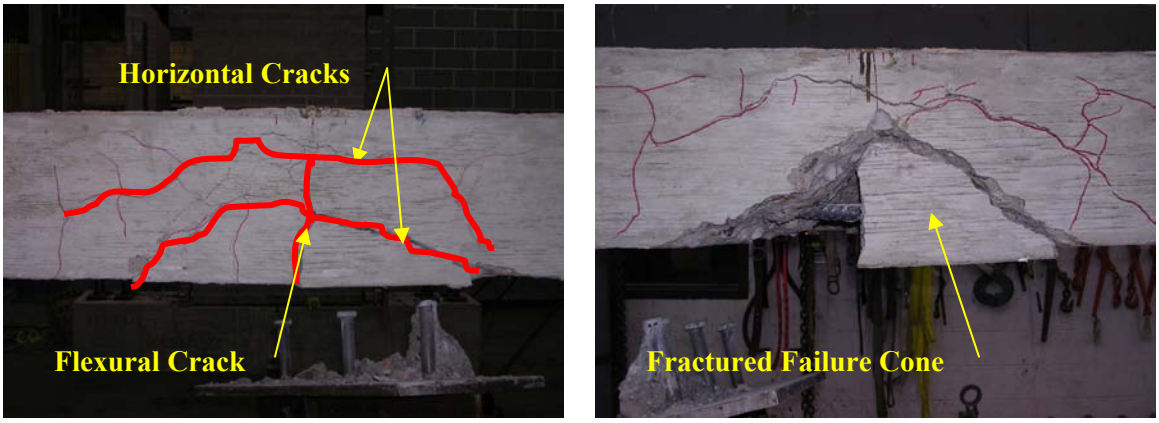

(a) ***(b)***

Figure 4.51: Failure of Dynamic Specimens 5:0-3LD (a) Cracking Patterns (b) Fractured Failure Cone

The failure behavior of three studs spaced longitudinally without a haunch is different than other dynamically loaded no-haunch specimens, though it is still similar to the respective static case. The specimens show considerable cracking, both flexural and horizontal, as shown in Figure 4.51(a). Horizontal cracking creates the characteristic ridge of concrete around the studs. While this ridge remains an intact block of concrete in static tests, for dynamic tests it fractures into multiple pieces as displacements increase. Some pieces of the fractured failure cone remain lodged against the rebar in the

specimen, as shown in Figure 4.51(b). The load-displacement curves have the same trend as in respective static cases, with peak load sustained over increasing displacement. After breakout, a rapid decrease in load occurs, down to approximately one-third of the peak strength. After this initial drop, the load continues to decrease very slowly as displacements increase. Load eventually begins to reach minimal levels after 3 in of displacement. All dynamic specimens without a haunch have displacements at peak load between 0.02 and 0.05 in, which are similar to the corresponding static displacements. The single exception is specimen 5:3-3Ta, which for unknown reasons has a peak load displacement of 0.08 in.

4.5.3 Shear Stud Gage Data

While the yield strength of steel elevates with increasing strain rates, the static yield strength is used exclusively in this analyses presented in this section. Static yield is used as a reference because the strain rates during testing varied, making determination of a single strain rate value for calculation of adjusted properties impractical. Because the static yield assumption underestimates true yield strength in each stud, percentage-of-yield calculations potentially overestimate the true percentage of yield. All data for Series IV shear studs are analyzed with the same procedures used in Section 4.2.3. With the exception of single-stud specimens, which in some cases achieved up to 95% of the static yield stress, most studs are stressed to less than 45% of static yield. The single exception is specimen 5:3-1Da, which has a peak strain of 144% of the static yield strain. This value is unrealistically high compared to the applied force, and may indicate that the strain gage was damaged either before or during the test.

Specimens with a Haunch

All of the dynamically loaded haunch specimens compare well with their static counterparts. Most specimens have calculated stud forces less than the applied force, with the difference again attributed to steel-concrete friction. For single-stud specimens, Figure 4.52 shows that the measured stud force is equal to or above the applied force near peak load, which is also reflected in Table 4.15. Both single-stud specimens have a degree of eccentric pullout, leading to the increase in stud force above applied load. For three studs spaced longitudinally, Figure 4.53 shows a variation in force among the three studs, with the center stud gaining force as load increases. Both specimens show a modest degree of concrete friction load transfer at peak load.

For three studs spaced transversely, Figure 4.54 shows that the center stud carries significantly more force (approximately 60% to 70% greater) than either of the two outer studs. The two outer studs carry approximately the same load, with minor variations. Specimen 5:3-3Tb shows a reasonable amount of concrete friction load transfer at peak load, while specimen 3:3-3Ta shows a very large amount of friction load transfer for reasons that are not clear.

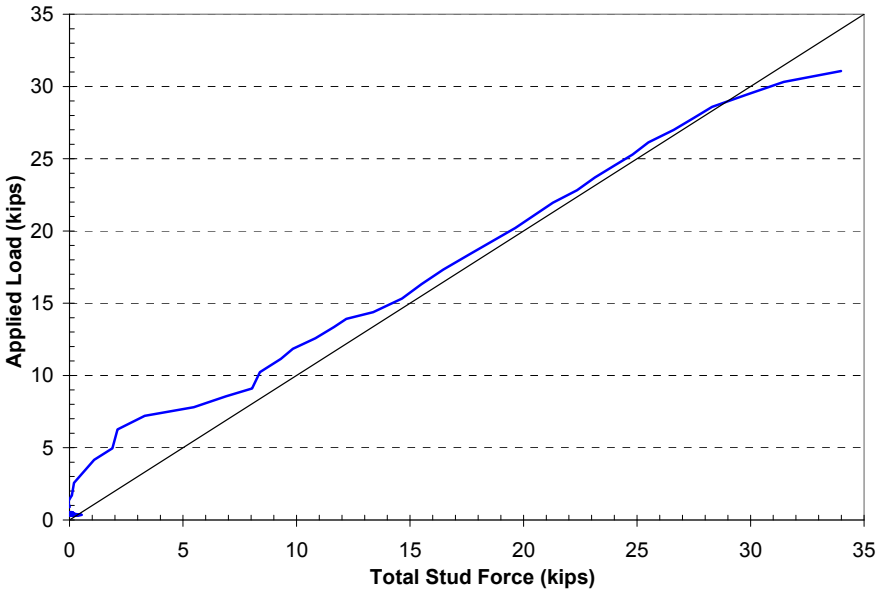

Figure 4.52: Applied Force vs. Stud Force, Specimens 5:3-1D

Table 4.15: Series IV Specimens, 3-in Haunch, Comparison of Stud and Applied Forces

Specimen	Stud Location	Strain (in/in)	Stress (ksi)	Force (kips)	% Total Stud Force	Total Stud Force (kips)	Applied Force (kips)	% Difference
5:3-1a	**Gage Malfunction**							
5:3-1b	Center	0.001949	56.52	33.99	100.0%	33.99	31.07	9.40%
5:3-3La	Left	0.000555	16.10	9.68	28.6%	33.80	36.24	-6.76%
	Center	0.000780	22.62	13.60	40.2%			
	Right	0.000603	17.49	10.52	31.1%			
5:3-3Lb	Left	0.000694	20.13	12.10	33.9%	35.68	36.53	-2.33%
	Center	0.000641	18.59	11.18	31.3%			
	Right	0.000711	20.62	12.40	34.8%			
5:3-3Ta	Left	0.000218	6.32	3.80	23.3%	16.30	21.85	-25.36%
	Center	0.000555	16.10	9.68	59.4%			
	Right	0.000162	4.70	2.83	17.3%			
5:3-3Tb	Left	0.000396	11.48	6.91	28.9%	23.89	25.27	-5.45%
	Center	0.000596	17.28	10.39	43.5%			
	Right	0.000378	10.96	6.59	27.6%			

Figure 4.53: Applied Force vs. Stud Force, Specimens 5:3-3LD

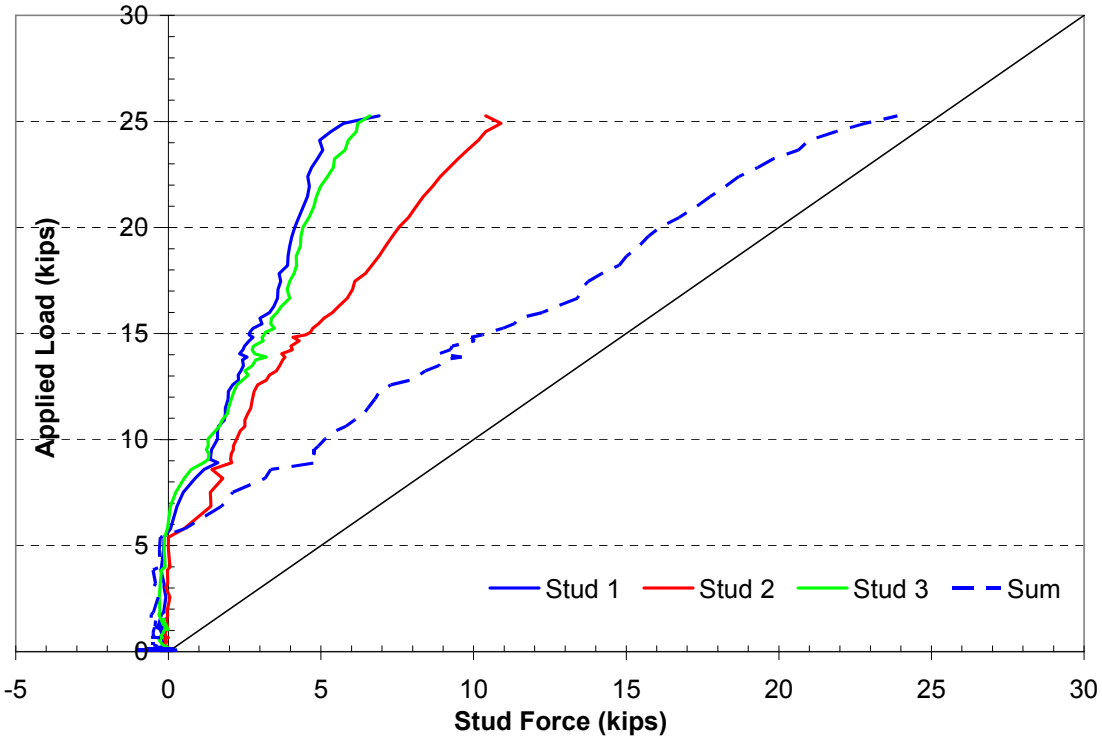

Figure 4.54: Applied Force vs. Stud Force, Specimens 5:3-3TD

Specimens with No Haunch

Dynamically loaded no-haunch specimens have force distributions in their studs similar to their respective static specimens. Single-stud specimens show a very good correlation between measured stud force and applied force as shown in Figure 4.55. Table 4.16 summarizes stud forces compared to measured peak forces.

For three studs spaced longitudinally without a haunch, Figure 4.56 shows that there is very little variation in forces among the three studs. Also, both specimens have very little load transfer by concrete friction. For three studs transversely, Figure 4.57 shows that the center stud carries much more force than the outer two studs, which each carry similar amounts of force.

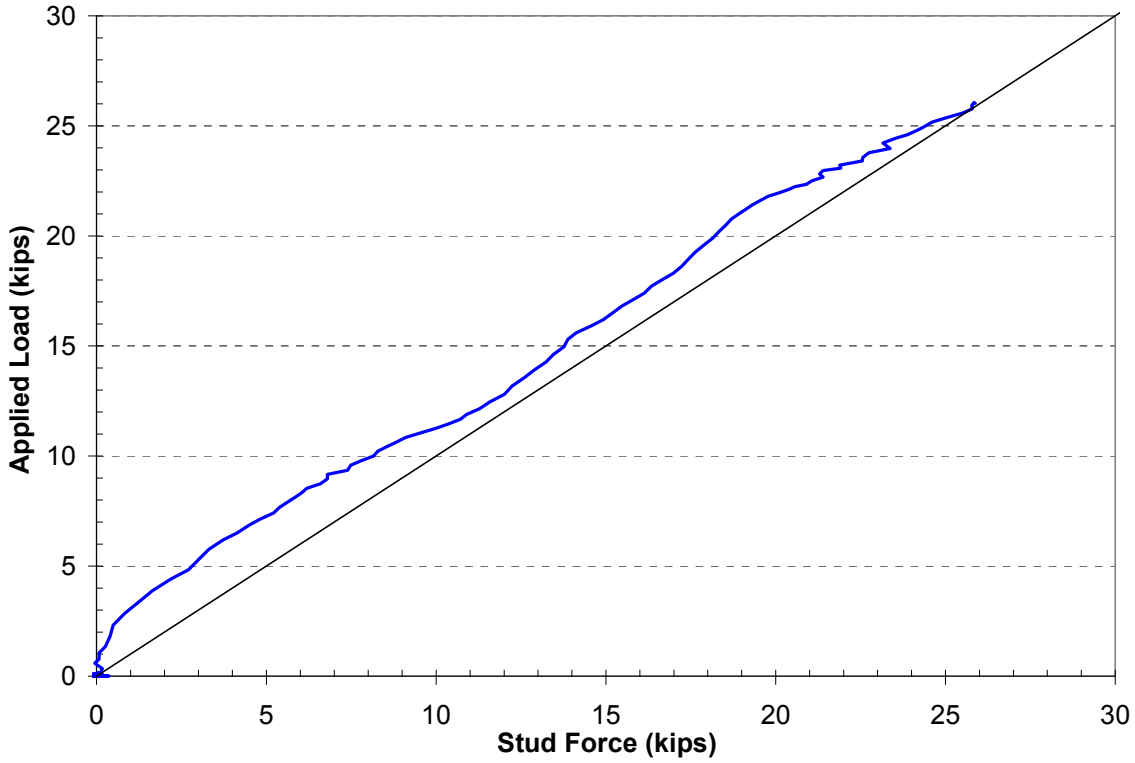

Figure 4.55: Applied Force vs. Stud Force, Specimens 5:0-1D

Table 4.16: Series IV Specimens, No Haunch, Comparison of Stud and Applied Forces

Specimen	Stud Location	Strain (in/in)	Stress (ksi)	Force (kips)	% Total Stud Force	Total Stud Force (kips)	Applied Force (kips)	% Difference
5:0-1a	Center	0.001481	42.95	25.83	100.0%	25.83	26.05	-0.84%
5:0-1b	Center	0.001648	47.79	28.74	100.0%	28.74	27.88	3.07%
5:0-3La	Left	0.000614	17.81	10.71	33.4%	32.09	32.48	-1.23%
	Center	0.000585	16.97	10.20	31.8%			
	Right	0.000641	18.59	11.18	34.8%			
5:0-3Lb	Left	0.000543	15.75	9.47	27.3%	34.63	35.42	-2.22%
	Center	0.000842	24.42	14.68	42.4%			
	Right	0.000601	17.43	10.48	30.3%			
5:0-3Ta	Left	0.000570	16.53	9.94	28.1%	35.42	33.94	4.35%
	Center	0.000908	26.33	15.83	44.7%			
	Right	0.000553	16.04	9.64	27.2%			
5:0-3Tb	**Load Cell Malfunction**							

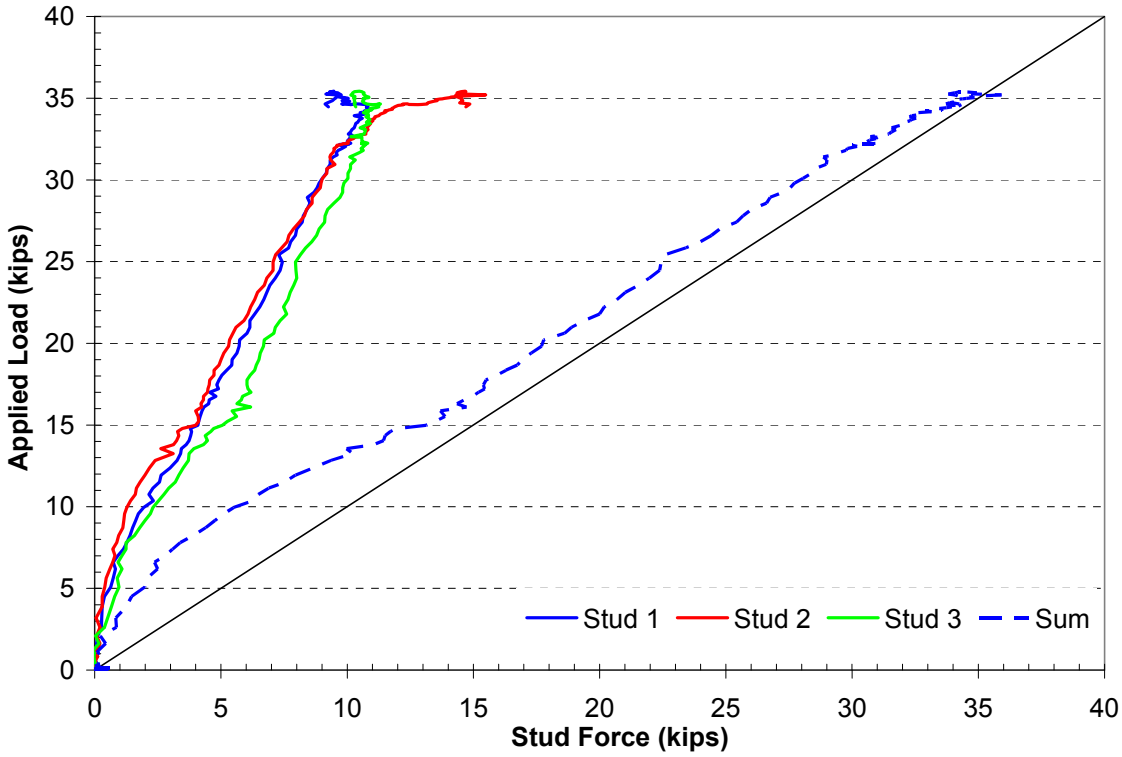

Figure 4.56: Applied Force vs. Stud Force, Specimens 5:0-3LD

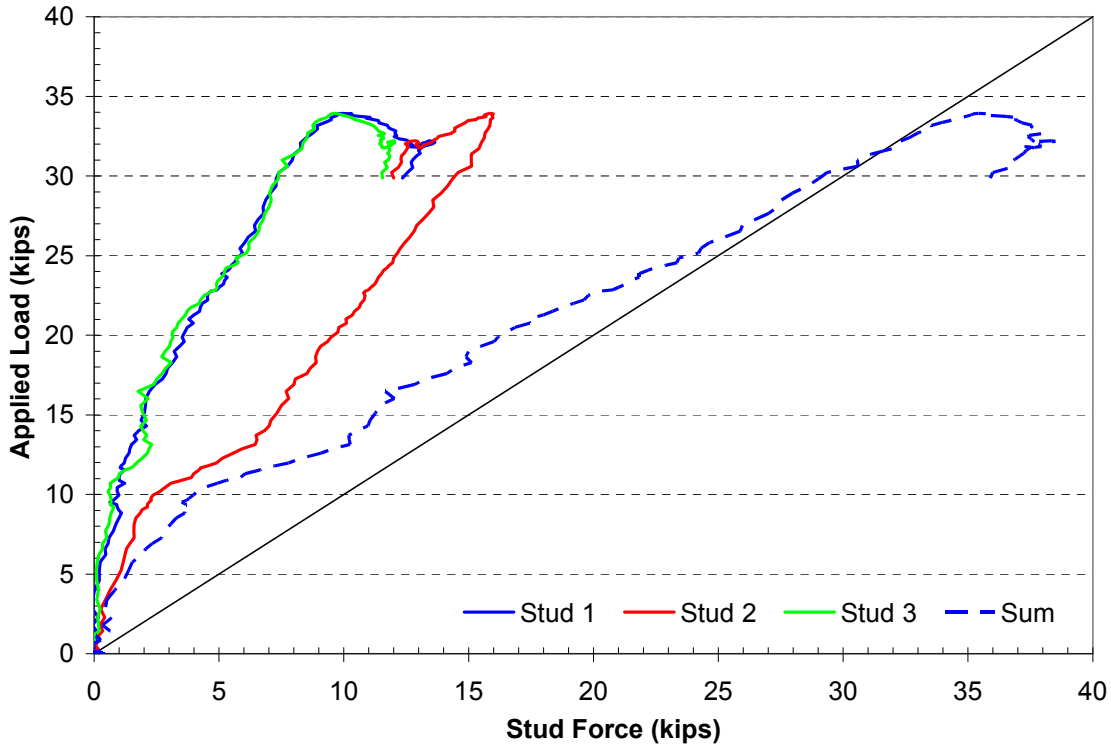

Figure 4.57: Applied Force vs. Stud Force, Specimens 5:0-3TD

4.5.4 Reinforcing Steel Gage Data

Cracking, yield, and ultimate loads for Series IV are predicted using the same methods as presented in Section 4.2.4. Strain rate effects increasing compressive strength of concrete and yield strength of the rebar are neglected for these calculations. The variability of strain rates during testing make establishing a single strain rate for calculation of adjusted material properties impractical. All "b" replicate specimens in Series IV have only the center two rebar in each mat instrumented. For Series IV, the compressive concrete strength has a mean value of 6.2 ksi, with a corresponding β_1 value of 0.74. Table 4.17 summarizes the critical points of slab behavior for Series IV.

Table 4.17: Series IV Slab Critical Loads

Slab State	Moment (kip-in)	Load (kips), No Haunch	Load (kips), 3-in Haunch
Cracking	151	7.8	9.2
First Yield	446	22.9	27.0
Ultimate Strength	549	28.2	33.3

Specimens with a Haunch

Dynamically loaded haunch specimens show different behavior depending on whether studs are spaced transversely (including the single stud case), or longitudinally. Figure 4.58 shows typical plots for both cases. All single-stud results are based on specimen 5:3-1b, because the replicate has considerable noise in the measured stud strains. For all specimens, the cracking load is elevated from the predicted 9.2 kips to between 13.0 and 14.0 kips, a dynamic increase of approximately 40%, which is very similar to the dynamic strength factor for the specimens' strengths.

After cracking, all rebar in the transversely spaced stud specimens begins to go into tension. Top mat rebar has little tensile strain prior to failure because of the low specimen strength. The top mat rebar shows little difference in strain among the individual bars, while the bottom mat of reinforcing shows significant differences in the strain, up to 40% between maximum and minimum strains. While all transverse specimens exceed the predicted static yield load, bottom mat yielding is very limited. For all transversely spaced stud specimens, strains reduce very little as applied force decreases after peak load.

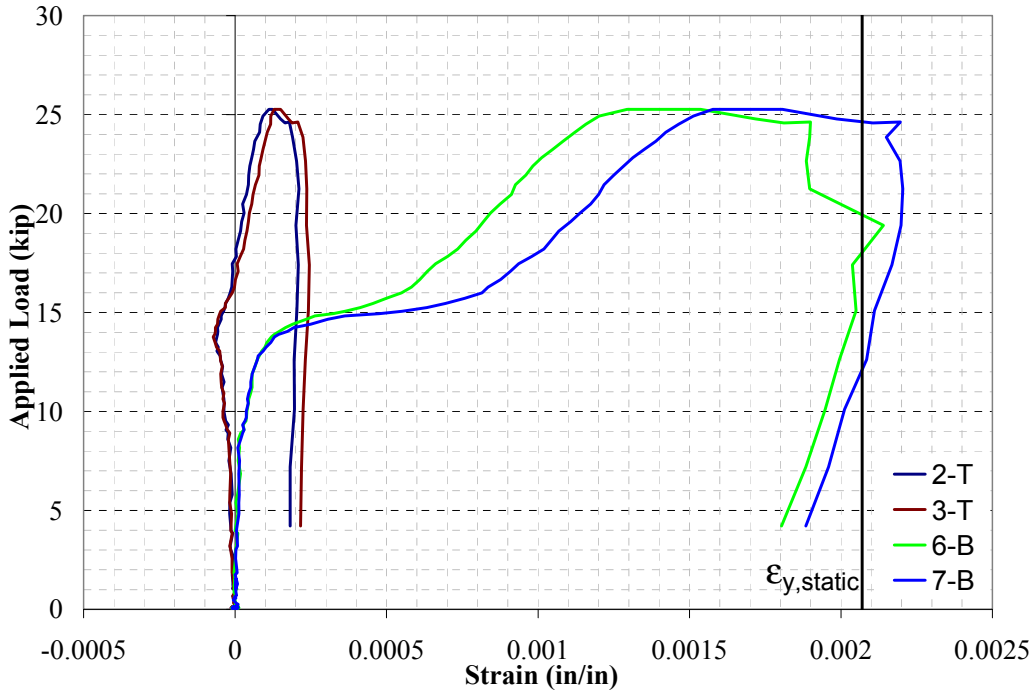

(a)

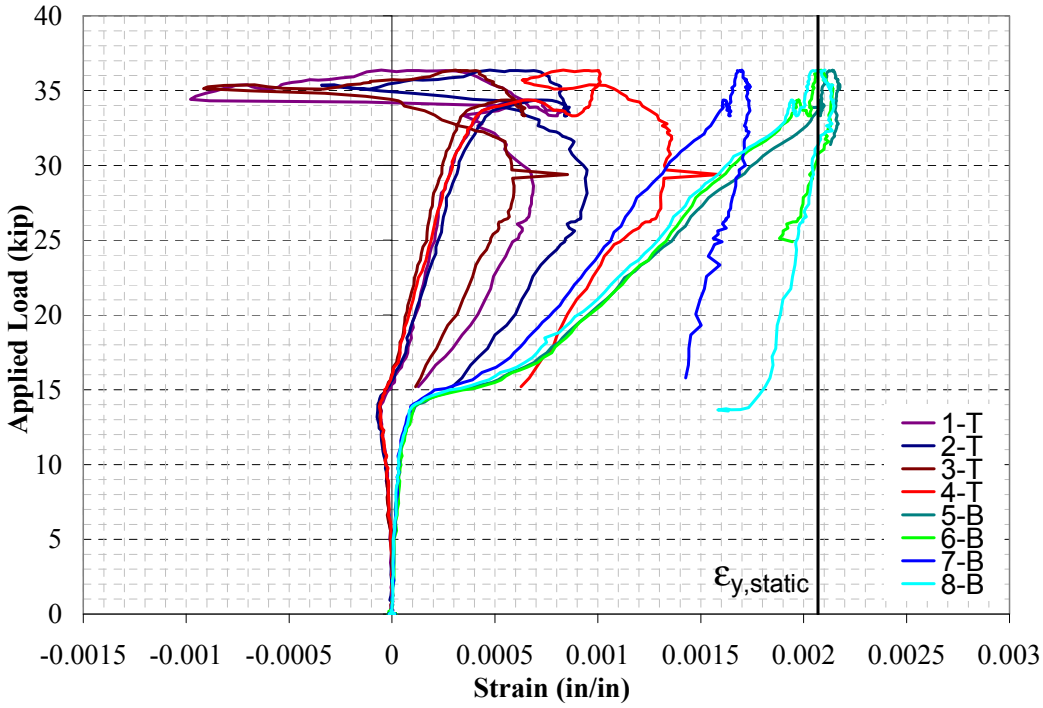

(b)

Figure 4.58: Applied Load vs. Rebar Strain Dynamically Loaded Haunch Specimens (a) with Studs Spaced Transversely (b) with Studs Spaced Longitudinally

For three studs spaced longitudinally in a haunch, all the rebar goes into tension above the cracking load, with all rebar in a single mat having nearly the same strain. At peak load (well above the

predicted ultimate load), some of the bottom rebar has just reached yield when load begins to decrease. The top mat rebar begins to experience large compressive strains at peak load, followed by a return to tensile strains as load decreases. The compressive strains are likely due to arching in the top mat reinforcement, while the tensile strains are due to bar flexure as the rebar continues to arch.

Specimens with No Haunch

Specimens with no haunch are grouped into two categories of rebar strain gage behavior: those with studs spaced transversely (including single studs), and those with studs spaced longitudinally. All specimens show considerable yielding of the rebar, with longitudinally spaced studs having strains much higher than studs spaced transversely. Representative load-rebar strain plots of each case are shown in Figure 4.59. Most specimens have a cracking load between 9.0 and 12.0 kips. These loads are much larger (around 50% greater) than the predicted static load, 7.75 kips. For unknown reasons, specimen 5:0-3La has an unusually high cracking load of 17.0 kips.

After cracking, specimens with transversely spaced studs have increasing tensile strains, with strains in both top and bottom mats showing only a small degree in variation among individual bars. Bottom bars in all transverse specimens yield between 23.0 and 24.0 kips of applied load, which is very close to the predicted static yield load of 22.9 kips. This similarity suggests that the dynamic increase of yield strength in the rebar plays a limited role for the tested loading rates. After peak load, all of the top mat reinforcement and most of the bottom mat reinforcement begin to lose strain. Some bottom bars in specimens with three studs spaced transversely continue to gain strain until the lead wires to the gages break.

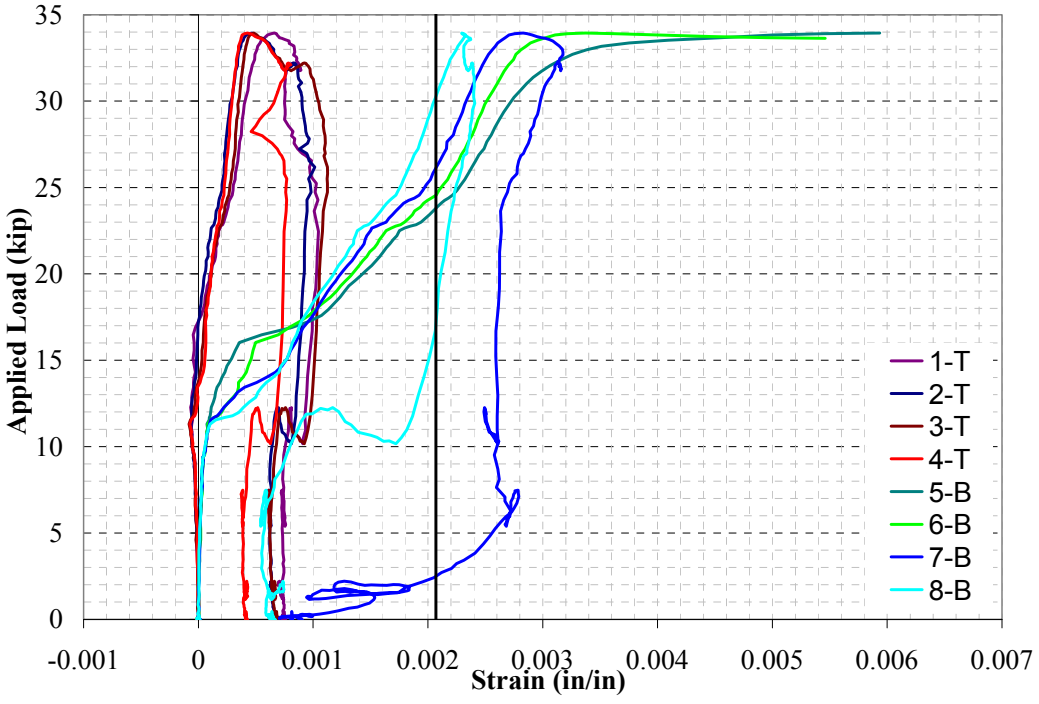

(a)

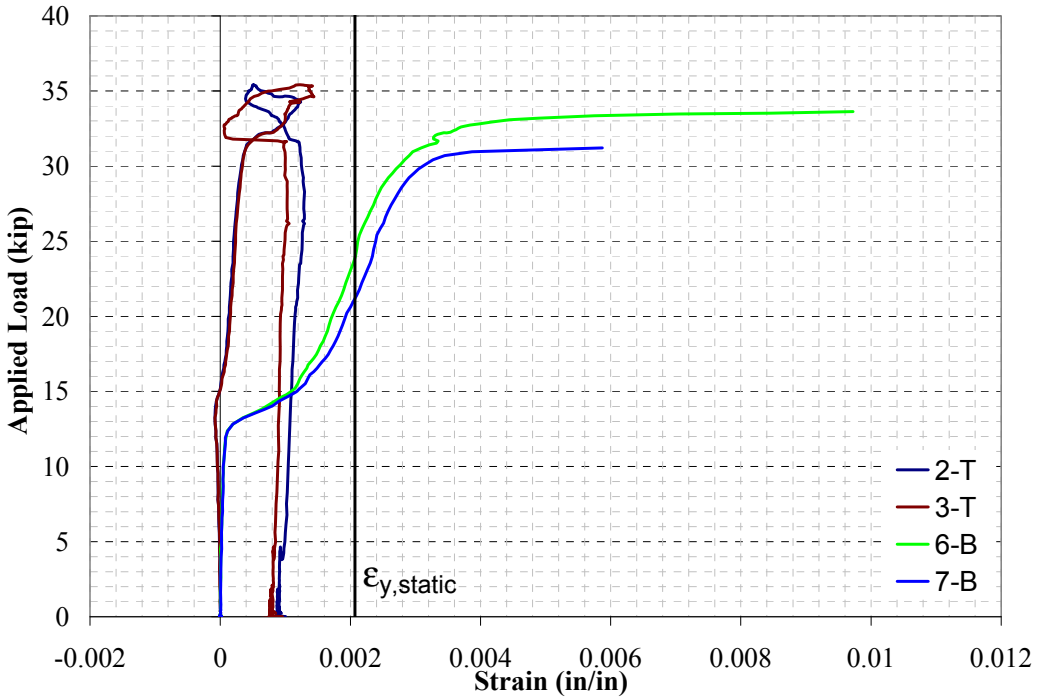

(b)

Figure 4.59: Applied Load vs. Rebar Strain Dynamically Loaded No-Haunch Specimens with (a) Studs Spaced Transversely (b) Studs Spaced Longitudinally

Specimens with studs spaced longitudinally have the same cracking behavior as other no-haunch specimens and, after cracking, all rebar goes into tension. Top mat rebar shows typical post-peak strain loss with decreasing load, while bottom mat rebar yields between 21.0 and 23.0 kips, close to the predicted yield load. At peak loads, all of the bottom mat rebar begins to gain strain rapidly without increasing loads and continues to gain strain until their lead wires break.

4.5.5 Slab Strength

No slab deflection measurements were taken for Series IV tests due to concerns that the sudden rebound of a specimen at failure would throw the measuring stand off the slab. However, visual examinations of the specimens after each test showed that dynamically loaded specimens behave similarly to their respective static tests. Specimens with three studs spaced longitudinally in a 3-in haunch both behave similarly to specimen 5:3-3La for Series II.

Concrete Cylinder Tests

Cylinder tests for Series IV were conducted statically at the strain rates prescribed by ASTM, and the results of compressive and split cylinder tests are summarized in Table 4.18. A significant delay between casting and testing occurred due to delays in receiving parts needed for the hydraulic system used in the dynamic tests. The concrete strength at testing was well in excess of the required minimum. The tensile strength of the concrete was 482 psi. This tensile strength is lower than the tensile strength of a weaker concrete (Series III) and higher than the tensile strength of a stronger concrete (Series II).

Table 4.18: Series IV Concrete Test Data

Compression Tests		**Split Cylinder Tensile Tests**		
Days after Casting	Mean Compressive Strengh, f'_c (psi)	Days after Casting	Cracking Tensile Strength, f_t (psi)	$f_t/\sqrt{f'_c}$
117	6,289	133	482	$f_t=6.1\sqrt{f'_c}$
132	6,225			
150	6,203			

Series Mean Strength: 6.2 ksi

Chapter 5: Analysis and Discussion of Test Results

5.1 Introduction

A considerable quantity of data was generated from the four series of tests presented in detail in Chapter 4. This chapter focuses on finding trends and conclusions from the accumulated data and on the development of design equations. The code-based calculations of shear stud tensile strengths in this chapter use the procedures of ACI 318-08, Appendix D, as discussed in Chapter 2. Recommended modifications to the ACI Code are covered in Section 5.3 for estimating the tensile capacity of the shear stud details used in bridges.

5.2 Evaluation of Tested Shear Stud Details

5.2.1 Strength

The most significant measure of the shear stud behavior is the peak load it carries. All tests in all series fail by concrete cone breakout, providing a common basis of comparison among specimen strengths. The strength of the stud, the weld connecting the stud to the flange, and the flange strength did not control the strength of the specimens. The strength of a shear stud connection is governed by three parameters: the stud configuration (longitudinal or transverse spacing), the stud height, and the presence or lack of a haunch. The influence of these variables for all the specimen configurations are reviewed below.

For longitudinally spaced 5-in studs with and without a haunch, strength increases from one to two studs, then shows virtually no increase in strength as more studs are added. The strength reaches a plateau at two studs because the failure cones of the studs have overlapped, and adding studs does not engage additional concrete. In general, specimens with a haunch have higher strengths than similar specimens without a haunch because the haunch prevents cracking around the studs. The single exception to this case is the transversely spaced 5-in stud specimens. The single stud test has a higher strength than those specimens without a haunch (because of no cracking in haunch). However, as more studs are added, significant strength is lost due to the outer studs' proximity to the edge of the haunch. Specimens with studs spaced transversely without a haunch show an increase in strength as studs are added because more concrete is being engaged by the studs. All dynamically tested specimens mimic the behavior of their respective static tests.

Tall studs spaced longitudinally show a similar trend to 5-in studs spaced longitudinally, though 9-in studs with a haunch carry slightly more and 7-in studs with a haunch carry slightly less load than the same number of 5-in studs without a haunch. This variation in strength is because 9-in studs in a haunch are effectively 1-in taller than 5-in studs without a haunch and 7-in studs are effectively 1-in shorter than 5-in studs without a haunch. Tall studs spaced longitudinally, as with 5-in studs, show very little increase in strength when more than two studs are present. The single difference between tall studs and 5-in studs is that tall single studs carry more load (close to the load carried by two 5 in. studs) than the single 5-in studs. Tall studs spaced transversely show a divergence in behavior; 7-in studs behave similarly to 5-in studs in a haunch, with strength decreasing as the number of studs increases due to the edge effect. For 9-in tall studs, the strength remains roughly constant from one to two studs, then increases with the addition of the third stud. This divergence is due to the 7-in studs, like the 5-in studs, only engaging haunch concrete and no reinforcement, while the 9-in studs are tall enough to engage the rebar as well as concrete outside the haunch.

For each series of tests, ACI 318, Appendix D is used to calculate a predicted strength based on the mean concrete strength for that series and the given stud configuration. To review the code's tensile cone breakout strength equations:

$$N_b = k_c \sqrt{f_c'} h_{ef}^{1.5} \qquad \text{Equation 5.1 (ACI 318-08)}$$

$$N_{cbg} = \frac{A_{Nc}}{A_{Nco}} \psi_{ec,N} \psi_{ed,N} \psi_{c,N} N_b \qquad \text{Equation 5.2 (ACI 318-08)}$$

where: N_b = concrete cone breakout strength of a single isolated stud in a continuous piece of cracked concrete (lb)
k_c = 24 for cast-in-place shear studs
f'_c = specified concrete compressive strength (psi)
h_{ef} = effective height of shear stud in concrete (in)
N_{cbg} = design concrete breakout strength of a stud or group of studs (lb)
A_{Nc} = projected concrete cone failure area of a stud group (in^2)
A_{Nco} = projected concrete cone failure area of a single stud in continuous concrete ($= 9h_{ef}^2$) (in^2)
$\psi_{ec,N}$ = eccentric load modification factor
$\psi_{ed,N}$ = edge distance modification factor (when distance is less than $1.5h_{ef}$)
$\psi_{c,N}$ = cracked concrete modification factor

The calculation of N_b is constant for each series and stud height. For each series, the mean concrete compressive strength is used in calculations. The effective height of a stud is the distance from the base of the installed stud to the underside of the stud head. Because the stud head is a standard 3/8-in thick for all heights of 7/8-in diameter studs, this configuration makes the effective height of a stud equal to 3/8 in less than the full height in all cases. The eccentric load factor, $\psi_{ec,N}$, is taken as 1.0 in all cases except the two eccentric load tests. The cracked concrete factor, $\psi_{c,N}$, is taken as 1.0 (cracking present in concrete) for all specimens without a haunch because flexural cracking occurs around the studs well in advance of peak load. For specimens with a haunch, the factor is taken as 1.25 (uncracked concrete) because no cracking occurs within the haunch until at or after failure cone formation. The edge distance factor, $\psi_{ed,N}$, varies depending on the geometry of the specimen and the height of the stud:

$$\psi_{ed,N} = 0.7 + 0.3 \frac{c_{a,\min}}{1.5h_{ef}} \text{ for } c_{a,min} < 1.5h_{ef} \qquad \text{Equation 5.3 (ACI 318-08)}$$

where: $\psi_{ed,N}$ = edge distance modification factor (when distance is less than $1.5h_{ef}$)
$c_{a,min}$ = smallest edge distance measured from center of stud to the edge of concrete (in)
h_{ef} = effective height of shear stud in concrete (in)

For specimens without a haunch, $c_{a,min}$ is taken as the longitudinal distance from the end of the concrete slab to the nearest stud. Using this distance typically produces very small edge effect strength reductions, with $\psi_{ed,N}$ often equaling 1.0 because $c_{a,min}$ is greater than or equal to $1.5h_{ef}$. For specimens with a haunch, the side of the haunch is taken as an edge in determining $c_{a,min}$ and results in significant

reductions in strength for studs spaced transversely. Table 5.1 tabulates values for $\psi_{ed,N}$ for each specimen along with the other major variables in the strength equation.

Table 5.1: Values used to Calculate ACI 318, Appendix D Specimen Strength

Series	Configuration	N_{cbg}, kips	A_{Nco}, in^2	A_{Nc}, in^2	h_{ef}, in	$c_{a,min}$, in	$\psi_{ed,N}$	$\psi_{c,N}$
Series I f'_c=5.9 ksi	5:0-1	18.3	192.5	192.5	4.625	12.0	1.000	1.00
	5:0-2T	23.6	192.5	248.0	4.625	12.0	1.000	1.00
	5:0-3T	28.9	192.5	303.5	4.625	12.0	1.000	1.00
	5:3-1	19.0	192.5	166.5	4.625	6.0	0.959	1.25
	5:3-2T	17.3	192.5	166.5	4.625	4.0	0.873	1.25
	5:3-3T	15.6	192.5	166.5	4.625	2.0	0.786	1.25
Series II f'_c=7.5 ksi	5:0-1	20.7	192.5	192.5	4.625	12.0	1.000	1.00
	5:0-2L	34.3	192.5	333.0	4.625	6.0	0.959	1.00
	5:0-3L	31.2	192.5	333.0	4.625	4.0	0.873	1.00
	5:0-4L	29.7	192.5	333.0	4.625	3.0	0.830	1.00
	5:3-2L	37.1	192.5	288.0	4.625	6.0	0.959	1.25
	5:3-3L	33.7	192.5	288.0	4.625	4.0	0.873	1.25
Series III f'_c=5.1 ksi	7:3-1	19.7	425.4	247.5	6.875	6.0	0.875	1.25
	7:3-2L	22.9	425.4	288.0	6.875	6.0	0.875	1.25
	7:3-3L	21.3	425.4	288.0	6.875	4.0	0.816	1.25
	7:3-2T	18.3	425.4	247.5	6.875	4.0	0.816	1.25
	7:3-3T	17.0	425.4	247.5	6.875	2.0	0.758	1.25
	9:3-1	19.2	708.9	288.0	8.875	6.0	0.835	1.25
	9:3-2L	19.2	708.9	288.0	8.875	6.0	0.835	1.25
	9:3-3L	18.2	708.9	288.0	8.875	4.0	0.790	1.25
	9:3-2T	18.2	708.9	288.0	8.875	4.0	0.790	1.25
	9:3-3T	17.1	708.9	288.0	8.875	2.0	0.745	1.25
Series IV f'_c=6.2 ksi	5:0-1D	18.8	192.5	192.5	4.625	12.0	1.00	1.00
	5:0-3TD	29.6	192.5	303.5	4.625	12.0	1.00	1.00
	5:0-3LD	28.4	192.5	333.0	4.625	4.0	0.87	1.00
	5:3-1D	19.5	192.5	166.5	4.625	6.0	0.96	1.25
	5:3-3TD	16.0	192.5	166.5	4.625	2.0	0.79	1.25
	5:3-3LD	30.7	192.5	288.0	4.625	4.0	0.87	1.25

The single failure cone breakout area, A_{Nco}, is computed using ACI 318, Appendix D as a square $3h_{ef}$ on a side, for an area of $9h_{ef}^2$. The group failure cone area, A_{Nc}, differs depending on whether a haunch is or is not present. If no haunch is present, the group failure cone area is defined by the total area covered by overlapping single stud failure cone areas. Figure 5.1 illustrates the method used to calculate a single stud failure cone area and a group failure cone area without a haunch. For specimens with a haunch, the sides of the haunch are assumed to act as an edge in confining the size of the failure cone area to the haunch region. Figure 5.2 shows the projected stud failure cone areas for specimens with transverse and longitudinal stud spacings in a haunch.

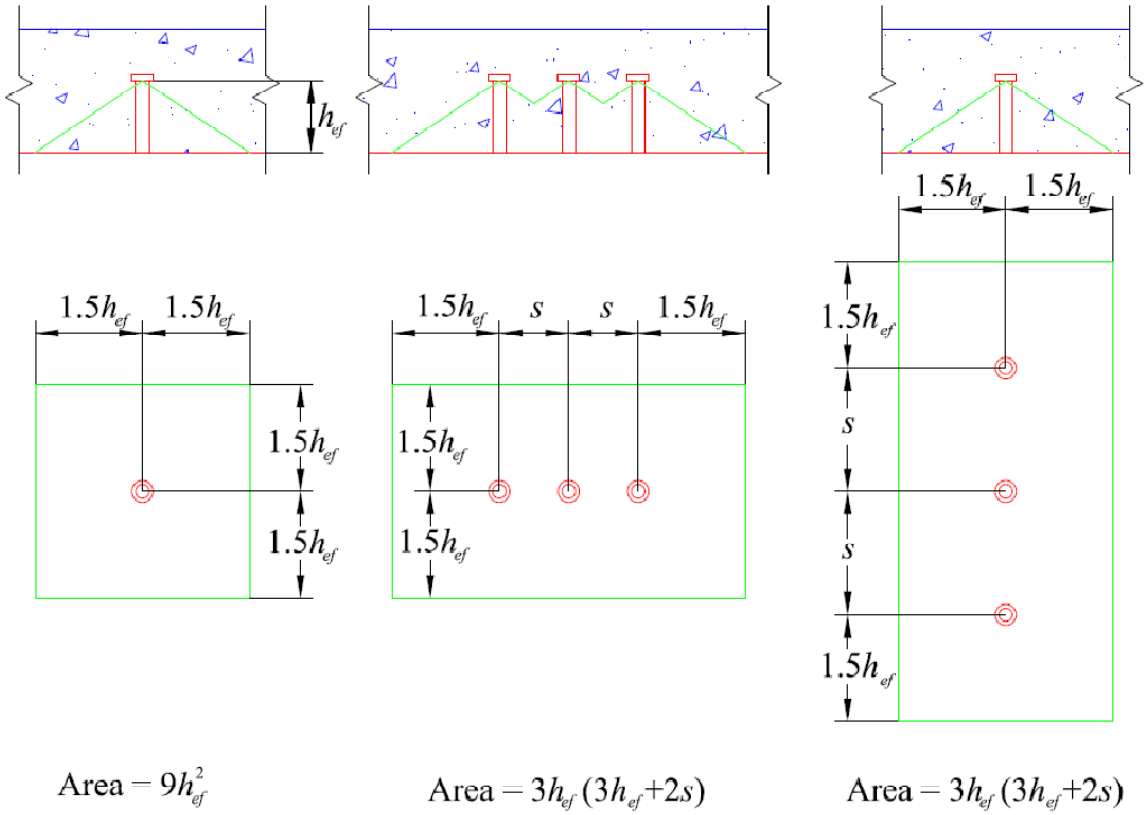

Figure 5.1: Dimensioned Projected Failure Cone Areas for (a) 1 Stud (b) 3 Studs Spaced Transversely (c) 3 Studs Spaced Longitudinally, all without a Haunch

Using the values in Table 5.1 to calculate predicted strengths for each specimen, the predicted strengths are compared to the mean of the measured specimen strengths. No strength reduction factor (ϕ) is included in the code calculations to compare nominal predicted strengths with measured values. Table 5.2 lists the comparisons for all four series. In the case of Series IV, the estimated static strengths of the dynamically tested specimens were calculated using ACI 318, Appendix D and then multiplied by the measured dynamic strength factor.

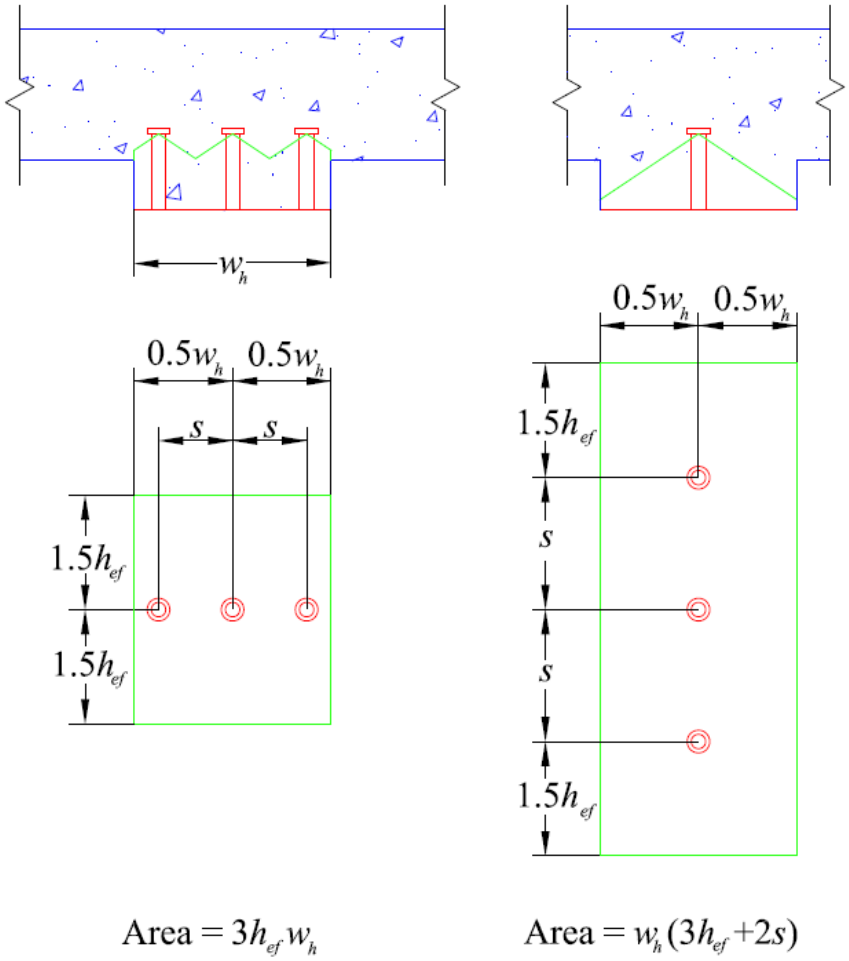

Figure 5.2: Dimensioned Projected Failure Cone Areas for (a) 3 Studs Spaced Transversely and (b) 3 Studs Spaced Longitudinally, both in a Haunch

Table 5.2: Comparison of Code Predicted and Measured Strengths

Series	Stud Configuration	P_{code}, kips	$P_{measured}$, kips	$P_{code}/P_{measured}$
Series I	5:0-1	18.3	20.9	0.88
	5:0-2T	23.6	24.6	0.96
	5:0-3T	28.9	25.9	1.12
	5:3-1	19.0	22.3	0.85
	5:3-2T	17.3	19.2	0.90
	5:3-3T	15.6	17.3	0.90
Series II	5:0-1	20.7	20.6	1.00
	5:0-2L	34.3	28.8	1.19
	5:0-3L	31.2	30.1	1.04
	5:0-4L	29.7	28.9	1.03
	5:3-1	21.4	22.3	0.96
	5:3-2L	37.1	32.7	1.13
	5:3-3L	33.7	32.6	1.04
Series III	7:3-1	19.7	26.2	0.75
	7:3-2L	22.9	27.2	0.84
	7:3-3L	21.3	28.3	0.75
	7:3-2T	18.3	25.1	0.73
	7:3-3T	17.0	20.3	0.84
	9:3-1	19.2	28.4	0.68
	9:3-2L	19.2	29.5	0.65
	9:3-3L	18.2	30.0	0.61
	9:3-2T	18.2	27.7	0.66
	9:3-3T	17.1	31.4	0.55
Series IV	5:0-1D	24.2	27.0	0.90
	5:0-3LD	33.5	34.5	0.97
	5:0-3TD	38.8	33.9	1.15
	5:3-1D	27.9	31.9	0.88
	5:3-3LD	35.3	36.6	0.97
	5:3-3TD	22.5	24.4	0.93
			Mean	0.89
			Std. Dev.	0.17

Figure 5.3 compares average measured connection strengths with strengths computed by ACI 318, Appendix D for 5-in studs loaded statically. The most important variable is whether the studs are spaced longitudinally or transversely. The strength of multiple studs spaced transversely is comparable to a single stud. Stud orientation affects how accurately the code can predict the actual connection strength. For nearly all of the specimens with studs spaced transversely, the code underpredicts the actual strength by a relatively small amount, less than 15% for all 5-in stud specimens. The single exception to this trend is for three studs spaced transversely without a haunch, where the code overpredicts the strength by 10%.

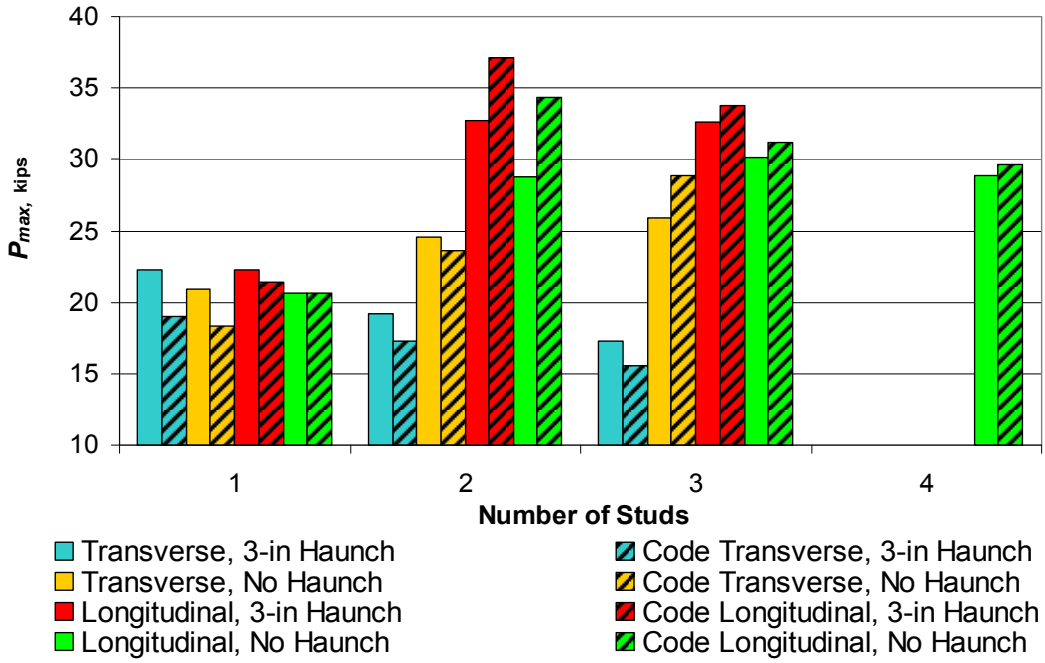

Figure 5.3: Measured and Predicted Strengths of 5-in Tall Studs Loaded Statically

For studs spaced longitudinally, there is a reasonable correlation between measured and predicted strengths, with the code never overestimating by more than 16% for 5-in studs. In the case of single-stud specimens, the code strength is often nearly exactly the same as the measured strength. As the number of studs increases, the code tends to overpredict the strength, significantly for two 5-in stud specimens (by 16%), then marginally for more than two 5-in studs (3% to 4% above the predicted value).

The key element determining the strength of a shear stud specimen in tension is the size and geometry of the tensile failure cone, represented mathematically in the code by the projected concrete failure cone area, A_{Nc}. For single studs without a haunch, the code is very accurate in predicting the strength of the specimen. This finding reaffirms the code assumption of a failure surface being pyramidal, spreading at a width-to-height ratio of 1.5:1 from the top of the effective stud height. While the code cone does not physically describe the failure surface, which is a cone of slope ratio 1:1 extending from the effective top of the stud, it does produce very good numerical results. Figure 5.4(a) shows the projected code failure cone area, overlaid with the actual failure cone for a single stud specimen without a haunch. Next to the figure is an image of the failure cone for a single stud without a haunch. For two and three studs spaced transversely without a haunch, the code also matches the predicted strength well, with only small deviations due to the close stud spacings. Figure 5.4(b) shows the multiple stud failure cones. Five-inch studs spaced transversely without a haunch increases in strength as the number of studs is increased, which is predicted well by the code.

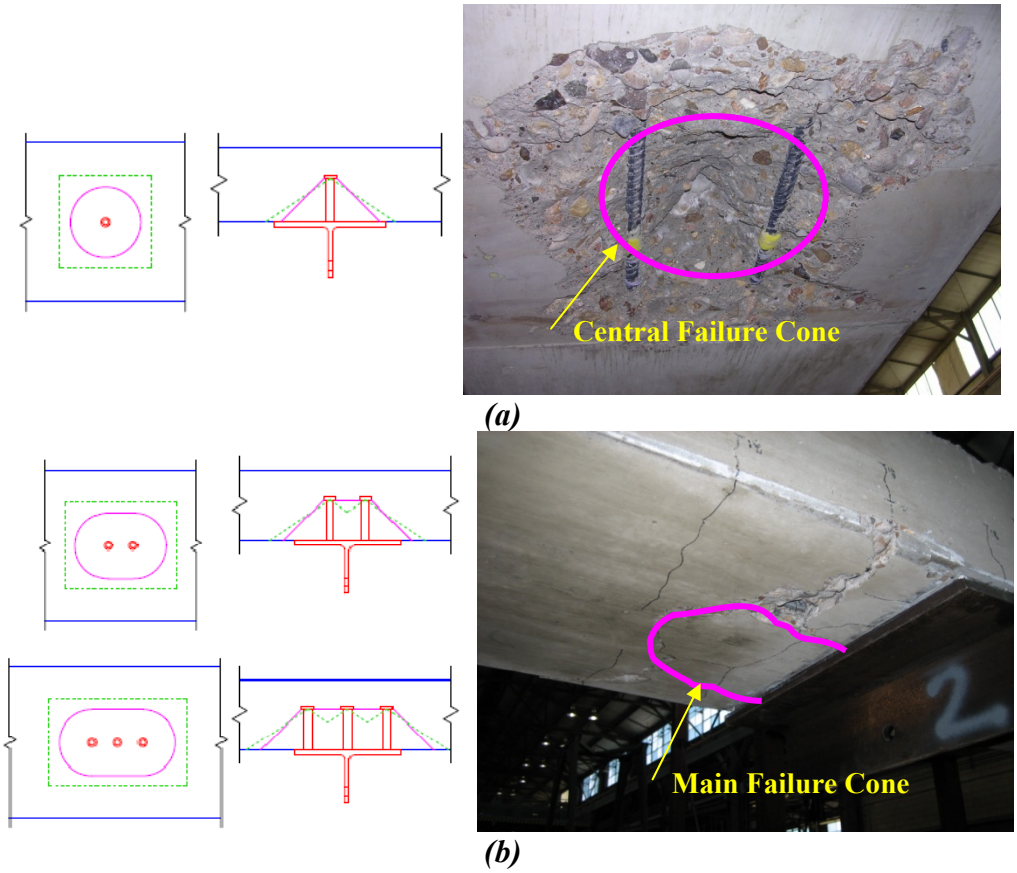

Figure 5.4: Code (Dashed) and Observed (Solid) Failure Cones with Pictures for (a) Single Studs without a Haunch (b) Multiple Studs without a Haunch

For 5-in studs spaced transversely in a haunch, the strength behavior is undesirable because adding studs decreases strength sharply. The code still predicts the stud strength well because of the edge effect modification factor. This factor appears to accurately capture the effect of the proximity of free faces to the studs has on the strength of a stud group. This effect increases in severity as the proximity of the studs to the edge of the haunch increases. Figure 5.5 shows the projected and actual failure cones for transversely spaced stud specimens with a haunch. Of note from Figure 5.5 is that, while the predicted strengths agree with measured results, the predicted failure cone bears no resemblance to the actual failure surface. The actual failure surface involves the haunch splitting and separating from the slab and not the cone pullout assumed in the ACI code.

ACI 318, Appendix D does not have provisions able to address a haunch's effect on the tensile behavior because the haunch represents a reduced concrete area around the base of a stud. The code assumes that either the failure cone extends the full stud height in solid concrete (Figure 5.6(a)) or that an edge extending the full height of the stud exists (Figure 5.6(b)). The haunch is neither of these cases because the concrete is missing around the base of the stud but not around the stud head as illustrated in Figure 5.6(c). The larger slab around the head of the stud still has the potential to be mobilized in the breakout cone. The haunch was treated as a free edge in the calculation of projected area and $c_{a,min}$ because it confines the projected concrete cone failure area. For 5-in studs, this assumption appears to work well.

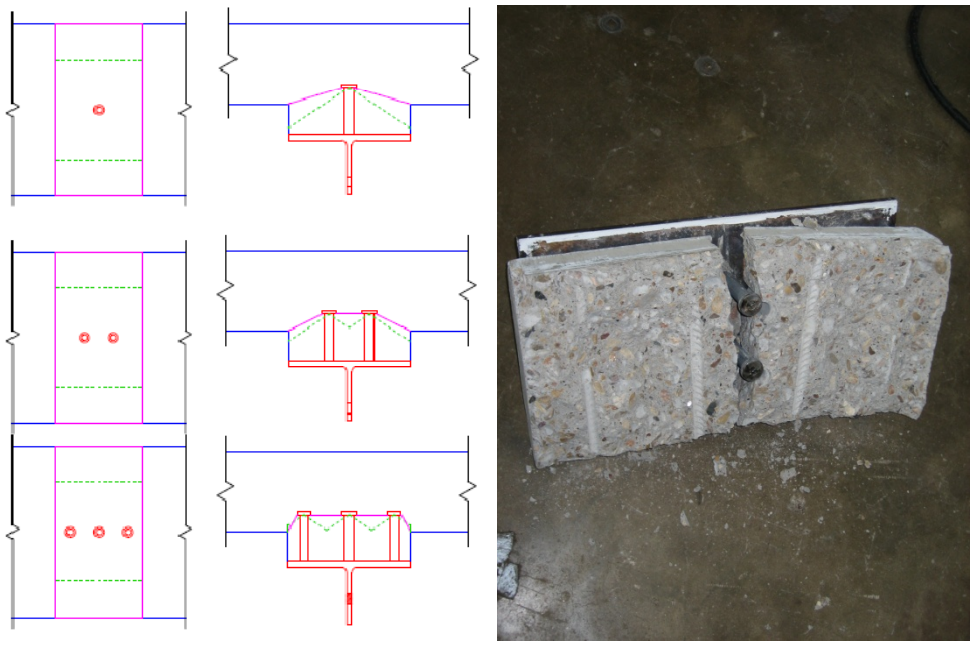

Figure 5.5: Code (Dashed) and Observed (Solid) Failure Cones with Picture for Studs Spaced Transversely in a Haunch

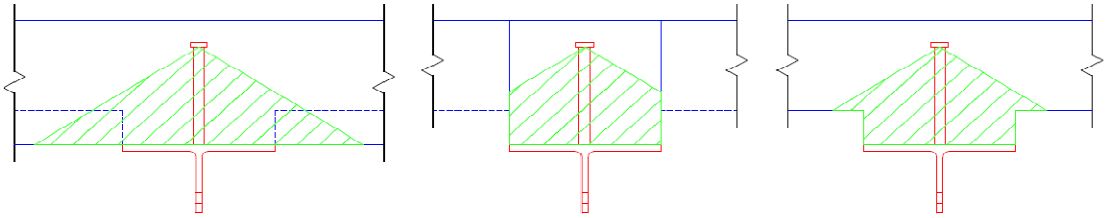

Figure 5.6: Methods of Dealing with Haunch Effect on Failure Cone Area (a) Full Height Action (b) Confined Haunch Action (c) Real Failure Cone

Five-inch studs spaced longitudinally without a haunch have a very favorable strength behavior, with a significant increase in load between one and two studs. Longitudinally spaced studs without a haunch have a higher strength than the same number of studs spaced transversely over a given length. The code predicts the strength well for large groupings of studs spaced closely together (8 in or less), but significantly overestimates strength when studs are spaced farther apart. As discussed in Chapter 4, once studs are spaced more closely than three times their effective height from one another, their failure cones overlap. However, while the code recognizes this overlap, it does not accurately predict the strength from this overlap until studs become more closely spaced. Figure 5.7 shows the projected failure areas and cones for longitudinal specimens without a haunch. As previously noted, when the failure cones of longitudinally spaced studs overlap, they form a continuous ridge of concrete, roughly trapezoidal in cross-section, down the axis of stud spacing.

For 5-in studs spaced longitudinally in a haunch, the strength behavior is still favorable. Because the haunch prevents cracking, the strength increases for a given number of studs above the same number without a haunch. Also, the longitudinal spacing helps to increase the strength because a larger area of concrete is engaged. Here again, the code has difficulties predicting the strength, both from the haunch and from the large spacings of some stud configurations. As seen with the transverse studs with a

haunch, treating the haunch as a free edge applies well, but the code still overpredicts the strength of studs spaced greater than 4-in apart. Figure 5.8 shows the projected failure areas and cones for longitudinal specimens with a haunch.

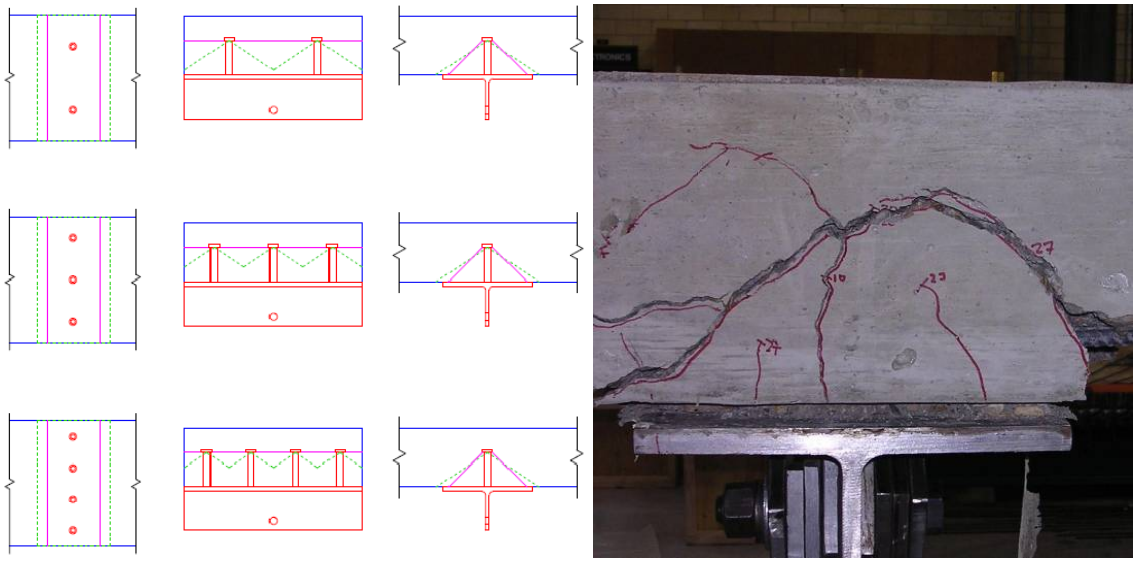

Figure 5.7: Code (Dashed) and Observed (Solid) Failure Cones with Picture for Studs Spaced Longitudinally without a Haunch

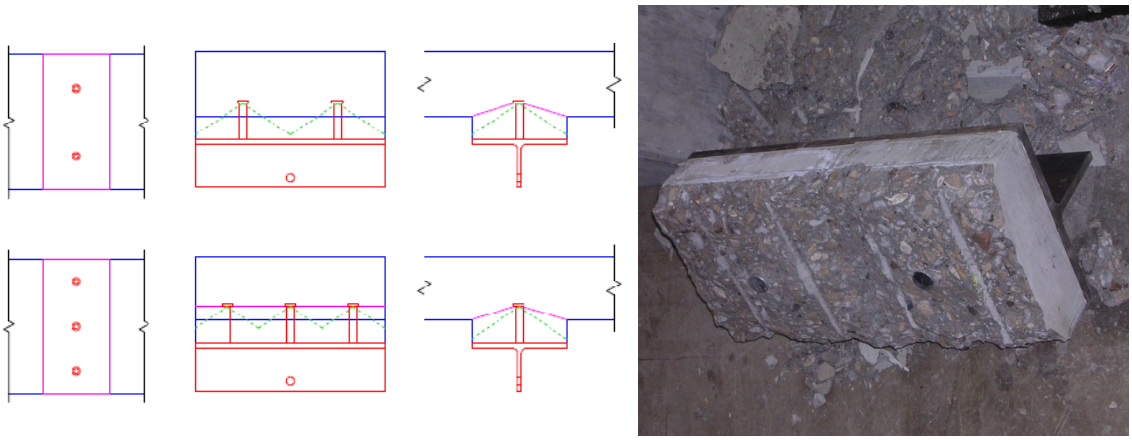

Figure 5.8: Code (Dashed) and Observed (Solid) Failure Cones with Picture for Studs Spaced Longitudinally with a Haunch

All dynamically tested specimens have similar failure cones and strength trends as their static counterparts with the exception of the 5:3-3LD specimens, which have similar strengths to specimen 5:3-3La. Because of rebar-stud interlock, the failure cone for 5:3-3LD specimens resembles the unified ridge of longitudinal specimens without a haunch rather than the more typical haunch separation of other specimens with a haunch. The code strength predictions, multiplied by the measured dynamic strength factor for each specimen, produce good results in all cases, as shown in Figure 5.9. The differences between code and measured strengths for dynamic loading are similar to the strength trends observed in static specimens. There is a distinct trend in the value of the dynamic strength factor. Specimens with studs spaced transversely with or without a haunch (including single-stud specimens) have higher dynamic strength factors (between 1.3 and 1.4) than specimens with studs spaced longitudinally with or without a haunch. Specimens with longitudinally spaced studs have dynamic strength factors between

1.15 and 1.18. The measured dynamic strength factor could not be correlated well to strain rates in either the reinforcing steel or the shear studs, so at this time there is no reliable way to match applied strain rate and the magnitude of the dynamic strength factor.

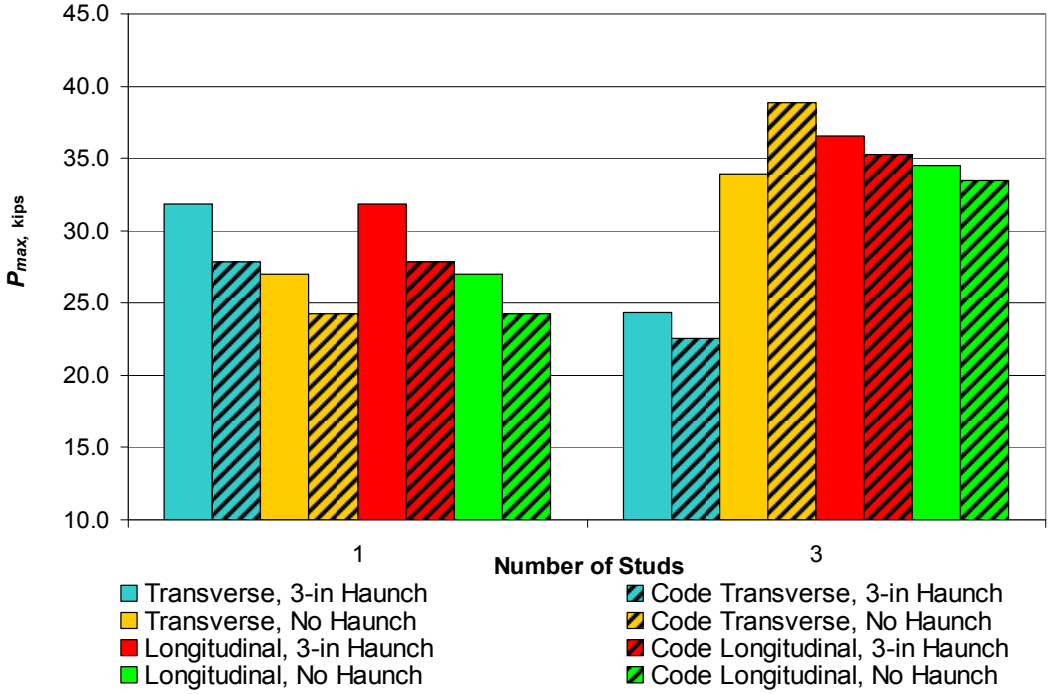

Figure 5.9: Measured and Predicted Strengths of Dynamically Loaded 5-in Studs Spaced

For tall studs (7-in and 9-in studs) spaced longitudinally with a haunch, the strength behavior is very desirable, as seen in Figure 5.10. Tall studs have high overall strengths, comparable to 5-in stud specimens without a haunch, and have higher strengths than the same number and height of studs spaced transversely. The taller 9-in studs exhibit a uniform increase in strength over the 7-in studs. Especially for the 9-in studs, the extra height over the 5-in studs allows the single stud case to develop a more complete failure ridge. Mobilizing the complete failure ridge increases the single stud strength to values similar to the group stud strength.

Figure 5.11 shows the projected and actual failure surfaces for the tall longitudinally spaced studs. The code is unable to accurately predict the specimen strength because of the presence of the haunch, underestimating it considerably. For two and three studs spaced longitudinally, measured strengths are 19% and 65% higher than the predicted strengths, respectively. This underestimated strength implies that a haunch does not act strictly as a full height edge for projected area calculations. Part of the underestimation comes from the edge effect modification factor, which gives more severe strength reductions for taller studs in a haunch than it does for 5-in studs in the same haunch. This change in reduction stems from the dependence of the edge effect factor on the effective stud height.

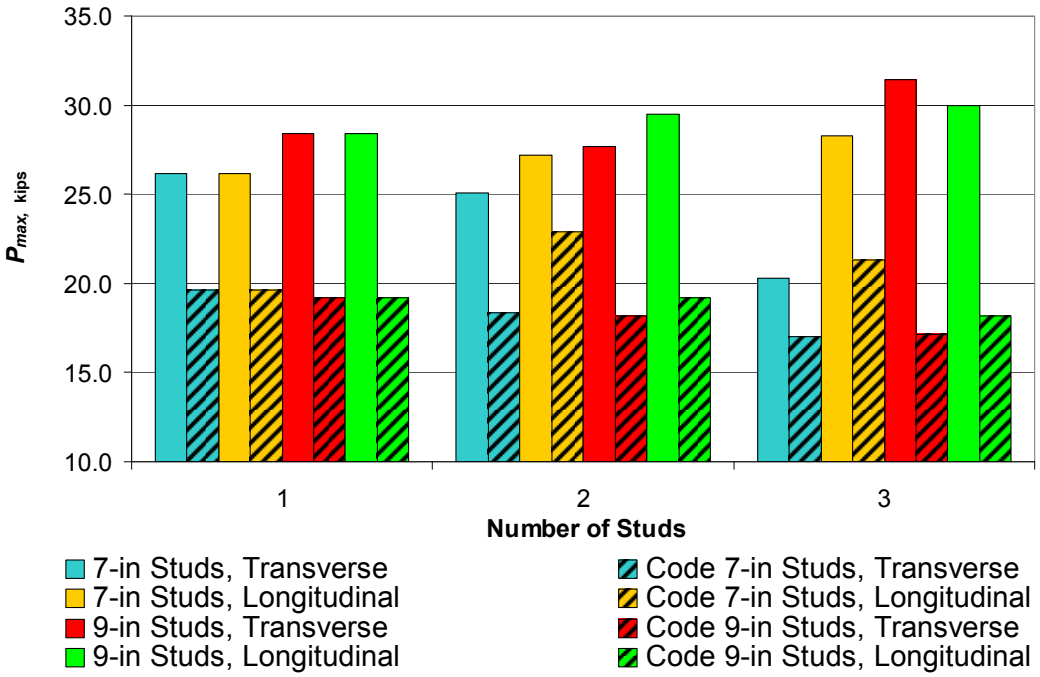

Figure 5.10: Measured and Predicted Strengths of 7-in and 9-in Tall Studs Spaced

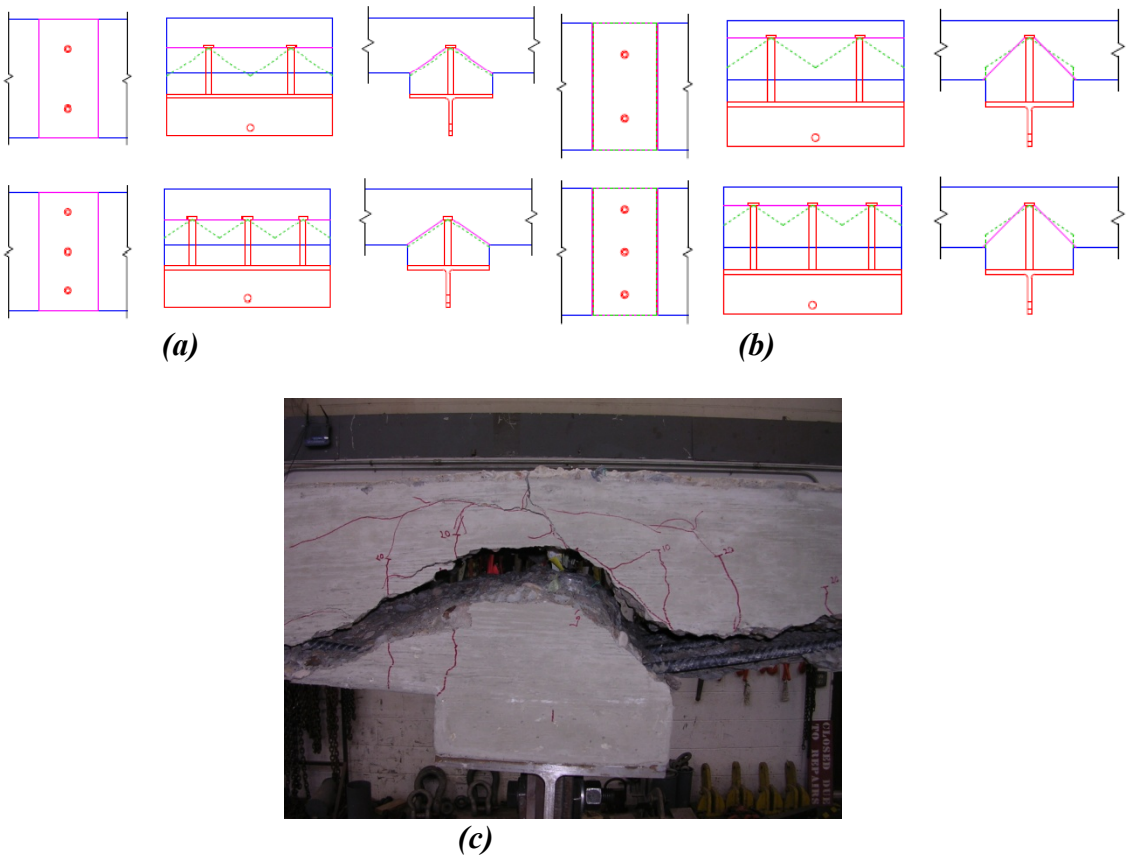

Figure 5.11: Code (Dashed) and Observed (Solid) Failure Cones for Studs Spaced Longitudinally (a) 7 in Tall (b) 9 in Tall (c) Picture of Failure Cone

As observed previously, there is a divergence in behavior for tall studs spaced transversely in a haunch. Seven-inch studs do not have a failure cone intersecting the reinforcement and, as a result, have limited strength and low ductility. While 7-in studs have a higher strength than 5-in studs in a haunch, they exhibit the same trend of decreasing strength with increasing number of studs. Nine-inch studs engage the reinforcement and thereby develop the full failure ridge, resulting in increasing strength with additional studs. Nine-inch studs have strengths similar to 5-in studs spaced longitudinally without a haunch, though there is little increase in strength with added studs. Figure 5.12 shows the projected and real failure cones for tall studs spaced transversely. Tall studs spaced transversely have the same problem as those spaced longitudinally in that the code does not properly address the haunch edge and severely underestimates the strengths of all specimens. For taller studs spaced transversely, the code highly underpredicts the measured strength, with measured strengths between 19% and 83% higher than predicted.

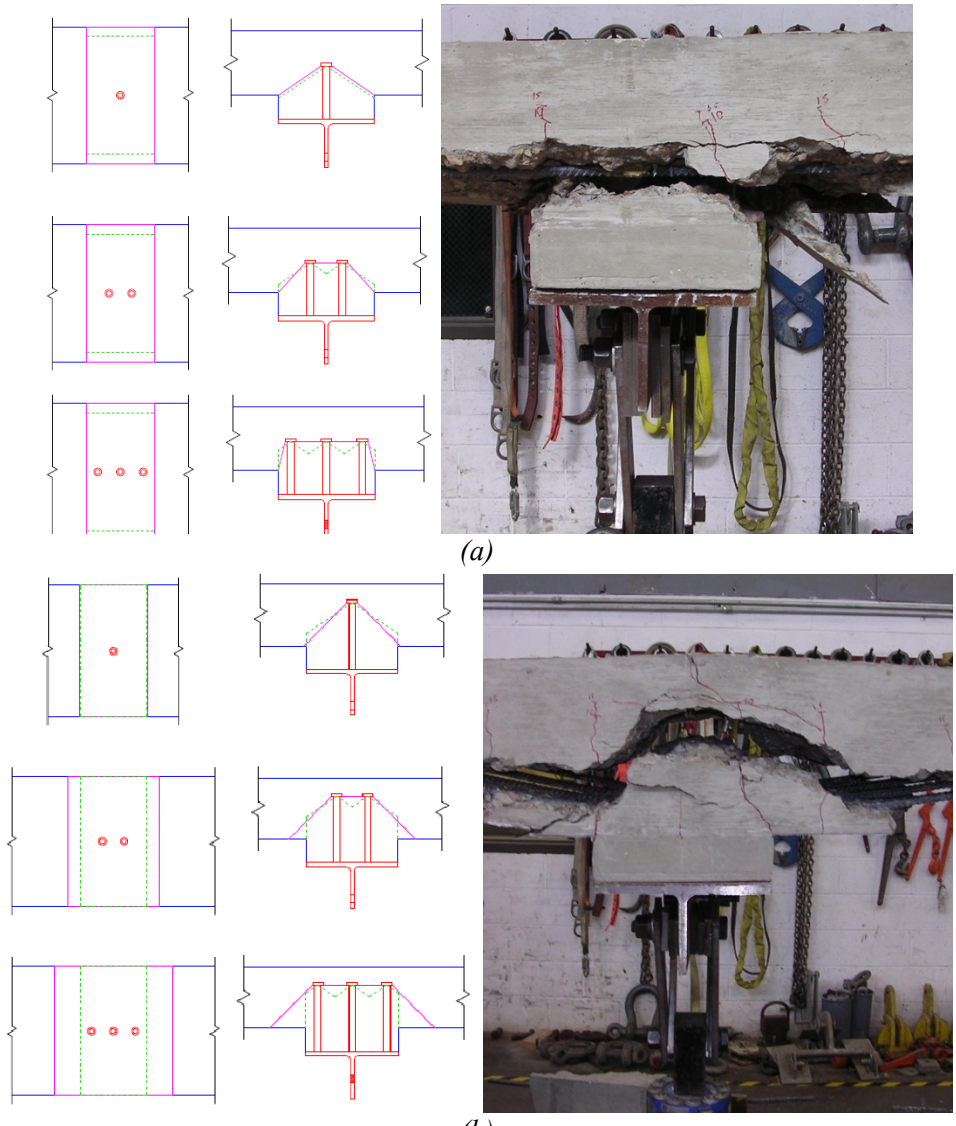

(a)

(b)

Figure 5.12: Code (Dashed) and Observed (Solid) Failure Cones with Pictures for Studs Spaced Transversely (a) 7 in Tall (b) 9 in Tall

Specimens loaded eccentrically fail similarly to their concentrically loaded counterparts. To calculate the code-based strength of the specimens for comparison, the eccentric load modification factor, $\psi_{ec,N}$, needs to be calculated based on Equation 5.4:

$$\psi_{ec,N} = \frac{1}{\left(1 + \frac{2e'_N}{3h_{ef}}\right)} \leq 1.0 \qquad \text{Equation 5.4 (ACI 318-08)}$$

where: $\psi_{ec,N}$ = eccentric load modification factor
e'_N = eccentricity of resultant stud tensile load
h_{ef} = effective height of shear stud in concrete (in)

For both specimens, the tensile load is applied with an eccentricity of 6 in from the center of the specimen. Table 5.3 lists the values of $\psi_{ec,N}$ and all other values used to compute the code-based tensile strength of the eccentrically loaded specimens. In addition to calculating the peak strength using the ACI code, another strength is computed using the load-displacement behavior from the concentric test. Assuming that the WT rotates as a rigid body, the displacement under each stud for a given rotation can be calculated. Using the load-displacement plot for the respective concentric test, the force in each stud (force per stud is assumed 1/3 of the total applied force on the concentric 3-stud specimen) and the total stud force are found for a given value of WT rotation. Performing this operation for multiple angles of rotation allows for the calculation of a complete load-displacement plot for each eccentric case and allows for determination of an approximate strength.

Table 5.3: Values used to calculate Eccentrically Loaded Specimen Strength

Series	Configuration	N_{cbg}, kips	A_{Nco}, in^2	A_{Nc}, in^2	h_{ef}, in	$c_{a,min}$, in	$\psi_{ed,N}$	$\psi_{c,N}$	$\psi_{ec,N}$
Series III	5:0-3LE	13.8	192.5	333.0	4.875	4.0	1.000	1.00	0.549
f'_c=5.1 ksi	5:3-3LE	14.9	192.5	288.0	4.875	4.0	1.000	1.00	0.549

Table 5.4: Comparison of Code-Predicted and Measured Strengths for Eccentrically Loaded Specimens

Stud Configuration	P_{code}, kips	P_{calc}, kips	P_{meas}, kips	P_{code}/P_{meas}	P_{calc}/P_{meas}
5:0-3LE	14.1	22.9	22.1	0.64	1.04
5:3-3LE	14.4	24.5	19.6	0.73	1.25
			Mean	0.69	1.14
			Std. Dev.	0.07	0.15

Table 5.4 shows the measured and predicted strengths, by code and calculation of the WT rotation, for both eccentric specimens. As the table shows, the code underestimates the actual strength of the specimens by a large margin. The calculated strengths are more accurate than the code predictions, but are unconservative in both cases, 25% so for the haunch specimen. The eccentric load does reduce strength from similar concentrically loaded specimens, but it does not have as severe an impact as the code would predict.

5.2.2 Ductility

After peak shear stud strength, the second most important parameter in a connection's behavior is the observed specimen ductility. The ductility in these tests is the ability to carry load at deflections greater than that of the peak load. Because all specimens fail by concrete cone breakout, no specimens exhibit the classic steel-type ductility of a plateau of strength at peak (yield) load. Instead, ductile specimens exhibit the ability to sustain some fraction of the peak load over large displacements. As previously discussed, ductility is important for this type of shear stud connection because, in the event of a girder fracture, many groups of studs must be engaged to support the girder weight and applied loads. The studs must have a degree of ductility to permit load redistribution among the groups, so that if one group is loaded past peak strength, it can continue to support load while the excess is shared with other stud groups. If no ductility is present, at peak strength a stud group will fail suddenly, disengaging the studs from the slab and transferring the entire load to the next stud group, which could also then be overloaded. This type of failure could result in an 'unbuttoning' of the girder that would result in part or the entire fractured girder detaching from the bridge deck. To avoid this potential mechanism, ductility in the connections is essential.

The single factor that determines whether or not a specimen exhibits ductility is the presence or absence of reinforcement within the failure cone of the shear studs. In the case of ductility, the cone in

question is the real, 45-degree failure cone and not the theoretical failure pyramid. Specimens with rebar present in the failure cone exhibit ductility. This ductility is a function of the stud spacing, which impacts how much reinforcement is included in the failure cone. Specimens without rebar present exhibit little to no ductility, and in many of these cases the WT, studs, and haunch concrete (if present) completely separate from the slab. ACI 318, Appendix D accounts for ductility not by an explicit process but by increasing the strength reduction factor from 0.70, when plain concrete breakout controls, to 0.75 if rebar crosses the controlling failure cone.

Very little ductility is achieved with 5-in studs spaced transversely for any configuration of studs. For all transversely spaced studs with a haunch, the connection has essentially no strength after peak load. The horizontal cracks form rapidly, causing separation of the haunch from the slab and reducing the load to virtually zero. In one case, the haunch completely disconnected from the slab, demonstrating exactly how brittle a concrete cone failure can be. Specimens without a haunch exhibit only limited amounts of ductility. The no-haunch specimens have very steep unloading curves down to minimal values of load, and within 0.5 in of displacement from this drop-off, load reduces to zero. This brittle failure happens even though the center bars of the bottom mat of reinforcing sit just inside of the actual failure cone, as shown in Figure 5.13. While the rebar is technically present, it is too close to the surface of the cone to engage the cone, which forms on only one side of the rebar. Overall, transversely spaced 5-in studs, regardless of haunch, have essentially no ductility.

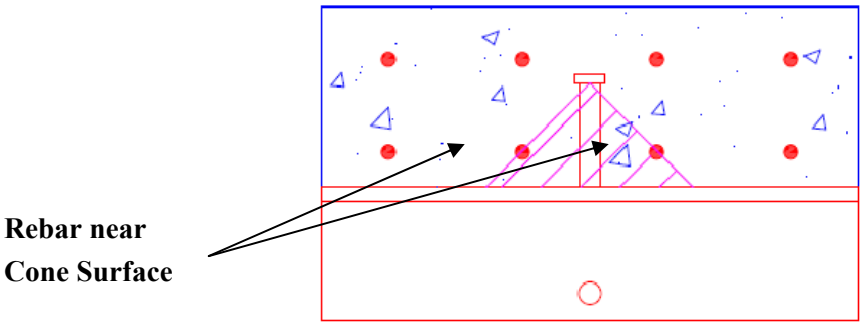

Figure 5.13: Failure Cone of a Stud Spaced Transversely, Showing Rebar near the edge of the Failure Surface

Five-inch studs spaced longitudinally vary substantially in ductility behavior depending on the presence of a haunch. All specimens with a haunch show very brittle failure at peak load, with the haunch fully separating in several cases. The single exception to this pattern is specimen 5:3-3La, where rebar-stud interlock forces the studs overlapping the rebar to develop the reinforcement. This interlock creates a failure ridge of concrete, resulting in a very ductile failure of 1/3 of the peak load for over 2 in of displacement. However, because the interlock is a coincidence of the geometry of the specimen, it cannot be directly relied upon to systematically provide ductility for the longitudinal haunch specimens. Specimens without a haunch show considerable ductility except for a single two-stud test, 5:0-2La. This specimen had a very eccentric pullout, changing its behavior with respect to the other tests. For single studs spaced longitudinally, the load drops steadily after peak strength. For all other numbers of studs, the strength plateaus at approximately 1/3 of the peak load, to deflections of at least 1.4 in for all cases, and up to 4.5 in for the case of a four-stud specimen. Overall, longitudinally spaced 5-in stud specimens have essentially no ductility if in a haunch. Conversely, if the no-haunch specimens have studs spaced closely enough to form a concrete ridge, the ductility is very good.

The dynamically tested specimens' ductility behavior is similar to their static counterparts. Dynamic testing does not change the ductility of haunch specimens over static tests and causes only slight reductions in ductility over static tests for specimens without a haunch. All studs longitudinally and transversely spaced with a haunch have essentially zero ductility, with the haunch separating from the

slab in nearly every test. The exceptions are the two replicates of 5:3-3LD, where rebar-stud interlock again creates a very ductile response, with the specimens carrying approximately 1/3 of the peak load to deflections exceeding 4 in. For specimens without a haunch, behavior depends on stud geometry. Single-stud tests show a steady decline of load to zero after peak strength, very similar to the static tests. Three studs spaced transversely show slightly more ductility than the static case, with a brief load plateau at 1/3 peak load to 3/4-in deflection before load begins to drop again. Three studs spaced longitudinally shows ductile behavior, but not as strongly as in the static tests; it maintains a load of slightly less than 1/3 the peak load up to 1.5 in before load begins to drop again.

Because all specimens with tall studs have a haunch, ductility is a function of the stud height and geometry alone. For 7-in studs spaced transversely, there is very little ductility in the specimens, and loads decrease steadily after peak strength in all cases. Seven-inch studs are not tall enough to engage the rebar, leading to these brittle failures. Failures in specimens with 7-in studs are not as brittle as 5-in studs where the haunch completely separates. Nine-inch studs spaced transversely are tall enough to engage the rebar fully and have a ductile response. However, because the cone only engages the rebar at its edges, as opposed to having the rebar pass though the interior of the failure cone (as shown in Figure 5.13), ductilities are somewhat limited. Nine-inch studs spaced transversely carry approximately 1/4 of the peak load to deflections in excess of 3 in. With the exception of a single 7-in stud, which acts similarly to a transversely spaced stud, all specimens with tall studs spaced longitudinally have very good ductility. Both 7-in and 9-in studs spaced longitudinally have ductile plateaus between 1/4 and 1/3 of the peak strength for displacements exceeding 2.5 in. This ductility is due to the merging of the failure cones of the studs, fully engaging the rebar inside of the concrete ridge. Seven-inch studs engage the rebar because the failure ridge runs straight across from one stud head to the next, as shown in Figure 5.14. Overall, if the studs are tall enough to fully engage the rebar, either by height alone or by longitudinal spacing utilizing the concrete ridge failure mode, very good ductility is achieved. If this condition is not met, specimens have essentially no ductility.

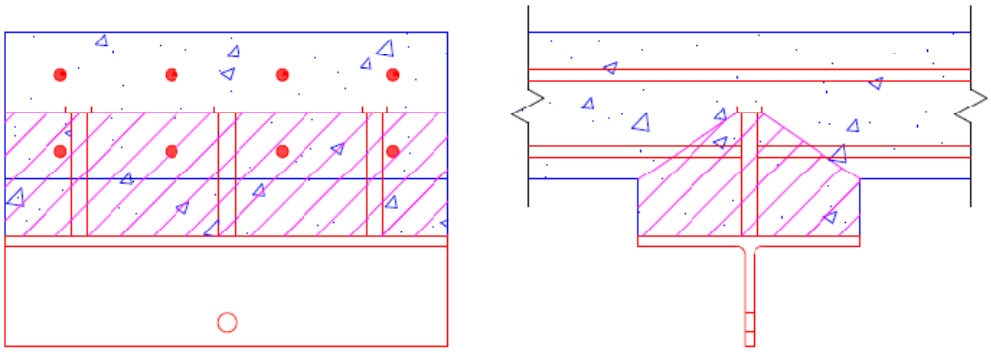

Figure 5.14: Failure Cone of 7-in Studs Spaced Longitudinally Enclosing Bottom Mat Reinforcement

As with the concentric tests, ductility in the eccentrically loaded specimens is a function of rebar engagement by the shear stud failure cones. Specimen 5:3-3LE, with a 3-in haunch, has essentially no ductility, with load dropping to zero when the horizontal crack forms at peak load. For specimen 5:0-3LE with no haunch, ductility is observed, with a load plateau of 1/4 of the peak load, but this plateau ends and begins losing load again after 1.2 in of deflection. These values mark a reduction in ductility from the concentrically loaded test, though not a severe one. Using the same WT rotation method as is utilized to find the calculated peak strength in Section 5.2.1, a calculated load-displacement curve is constructed for both specimens. Figures 5.15 and 5.16 show the measured and calculated load-displacement plots for no haunch and 3-in haunch specimens, respectively. For the no-haunch case, the WT-rotation-based load-displacement plot roughly parallels the measured results, though, as with the peak strength, it is unconservative. For the haunch specimen, the calculated curve shows a sharp drop when the first

horizontal crack forms, but it occurs at twice the measured peak-load displacement. However, the calculated curve shows residual load being carried by the other two studs when in reality the crack propagates all the way across the specimen and strength drops to zero. Overall, the calculation methods produce reasonably accurate prediction of the response, but they are unconservative for both cases in terms of both ductility and strength.

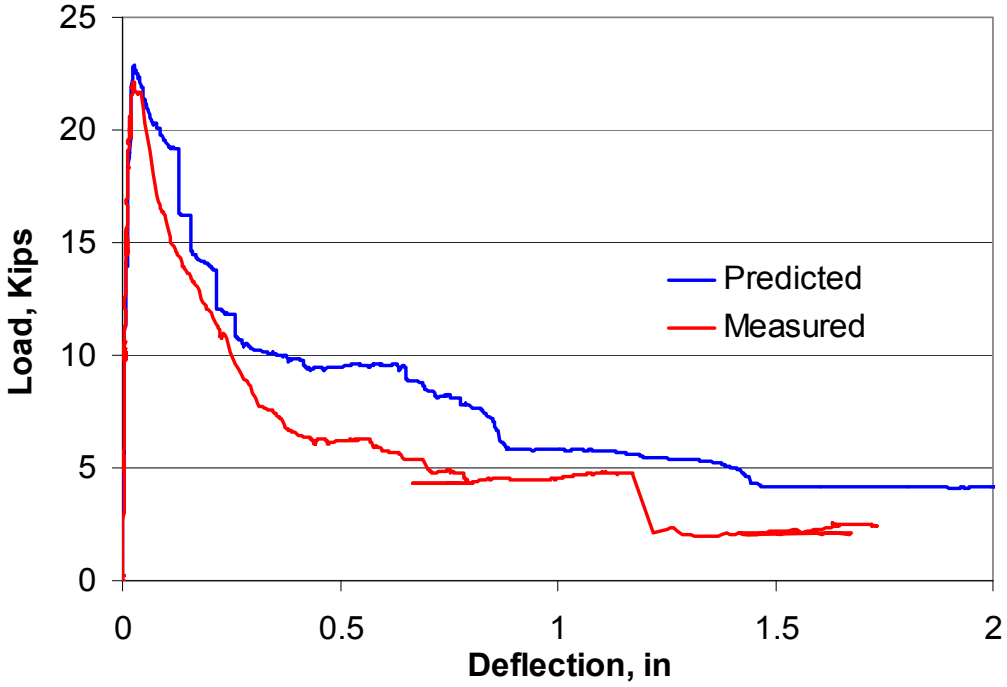

Figure 5.15: Measured and WT-Rotation-Predicted Load-Displacement Plots for Specimen 5:0-3LE

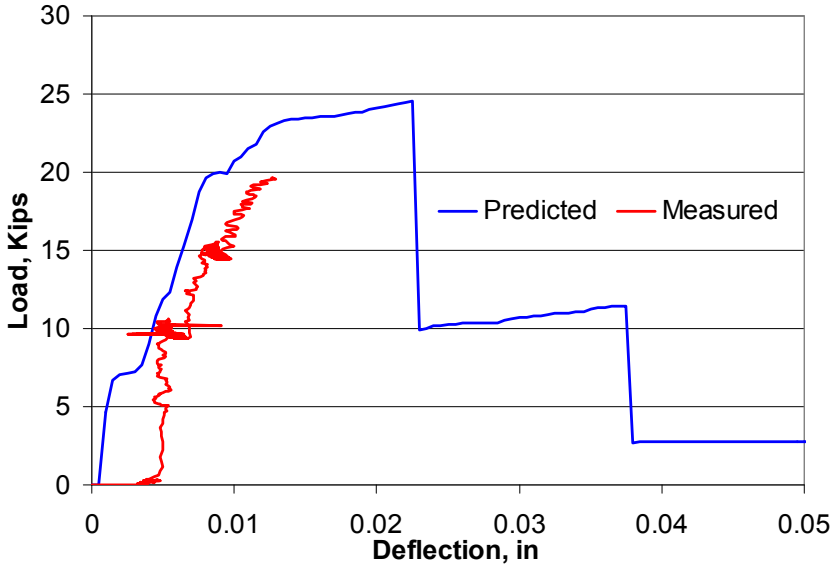

Figure 5.16: Failure Measured and WT-Rotation-Predicted Load-Displacement Plots for Specimen 5:3-3LE

5.2.3 Efficiency

The tensile efficiency of shear stud connections is a function of the force each stud in a group carries for a given applied load and is measured by the stress in each stud at peak load. All of the tests are governed by concrete breakout and not the strength of the studs. Therefore, there is not a simple relationship between the number of studs in a specimen and the strength of the specimen. Even for longitudinally spaced studs, the strength increases are small when additional studs are added after the concrete cones merge. The stress in the studs decreases for a given load as the number of studs is increased, which results in an inefficient use of materials. This trend is true for all longitudinally spaced stud configurations, dynamic and static, as well as transversely spaced studs tall enough to engage the rebar (5-in studs without a haunch and 9-in studs in a haunch). For transversely spaced specimens with studs not tall enough to engage the rebar (5-in studs in a haunch and 7-in studs in a haunch), this inefficiency is magnified considerably because adding studs reduces the total strength, causing individual stud utilization to drop even more rapidly than in longitudinal configurations.

Because of this drop in efficiency with added studs, the optimal configuration for shear studs, considering only the tensile strength, is to use the minimum number of studs needed to achieve a group failure. For the series tested in this research, the optimal number of studs for transverse spacing is two, both for specimens that engage the rebar (where adding a third stud gains very little strength), and for those that do not engage the rebar (where strength drops with the third stud). For specimens spaced longitudinally, the optimal configuration utilizes studs spaced just less than three times the effective height from one another, which causes their failure cones to overlap and form a concrete ridge. For the specimens in this study, this spacing corresponds to two studs. For either case, adding more studs than the optimal number will add little strength to the capacity.

5.2.4 Summary

There are many possible variations of shear studs connecting a bridge deck to a girder, but there are only three key questions that must be considered when evaluating the tensile strength of the studs:

1) Are the studs tall enough to engage the reinforcement?
2) Is there a haunch present or not?
3) Are the studs spaced longitudinally or transversely?

The answers to these three questions will govern the studs' tensile behavior. If the studs are tall enough to engage the reinforcement, strength is noticeably enhanced and ductility is greatly increased over studs that do not engage the reinforcement. However, if the studs are not tall enough to engage the reinforcing, there is virtually no ductility.

The presence of a haunch can help or hinder strength and ductility, depending on the height of the studs. If the studs are tall enough to engage the rebar, the haunch improves strength for the connection by preventing cracking around the base of the studs. Specimens without a haunch will also have satisfactory strength and ductility as long as the shear studs engage the reinforcement. If the studs are not tall enough to engage the reinforcement, a haunch is detrimental as it reduces the ductility of the specimens. If the studs do not engage the reinforcement, no haunch is the much better option to preserve some ductility and strength in the connection. Because the use of haunches is a typical part of bridge construction, it is strongly urged that the studs are tall enough to engage the rebar so that ductility can be achieved.

The spacing of the studs greatly aids the ductility of a connection. If studs are spaced longitudinally and close enough that their failure cones overlap (within three times the effective height from one another), specimen ductility is greatly increased by assuring rebar penetration into the failure ridge. This benefit occurs regardless of the presence of a haunch. If studs are spaced far enough apart that their failure cones do not overlap, they should be treated as single studs spaced transversely. Transversely spaced studs that engage the reinforcement are ductile, but because they will not fully engage the

surrounding rebar on all sides, the ductility is not as great as longitudinally spaced studs of the same height. If the studs are not tall enough to engage the reinforcement and there is a haunch, transversely spaced studs are not recommended because they have low strength and virtually no ductility. Figure 5.17 shows a flow chart of the questions to be asked in determining the tensile strength of shear studs and indicates what details should and should not be used. As a reference, Table 5.5 lists the eight major stud configurations tested for this research and ranks them best to worst (1 to 8) by their strength and ductility behavior.

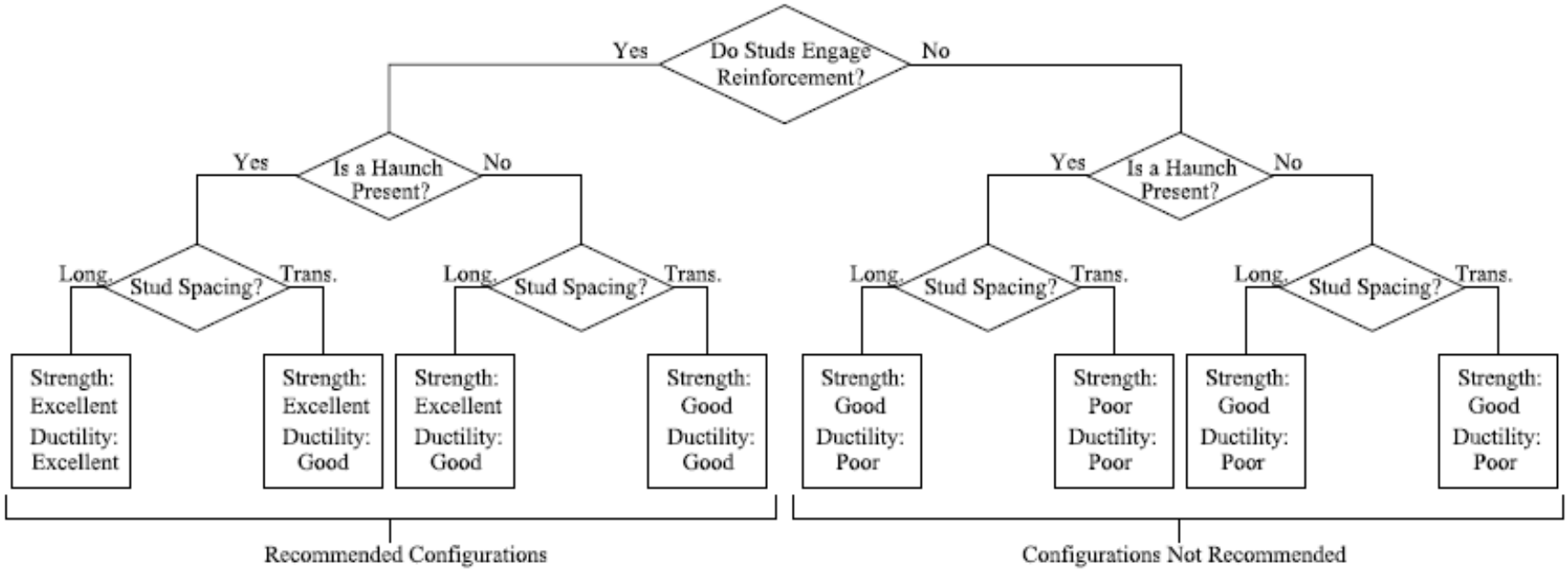

Figure 5.17: Flowchart Showing Possible Configuration Options and their Strength and Ductility Behavior

Table 5.5: Comparative Ranking of Major Stud Configurations

Rank	Stud Height	Configuration	Haunch Height	Strength	Ductility	Recommended
1	9 in	Longitudinal	3 in	Excellent	Excellent	Yes
2	5 in	Longitudinal	0 in	Excellent	Good	Yes
3	9 in	Transverse	3 in	Excellent	Good	Yes
4	7 in	Longitudinal	3 in	Good	Excellent	Yes
5	5 in	Longitudinal	3 in	Good	None	No
6	5 in	Transverse	0 in	Good	Poor	No
7	7 in	Transverse	3 in	Poor	Poor	No
8	5 in	Transverse	3 in	Poor	None	No

5.3 Proposed Shear Stud Configurations and Modifications to Code Strength Calculations

5.3.1 General Comments

Section 5.2 covers the behavior of the various shear stud connection configurations and describes which configurations have the most desirable ductility and strength. These determinations of strength and ductility are based on test data and hold true irrespective of the methods used to predict specimen strength. However, it is of great benefit to a designer to have equations that accurately predict a connection's strength. ACI 318, Appendix D serves as a good basis for predicting the tensile strength of shear studs, but the code does not adequately address the connections in this research. Because the code does not consider these connections, it does not always predict the strength accurately, especially when the detail has a haunch. Below are proposed modifications to ACI 318, Appendix D that will allow designers to better predict stud strength.

5.3.2 Code Modifications - Haunch Effect

While the haunch does not appear to cause inaccuracies in predicting the strengths for 5-in studs in a haunch using ACI 318, Appendix D, it does cause major discrepancies in the predicted strengths for 7-in and 9-in studs in a haunch. The code severely underestimates the strength of specimens with tall studs for both longitudinal and transverse spacings. While treating the haunch as a free edge works well for short studs whose cones do not extend over the top of the haunch, this assumption ceases to produce accurate results as the studs becomes tall enough to have their cones extend over the top of the haunch, as shown previously in Figure 5.6. To compensate for this discrepancy, it is proposed, for connections with a haunch, to replace the existing effective stud height term, h_{ef}, with an effective height of the stud above the top of the haunch, h_h. Equation 5.5 shows the calculation of h_h:

$$h_h = h_{ef} - d_h \geq \frac{w_h}{3} \qquad \text{Equation 5.5}$$

where: h_h = effective height of the stud above the top of the haunch (in)
h_{ef} = effective height of shear stud in concrete (in)
d_h = depth of the haunch (in)
w_h = width of haunch perpendicular to bridge span axis (in)

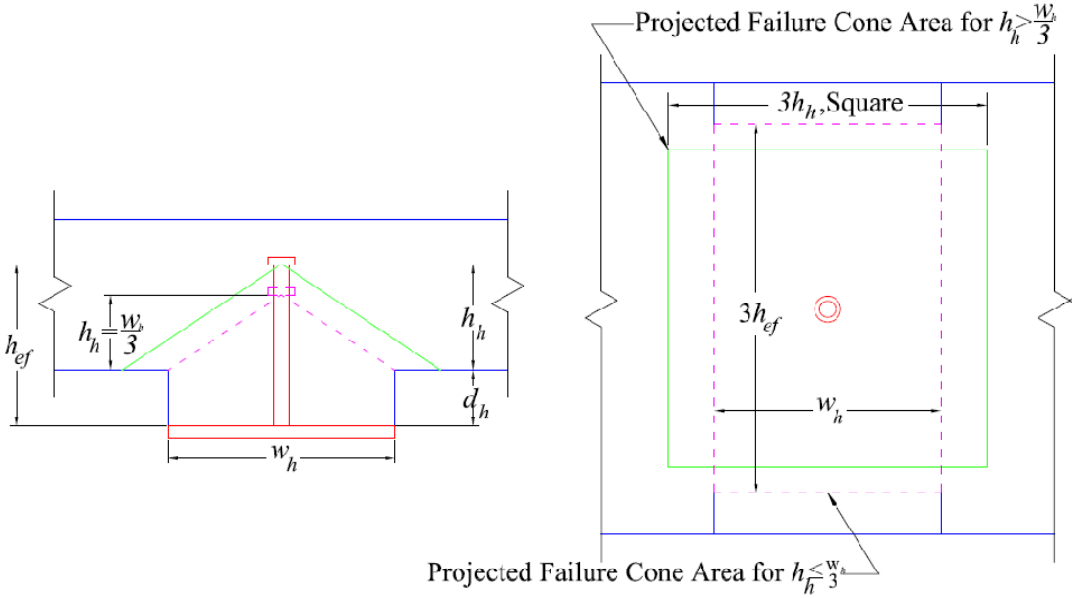

Figure 5.18: Pictorial Definition of Terms for Effective Stud Height Term

Figure 5.18 illustrates the terms of Equation 5.5, with d_h equaling 3 in and w_h equaling 12 in for all the haunch tests in this research. The limit of $w_h/3$ reflects the fact that, regardless of actual stud height, specimens with a haunch always engage the entire haunch region as their failure surface, regardless of what the ACI Code predicts as the projected failure cone area. The limit enforces that the effective haunch stud height will always engage the entire width of the haunch when the projected failure cone area is calculated. Thus, when the limit controls, the width of the projected failure area becomes $3w_h/3$, equal to simply w_h. When the $w_h/3$ limit controls, the projected failure cone area, A_{Nc}, becomes the area using h_{ef}, the full effective stud height, with the sides of the haunch acting as an edge, as shown in Figure 5.18. If $w_h/3$ does not limit h_h, the group projected failure cone area is the area calculated with h_h, the haunch effective stud height, and is not confined by the haunch edges. In both cases, the single stud projected failure area is still calculated with the haunch effective stud height, h_h.

The effective haunch stud height replaces the effective height in all breakout cone equations in the code, including the calculation of modification factors such as edge distance, $\psi_{ed,N}$. After adjusting the height, the haunch sides are still considered an edge for the calculation of the edge distance factor. Because the haunch inhibits cracking around the studs, it is permitted to treat the concrete as uncracked for the purposes of the cracked concrete modification factor, $\psi_{c,N}$. If a haunch is wide enough not to confine the projected failure cone area of the full effective height, then the studs should be considered as not in a haunch.

Figure 5.19 shows the original and proposed projected failure cones for 9-in studs in a haunch. All other configurations have the same projected area, but all specimens with a haunch use h_h in lieu of h_{ef}. The modification of the stud height in the haunch allows the effect of the haunch to be considered, and it correctly accounts for whether the failure cone does or does not engage concrete beyond the edges of the haunch. Numerical comparisons of the proposed height modification to test data are given in Sections 5.3.3 and 5.3.4.

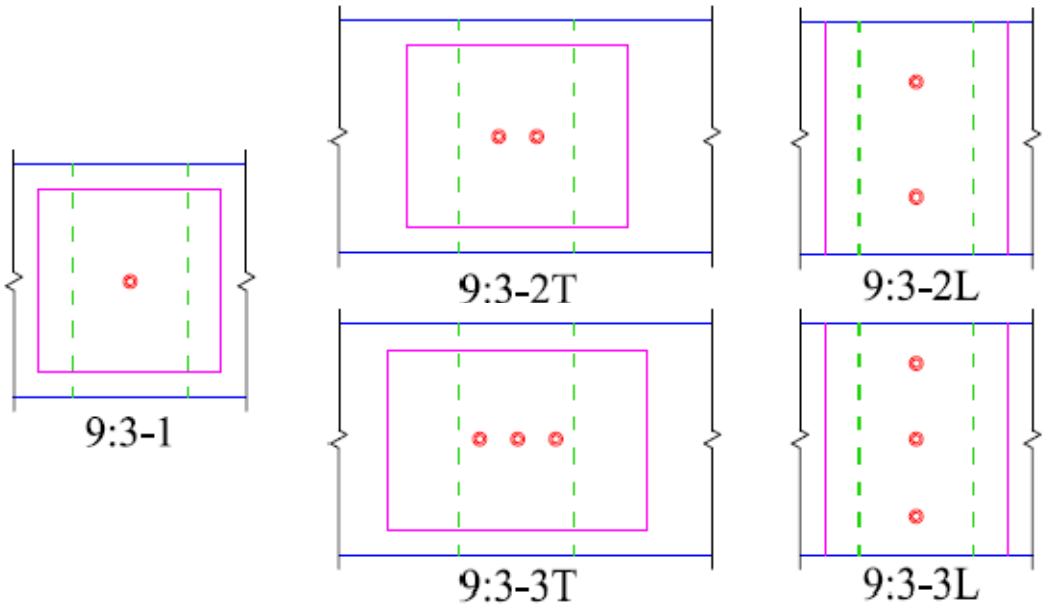

Figure 5.19: Code (Dashed) and Proposed Modified (Solid) Failure Cones for 9 in. Studs (Configurations Not Pictured had no Change in Cone Projected Area)

5.3.3 Code Modifications - Transversely Spaced Studs

As noted previously, the existing ACI code provisions are able to handle group effects of studs spaced closely together, such as those spaced transversely on a bridge girder. However, it does overpredict the strength of these closely spaced stud groups by a small amount. To adjust for this over prediction, a group effect modification factor, $\psi_{g,N}$, is proposed to be added to the breakout strength equation, resulting in Equation 5.6:

$$N_{cbg} = \frac{A_{Nc}}{A_{Nco}} \psi_{g,N} \psi_{ec,N} \psi_{ed,N} \psi_{c,N} N_b \qquad \text{Equation 5.6}$$

where: $\psi_{g,N}$ = group effect modification factor for studs on a bridge girder
All other variables as previously defined for Equation 5.2

This factor helps to account for the reduction in stud efficiency as more studs are added to a group. To determine the value of the group effect modification factor for studs spaced transversely, the measured strength of each specimen was divided by the predicted strength using the haunch effective height as covered in Section 5.3.2. For dynamically loaded specimens, the predicted strength was multiplied by the measured dynamic strength factor for comparison with measured strengths. These strength ratios for transversely spaced stud configurations, along with the average ratio for each number of studs, are shown in Table 5.6. As Table 5.6 shows, for a single stud the modified code underpredicts the measured strength by an average of 4.0% (a strength ratio of 1.04); this underprediction is conservatively neglected and the group effect factor is taken as 1.0. For two studs spaced transversely the average strength ratio is 0.97. Because of the large scatter in the two-stud strength ratios, the group effect factor is taken as 0.95 so that the modified code conservatively underestimates the measured capacity for most specimens. The same logic is applied to three studs with an average strength ratio of 0.92, and the group effect factor conservatively taken as 0.90.

Table 5.6: Measured Strength to Haunch-Height-Modified Strength Ratios for Studs Spaced Transversely

Number of studs	h_h Modified Strength, kips	$P_{measured}/P_{Modified}$	h_h Modified Strength, kips	$P_{measured}/P_{Modified}$	h_h Modified Strength, kips	$P_{measured}/P_{Modified}$
	5-in Studs, No Haunch		5-in Studs, 3-in Haunch		7-in Studs, 3-in Haunch	
1	18.3	1.14	21.3	1.05	29.5	0.89
2	23.6	1.04	19.2	1.00	26.5	0.95
3	28.9	0.90	17.1	1.01	23.6	0.86
Number of studs	9-in Studs, 3-in Haunch		Dynamic Loading, 5-in Studs, No Haunch		Dynamic Loading, 5-in Studs, 3-in Haunch	
1	27.6	1.03	24.3	1.11	31.3	1.02
2	31.3	0.88				
3	34.1	0.92	38.8	0.87	24.7	0.99

Number of studs	Average Ratio $P_{measured}/P_{modified}$
1	1.04
2	0.97
3	0.92

Table 5.7 summarizes the values of the group effect factor for studs spaced transversely, for any height. For the case where stud spacing or configuration changes down the length of a bridge, each configuration should have its strength calculated separately. The group effect factor is applied separately to each similar stud group. Table 5.8 compares the original code predicted strengths and strengths from the proposed modifications with the measured strengths, including the effective haunch height as appropriate. Figures 5.20, 5.21, and 5.22 plot the original code strengths, proposed modified strengths, and measured strengths versus the number of studs for static, dynamic, and tall stud transverse configurations, respectively.

Table 5.7: Values of the Group Effect Modification Factor for Studs Spaced Transversely

Number of Studs	$\psi_{g,N}$
1	1.00
2	0.95
3	0.90

Table 5.8: Comparison of Modified Code Strengths to Original Code and Measured Strengths for Studs Spaced Transversely

Series	Stud Configuration	P_{adj}, kips	P_{code}, kips	$P_{measured}$, kips	$P_{adj}/P_{measured}$	$P_{code}/P_{measured}$
Series I	5:0-1	18.3	18.3	20.9	0.88	0.88
	5:0-2T	22.4	23.6	24.6	0.91	0.96
	5:0-3T	26.0	28.9	25.9	1.00	1.12
	5:3-1	21.3	19.0	22.3	0.96	0.85
	5:3-2T	18.2	17.3	19.2	0.95	0.90
	5:3-3T	15.4	15.6	17.3	0.89	0.90
Series III	7:3-1	29.5	19.7	26.2	1.13	0.75
	7:3-2T	25.2	18.3	25.1	1.00	0.73
	7:3-3T	21.2	17.0	20.3	1.05	0.84
	9:3-1	27.6	19.2	28.4	0.97	0.68
	9:3-2T	29.7	18.2	27.7	1.07	0.66
	9:3-3T	30.7	17.1	31.4	0.98	0.55
Series IV	5:0-1D	24.3	24.2	27.0	0.90	0.90
	5:0-3TD	34.9	38.8	33.9	1.03	1.15
	5:3-1D	31.3	27.9	31.9	0.98	0.88
	5:3-3TD	22.2	22.5	24.4	0.91	0.93
				Mean	0.98	0.85
				Std. Dev.	0.07	0.16

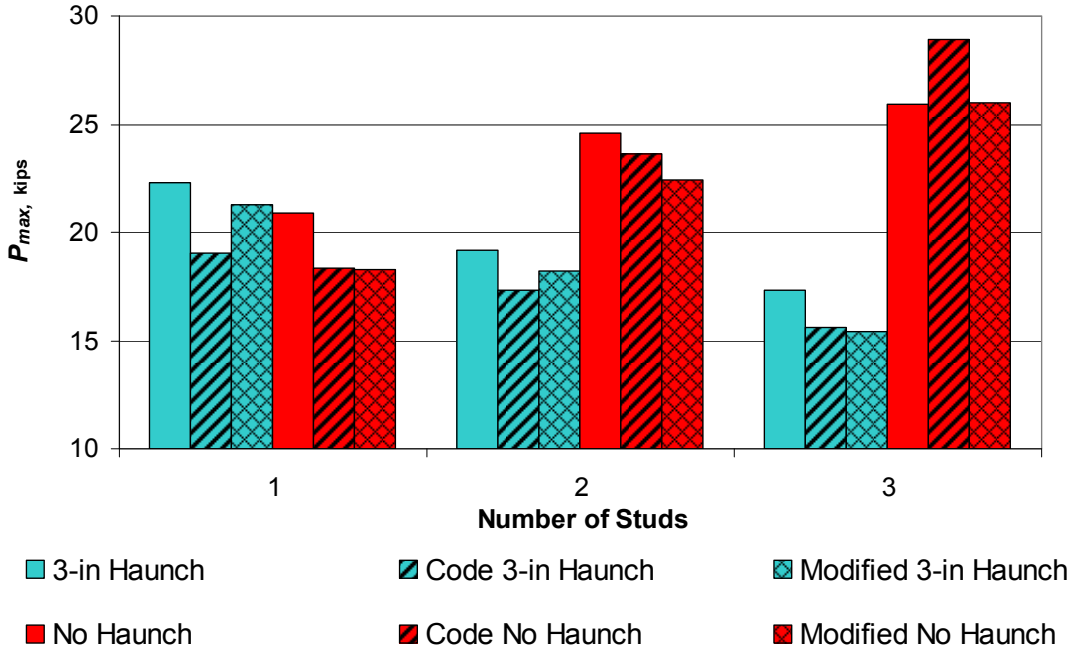

Figure 5.20: Comparison of Modified Code Strengths to Measured Strengths for Statically Loaded Studs Spaced Transversely

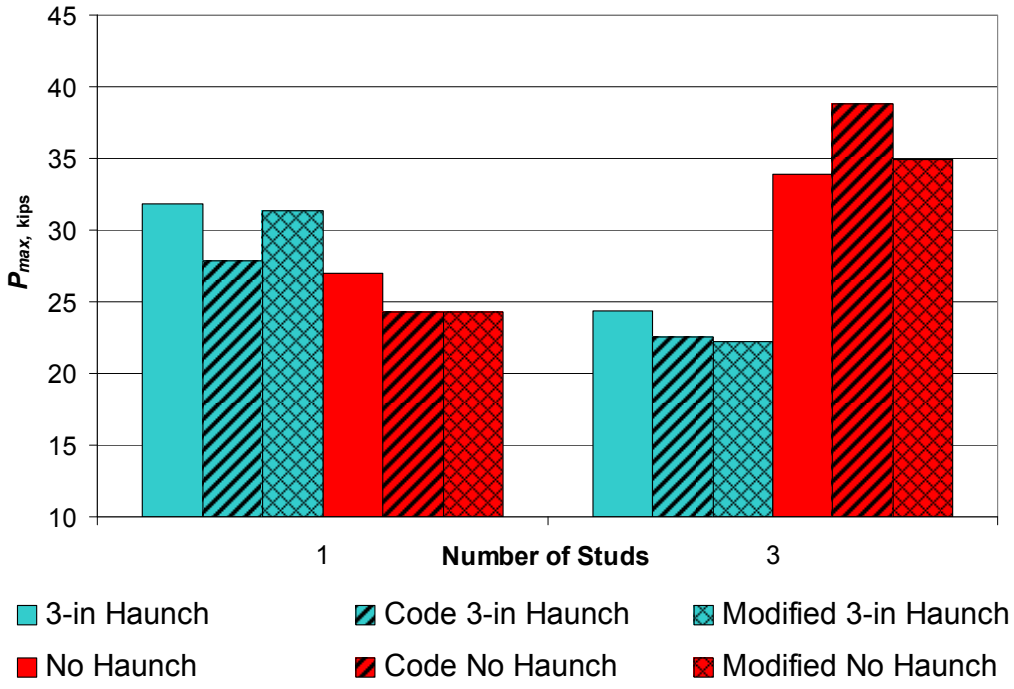

Figure 5.21: Comparison of Modified Code Strengths to Measured Strengths for Dynamically Loaded Studs Spaced Transversely

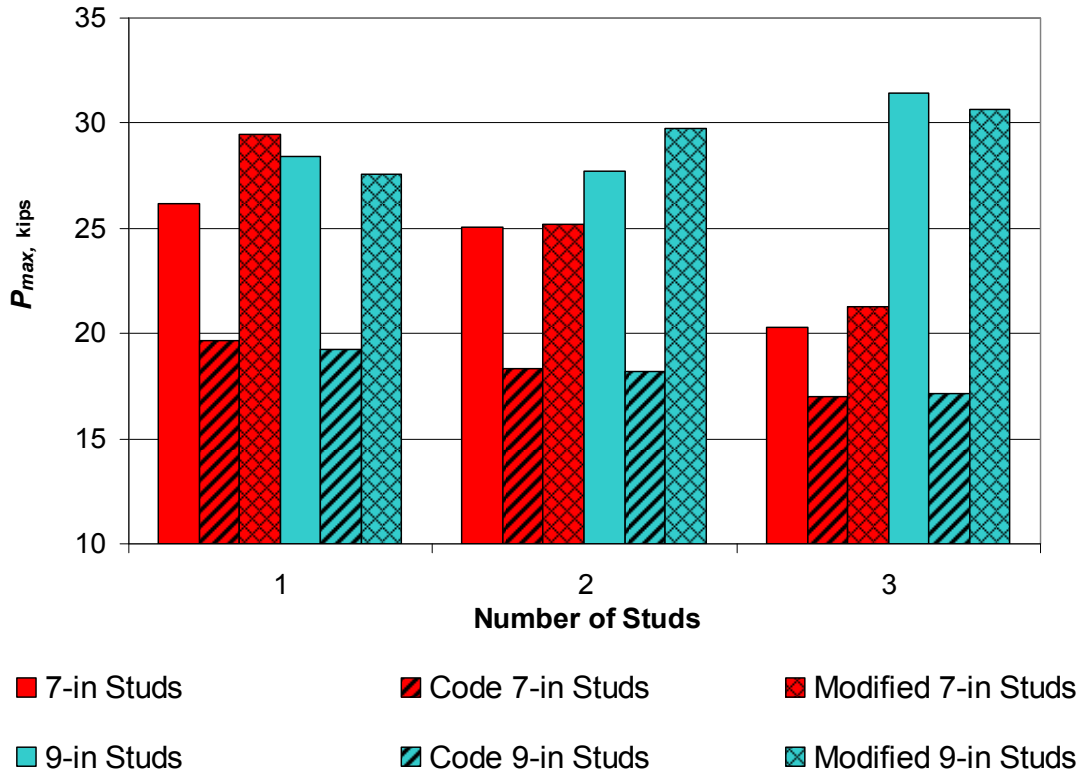

Figure 5.22: Comparison of Modified Code Strengths to Measured Strengths for Taller Studs Spaced Transversely

The proposed modifications of group effect and effective stud height above the haunch predict well the actual failure strength of most of the specimens. The mean of the existing code strength to measured strength ratio for transversely spaced studs is 0.85, with a standard deviation of 0.16. The mean of the modified strength to measured strength ratio is 0.98, with a standard deviation of 0.07, indicating that the modified strengths more accurately and consistently predict the measured strength. For 5-in studs spaced transversely without a haunch, the modifications eliminate the code overprediction for groups of studs, resulting in a uniform margin of safety between experimental and predicted results. For 5-in studs spaced transversely with a haunch, the modifications (principally the stud height modification) predict the actual measured strength more exactly than the original code equation while still being conservative.

The proposed modifications provide a better prediction of the test strengths of the dynamically loaded specimens with studs spaced transversely than the original code equations. The code and modified values in Figure 5.21 have been multiplied by the appropriate dynamic strength factor for the purpose of comparison. For specimens with tall studs spaced transversely, the modifications provide reasonably accurate strengths predicted for most of the tested specimens. The modifications are slightly unconservative for specimens 7:3-1 and 9:3-2T, but by less than 8.0% in both cases. No replicates were preformed on these two geometries; consequently, the variability of the results relative to the predicted strength cannot be judged. Overall, the proposed modification factors for transversely spaced studs provide a designer with a much more accurate prediction of the tensile strength of a stud group than the existing ACI equations. The proposed modifications are also conservative in nearly all places for the nominal strength and very conservative once strength reduction (ϕ) factors of ACI 318, Appendix D are applied.

5.3.4 Code Modifications — Longitudinally Spaced Studs

While the current code provisions are able to reasonably predict the strength of closely spaced studs, they are unable to do so for studs spaced longitudinally farther apart but still creating a group failure. To correct for this deficiency, it is proposed that longitudinally spaced studs make use of the group effect modification factor, $\psi_{g,N}$. As was done for studs spaced transversely, the modified predicted strength is divided by the measured strength for each specimen with studs spaced longitudinally, shown in Table 5.9. Modified strengths for dynamically loaded specimens have been multiplied by their respective measured dynamic strength factors, and the average of the strength ratio for studs spaced greater than $3h_{ef}$ apart (one stud) and less than $3h_{ef}$ apart (two and three studs) is tabulated. For studs spaced further apart than three times the effective height, the failure cones do not overlap, and they behave as single studs, which the modified strength predicts well without adjustment. Therefore, for a single stud without an overlapping failure cone, the group effect factor is conservatively taken as 1.0. If the studs are spaced more closely than three times the effective height, the failure cones overlap and form a continuous failure surface whose capacity is roughly constant as the number of studs on a given length of girder increases. Taking all studs with overlapping cones together, the average strength ratio is 0.83. To conservatively estimate the capacity of various longitudinally spaced stud configurations, the group effect factor for studs spaced longitudinally less than three times the effective stud height is taken as 0.80. Table 5.10 lists the proposed values of the factor for longitudinally spaced studs as a function of their spacing.

Table 5.9: Measured Strength to Haunch-Height-Modified Strength Ratios for Studs Spaced Longitudinally

Number of Studs	h_h Modifed Strength (kips)	$P_{measured}/P_{modified}$	h_h Modifed Strength (kips)	$P_{measured}/P_{modified}$	h_h Modifed Strength (kips)	$P_{measured}/P_{modified}$
	5-in Studs, No Haunch		5-in Studs, 3-in Haunch		7-in Studs, 3-in Haunch	
1	20.67	1.00			29.5	0.89
2	35.6	0.81	41.57	0.79	34.28	0.79
3	35.6	0.85	41.57	0.78	34.28	0.82
4	35.6	0.81				
Number of Studs	9-in Studs, 3-in Haunch		Dynamic Loading, 5-in Studs, No Haunch		Dynamic Loading, 5-in Studs, 3-in Haunch	
1	27.59	1.03	24.3	1.11	24.3	1.31
2	37.57	0.79				
3	37.57	0.80	38.4	0.90	38.4	0.95

Stud Spacing, s	Number of Studs	Average Ratio $P_{measured}/P_{modified}$
$s > 3h_{ef}$	1	1.07
$s \leq 3h_{ef}$	2, 3, 4	0.83

Table 5.10: Values of the Group Effect Modification Factor for Studs Spaced Longitudinally

Stud Spacing, s	$\psi_{g,N}$
$s > 3h_{ef}$	1.00
$s \leq 3h_{ef}$	0.80

When the concrete failure cones overlap, a continuous concrete ridge failure surface develops, and its size does not change if more studs are added over a given length. When this overlap happens, the group projected failure cone area, A_{Nc}, becomes the area projected by all of the studs in tension along the entire longitudinal line. This area does not change as more studs are added; therefore, the strength of the group does not change as more studs are added over the same longitudinal length. For all multiple stud cases, the edge effect modification factor should be calculated with the minimum edge distance present when the studs are spaced at $3h_{ef}$. Table 5.11 lists the measured, code predicted, and proposed modified code strengths for studs spaced longitudinally.

Figures 5.23, 5.24, and 5.25 plot the original code strengths, proposed modified strengths, and measured strengths versus the number of studs for static, dynamic, and tall stud longitudinal configurations, respectively. As these figures show, the proposed longitudinal group effect and effective haunch height modification factors do a very good job of predicting (in the case of studs without a haunch, slightly conservatively predicting) the connection strength. For statically loaded 5-in tall studs spaced longitudinally, the modifications produce a close but conservative prediction for both haunch and no-haunch cases and reflects the relative plateau of strength once group failure action is reached.

Table 5.11: Comparison of Modified Code Strengths to Original Code and Measured Strengths for Studs Spaced Longitudinally

Series	Stud Configuration	$P_{adj,}$ kips	$P_{code,}$ kips	$P_{measured,}$ kips	$P_{adj}/P_{measured}$	$P_{code}/P_{measured}$
Series II	5:0-1	20.7	20.7	20.6	1.00	1.00
	5:0-2L	28.5	34.3	28.8	0.99	1.19
	5:0-3L	28.5	31.2	30.1	0.95	1.04
	5:0-4L	28.5	29.7	28.9	0.99	1.03
	5:3-2L	33.3	37.1	32.7	1.02	1.13
	5:3-3L	33.3	33.7	32.6	1.02	1.04
Series III	7:3-1	29.5	19.7	26.2	1.13	0.75
	7:3-2L	27.4	22.9	27.2	1.01	0.84
	7:3-3L	27.4	21.3	28.3	0.97	0.75
	9:3-1	27.6	19.2	28.4	0.97	0.68
	9:3-2L	30.1	19.2	29.5	1.02	0.65
	9:3-3L	30.1	18.2	30.0	1.00	0.61
Series IV	5:0-1D	24.3	24.2	27.0	0.90	0.90
	5:0-3LD	30.7	33.5	34.5	0.89	0.97
	5:3-1D	24.3	27.9	31.9	0.76	0.88
	5:3-3LD	30.7	35.3	36.6	0.84	0.97
				Mean	0.97	0.90
				Std. Dev.	0.08	0.17

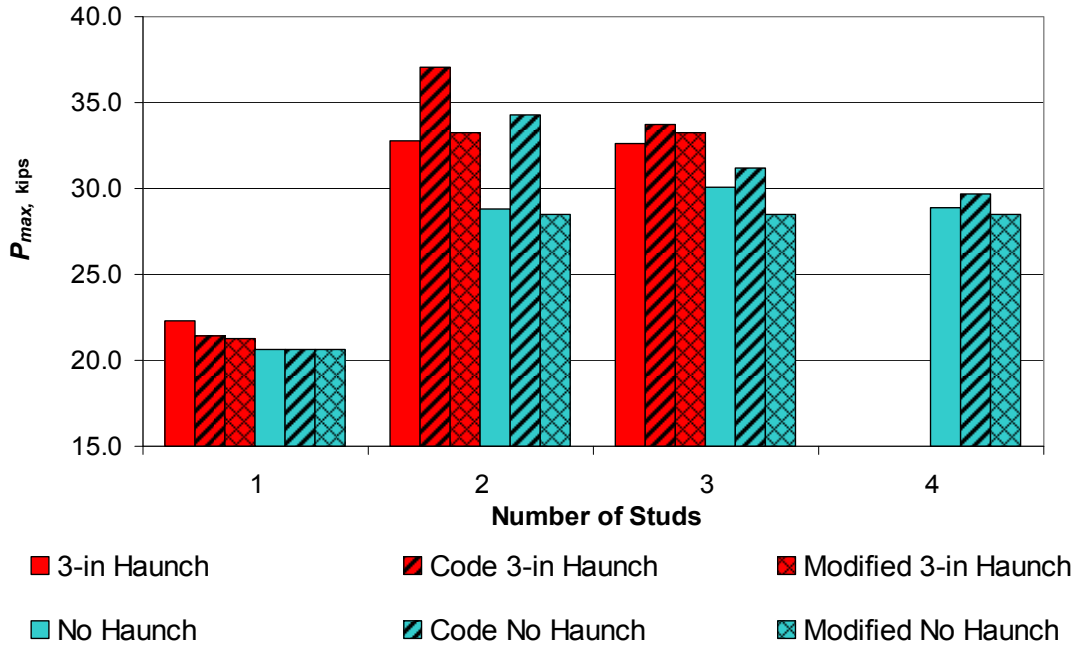

Figure 5.23: Comparison of Modified Code Strengths to Measured Strengths for Statically Loaded Studs Spaced Longitudinally

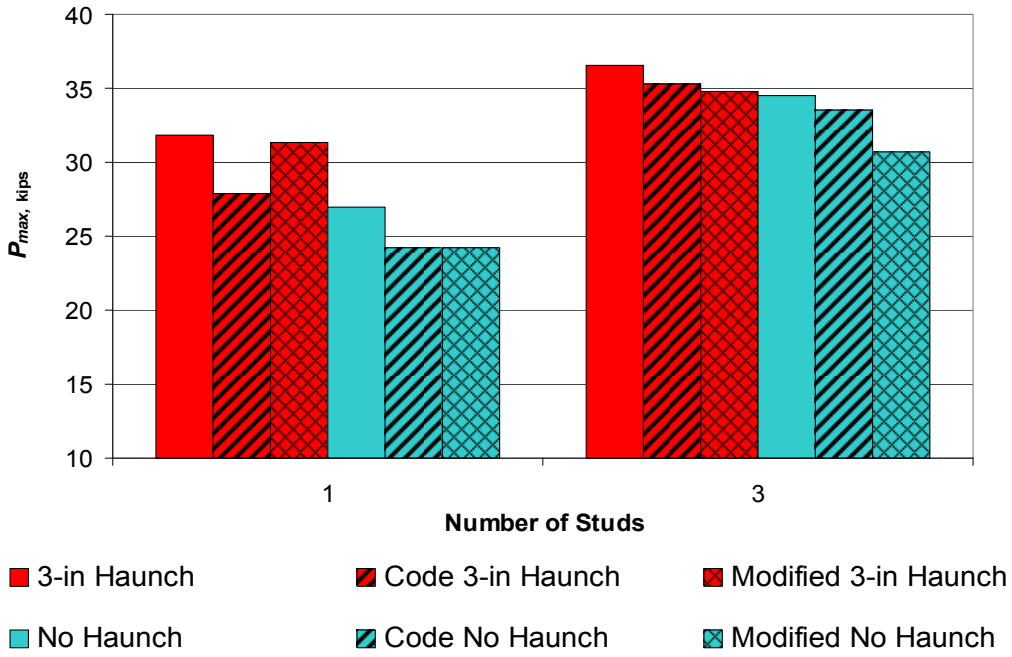

Figure 5.24: Comparison of Modified Code Strengths to Measured Strengths for Dynamically Loaded Studs Spaced Longitudinally

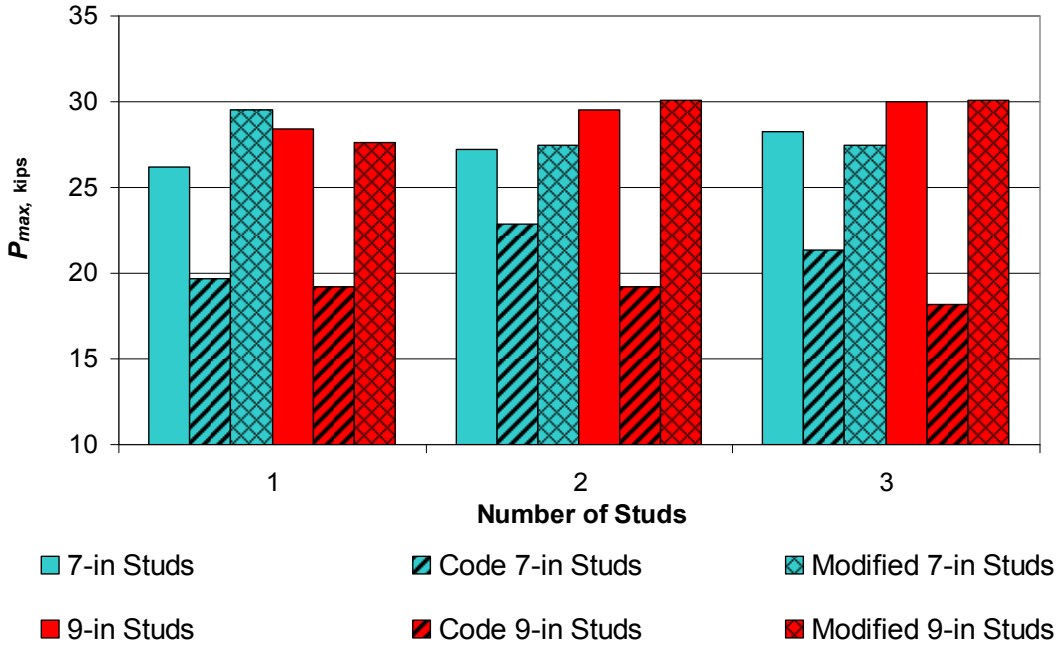

Figure 5.25: Comparison of Modified Code Strengths to Measured Strengths for Taller Studs Spaced Longitudinally

For 5-in tall studs spaced longitudinally, the modifications again do a very good job of predicting the actual failure strength. The existing code mean predicted-to-measured strength ratio is 0.90 with a standard deviation of 0.17, while the modified mean predicted-to-measured strength ratio is 0.97 with a standard deviation of 0.08. These ratios show that the proposed modifications are both more accurate and

more consistent than the existing code equations at predicting the measured capacity for all studs spaced longitudinally. All dynamic strengths are multiplied by the respective measured dynamic strength factors for the purposes of comparison. For 9-in studs spaced longitudinally, the modifications of group effect and effective height do an excellent job of accurately predicting the measured strength. The same is true for the 7-in studs, with the exception of a single 7-in stud, whose discrepancy was explained previously.

For longitudinally spaced studs loaded eccentrically, the effective haunch height factor applies well, but the eccentric failure appears to negate the need for the utilization of a group effect factor ($\psi_{g,N}$=1.0). Table 5.12 compares the measured and modified code strengths for eccentrically loaded specimens. While the proposed modifications are more accurate than the original code strengths with a mean modified predicted-to-measured strength ratio of 0.79, compared to the mean code predicted-to-measured strength ratio of 0.69, they are still conservative estimations and need more refinement.

Table 5.12: Comparison of Modified Code Strengths to Measured Strengths for Eccentrically Loaded Specimens

Stud Configuration	$\psi_{ec,N}$, Code	$\psi_{ec,N}$, Modified	$P_{adj,}$ kips	$P_{code,}$ kips	$P_{measured,}$ kips	$P_{adj}/P_{measured}$	$P_{code}/P_{measured}$
5:0-3LE	0.549	0.549	15.4	14.1	22.1	0.70	0.64
5:3-3LE	0.549	0.500	17.2	14.4	19.6	0.88	0.73
					Mean	0.79	0.69
					Std. Dev.	0.13	0.07

Overall, the longitudinal stud group modification factor and the effective stud haunch height produce results much more accurate (but still conservative) than the original code predictions.

5.3.5 Code Modifications - Summary

The proposed modifications to ACI 318, Appendix D that rely on the use of the effective stud height in the haunch and the group effect modification factor show an increase in overall accuracy over the original code provisions in predicting the measured capacity. Table 5.13 summarizes the mean and standard deviation of the modified strength-to-measured strength and code predicted strength-to-measured strength ratios for all forty-eight test specimens. As Table 5.13 shows, the proposed modifications are both more accurate and more consistent with the measured test data than the original code.

Table 5.13: Predicted-to-Measured Strength Ratios for Code and Modified Strengths of all Test Specimens

	$P_{adj}/P_{measured}$	$P_{code}/P_{measured}$
Mean	0.96	0.87
Std. Dev.	0.09	0.17

To concisely present the proposed modifications to ACI 318, Appendix D, the modified breakout strength equations are listed below, incorporating the effective haunch height and the group effect modification factor.

$$N_b = k_c \sqrt{f_c'} h_h^{1.5} \qquad \text{Equation 5.7}$$

$$N_{cbg} = \frac{A_{Nc}}{A_{Nco}} \psi_{g,N} \psi_{ec,N} \psi_{ed,N} \psi_{c,N} N_b \qquad \text{Equation 5.8}$$

$$h_h = h_{ef} - d_h \geq \frac{w_h}{3}$$ Equation 5.9

$$\psi_{ed,N} = 0.7 + 0.3\frac{c_{a,\min}}{1.5h_h} \leq 1.0$$ Equation 5.10

$$\psi_{ec,N} = \frac{1}{\left(1 + \frac{2e'_N}{3h_h}\right)} \leq 1.0$$ Equation 5.11

$\psi_{g,N}$:

Stud Configuration	$\psi_{g,N}$
1 Stud, No Group Failure Cone	1.00
2 Studs Spaced Transvesely	0.95
3 Studs Spaced Transvesely	0.90
Studs Spaced Longitudianly $\geq 3h_{ef}$	0.80

$\psi_{c,N}$:

Concrete Condition	$\psi_{c,N}$
Cracked or no Haunch	1.00
Uncracked or with Haunch	1.25

where: N_b = concrete cone breakout strength of a single isolated stud in a continuous piece of cracked concrete (lb)
k_c = 24 for cast-in-place shear studs
f'_c = specified concrete compressive strength (psi)
h_h = effective height of the stud above the top of the haunch (in)
N_{cbg} = design concrete breakout strength of a stud or group of studs (lb)
A_{Nc} = projected concrete cone failure area of a stud group (in^2)
A_{Nco} = projected concrete cone failure area of a single stud in continuous concrete ($= 9h_h^2$) (in^2)
$\psi_{g,N}$ = group effect modification factor for studs on a bridge girder
$\psi_{ec,N}$ = eccentric load modification factor
$\psi_{ed,N}$ = edge distance modification factor (when distance is less than $1.5h_h$)
$\psi_{c,N}$ = cracked concrete modification factor
h_{ef} = effective height of shear stud in concrete (in)
d_h = depth of the haunch (in)
w_h = width of haunch perpendicular to bridge span axis (in)
$c_{a,min}$ = smallest edge distance measured from center of stud to the edge of concrete (in)
e'_N = eccentricity of resultant stud tensile load

For the above equations, if there is no haunch or the haunch does not limit the projected failure cone area, h_h is equal to h_{ef}. When a haunch is present and $h_h<w_h/3$ the group projected failure cone area, A_{Nc}, is confined by the haunch and calculated using h_{ef}. If $h_h>w_h/3$ the haunch does not confine the group projected failure cone area and is calculated using h_h. The group effect modification factor is applied separately to each stud configuration on a bridge girder, and the strengths of each configuration are added to produce a total strength for a girder.

To illustrate how stud height and orientation using the proposed modifications impact strength, an example connection is considered. A girder has a 3-in haunch, 12-in wide, and a deck slab with a concrete compressive strength of 6.0 ksi and rebar configuration the same as in the test specimens. If single 5-in studs are spaced 24-in on center, the stud strength per 24-in of girder is 21.5 kips. If three 5-in studs are spaced transversely (outer studs 2-in from the haunch edge) 24-in on center down the girder, the strength per 24-in of girder drops to 15.5 kips. If the same three 5-in studs are reoriented longitudinally over 24-in of girder (spaced 8-in on center down the girder), the capacity increases to 29.8 kips. If the same longitudinal spacing is used and the stud height is increased to 7 in, the strength drops slightly to 27.4 kips for a 24-in length of girder. This 7-in configuration has a ductile failure, while all of the 5-in stud configurations have brittle failures. If the 7-in stud longitudinal spacing is increased to 20 in on center (just outside the $3h_{ef}$ group failure spacing but engaging almost the same failure cone area as a group breakout), the capacity increases to an average of 37.0 kips per 24-in of girder. While this strength is much higher than closer spacing, the tradeoff is a loss in ductility because the 20-in spacing has a brittle breakout. To have a ductile failure for studs spaced transversely, 9-in studs are needed, spaced at 26-in on center and 2-in from the haunch edge. This configuration produces strength of 24.6 kips for a 24-in girder length and a ductile failure. In general, increasing stud height increases strength and ductility. Transverse groups of studs have less strength than the same number of studs spaced longitudinally over the same length. If longitudinal studs are spaced out far enough to have individual cone failures, they have a higher strength but lower ductility than studs in a group failure engaging the same projected failure cone area. Longitudinal stud spacings that create a group failure and are tall enough to engage the reinforcement are the recommended stud configuration to provide both high strength and ductility.

5.3.6 Recommended Additional Testing

While the four series of tests covered many possible connection configurations, it is not possible to cover every variation. Also, the research performed suggests further avenues of investigation that might help improve stud connection details in the future.

A significant point to note is that all of the tests performed were loaded under either pure tension or tension and moment (eccentric load tests). However, shear studs in use in a bridge could also be carrying shear, which can interact with tension to reduce the overall tensile strength of a group of studs. Two reasons support why the tests performed still give valid results even though no shear is applied. First, as previously discussed, the shear near a fracture in a girder in the positive moment region of a bridge is expected to be low. Second, for low values of shear, ACI 318, Appendix D shows the interaction between shear and tension is small and states that for values of shear less than 20% of the shear strength, the tensile strength is not affected at all. While these two factors should mitigate the effect of shear in the tensile behavior of shear stud connections, tests to prove this behavior are highly recommended.

For all 48 tests, the cross-sectional area of the rebar in the specimens was the same, eight #5 bars. All of the static specimens that did show ductility have strength plateaus between 25% and 33% of the peak strength, which translates into loads between 5 kips and 12 kips. Because ductile behavior relies heavily on the flexural and tensile strength of the rebar as the studs experience large deflections, it is likely that increasing the area of steel intersecting the concrete failure cone could increase the value of the load carried at large deflections. The ductility of a specimen is not explicitly recognized in both the code and the proposed changes from this research. Rather, it is handled by allowing ductile specimens to have a strength reduction factor, $\phi = 0.75$, that is higher than the value of $\phi = 0.70$ for specimens that exhibit brittle failure behavior. Additional testing where the area of steel intersecting the failure cone is varied could lead to a quantitative relationship between post-peak load ductile strength and reinforcing steel area, allowing for the ductility to be accounted for explicitly. Explicitly accounting for the ductility would allow designers an extra degree of freedom and certainty in their designs by having a known ductile load that the studs can support while redistributing forces.

As previously observed, there appears to be a correlation between the test configuration geometry and the dynamic strength factor. Longitudinal stud configurations have a dynamic strength factor between 1.15 and 1.18, while transversely spaced stud configurations have a higher dynamic strength factor between 1.29 and 1.43. However, these twelve tests are insufficient to fully characterize the behavior for all connection geometries, especially those utilizing studs taller than 5 in. Because of these limitations, the proposed modifications to the code conservatively neglect the dynamic strength factor, as it is always greater than 1.0. Additional testing to examine the dynamic response of tall stud configurations, to collect more data on the previously tested connection configurations, and to investigate what strain rates a fracture event in a girder will impose on the shear studs might allow some degree of dynamic strength increase to be utilized in the code computed strength.

As was observed in specimens 5:3-3La, 5:3-3LDa, and 5:3-3LDb, rebar-stud interlock produces a very strong, ductile behavior in a specimen that would have otherwise had a brittle failure mode. It may be possible that, rather than rearranging the studs and making them tall enough to engage the rebar, the rebar could be laid out directly underneath the stud heads to force rebar-stud interlock in the connection. This configuration would alleviate the need to use the new stud configurations proposed above. Further testing is needed to determine if rebar-stud interlock can be predictably repeated and what proximity to stud and size of rebar are needed for it to occur.

Tests to date have looked at stud spacings that are either multiple studs grouped transversely to the bridge span or spaced single file longitudinally down the bridge axis. Another possible configuration is often encountered when shear demand is large in which the rows of studs are spaced less than three times the effective stud height from each other longitudinally. A variant of this configuration would be studs spaced longitudinally down the web but staggered transversely to create a zigzag pattern. Both configurations have the potential to realize strength increases and behave as a longitudinal grouping if the studs are tall enough to engage the reinforcement, or they could behave in a brittle fashion if studs do not engage reinforcement. Additional testing is needed to assess how longitudinally overlapping transverse stud groups and staggered stud groups will behave in comparison to a single transverse row or only longitudinal configurations examined in this study.

For connections loaded eccentrically, the current code greatly underpredicts the actual strength. While the proposed modifications to the code improve the predicted accuracy, there is still a large discrepancy between calculated and measured eccentric load strength. More research is needed to better define the relationship between high eccentricity and connection strength.

5.3.7 Summary

While work remains to be done to fully characterize the tensile strength of embedded shear studs, this research has shown that the current code previsions of ACI 318, Appendix D provide a good starting point for tensile strength prediction. With the modifications proposed to effective stud height in a haunch and to the group effect of studs spaced transversely and longitudinally, the code provisions can be adapted to produce very accurate yet safe results. Certain configurations of shear studs have been shown to have significantly better behavior than others, with studs spaced longitudinally having more tensile strength than those spaced transversely. Also, studs tall enough to engage reinforcement in their failure cones are dramatically more ductile than those configurations that do not engage the rebar. The presence of a haunch can be beneficial or detrimental, depending on whether the connection is ductile or brittle. Ductile specimens with a haunch experience an increased strength over similar specimens without it, while brittle specimens see a marked reduction in strength under the same conditions. Overall, the analysis here shows that, with a few changes in current shear stud standard configurations for bridges and to the relatively simple and existing code provisions, designers can satisfy strength and ductility requirements in their shear stud connection designs in the event of a girder fracture.

Chapter 6: Conclusions and Recommendations

6.1. Summary and Objectives

Steel box girder bridges are fracture critical only if they are unable to support load after a fracture event. Key to bridge survival after a fracture is support of the fractured girder by the remaining structure through the transfer of load by the shear studs acting in tension. The ability of the shear stud connections to carry these tensile loads in a ductile fashion is vital to supporting a fractured girder.

The current TxDOT standard shear stud detail in a haunch has been shown to have both a very low tensile strength and virtually no ductility. Different configurations of the shear stud connections were evaluated to find alternate geometries with better strength and ductility characteristics. The effects of dynamic loading from a fracture event were also investigated, along with the effects of eccentric loading of the connections.

6.2 Conclusions

Tests on the 48 shear stud connection specimens produced several clear conclusions on the connection behavior:

1) If the studs are tall enough that their failure cones (which propagate at 45 degrees) enclose reinforcement in the breakout cone concrete, the connection will have a high tensile strength and substantial ductility.
2) For connections with studs tall enough to engage the reinforcement, longitudinal spacings of the shear studs less than three times their effective stud height apart develop the most ductile behavior. Studs spaced longitudinally greater than three times their effective stud height apart have a higher strength than a similar number of studs in a group failure, but with less ductility. Once studs are spaced less than three times their effective stud height apart, their failure cones overlap and closer stud spacings will not increase connection strength. Therefore, the most efficient spacing is exactly three times the effective stud height. The full engagement of multiple bars of reinforcement also helps increase the strength. Once studs are spaced within the distance needed to create cone overlap, additional studs will not significantly increase a connection's strength.
3) For connections with studs tall enough to engage the reinforcement, transverse spacing of the studs can develop both strength and ductility, though not as much as for studs spaced longitudinally. This limited benefit is due to transverse studs only being able to engage rebar near the edge of the breakout cone, making the rebar more prone to separation at large displacements.
4) Connections without studs tall enough to engage the reinforcement have lower strengths and little to no ductility compared to configurations that do engage the rebar. This lack of ductility applies regardless of whether the studs are spaced longitudinally or transversely.
5) For connections with ductile behavior, the presence of a haunch can improve strength by reducing flexural cracking around the shear studs. This lack of cracking prior to peak load allows monolithic concrete cone breakout. For connections that exhibit brittle behavior, the haunch is detrimental. For brittle connections with studs spaced longitudinally, the haunch does not contribute any ductility to the connection, while for brittle connections with studs spaced transversely, the haunch reduces strength and ductility.
6) Dynamic loading of shear stud connections in tension increases the strength of the connection, with the level of increase related to the configuration of the studs in the connection. Longitudinal stud spacings have a dynamic strength factor between 1.15 and 1.18, while transverse and single

stud spacings have a dynamic strength factor between 1.29 and 1.43. Dynamic loading slightly reduces the ductility of connections, but otherwise does not change their behavior from static loading conditions. Eccentric loading of shear stud connections reduces the strength from concentric loading, but causes only a small reduction in the ductility.

6.3 Recommendations for Design and Future Work

Based on the conclusions drawn from the tests performed as part of this research, several recommendations can confidently be given on how to design and improve shear stud connection details. While the current research provides a strong basis for changes in tensile strength design of shear stud connections, some aspects of the connection behavior have not been fully examined and merit further testing. Below are recommendations for shear stud design based on the current research and suggestions for future work.

1) Shear studs on fracture critical girders should be tall enough to engage the reinforcement of the deck slab. Longitudinal spacing of the studs, close enough that their failure cones overlap (less than or equal to three times the effective stud height), is encouraged, but transverse spacings are also strong and ductile if the studs engage the reinforcement. Longitudinal spacings with failure cones that do not overlap have a higher strength than the same number of studs in a group failure but have less ductility and are only recommended if ductility is not needed. For this research, 7-in studs spaced longitudinally in a 3-in haunch were tall enough to engage the reinforcement. The center of this reinforcement was 2-3/8 in below the bottom of the stud head (the top of the effective stud height) and 3 in away from the center of the stud. The effective stud height was 3/8 in (the stud head thickness) less than the overall stud height. For transverse spacings, 9-in studs in a 3-in haunch were needed to develop ductility, with the center of the reinforcement 4-3/8 in below the top of the effective stud height and 3 in away from the center of the stud. The typical construction practice of a haunch helps the strength of these ductile connections. Connections with shear studs not tall enough to engage the reinforcement are strongly discouraged as they have poor strength and no practically ductility, both of which are essential to non-fracture critical behavior of the bridge.
2) In order to predict the tensile strength of shear studs in a haunch, an effective haunch height term should be used in place of the effective height term in ACI 318, Appendix D, taking into account only the portion of the stud above the haunch. This effective haunch height has a lower bound limit to account for complete utilization of the haunch in the breakout cone.
3) To more accurately predict the tensile strength of shear studs, a group effect modification factor is proposed for ACI 318, Appendix D. This factor accounts for the diminishing returns seen as more studs are spaced in close proximity to one another, such as with studs spaced transversely. The factor also accounts for the maximum concrete engagement seen when the failure cones of studs spaced longitudinally overlap one another to create a continuous group cone.
4) Current testing considers only shear studs loaded in tension. The possibility exists for a shear stud connection to see both tension and shear during a fracture event, and further research is recommended to examine if there is strong shear and tension interaction on the connection behavior. The area of reinforcing intersecting a failure cone should also be examined to see if increased areas of steel can increase the ductile load strengths of a connection. Additional dynamic tests are recommended to validate a strong relationship between stud configuration and the magnitude of the dynamic strength factor. Likewise, the proximity of the shear studs to the rebar should be examined to discover how close reinforcement must be to the head of a shear stud before rebar-stud interlock creates strong, ductile behavior. Combined longitudinal and transverse stud spacings should be examined to determine if transverse group effects hinder full longitudinal strength development. Lastly, additional eccentric load testing is needed to define the strength-eccentricity relationship.

Appendix A

Selected Tensile Strength Calculations using ACI Appendix D Existing Provisions and Proposed Modifications

5:0-1 Single 5-in Stud without a Haunch

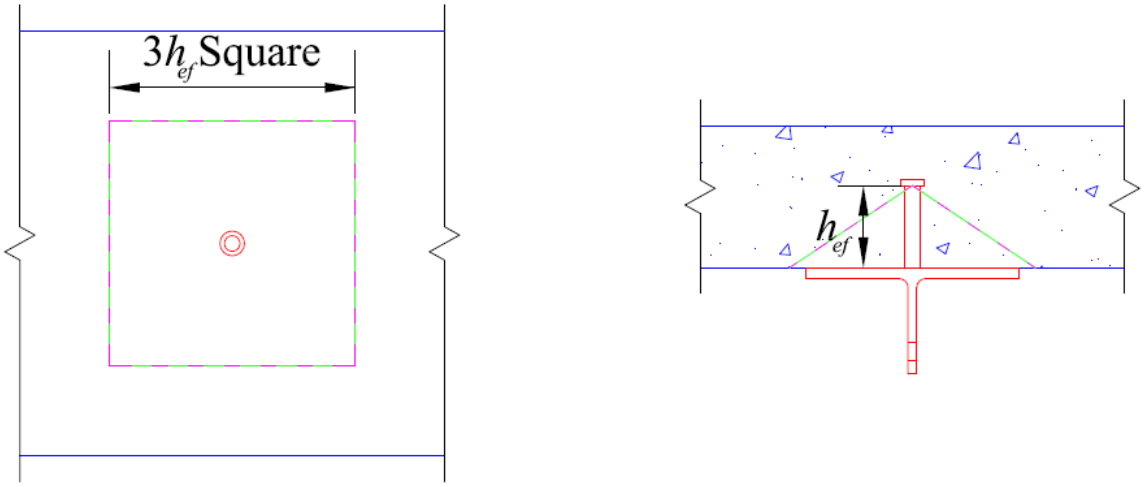

Figure A.1: Code (Green) and Proposed (Purple) Projected Failure Cone Areas for 5:0-1

Existing Code Method:

f'_c = 5900 psi
d_h = 0.0 in
h = 5.0 in
h_{ef} = 5-0.375 = 4.625 in
$c_{a,min}$ = 12.0 in
k_c=24, cast in place anchor

$$N_b = k_c\sqrt{f'_c}\,h_{ef}^{1.5} = 24\sqrt{5900}\times 4.625^{1.5} = 18{,}336 \text{ lbs}$$

$$A_{Nco} = 9h_{ef}^2 = 9\times 4.625^2 = 192.5 \text{ in}^2$$

For a single stud, no haunch, $A_{Nc} = A_{Nco}$ = 192.5 in^2
$\psi_{ec,N}$ = 1.0, Concentric Loading
$\psi_{ed,N}$ = 1.0, $c_{a,min} > 1.5h_{ef}$
$\psi_{ec,N}$ = 1.00, Cracked concrete (no haunch)

$$N_{cbg} = \frac{A_{Nc}}{A_{Nco}}\psi_{ec,N}\psi_{ed,N}\psi_{c,N}N_b = \frac{192.5}{192.5}1.0\times 1.0\times 1.0\times\frac{18{,}336}{1000} = 18.3 \text{ kips}$$

ACI Code Strength = 18.3 kips

Proposed Modified Method has no changes to this case.

5:3-1 Single 5-in Stud with a 3-in Haunch

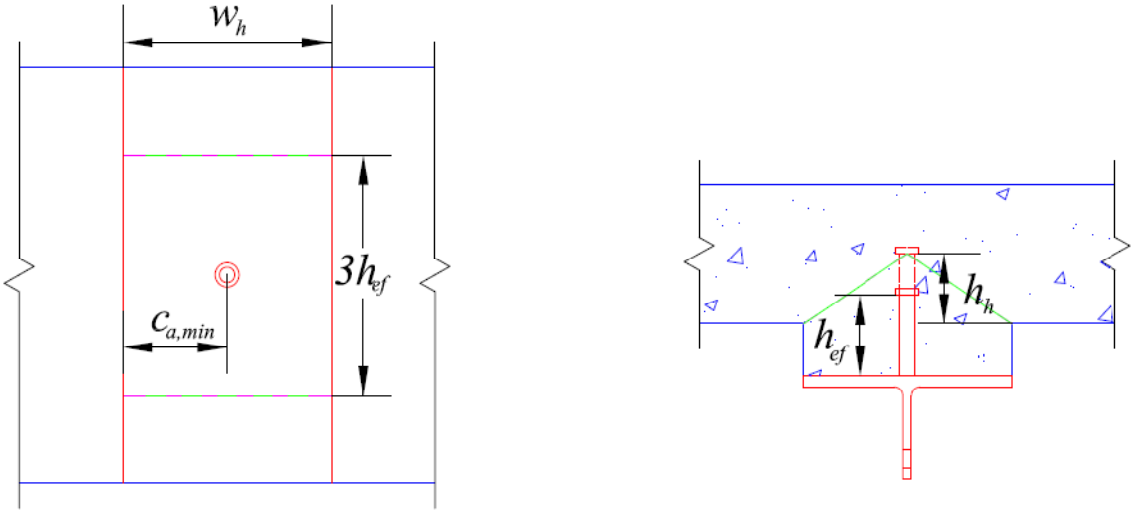

Figure A.2: Code (Green) and Proposed (Purple) Projected Failure Cone Areas for 5:3-1

Existing Code Method:

f'_c = 5900 psi
d_h = 3.0 in
h = 5.0 in
h_{ef} = 5-0.375 = 4.625 in
$c_{a,min}$ = 6.0 in
k_c=24, cast in place anchor

$$N_b = k_c\sqrt{f'_c}\,h_{ef}^{1.5} = 24\sqrt{5900}\times 4.625^{1.5} = 18{,}336 \text{ lbs}$$
$$A_{Nco} = 9h_{ef}^2 = 9\times 4.625^2 = 192.5 \text{ in}^2$$

Haunch confines projected cone area:

$$A_{Nc} = 3h_{ef}\,w_h = 3\times 4.625\times 12 = 166.5 \text{ in}^2$$

$\psi_{ec,N}$ = 1.0, Concentric Loading

$$\psi_{ed,N} = 0.7 + 0.3\frac{c_{a,\min}}{1.5h_{ef}} = 0.7 + 0.3\frac{6}{1.5\times 4.625} = 0.959$$

$\psi_{ec,N}$ = 1.25, Uncracked concrete (haunch)

$$N_{cbg} = \frac{A_{Nc}}{A_{Nco}}\psi_{ec,N}\psi_{ed,N}\psi_{c,N}N_b = \frac{166.5}{192.5}1.0\times 0.959\times 1.25\times\frac{18{,}336}{1000} = 19.0 \text{ kips}$$

ACI Code Strength = 19.0 kips

Proposed Modified Method:

f'_c = 5900 psi

d_h = 3.0 in
h = 5.0 in
h_{ef} = 5-0.375 = 4.625 in

$$h_h = h_{ef} - d_h \geq \frac{w_h}{3} = 4.525 - 3 \geq \frac{12}{3} = 1.625 < 4; h_h = 4.0 \text{ in}$$

$c_{a,min}$ = 6.0 in
k_c=24, cast in place anchor

$$N_b = k_c \sqrt{f_c'} h_h^{1.5} = 24\sqrt{5900} \times 4.0^{1.5} = 14{,}748 \text{ lbs}$$
$$A_{Nco} = 9h_h^2 = 9 \times 4.0^2 = 144 \text{ in}^2$$

Haunch confined full height projected cone area:

$$A_{Nc} = 3h_{ef} w_h = 3 \times 4.625 \times 12 = 166.5 \text{ in}^2$$

$\psi_{ec,N}$ = 1.0, Concentric Loading
$\psi_{ed,N}$ = 1.0, $c_{a,min}$ = $1.5h_{ef}$
$\psi_{ec,N}$ = 1.25, Uncracked concrete (haunch)
$\psi_{g,N}$ = 1.0, Single Stud

$$N_{cbg} = \frac{A_{Nc}}{A_{Nco}} \psi_{g,N} \psi_{ec,N} \psi_{ed,N} \psi_{c,N} N_b = \frac{166.5}{144} 1.0 \times 1.0 \times 1.0 \times 1.25 \times \frac{14{,}748}{1000} = 21.3 \text{ kips}$$

<u>Proposed Modified Strength = 21.3 kips</u>

5:3-3T Three 5-in Studs Spaced Transversely with a 3-in Haunch

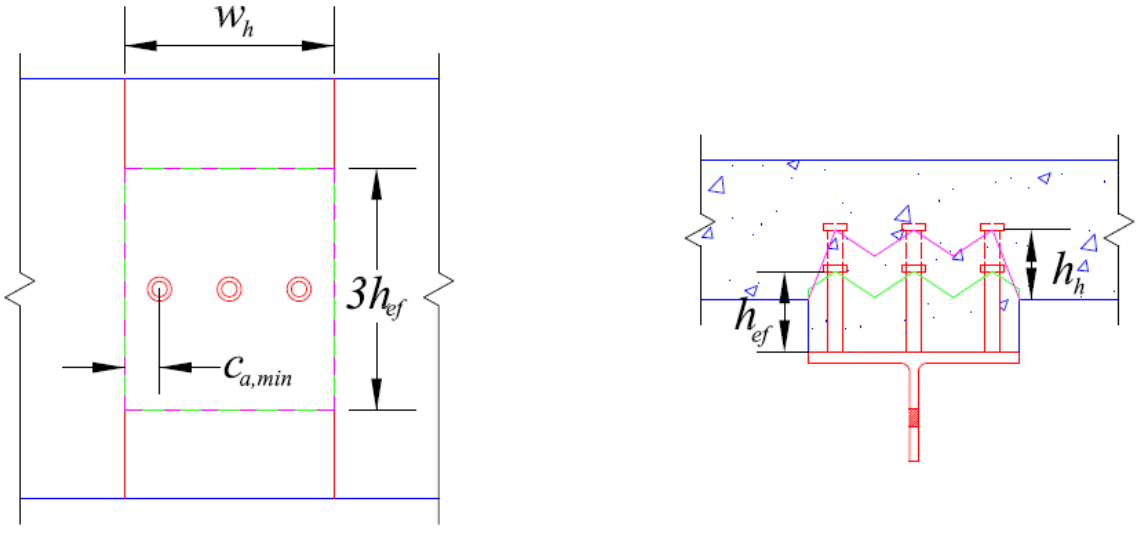

Figure A.3: Code (Green) and Proposed (Purple) Projected Failure Cone Areas for 5:3-3T

<u>Existing Code Method:</u>

f'_c = 5900 psi
d_h = 3.0 in

h = 5.0 in
h_{ef} = 5-0.375 = 4.625 in
$c_{a,min}$ = 2.0 in
k_c=24, cast in place anchor

$$N_b = k_c\sqrt{f_c'}h_{ef}^{1.5} = 24\sqrt{5900}\times 4.625^{1.5} = 18{,}336 \text{ lbs}$$
$$A_{Nco} = 9h_{ef}^2 = 9\times 4.625^2 = 192.5 \text{ in}^2$$

Haunch confined projected cone area:

$$A_{Nc} = 3h_{ef}w_h = 3\times 4.625\times 12 = 166.5 \text{ in}^2$$
$\psi_{ec,N}$ = 1.0, Concentric Loading

$$\psi_{ed,N} = 0.7 + 0.3\frac{c_{a,\min}}{1.5h_{ef}} = 0.7 + 0.3\frac{2}{1.5\times 4.625} = 0.786$$
$\psi_{ec,N}$ = 1.25, Uncracked concrete (haunch)
$$N_{cbg} = \frac{A_{Nc}}{A_{Nco}}\psi_{ec,N}\psi_{ed,N}\psi_{c,N}N_b = \frac{166.5}{192.5}1.0\times 0.786\times 1.25\times\frac{18{,}336}{1000} = 15.6 \text{ kips}$$

ACI Code Strength = 15.6 kips

Proposed Modified Method:

f'_c = 5900 psi
d_h = 3.0 in
h = 5.0 in
h_{ef} = 5-0.375 = 4.625 in
$$h_h = h_{ef} - d_h \ge \frac{w_h}{3} = 4.625 - 3 \ge \frac{12}{3} = 1.625 < 4; h_h = 4.0 \text{ in}$$
$c_{a,min}$ = 2.0 in
k_c=24, cast in place anchor

$$N_b = k_c\sqrt{f_c'}h_h^{1.5} = 24\sqrt{5900}\times 4.0^{1.5} = 14{,}748 \text{ lbs}$$
$$A_{Nco} = 9h_h^2 = 9\times 4.0^2 = 144 \text{ in}^2$$

Haunch confined full height projected cone area:

$$A_{Nc} = 3h_{ef}w_h = 3\times 4.625\times 12 = 166.5 \text{ in}^2$$
$\psi_{ec,N}$ = 1.0, Concentric Loading
$$\psi_{ed,N} = 0.7 + 0.3\frac{c_{a,\min}}{1.5h_{ef}} = 0.7 + 0.3\frac{2}{1.5\times 4.0} = 0.80$$
$\psi_{ec,N}$ = 1.25, Uncracked concrete (haunch)
$\psi_{g,N}$ = 0.90, Three studs spaced transversely

$$N_{cbg} = \frac{A_{Nc}}{A_{Nco}} \psi_{g,N} \psi_{ec,N} \psi_{ed,N} \psi_{c,N} N_b = \frac{166.5}{144} 0.90 \times 1.0 \times 0.8 \times 1.25 \times \frac{14{,}748}{1000} = 15.3 \text{ kips}$$

Proposed Modified Strength = 15.3 kips

5:0-3L Three 5-in Studs Spaced Longitudinally with no Haunch

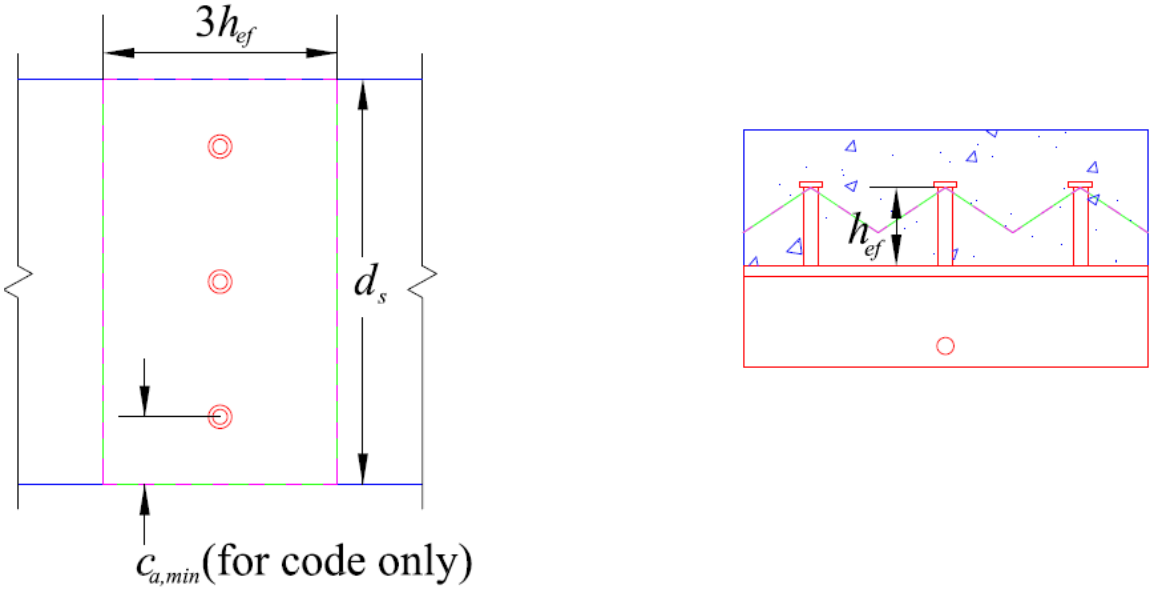

Figure A.4: Code (Green) and Proposed (Purple) Projected Failure Cone Areas for 5:0-3L

Existing Code Method:

f'_c = 7500 psi
d_h = 0.0 in
h = 5.0 in
h_{ef} = 5-0.375 = 4.625 in
$c_{a,min}$ = 4.0 in (to edge of slab)
k_c=24, cast in place anchor

$$N_b = k_c \sqrt{f'_c} h_{ef}^{1.5} = 24\sqrt{7500} \times 4.625^{1.5} = 20{,}673 \text{ lbs}$$

$$A_{Nco} = 9h_{ef}^2 = 9 \times 4.625^2 = 192.5 \text{ in}^2$$

Projected cone area confined by slab edges:

$$A_{Nc} = d_s \, 3h_{ef} = 24 \times 3 \times 4.625 = 333 \text{ in}^2$$

$\psi_{ec,N}$ = 1.0, Concentric Loading

$$\psi_{ed,N} = 0.7 + 0.3 \frac{c_{a,\min}}{1.5h_{ef}} = 0.7 + 0.3 \frac{4}{1.5 \times 4.625} = 0.873$$

$\psi_{ec,N}$ = 1.0, Cracked concrete (no haunch)

$$N_{cbg} = \frac{A_{Nc}}{A_{Nco}} \psi_{ec,N} \psi_{ed,N} \psi_{c,N} N_b = \frac{333}{192.5} 1.0 \times 0.873 \times 1.00 \times \frac{20{,}673}{1000} = 31.2 \text{ kips}$$

ACI Code Strength = 31.2 kips

Proposed Modified Method:

f'_c = 7500 psi
d_h = 0.0 in
h = 5.0 in
h_{ef} = 5-0.375 = 4.625 in
$h_h = h_{ef} = 4.625$ in (no haunch, no change in effective height)
$c_{a,min}$ = none (slab edge neglected for proposed method)
k_c=24, cast in place anchor

$$N_b = k_c \sqrt{f'_c} h_h^{1.5} = 24\sqrt{7500} \times 4.625^{1.5} = 20{,}673 \text{ lbs}$$
$$A_{Nco} = 9h_h^2 = 9 \times 4.625^2 = 192.5 \text{ in}^2$$

Full height projected cone area confined by slab edges:

$$A_{Nc} = d_s\, 3h_{ef} = 24 \times 3 \times 4.625 = 333 \text{ in}^2$$

$\psi_{ec,N}$ = 1.0, Concentric Loading
$\psi_{ed,N}$ = 1.0, no $c_{a,min}$
$\psi_{ec,N}$ = 1.0, Cracked concrete (no haunch)
$\psi_{g,N}$ = 0.80, Three studs spaced longitudinally

$$N_{cbg} = \frac{A_{Nc}}{A_{Nco}} \psi_{g,N} \psi_{ec,N} \psi_{ed,N} \psi_{c,N} N_b = \frac{333}{192.5} 0.80 \times 1.0 \times 1.0 \times 1.0 \times \frac{20{,}673}{1000} = 28.6 \text{ kips}$$

Proposed Modified Strength = 28.6 kips

5:3-3L Three 5-in Studs Spaced Longitudinally with a 3-in Haunch

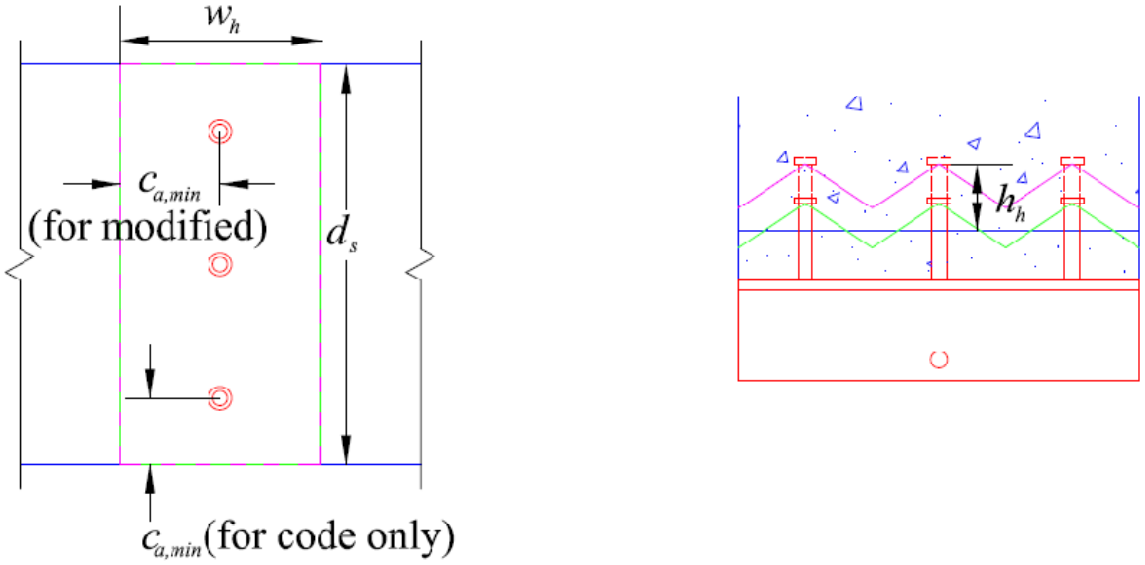

Figure A.5: Code (Green) and Proposed (Purple) Projected Failure Cone Areas for 5:3-3L

Existing Code Method:

f'_c = 7500 psi
d_h = 3.0 in
h = 5.0 in
h_{ef} = 5-0.375 = 4.625 in
$c_{a,min}$ = 4.0 in (to edge of slab)
k_c=24, cast in place anchor

$$N_b = k_c\sqrt{f'_c}\,h_{ef}^{1.5} = 24\sqrt{7500}\times 4.625^{1.5} = 20{,}673 \text{ lbs}$$

$$A_{Nco} = 9h_{ef}^2 = 9\times 4.625^2 = 192.5 \text{ in}^2$$

Haunch confined projected cone area:

$$A_{Nc} = d_s w_h = 24\times 12 = 288 \text{ in}^2$$

$\psi_{ec,N}$ = 1.0, Concentric Loading

$$\psi_{ed,N} = 0.7 + 0.3\frac{c_{a,\min}}{1.5h_{ef}} = 0.7 + 0.3\frac{4}{1.5\times 4.625} = 0.873$$

$\psi_{ec,N}$ = 1.25, Uncracked concrete (haunch)

$$N_{cbg} = \frac{A_{Nc}}{A_{Nco}}\psi_{ec,N}\psi_{ed,N}\psi_{c,N}N_b = \frac{288}{192.5}1.0\times 0.873\times 1.25\times\frac{20{,}673}{1000} = 33.7 \text{ kips}$$

ACI Code Strength = 33.7 kips

Proposed Modified Method:

f'_c = 7500 psi
d_h = 3.0 in
h = 5.0 in
h_{ef} = 5-0.375 = 4.625 in

$$h_h = h_{ef} - d_h \geq \frac{w_h}{3} = 4.625 - 3 \geq \frac{12}{3} = 1.625 < 4; h_h = 4.0 \text{ in}$$

$c_{a,min}$ = 6.0 in (edge distance to haunch, slab edge neglected for proposed method)
k_c=24, cast in place anchor

$$N_b = k_c \sqrt{f'_c} h_h^{1.5} = 24\sqrt{7500} \times 4.0^{1.5} = 16{,}628 \text{ lbs}$$
$$A_{Nco} = 9h_h^2 = 9 \times 4.0^2 = 144 \text{ in}^2$$

Haunch confined full height projected cone area:

$$A_{Nc} = d_s w_h = 24 \times 12 = 288 \text{ in}^2$$

$\psi_{ec,N}$ = 1.0, Concentric Loading
$\psi_{ed,N}$ = 1.0, $c_{a,min} = 1.5h_{ef}$
$\psi_{ec,N}$ = 1.25, Uncracked concrete (haunch)
$\psi_{g,N}$ = 0.80, Three studs spaced longitudinally

$$N_{cbg} = \frac{A_{Nc}}{A_{Nco}} \psi_{g,N} \psi_{ec,N} \psi_{ed,N} \psi_{c,N} N_b = \frac{288}{144} 0.80 \times 1.0 \times 1.0 \times 1.25 \times \frac{16{,}628}{1000} = 33.3 \text{ kips}$$

Proposed Modified Strength = 33.3 kips

9:3-3T Three 9-in Studs Spaced Transversely with a 3-in Haunch

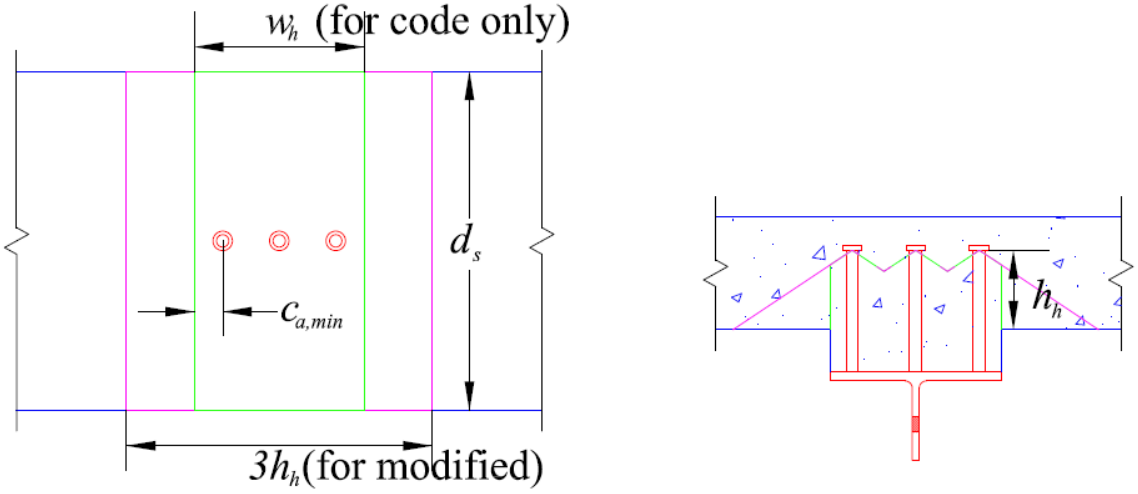

Figure A.6: Code (Green) and Proposed (Purple) Projected Failure Cone Areas for 9:3-3T

Existing Code Method:

f'_c = 5100 psi
d_h = 3.0 in
h = 9.25 in (as-installed height from fillet welding)
h_{ef} = 9.25-0.375 = 8.875 in
$c_{a,min}$ = 2.0 in (to edge of haunch)
k_c=24, cast in place anchor

$$N_b = k_c\sqrt{f'_c}h_{ef}^{1.5} = 24\sqrt{5100}\times 8.875^{1.5} = 45{,}316 \text{ lbs}$$
$$A_{Nco} = 9h_{ef}^2 = 9\times 8.875^2 = 708.9 \text{ in}^2$$

Haunch confined projected cone area (Area abounded by haunch and ends of slab):

$$A_{Nc} = d_s w_h = 24\times 12 = 288 \text{ in}^2$$
$\psi_{ec,N}$ = 1.0, Concentric Loading

$$\psi_{ed,N} = 0.7 + 0.3\frac{c_{a,\min}}{1.5h_{ef}} = 0.7 + 0.3\frac{2}{1.5\times 8.875} = 0.745$$

$\psi_{ec,N}$ = 1.25, Uncracked concrete (haunch)

$$N_{cbg} = \frac{A_{Nc}}{A_{Nco}}\psi_{ec,N}\psi_{ed,N}\psi_{c,N}N_b = \frac{288}{708.9}1.0\times 0.745\times 1.25\times\frac{45{,}316}{1000} = 17.1 \text{ kips}$$

ACI Code Strength = 17.1 kips

Proposed Modified Method:
f'_c = 5100 psi
d_h = 3.0 in
h = 9.25 in (as-installed height from fillet welding)
h_{ef} = 9.25-0.375 = 8.875 in

$$h_h = h_{ef} - d_h \geq \frac{w_h}{3} = 8.875 - 3 \geq \frac{12}{3} = 5.875 < 4; h_h = 5.875 \text{ in}$$

$c_{a,min}$ = 2.0 in (edge distance to haunch)
k_c=24, cast in place anchor

$$N_b = k_c\sqrt{f'_c}h_h^{1.5} = 24\sqrt{5100}\times 5.875^{1.5} = 24{,}407 \text{ lbs}$$
$$A_{Nco} = 9h_h^2 = 9\times 5.875^2 = 310.6 \text{ in}^2$$

Stud effective height above haunch projected cone area, not confined by haunch:

$$A_{Nc} = 3h_h(3h_h + 2s) = 3\times 5.875(3\times 5.875 + 2\times 4) = 451.6 \text{ in}^2$$
$\psi_{ec,N}$ = 1.0, Concentric Loading

$$\psi_{ed,N} = 0.7 + 0.3\frac{c_{a,\min}}{1.5h_h} = 0.7 + 0.3\frac{2}{1.5\times 5.875} = 0.768$$

$\psi_{ec,N}$ = 1.25, Uncracked concrete (haunch)
$\psi_{g,N}$ = 0.90, Three studs spaced transversely

$$N_{cbg} = \frac{A_{Nc}}{A_{Nco}}\psi_{g,N}\psi_{ec,N}\psi_{ed,N}\psi_{c,N}N_b = \frac{451.6}{310.6}0.90\times 1.0\times 0.768\times 1.25\times\frac{24{,}407}{1000} = 30.7 \text{ kips}$$

Proposed Modified Strength = 30.7 kips

9:3-3L Three 9-in Studs Spaced Longitudinally with a 3-in Haunch

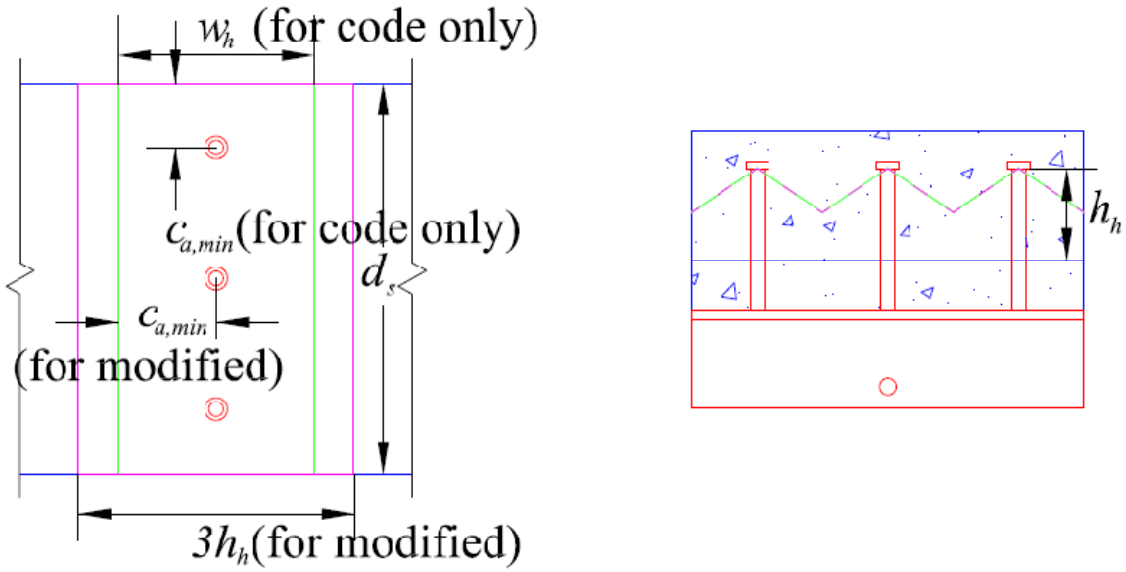

Figure A.7: Code (Green) and Proposed (Purple) Projected Failure Cone Areas for 9:3-3L

Existing Code Method:

f'_c = 5100 psi
d_h = 3.0 in
h = 9.25 in (as-installed height from fillet welding)
h_{ef} = 9.25-0.375 = 8.875 in
$c_{a,min}$ = 4.0 in (to edge of slab)
k_c=24, cast in place anchor

$$N_b = k_c\sqrt{f'_c}h_{ef}^{1.5} = 24\sqrt{5100}\times 8.875^{1.5} = 45{,}316 \text{ lbs}$$

$$A_{Nco} = 9h_{ef}^2 = 9\times 8.875^2 = 708.9 \text{ in}^2$$

Haunch confined projected cone area (Area abounded by haunch and ends of slab):

$$A_{Nc} = d_s w_h = 24\times 12 = 288 \text{ in}^2$$

$\psi_{ec,N}$ = 1.0, Concentric Loading

$$\psi_{ed,N} = 0.7 + 0.3\frac{c_{a,\min}}{1.5h_{ef}} = 0.7 + 0.3\frac{4}{1.5\times 8.875} = 0.790$$

$\psi_{ec,N}$ = 1.25, Uncracked concrete (haunch)

$$N_{cbg} = \frac{A_{Nc}}{A_{Nco}}\psi_{ec,N}\psi_{ed,N}\psi_{c,N}N_b = \frac{288}{708.9}1.0\times 0.790\times 1.25\times\frac{45{,}316}{1000} = 18.2\,\text{kips}$$

ACI Code Strength = 18.2 kips

Proposed Modified Method:

f'_c = 5100 psi
d_h = 3.0 in
h = 9.25 in (as-installed height from fillet welding)
h_{ef} = 9.25-0.375 = 8.875 in

$$h_h = h_{ef} - d_h \geq \frac{w_h}{3} = 8.875 - 3 \geq \frac{12}{3} = 5.875 < 4; h_h = 5.875 \text{ in}$$

$c_{a,min}$ = 6.0 in (edge distance to haunch, slab edge neglected for proposed method)
k_c=24, cast in place anchor

$$N_b = k_c\sqrt{f'_c}h_h^{1.5} = 24\sqrt{5100}\times 5.875^{1.5} = 24{,}407 \text{ lbs}$$

$$A_{Nco} = 9h_h^2 = 9\times 5.875^2 = 310.6 \text{ in}^2$$

Stud effective height above haunch projected cone area, not confined by haunch:

$$A_{Nc} = 3h_h d_s = 3\times 5.875\times 24 = 423 \text{ in}^2$$

$\psi_{ec,N}$ = 1.0, Concentric Loading

$$\psi_{ed,N} = 0.7 + 0.3\frac{c_{a,\min}}{1.5h_h} = 0.7 + 0.3\frac{6}{1.5\times 5.875} = 0.904$$

$\psi_{ec,N}$ = 1.25, Uncracked concrete (haunch)
$\psi_{g,N}$ = 0.80, Three studs spaced longitudinally

$$N_{cbg} = \frac{A_{Nc}}{A_{Nco}}\psi_{g,N}\psi_{ec,N}\psi_{ed,N}\psi_{c,N}N_b = \frac{423}{310.6}0.80\times 1.0\times 0.904\times 1.25\times\frac{24{,}407}{1000} = 30.0\,\text{kips}$$

Proposed Modified Strength = 30.0 kips

5:3-3LE Three 5-in Studs Spaced Longitudinally with a 3-in Haunch, Loaded Eccentrically

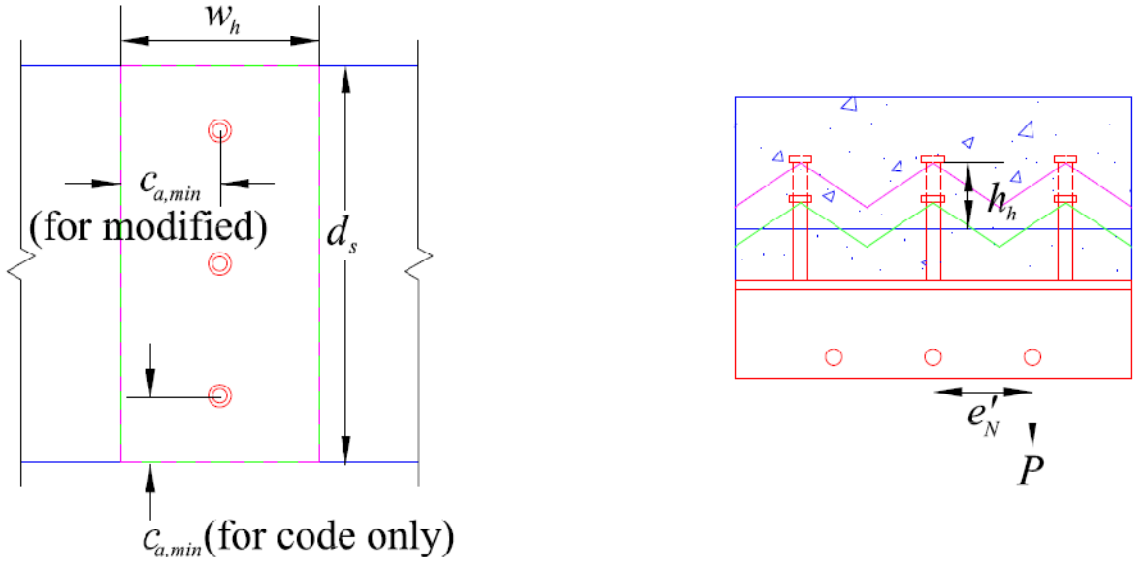

Figure A.8: Code (Green) and Proposed (Purple) Projected Failure Cone Areas for 5:3-3LE

Existing Code Method:

f'_c = 5100 psi
d_h = 3.0 in
h = 5.25 in (as-installed height from fillet welding)
h_{ef} = 5.25-0.375 = 5.875 in
$c_{a,min}$ = 4.0 in (to edge of slab)
e'_N = 6.0 in, applied load eccentricity
k_c=24, cast in place anchor

$$N_b = k_c\sqrt{f'_c}h_{ef}^{1.5} = 24\sqrt{5100}\times 4.875^{1.5} = 18{,}448 \text{ lbs}$$
$$A_{Nco} = 9h_{ef}^2 = 9\times 4.875^2 = 213.9 \text{ in}^2$$

Haunch confined projected cone area (area abounded by haunch and ends of slab):

$$A_{Nc} = d_s w_h = 24\times 12 = 288 \text{ in}^2$$
$$\psi_{ec,N} = \frac{1}{\left(1+\frac{2e'_N}{3h_{ef}}\right)} \le 1.0 = \frac{1}{\left(1+\frac{2\times 6}{3\times 4.875}\right)} \le 1.0 = 0.549 < 1.0; \psi_{ec,N} = 0.549$$

$$\psi_{ed,N} = 0.7 + 0.3\frac{c_{a,\min}}{1.5h_{ef}} = 0.7 + 0.3\frac{4}{1.5\times 4.875} = 0.846$$

$\psi_{ec,N}$ = 1.25, Uncracked concrete (haunch)

$$N_{cbg} = \frac{A_{Nc}}{A_{Nco}}\psi_{ec,N}\psi_{ed,N}\psi_{c,N}N_b = \frac{288}{213.9}0.549\times 0.846\times 1.25\times\frac{18{,}448}{1000} = 14.4 \text{ kips}$$

ACI Code Strength = 14.4 kips

Proposed Modified Method:

f'_c = 5100 psi
d_h = 3.0 in
h = 5.25 in (as-installed height from fillet welding)
h_{ef} = 5.25-0.375 = 4.875 in

$$h_h = h_{ef} - d_h \geq \frac{w_h}{3} = 4.875 - 3 \geq \frac{12}{3} = 1.875 < 4; h_h = 4 \text{ in}$$

$c_{a,min}$ = 6.0 in (edge distance to haunch, slab edge neglected for proposed method)
e'_N = 6.0 in, applied load eccentricity
k_c=24, cast in place anchor

$$N_b = k_c \sqrt{f'_c} h_h^{1.5} = 24\sqrt{5100} \times 4.0^{1.5} = 13{,}712 \text{ lbs}$$

$$A_{Nco} = 9h_h^2 = 9 \times 4.0^2 = 144 \text{ in}^2$$

Stud effective height above haunch projected cone area, confined by haunch and slab edges:

$$A_{Nc} = d_s w_h = 24 \times 12 = 288 \text{ in}^2$$

$$\psi_{ec,N} = \frac{1}{\left(1 + \frac{2e'_N}{3h_h}\right)} \leq 1.0 = \frac{1}{\left(1 + \frac{2 \times 6}{3 \times 4}\right)} \leq 1.0 = 0.5 < 1.0; \psi_{ec,N} = 0.5$$

$\psi_{ed,N}$ = 1.0, $c_{a,min} = 1.5h_{ef}$
$\psi_{ec,N}$ = 1.25, Uncracked concrete (haunch)
$\psi_{g,N}$ = 1.0, Eccentrically loaded

$$N_{cbg} = \frac{A_{Nc}}{A_{Nco}} \psi_{g,N} \psi_{ec,N} \psi_{ed,N} \psi_{c,N} N_b = \frac{288}{144} 1.0 \times 0.5 \times 1.0 \times 1.25 \times \frac{13{,}712}{1000} = 17.2 \text{ kips}$$

Proposed Modified Strength = 17.2 kips

Appendix B

Complete Test Specimen Details

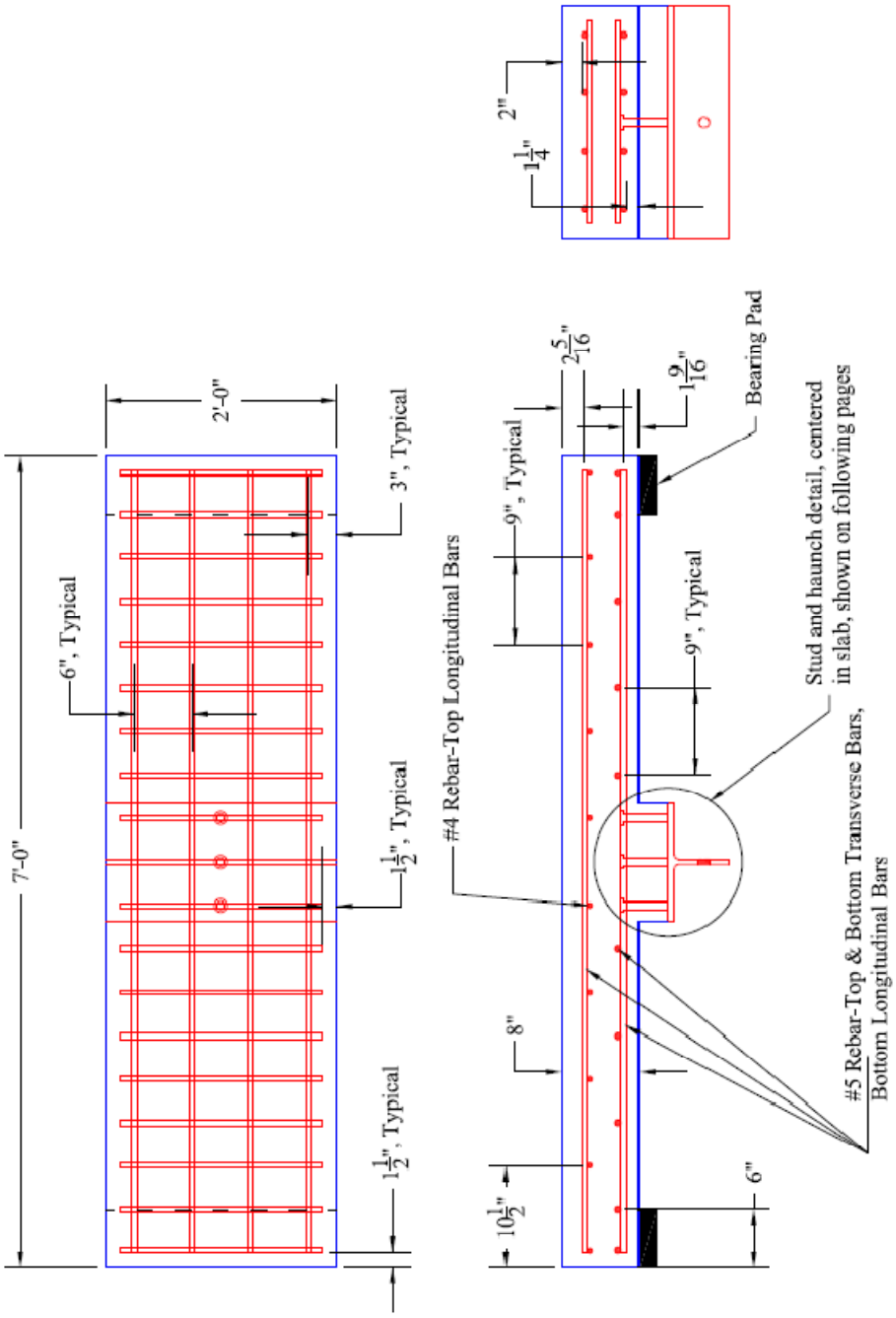

Figure B.1: Standard Specimen Slab Details

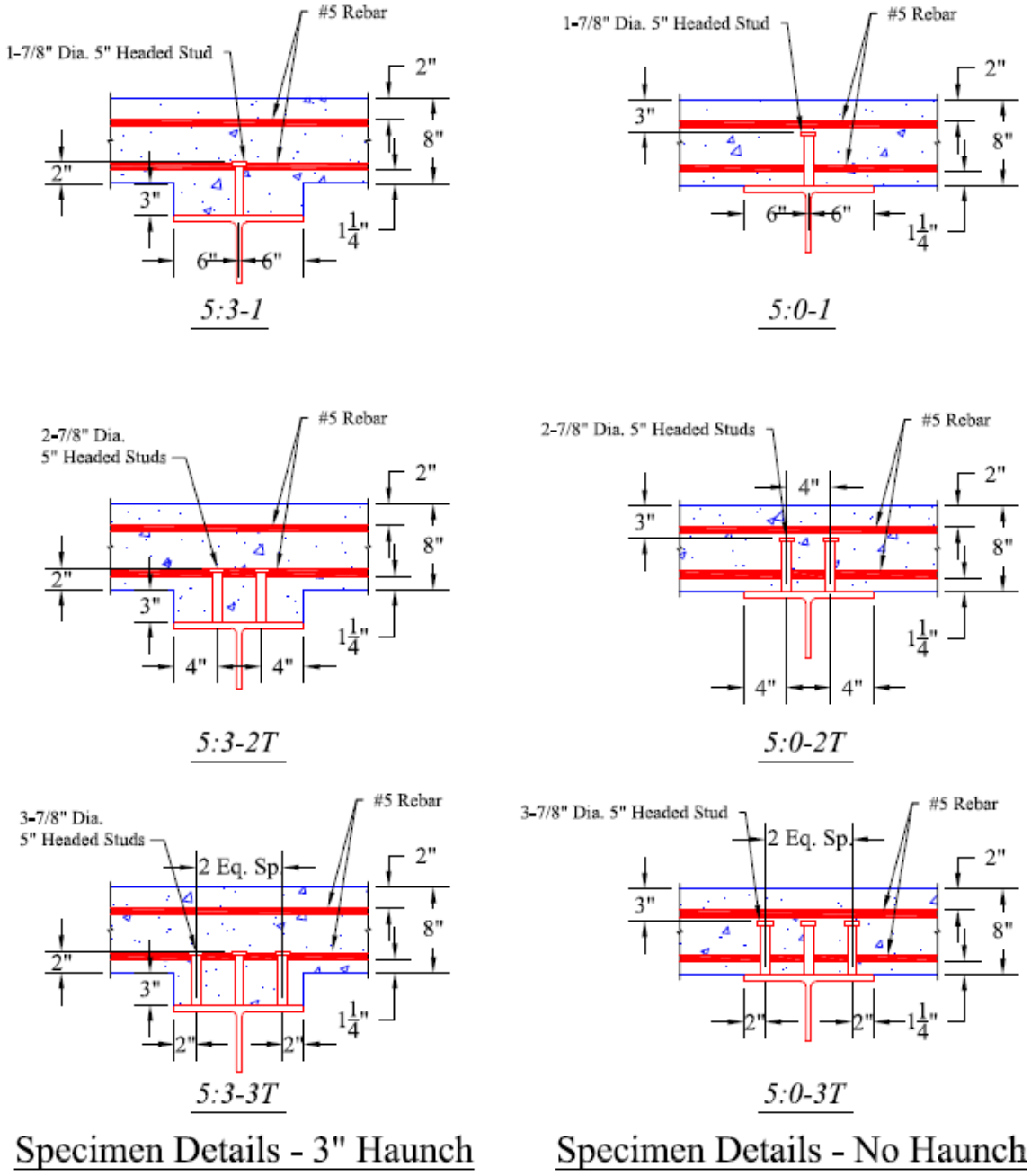

Figure B.2: Shear Studs Details, 5-in Studs Spaced Transversely

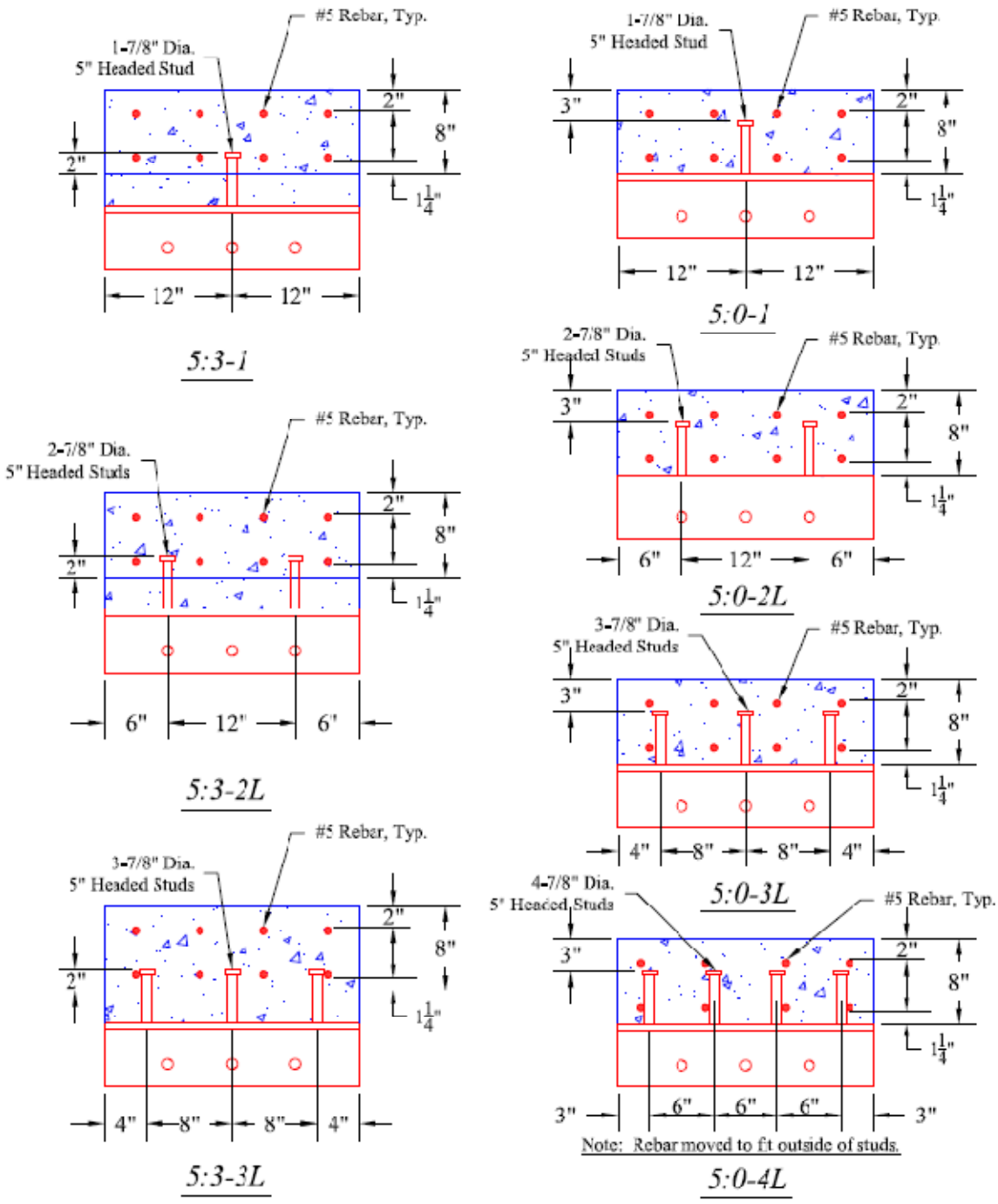

Figure B.3: Shear Studs Details, 5-in Studs Spaced Longitudinally

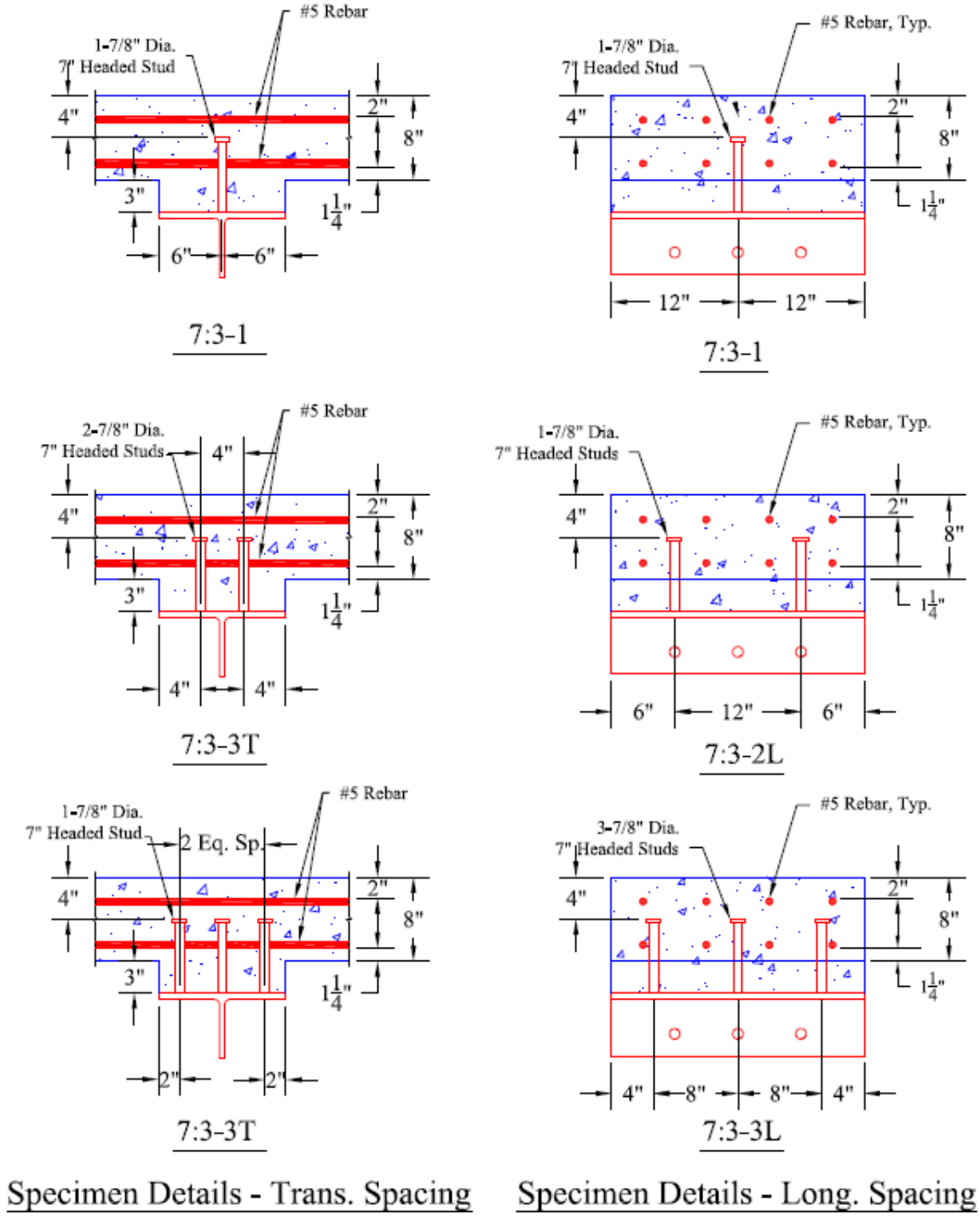

Figure B.4: Shear Studs Details, 7-in Studs

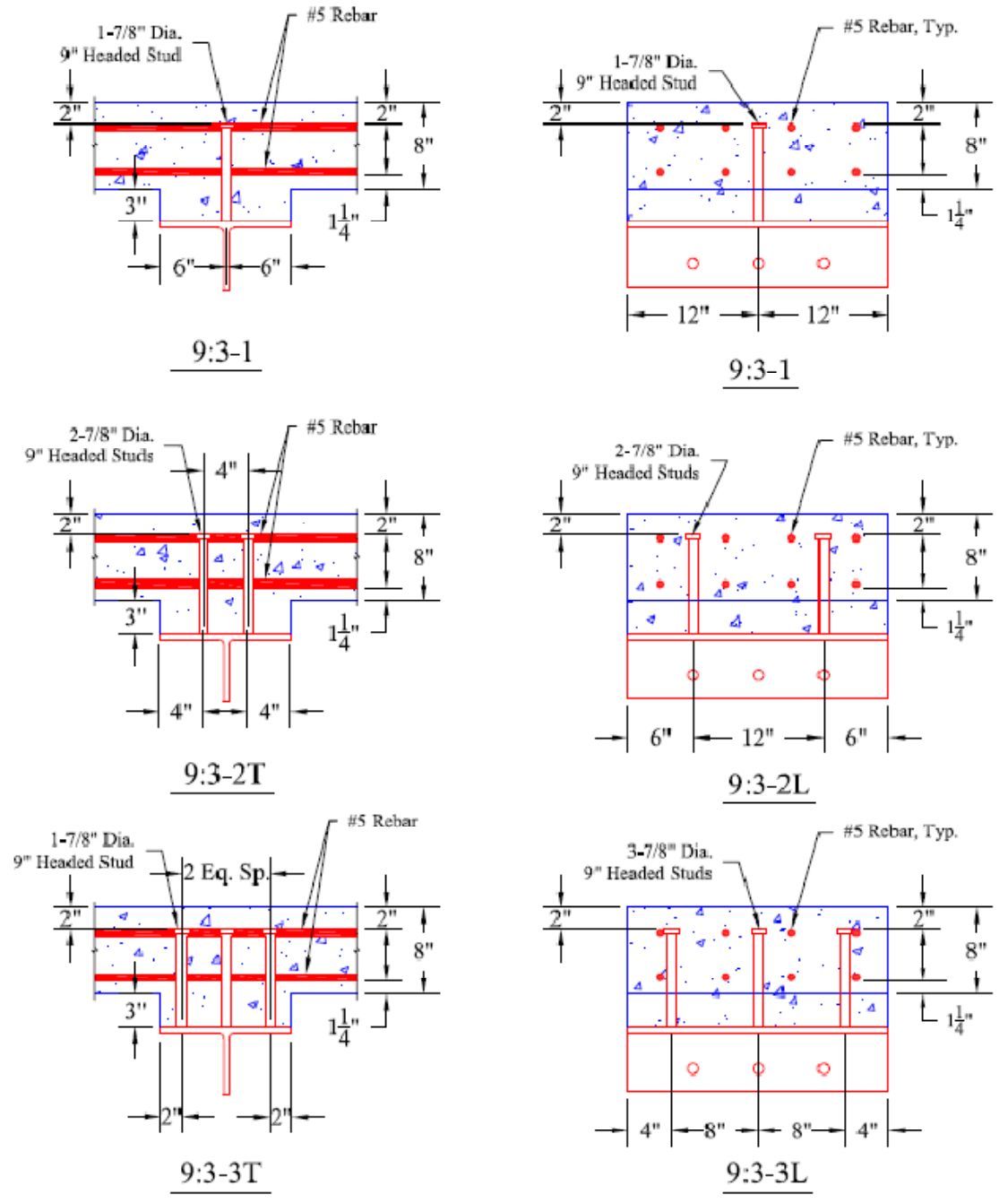

Figure B.5: Shear Studs Details, 9-in Studs

REFERENCES

ACI Committee 318. (2008). *Building Code Requirements for Structural Concrete (ACI 318-05) and Commentary (ACI 318R-08)*. American Concrete Institute, Farmington Hills, MI.

American Association of State Highway Transportation Officials. (2007). *AASHTO LRFD Bridge Design Specifications*. Washington, D.C.

American Association of State Highway Transportation Officials/American Welding Society. (2002). *AASHTO/AWS D1.5M/D1.5:2002 Bridge Welding Code*. AASHTO/AWS, Washington D.C./Miami, FL.

Connor, Robert J., Dexter, Robert, and Mahmoud, Hussam. (2005). "Inspection and Management of Bridges with Fracture-Critical Details." *National Cooperative Highway Research Program Synthesis 354*. Transportation Research Board, National Academy Press, Washington, D.C.

Department of the Army Technical Manual TM 5-1300. (1990). *Structures to Resist the Effects of Accidental Explosions,* Washington D.C.

Fuchs, Werner, Eligehausen, Rolf, and Breen, John E. (1995). "Concrete Capacity Design (CCD) Approach for Fastening to Concrete." *ACI Structural Journal*, vol. 92, no. 1, pp. 73-94.

Idriss, R. L., White, K. R., and Woodward, C. B., and Jauregui, D. V. (1995). "Evaluation and Testing of a Fracture Critical Bridge" *NDT&E International*, vol. 28, no. 6, pp. 339-347.

Quiel, Spencer, (2003). "Forensic Analysis of the Steel Girder Facture in the I-95 Brandywine River Bridge" *Research Experience for Undergraduates Report, University of Notre Dame*

Shirvani, Mansour, Klingner, Richard E., and Graves III, Herman L. (2004). "Breakout Capacity of Anchors in Concrete – Part 1: Tension." *ACI Structural Journal*, vol. 101, no. 6, pp. 812-820.

Sutton, James P. (2007). "Evaluating the Redundancy of Steel Bridges: Effect of a Bridge Haunch on the Strength and Behavior of Shear Stud under Tensile Loading" *M.S. Thesis, University of Texas at Austin*